

Faculty of Applied Engineering  
Research group Applied Electrochemistry  
and Catalysis (ELCAT)



# Integrated capture and electrochemical conversion of CO<sub>2</sub>

This thesis is submitted in fulfilment of the requirements for the degree of  
Doctor in Applied Engineering  
(Doctor in de toegepaste ingenieurswetenschappen)

**Oriol Gutiérrez-Sánchez**

Promotor(s): Prof. Dr Ing. Tom Breugelmans (ELCAT, University of Antwerp)  
Dr Ir. Metin Bulut (Flemish Institute for Technological Research, VITO)

Antwerp 2022

#### Disclaimer

The author allows to consult and copy parts of this work for personal use. Further reproduction or transmission in any form or by any means, without the prior permission of the author is strictly forbidden.

## **Integrated capture and electrochemical conversion of CO<sub>2</sub>**

Oriol Gutiérrez-Sánchez

### **Members of the Jury**

Prof. Dr Vera Meynen	President of the jury LADCA, University of Antwerp
Dr Nick Daems	Secretary of the jury ELCAT, University of Antwerp
Prof. Dr Tom Breugelmans	Promotor ELCAT, University of Antwerp
Dr Metin Bulut	Promotor VITO
Prof. Dr Shoubhik Das	Jury member ORSY, University of Antwerp
Dr Deepak Pant	External jury member VITO
Dr Carlos M. Sanchez-Sanchez	External jury member LISE, University Pierre et Marie Curie



# Acknowledgements

Since I had the opportunity, I took the chance to leave home and explore the world abroad, not only for leisure, but to temporarily settle, find new challenges, and enrich myself. As a well-defined expat, changing your home, starting from the scratch, and spending time alone were not new experiences to me, however, it is easy to get lost by leaving everything behind and fully depending on yourself. One of my favourite authors, J.R.R. Tolkien, once quoted “not all those who wander are lost”. Even by starting over in a new adventure, facing a challenge such as a PhD, it is impossible to success and find your way without support and letting people in, using these inputs as a guide to your new life. For this reason, I want to open this thesis by acknowledging those who helped me fulfill my PhD, both directly and indirectly.

I would like to start thanking my promotors, Tom and Metin, for giving me the opportunity to come to Belgium to perform my PhD. I still remember it was not easy at the beginning to get used to the new life and the responsibilities both at ELCAT and VITO, but I always felt trusted and supported by you two. Additionally, I have observed you and learnt a lot during these four years. Tom, you are an example of commitment and hard-working. I respect you for what you achieved and for how you can manage a research group (duplicating its members in short time), being the dean and a caring father. You made me always look higher and be more ambitious, both professionally and personally. Metin, from the first day you had unconditional trust on me, always standing up for my choices and giving me confidence to face difficult situations. If I am ever a boss, I would be lucky if I am a fraction of what you are today. Furthermore, you showed me a new way to see science, linked to industry and with a direct impact to society, which I fell for from the first day. I hope that I can continue learning from you now from VITO, too.

Next, I would like to thank my colleagues and ex-colleagues from ELCAT (formerly ART) for their daily company of my journey. I remember how, at the start of my PhD, I was the first foreigner ever in the group, which shocked me, however, from the first day I felt like one more. Without a non-engineering background, I had evident lack of knowledge upon assembling reactors and operating certain complex systems, among others. Nevertheless, you always helped me when I needed it, and I learnt a lot from it. Today, I can say I consider myself a bit of an engineer (still far from you) all thanks to you! I hope we can still see each other and continue to collaborate and hang out. I had great time guys!

I will continue thanking my colleagues and ex-colleagues from ELEC for the good vibes, professionalism, and partnership. I remember those brainstorm sessions during our meetings where we let ourselves be carried away, sometimes for too long. Thanks to those meetings, we were able solve many clues during my thesis. Specially, I want to thank Deepak for his continuous support and guidance. I learnt so much about the scientific world from you and you are such a role-model for a scientist. I'm looking forward continue working alongside you in my following years.

Por último, no podía dejar a mi gente atrás. A los de toda la vida, aunque hayan sido más de cuatro años desde que me fui, siempre habéis estado ahí como si nunca lo hubiera hecho. Habéis sido un apoyo durante toda mi vida, y este periodo tan importante para mí no ha sido una excepción, siempre os agradeceré vuestra amistad. A los que aparecieron durante este tiempo, gracias por permitirme forjar una nueva vida, especialmente a ti, Lien, por ser un apoyo en los mejores y peores momentos. Ja per acabar, papa, mama i Alba sempre heu estat el pilar de la meva vida i m'heu donat força per continuar endavant, mai serà suficient per agrair-vos el vostre suport així que continuaré intentant fer-vos sentir orgullosos de mi.

Oriol.

## Scientific contributions

This PhD thesis was executed in a strategic collaboration of ELCAT with the Flemish Institute for Technological Research (VITO), bringing VITO's technology domain of electrochemistry and techno-economic assessment to the expertise electrocatalysis and reactor engineering of the ELCAT group of the University of Antwerp. Oriol Gutiérrez-Sánchez was awarded with a VITO's strategic funds PhD Grant (n. 1810257) for the elaboration of this thesis. In addition to the daily duties at ELCAT, the candidate took part in the daily duties as an employee of the Separation and Conversion Technology (SCT) unit of VITO within the frame of the CAPTIN and CAPTIN-2 project (under the Moonshot initiative of VLAIO/Catalisti, Grant number HBC.2019.0076 and HBC.2021.0255).





# Abstract

The level of CO<sub>2</sub> in the atmosphere is increasing to unprecedented levels leading to a global warming era. Reducing the amount of CO<sub>2</sub> from the atmosphere by capturing it is crucial to decrease the effects of climate change and eventually revert it. However, capturing CO<sub>2</sub> is costly and inefficient if it cannot be valorised afterwards. Capturing CO<sub>2</sub> and utilizing it to produce chemical building blocks within the frame of Carbon Capture and Utilization (CCU) technologies is receiving a lot of attention. In this respect, using alkaline solutions to capture CO<sub>2</sub> and the electrochemical CO<sub>2</sub> reduction are promising technologies to convert CO<sub>2</sub> into valuable products and as such reduce greenhouse emissions while valorising the CO<sub>2</sub>. However, the capture and electrochemical CO<sub>2</sub> conversion have been investigated almost exclusively as separate processes. A disadvantage is that gaseous CO<sub>2</sub> is desorbed and compressed to be fed to the electrolyser, with an important contribution to operational costs. To improve the valorisation, integrating the capture and conversion steps by utilizing the post-capture solution, in the form of bicarbonate, directly as a CO<sub>2</sub> source for the electrochemical CO<sub>2</sub> reduction is a promising approach. This technology is however limited by the slow CO<sub>2</sub> release rate at the catalytic interphase and the high competition with undesired co-reactions like the Hydrogen Evolution Reaction (HER) being the main reasons for low Faradaic efficiencies and partial current densities. To increase the feasibility of the integrated concept and delivering the know-how of the technology, this doctoral thesis is elaborated.

In the first part, an overview of the context is given, discussing the role of CCU in the battle against global warming. In addition, the most fundamental aspects of the CCU value chain are explained.

In the second part, the reader is provided with the most recent information on the industrialization of CO<sub>2</sub> electroreduction and the integration of CO<sub>2</sub> capture and electrochemical conversion in two literature reviews. It is shown the technology is promising and hence still in its early stages of development where engineering and energetic aspects limit the up-scalability towards application. These shortcomings formed the starting point for this thesis.

The third part consists of three experimental chapters. A fundamental study on the mechanism of bicarbonate electrolysis is provided. It was proven how bicarbonate was not the substrate of the electrochemical reaction but instead, the CO<sub>2</sub> supplied via an equilibrium of bicarbonate in water. In addition, bicarbonate was found to be a proton donor species, promoting the HER, the main co-reaction, thus limiting the efficiency of the reaction. A strategy to inhibit the Hydrogen Evolution Reaction was proposed, increasing the faradaic efficiency of the reaction. Additionally, based on the findings of these chapters, a novel integrated capture and conversion system involving biomimetic catalysis is proposed.

Lastly, an upscaled bicarbonate electrolyser was built. The engineering aspects of the electrolyser were studied, and the parameters were screened to identify the most energy-efficient operational window. These optimal parameters were later used for a proof-of-concept Direct Air Capture electrolyser. For the first time, CO<sub>2</sub> was captured from the air and then directly converted, electrochemically, to formate and carbon monoxide (CO).

By the realisation of this thesis, we provide the necessary background on bicarbonate electrolysis, which enables further research focused on upscaling the integrated concept. Additionally, we have benchmarked a procedure to capture and convert CO<sub>2</sub> in one and a single system which, although it is still in its early stages, contributes to a great extend the development of the technology to higher Technology Readiness Levels.

# Samenvatting

De CO<sub>2</sub>-gehalte in de atmosfeer stijgt tot nooit eerder geziene niveaus, wat leidt tot een tijdperk van opwarming van ons planeet. Het verminderen van de hoeveelheid CO<sub>2</sub> in de atmosfeer door het af te vangen is cruciaal om de effecten van klimaatverandering te beperken en uiteindelijk terug te schroeven. Het afvangen van CO<sub>2</sub> is echter kostbaar en economisch inefficiënt als het achteraf niet gevaloriseerd kan worden. Het gebruik van CO<sub>2</sub> als grondstof om chemische bouwstenen te produceren in het kader van *Carbon Capture and Utilization* krijgt veel aandacht. In dit opzicht hebben amine-gebaseerde of, in het algemeen, alkalische oplossingen bewezen efficiënte CO<sub>2</sub>-afvangoplossingen te zijn en de elektrochemische CO<sub>2</sub>-conversie is een veelbelovende technologie. Beide processen worden echter bijna uitsluitend als afzonderlijke processen onderzocht. Een complexiteit van afvang is de desoptie van CO<sub>2</sub> uit de opvangoplossing en vervolgens de compressie voordat het naar de elektrolyser wordt gestuurd, en omgezet. Deze factoren hebben een belangrijke contributie in de operationele kost van de toepassing. Om de economische haalbaarheid te verbeteren, kunnen de afvang- en conversiestappen idealiter geïntegreerd worden, waarbij de post-capture-oplossing, die CO<sub>2</sub> geconcentreerd in de vorm van bicarbonaat bevat, en direct als CO<sub>2</sub>-bron voor de elektrochemische CO<sub>2</sub>-reductie kan dienen. Deze technologie wordt echter beperkt door lage Faraday-efficiëntie en partiële stroomdichtheden, wat leidt tot een langzame CO<sub>2</sub>-afgifte bij de katalytische interfase en de hoge competitie met nevenreacties zoals de waterstofevolutiereactie.

Eerst wordt een overzicht gegeven van de context waarin dit onderzoek zich afspeelt, waarbij de rol van CO<sub>2</sub> als broeikaseffect wordt besproken en de *Carbon Capture & Utilization* wordt voorgeteld om dit tegen te gaan. Daarnaast worden de meest fundamentele aspecten van afvang en elektrochemische CO<sub>2</sub>-conversie toegelicht.

Vervolgens, wordt de lezer met twee literatuurstudies-voorzien van de meest recente informatie over de industrialisatie van CO<sub>2</sub>-elektroreductie en over het geïntegreerd concept. Hier wordt aangetoond in welke mate, hoewel het veelbelovend is, de technologie nog in zijn kinderschoenen staat, naast de technische en energetische aspecten die de opschaalbaarheid beperken. Vanuit deze tekortkomingen is het onderzoekskader van dit proefschrift ontstaan.

In het derde deel zijn drie experimentele hoofdstukken te vinden. Er wordt een fundamentele studie gegeven over het mechanisme van bicarbonaatelektrolyse, en bewezen dat bicarbonaat niet ageert als substraat van de elektrochemische reactie, maar in wel CO<sub>2</sub> in de evenwichtreactie met water. Bovendien bleek bicarbonaat een protondonorsoort te zijn, die de waterstofevolutiereactie, de belangrijkste nevenreactie, bevordert, waardoor de reactie-efficiëntie beperkt wordt. Er werd een strategie voorgesteld om de waterstofevolutie-reactie te onderdrukken, waardoor de Faraday-efficiëntie van de beoogde reactie werd bevorderd. Daarnaast wordt, op basis van de bevindingen van *Hoofdstukken 6 en 7*, een nieuw geïntegreerd vang- en conversiesysteem voorgesteld, op basis van biomimetische katalyse.

Ten slotte werd, een opgeschaalde bicarbonaatelektrolyse-apparaat gebouwd. De technische aspecten van de elektrolyseur werden bestudeerd om de parameters-instellingen voor een energiezuiniger systeem te identificeren. Deze werden vervolgens gebruikt in een *proof-of-concept* experiment, met de integratie van de *Direct Air Capture*-toegepassing en -de (bicarbonaat) elektrolyzer. Voor het eerst werd CO<sub>2</sub> uit de lucht opgevangen en de afvangoplossing vervolgens gebruik in de elektrochemische omzetting in formiaat en CO.

# Table of contents

<b>ACKNOWLEDGEMENTS</b> .....	<b>V</b>
<b>SCIENTIFIC CONTRIBUTIONS</b> .....	<b>VII</b>
<b>ABSTRACT</b> .....	<b>IX</b>
<b>SAMENVATTING</b> .....	<b>XI</b>
<b>TABLE OF CONTENTS</b> .....	<b>XIII</b>
<b>NOMENCLATURE</b> .....	<b>XIX</b>
<b>LIST OF SYMBOLS</b> .....	<b>XXI</b>
<b>PART I INTRODUCTION</b> .....	<b>XXIII</b>
<b>CHAPTER 1 CARBON CAPTURE AND THE ELECTROCHEMICAL REDUCTION OF CO<sub>2</sub></b> .....	<b>1</b>
1.1 A STRATEGY TO REDUCE EMISSIONS: THE CAPTURE AND CONVERSION OF CO <sub>2</sub> .....	2
1.1.1 CO <sub>2</sub> and the global warming .....	2
1.1.2 Carbon Capture & Utilization .....	4
1.2 CO <sub>2</sub> CAPTURE .....	7
1.3 ELECTROCHEMICAL CO <sub>2</sub> CONVERSION .....	9
1.4 INTEGRATING THE CAPTURE AND THE CONVERSION OF CO <sub>2</sub> .....	12
1.5 TECHNO-ECONOMIC ASSESSMENT: INTEGRATED VS. TWO-STEP ROUTE .....	14
<b>CHAPTER 2 SCOPE AND OUTLINE</b> .....	<b>25</b>
2.1 SCOPE .....	26
2.2 STRATEGY.....	27
2.3 OUTLINE .....	28
<b>PART II LITERATURE REVIEW ON THE STATE-OF-THE-ART OF UPSCALING CO<sub>2</sub> CAPTURE AND ELECTROCHEMICAL CONVERSION SYSTEMS</b> .....	<b>31</b>
<b>CHAPTER 3 RECENT ADVANCES IN INDUSTRIAL CO<sub>2</sub> ELECTROREDUCTION</b> .....	<b>33</b>
3.1 INTRODUCTION .....	34
3.2 STATUS QUO OF INDUSTRIAL CO <sub>2</sub> R TECHNOLOGIES .....	35
3.3 REACTOR CONFIGURATION .....	40
3.4 ELECTRODE STRUCTURE .....	42
3.5 ANODE REACTION .....	47
3.6 MEMBRANES .....	48
3.7 CONCLUSIONS.....	49
<b>CHAPTER 4 STATE-OF-THE-ART ON INTEGRATED CO<sub>2</sub> CAPTURE AND ELECTROCHEMICAL CONVERSION SYSTEMS</b> .....	<b>51</b>
4.1 INTRODUCTION .....	52
4.2 CO <sub>2</sub> SOURCE: CAPTURE AND DELIVERY TECHNOLOGIES .....	52

4.2.1 CO <sub>2</sub> from the air: Direct Air Capture .....	52
4.2.2 CO <sub>2</sub> from flue gas .....	54
4.2.3 Catalytic CO <sub>2</sub> capture: improving capture rates .....	56
4.3 POST-CAPTURE ELECTROCHEMICAL CO <sub>2</sub> CONVERSION .....	59
4.3.1 CO <sub>2</sub> conversion from carbamate .....	59
4.3.2 CO <sub>2</sub> conversion from bicarbonate .....	60
4.4 EMERGING TECHNOLOGIES: CO <sub>2</sub> CAPTURE AND CONVERSION FROM IONIC LIQUIDS AND COVALENT ORGANIC FRAMEWORKS .....	63
4.5 CONCLUSIONS .....	64
<b>PART III STUDY OF THE MECHANISM OF BICARBONATE ELECTROLYSIS. ROLE OF THE BICARBONATE ANION, CO-REACTIONS, AND PROPOSED APPROACH.....</b>	<b>67</b>
<b>CHAPTER 5 THE ROLE OF THE BICARBONATE ANION AS PROTON DONOR IN CO<sub>2</sub> REDUCTION SYSTEMS: A STRATEGY TO INCREASE THE FARADAIC EFFICIENCY OF BICARBONATE ELECTROLYSIS .....</b>	<b>69</b>
5.1 INTRODUCTION .....	70
5.2 EXPERIMENTAL .....	72
5.2.1 Materials and solutions .....	72
5.2.2 Instruments .....	73
5.2.3 Experimental set up and procedure .....	74
5.3 RESULTS AND DISCUSSION .....	75
5.4 CONCLUSIONS .....	83
5.5 SUPPORTING INFORMATION .....	84
<b>CHAPTER 6 A DEEP STUDY ON THE HER INHIBITION MECHANISM OF CATIONIC SURFACTANTS DURING BICARBONATE ELECTROLYSIS .....</b>	<b>85</b>
6.1 INTRODUCTION .....	86
6.2 EXPERIMENTAL .....	89
6.2.1 Materials and solutions .....	89
6.2.2 Experimental set up and procedure .....	90
6.2.3 Analytical techniques .....	91
6.3 RESULTS AND DISCUSSION .....	92
6.3.1 Electrocatalytic reduction of CO <sub>2</sub> in presence of surfactants .....	92
6.3.2 Study of the surfactant-electrode interface by Linear Sweep Voltammetry....	94
6.3.3 Determination of the hydrophobicity of the electrode by electrochemical impedance spectroscopy .....	101
6.3.4 Benzyl functional groups as HER inhibitor promoters .....	105
6.3.5 Impurities in surfactants: analysis and electrochemical consequences .....	107
6.4 CONCLUSIONS .....	109
6.5 SUPPORTING INFORMATION .....	111
<b>CHAPTER 7 DEVELOPMENT OF A BIOMIMETIC BIFUNCTIONAL CATALYST FOR THE INTEGRATED CAPTURE AND ELECTROCHEMICAL CONVERSION OF CO<sub>2</sub>.....</b>	<b>123</b>

7.1 INTRODUCTION .....	124
7.2 EXPERIMENTAL.....	128
7.2.1 <i>Materials and solutions</i> .....	128
7.2.2 <i>CO<sub>2</sub> capture set-up and procedure</i> .....	129
7.2.3 <i>Bicarbonate electrolysis: set-up and procedure</i> .....	133
7.3 RESULTS AND DISCUSSION: BIOMIMETIC CATALYSIS OF THE CO <sub>2</sub> CAPTURE .....	135
7.3.1 <i>Effect of the nature of the ligand</i> .....	135
7.3.2 <i>Effect of the concentration of catalyst</i> .....	138
7.3.3 <i>Effect of the temperature of the solution</i> .....	139
7.4 RESULTS AND DISCUSSION: PROMOTED BICARBONATE ELECTROLYSIS .....	141
7.5 CONCLUSIONS.....	146
7.6 SUPPORTING INFORMATION .....	147
<b>PART IV UPSCALING A BICARBONATE ELECTROLYSER: ENGINEERING APPROACH AND TECHNOLOGICAL PROOF OF CONCEPT .....</b>	<b>153</b>
<b>CHAPTER 8 ENGINEERING ASPECTS FOR THE DESIGN OF A BICARBONATE ZERO-GAP FLOW ELECTROLYSER.....</b>	<b>155</b>
8.1 INTRODUCTION .....	156
8.2 MATERIALS AND METHODS.....	159
8.2.1 <i>Materials and solutions</i> .....	159
8.2.2 <i>Working electrode manufacturing</i> .....	159
8.2.3 <i>Electrolysis</i> .....	160
8.2.4 <i>Product analysis</i> .....	162
8.3 RESULTS AND DISCUSSION.....	162
8.3.1 <i>Catalyst configuration: binder material and oxidation state</i> .....	162
8.3.2 <i>Effect of the inlet flow rate</i> .....	164
8.3.3 <i>Effect of the temperature of the electrolyser</i> .....	168
8.3.4 <i>Effects of the concentration of carbon load (bicarbonate)</i> .....	171
8.4 CONCLUSIONS.....	174
8.5 SUPPORTING INFORMATION .....	175
<b>CHAPTER 9 ELECTROCHEMICAL CO<sub>2</sub> CONVERSION FROM DIRECT AIR CAPTURE SOLUTIONS.....</b>	<b>177</b>
9.1 INTRODUCTION .....	178
9.2 EXPERIMENTAL.....	178
9.2.1 <i>Materials and solutions</i> .....	178
9.2.2 <i>Direct Air Capture: Procedure</i> .....	179
9.2.3 <i>Working electrode manufacturing</i> .....	179
9.2.4 <i>(Bi)carbonate electrolysis: setup and procedure</i> .....	180
9.3 PRODUCT ANALYSIS AND CHARACTERIZATION.....	181
9.3.1 <i>Characterization of DAC solutions</i> .....	181
9.3.2 <i>(Bi)carbonate electrolysis product analysis</i> .....	184

9.4 RESULTS AND DISCUSSION .....	185
9.4.1 (Bi)carbonate solution obtained from Direct Air Capture .....	185
9.4.2 Electrolysis of the Direct Air Capture solution .....	188
9.5 CONCLUSIONS.....	191
<b>PART V CONCLUSIONS AND FUTURE PERSPECTIVES .....</b>	<b>193</b>
<b>CHAPTER 10 CONCLUSIONS AND FUTURE PERSPECTIVES .....</b>	<b>195</b>
10.1 CONCLUSIONS.....	196
10.1.1 Current state of the industrial eCO <sub>2</sub> R .....	196
10.1.2 Bicarbonate electrolysis.....	197
10.1.3 Integrated capture and conversion of CO <sub>2</sub> .....	198
10.2 FUTURE PERSPECTIVES.....	199
<b>ANNEX.....</b>	<b>205</b>
<b>ANNEX FUNDAMENTAL CONCEPTS AND EXPERIMENTAL TECHNIQUES.....</b>	<b>207</b>
A.1 PHYSICOCHEMICAL CONCEPTS OF THE CAPTURE OF CO <sub>2</sub> USING MEMBRANE CONTACTORS .....	208
A.1.1 CO <sub>2</sub> capture with membrane contactors.....	208
A.1.2 CO <sub>2</sub> capture solution .....	210
A.2 BASIC PRINCIPLES ON ELECTROCATALYSIS.....	211
A.2.1 Electrocatalysis.....	212
A.2.2 Electrochemical thermodynamics: the cell potential.....	214
A.2.3 Applied potential, equilibrium potential and overpotential .....	216
A.2.4 The electrode-electrolyte interface: the electrochemical double layer .....	221
A.2.5 The Faraday's law, the cell efficiency and the energy efficiency .....	224
A.3 REACTOR ASPECTS FOR INTEGRATING THE CAPTURE AND CONVERSION OF CO <sub>2</sub> .....	225
A.3.1 Bicarbonate as CO <sub>2</sub> source .....	226
A.3.2 Bicarbonate electrolysis and membrane engineering.....	229
A.4 CO <sub>2</sub> CAPTURE: EXPERIMENTAL SET-UP .....	230
A.4.1 CO <sub>2</sub> capture set-up for kinetic studies .....	232
A.4.2 Air tunnel for Direct Air Capture applications .....	233
A.5 ELECTROCHEMICAL CELL: EXPERIMENTAL SET-UP.....	235
A.5.1 H-Cell for batch operation .....	237
A.5.2 Zero-gap electrolyser for continuous flow operation.....	238
A.6 EXPERIMENTAL TECHNIQUES .....	239
A.6.1 Lineal sweep voltammetry .....	239
A.6.2 Chronoamperometry and chronopotentiometry .....	242
A.6.3 Electrochemical Impedance Spectroscopy .....	243
<b>LIST OF FIGURES.....</b>	<b>249</b>
<b>LIST OF TABLES .....</b>	<b>261</b>
<b>BIBLIOGRAPHY.....</b>	<b>263</b>
<b>PERSONAL INFORMATION .....</b>	<b>293</b>



PUBLICATIONS IN INTERNATIONAL PEER-REVIEWED JOURNALS .....	293
PUBLICATIONS IN REVIEW IN INTERNATIONAL PEER-REVIEWED JOURNALS .....	294
ORAL PRESENTATIONS AT INTERNATIONAL CONFERENCES .....	294
ORAL PRESENTATIONS AT A NATIONAL CONFERENCE .....	295
POSTER PRESENTATIONS AT INTERNATIONAL CONFERENCES .....	295



# Nomenclature

AEM	Anion exchange membrane
BPM	Bipolar membrane
BTAC	benzyl trimethylammonium chloride
CA	Chronoamperometry
CAH	Carbonic anhydrase
CAPEX	Capital expenditures
CCS	Carbon Capture & Storage
CCU	Carbon Capture & Utilisation
CD	Current density
CE	Cell efficiency
CEM	Cation exchange membrane
CKC	Cetalkonium chloride
CL	Catalyst layer
COF	Covalent-organic framework
CP	Chronopotentiometry
CPE	Constant phase element
CTAB	Cetrimonium bromide
CTAC	Cetrimonium chloride
DAC	Direct Air Capture
DSP	Downstream process
DIC	Dissolved inorganic carbon
eCO <sub>2</sub> R	Electrochemical CO <sub>2</sub> reduction
EDL	Electrochemical double layer
EE	Energy Efficiency
EIS	Electrochemical impedance spectroscopy
FE	Faradaic efficiency
F-T	Fischer-Tropsch

FT-IR	Fourier Transformed - Infrared Spectroscopy
GDE	Gas diffusion electrode
GDL	Gas diffusion layer
HER	Hydrogen evolution reaction
HPLC	High-performance liquid chromatography
IHP	Inner Helmholtz Plane
IL	Ionic liquid
LC-MS	Liquid chromatography-mass spectroscopy
LSV	Linear sweep voltammetry
LUMO	Lowest Unoccupied Molecular Orbital
MEA	Monoethanolamine
MOF	Metal-organic framework
MPL	Microporous layer
MWCNT	Multi-walled carbon nanotubes
OER	Oxygen evolution reaction
OHP	Outer Helmholtz Plane
PTFE	Polytetrafluoroethylene
PV	Photovoltaic
PZC	Potential of zero charge
RDE	Rotating disc electrode
RHE	Reversible hydrogen electrode
RT	Retention time
SDS	Sodium dodecyl sulfate
SOE	Solid oxide electrolyser
TEA	Techno-economic analysis
TRL	Technology readiness level
WACC	Weighted average cost of capital

## List of symbols

$A$	Warburg coefficient [ $\Omega \text{ s}^{-1/2}$ ]
$a$	Activity [ $\text{mol L}^{-1}$ ]
$\alpha$	Charge transfer coefficient
$C^*$	Bulk concentration [ $\text{mol L}^{-1}$ ]
$C_i$	Concentration of reactant [ $\text{mol L}^{-1}$ ]
$C_{dl}$	Double-layer capacitance [ $\Omega \text{ cm}^{-2}$ ]
$C_c$	Coating capacitance [ $\Omega \text{ cm}^{-2}$ ]
$D$	Diffusion constant [ $\text{cm}^2 \text{ s}^{-1}$ ]
$\Delta G^\circ$	Standard Gibbs free energy [ $\text{J mol}^{-1}$ ]
$\delta$	Thickness of the diffusion layer [ $\text{cm}$ ]
$E_{eq}$	Equilibrium potential [V]
$E^\circ_{eq}$	Standard equilibrium potential [V]
$E^\circ_{red}$	Standard reduction potential [V]
$E$	Applied potential [V]
$E_o$	Amplitude [V]
$\eta$	Overpotential [V]
$f$	Frequency [Hz]
$F$	Faraday constant [96485 C]
$I$	Intensity [A]
$I_o$	Current response to amplitude [A]
$j$	Current density [ $\text{A cm}^{-2}$ ]
$j_o$	Exchange current density [ $\text{A cm}^{-2}$ ]
$k_c$	Rate constant
$K^*_c$	(Pseudo)rate constant [ $\text{s}^{-1}$ ]
$K_a$	Acidity constant
$k_b$	Binding constant [ $\text{L mol}^{-1}$ ]
$\kappa$	Conductivity [ $\Omega^{-1} \text{ cm}^{-1}$ ]
$n$	Amount of product [mol]

$N$	Capacitance ideal factor
$v$	Reaction rate [mol s <sup>-1</sup> ]
$v_i$	Vibrational mode
$\omega$	Radial frequency [rad s <sup>-1</sup> ]
$\Phi$	Phase shift [rad]
$Q$	Total charge [C]
$Q_i$	Dedicated charge [C]
$R$	Ideal gas constant [J K <sup>-1</sup> mol <sup>-1</sup> ]
$R_i$	Resistance [ $\Omega$ ]
$\rho$	Resistivity [ $\Omega$ cm]
$R_s$	Resistance of the electrolyte [ $\Omega$ ]
$R_{ct}$	Charge transfer resistance [ $\Omega$ ]
$R_p$	Pore resistance [ $\Omega$ ]
$S$	Area of the electrode [cm <sup>2</sup> ]
$t$	Time [s]
$T$	Temperature [K]
$V_{Cell}$	Cell voltage [V]
$V_{RHE}$	Potential vs RHE [V]
$W_r$	Warburg resistance [ $\Omega$ ]
$z$	Number of electrons
$Z$	Impedance [ $\Omega$ ]
$Z'$	Real impedance [ $\Omega$ ]
$Z''$	Imaginary impedance [ $\Omega$ ]
$Z_o$	Impedance response to amplitude [ $\Omega$ ]

# **Part I**

## **Introduction**





# CHAPTER 1

## Carbon capture and the electrochemical reduction of CO<sub>2</sub>

IN THIS FIRST CHAPTER OF THE THESIS, AN INTRODUCTION IS PROVIDED TO ENSURE THE READERS CAN EASILY UNDERSTAND AND FOLLOW THE TOPICS AND DISCUSSION OF THIS WORK. AN OVERVIEW OF THE STRATEGY FOLLOWED TO CAPTURE AND CONVERT THE CO<sub>2</sub>, THE INTEGRATED CAPTURE AND ELECTROCHEMICAL CO<sub>2</sub> REDUCTION, WILL BE REVIEWED.

The techno-economic assessment of the integrated and the two-step strategy (section 1.5) was performed in a collaboration with Pieterjan Debergh from VITO.

## 1.1 A strategy to reduce emissions: the capture and conversion of CO<sub>2</sub>

### 1.1.1 CO<sub>2</sub> and the global warming

Current carbon dioxide (CO<sub>2</sub>) levels are higher than at any point in at least the past 800,000 years (Figure 1.1).[1] The last time that these levels were reached was more than three million years ago when the temperature was ~3 °C higher than during the pre-industrial era and the sea level ~20× higher than today.[2]

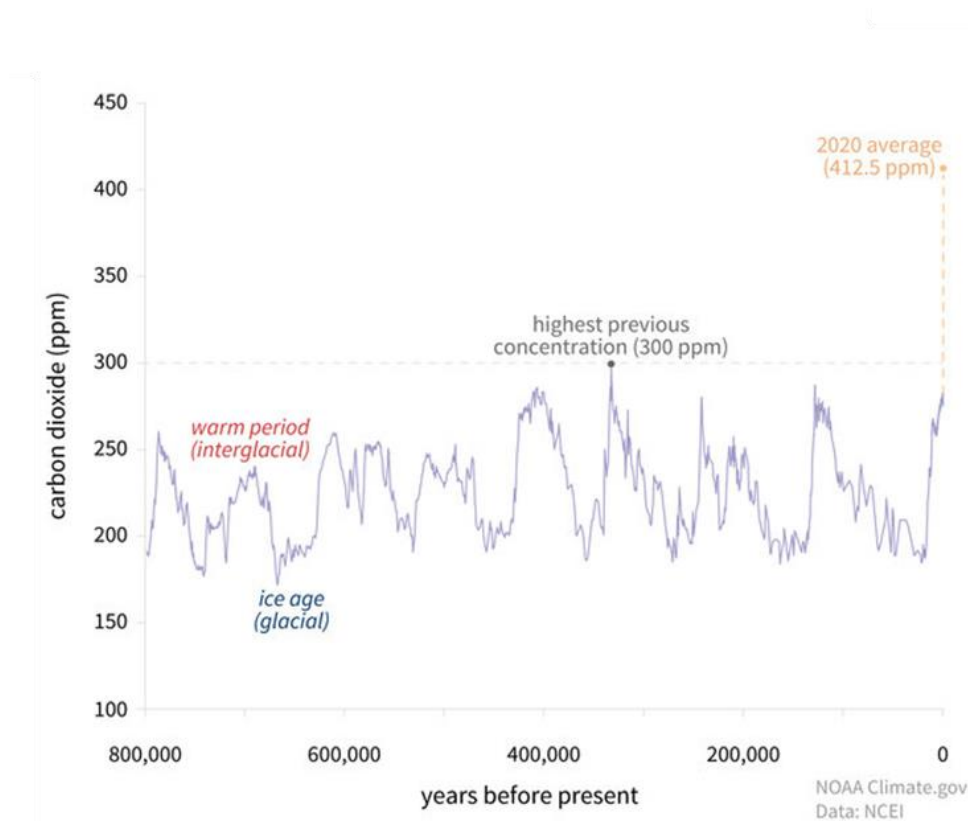


**Figure 1.1.** Global atmospheric carbon dioxide concentrations (CO<sub>2</sub>) in parts per million (ppm) for the past 800,000 years. Graph by NOAA Climate.gov based on data from Lüthi, *et al.*, 2008, via NOAA NCEI Paleoclimatology Program.[1]

The rise of atmospheric CO<sub>2</sub> levels (currently over 400 ppm) is mostly caused by anthropogenic activity such as industrial waste generation, energy production or fueled

transportation.[3,4] During millions of years, the plants pulled out the atmospheric CO<sub>2</sub> through photosynthesis and, in a little more than one century, we have returned that CO<sub>2</sub> back to the atmosphere.[5] Every year, more CO<sub>2</sub> is liberated into the atmosphere than natural processes can remove, increasing the yearly net amount of atmospheric CO<sub>2</sub>. In the last decade, the growth rate was already 2.3 ppm year<sup>-1</sup>.

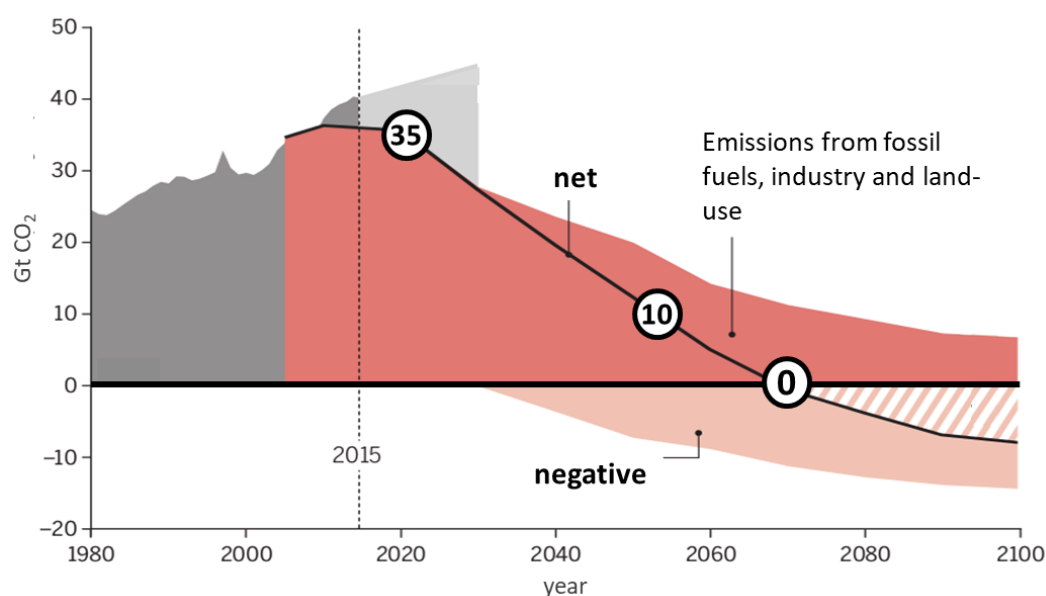


**Figure 1.2.** Amount of CO<sub>2</sub> emitted per year (grey). The International Panel for Climate Change set a scenario for the global CO<sub>2</sub> emissions to achieve a temperature anomaly of no more than 2 °C, ideally 1.5 °C (red). A net CO<sub>2</sub> emission approaches 10 Gt in 2050 and is zero in 2070.[6]

The CO<sub>2</sub> molecule, unlike other abundant gases in the atmosphere like O<sub>2</sub> or N<sub>2</sub>, absorbs energy in a variety of wavelengths (2000-12000 nm) within the infrared (IR) range. When irradiated by infrared sunlight, the CO<sub>2</sub> absorbs this energy and re-emits it towards every direction (which includes Earth) gradually over time, causing the greenhouse effect and therefore an increase in temperature in the Earth. Although greenhouse gases are necessary to maintain the living conditions on Earth (i.e., they maintain the temperature constant and within life conditions), an unbalance of these, as is the case of CO<sub>2</sub>, may

cause an uncontrolled rise in Earth's average temperature.[7] This consequence is called global warming. Global warming is posing a threat to the safety of society as it can result in many alterations to the environment, eventually impacting human health and quality of life. Those alterations include the rise of the sea levels, the acidification of the oceans, more drastic weather, and the regularity of natural catastrophes such as floods or droughts.

Reducing the amount of CO<sub>2</sub> present in the atmosphere is thus crucial to avoid these effects and, eventually, revert the situation (Figure 1.2). Decreasing the emissions and the production of CO<sub>2</sub> is the most straightforward strategy to reduce the atmospheric CO<sub>2</sub> concentration however, although several global commitments have been imposed during the last decade, the levels of atmospheric CO<sub>2</sub> are far from being reduced and are still increasing.[8,9] Therefore, capturing the CO<sub>2</sub> must be included in the strategy. Several technologies have been proposed to tackle the challenge of reducing atmospheric CO<sub>2</sub> levels, being Carbon Capture & Utilization (CCU) one of the most promising.[10]

### **1.1.2 Carbon Capture & Utilization**

CCU, which aims to valorise the CO<sub>2</sub>, is a technology where CO<sub>2</sub> is captured from a gaseous medium, like the atmosphere or flue gas, to be converted to valuable products such as chemical precursors (like formic acid, CO), plastics, and fuels (Figure 1.3).[11] When the capture of CO<sub>2</sub> (from fossil, biogenic sources or directly from the air) is considered, different types of emission reductions can be identified that contribute to the International Panel on Climate Change (IPCC) scenario: 1) Capture from fossil-derived CO<sub>2</sub> and utilization (i.e., CO<sub>2</sub> feedstock is used for fuel recycling); 2) Capture from fossil-derived CO<sub>2</sub> and utilization via mineralization or permanent CO<sub>2</sub> storage, where the intended CO<sub>2</sub> emissions are not released into the atmosphere and therefore avoided (i.e., permanent incorporation of CO<sub>2</sub> into building materials based on concrete); 3) Use of biogenic CO<sub>2</sub> (i.e., directly captured from the air) and utilization (where the CO<sub>2</sub> is

captured and used in the chemical/fuel industry and then released cyclically); and 4) Capture of biogenic CO<sub>2</sub> (as described in 3) combined with utilization via mineralization or permanent CO<sub>2</sub> storage (as described in 2). The third case offers an optimistic scenario where anthropogenic CO<sub>2</sub> is introduced into the chemical industry as a chemical building block, thus increasing the valorisation of CCU.

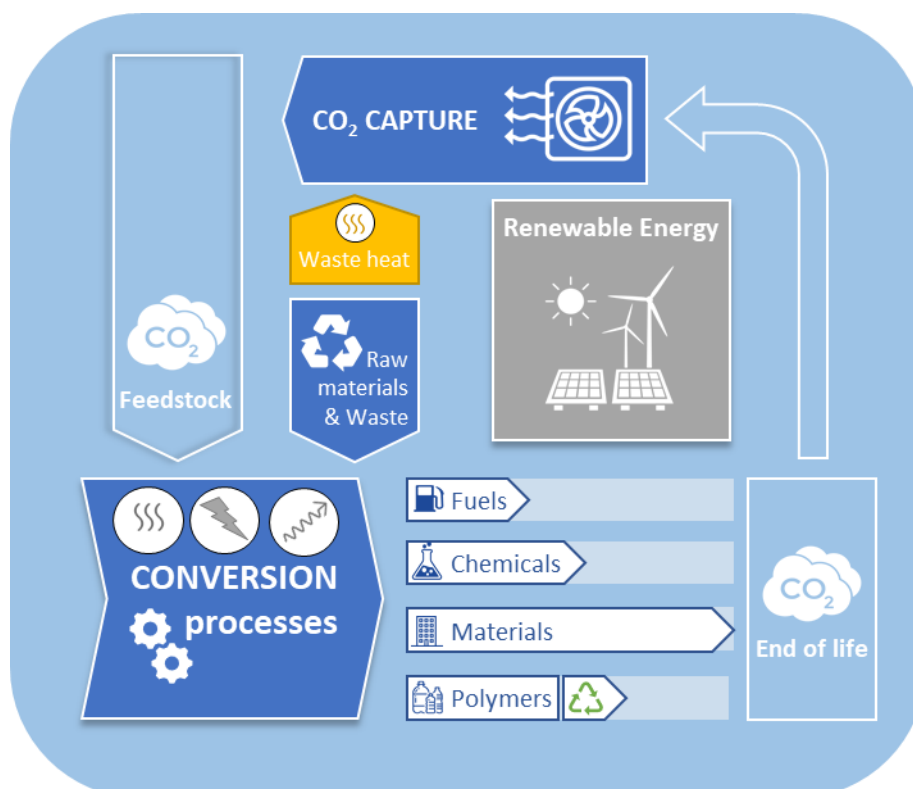


**Figure 1.3.** CO<sub>2</sub> net cycle proposed in the CCU technology

CCU consist of two separate steps: the capture and the conversion steps. While the overall efficiency of the process depends on their combination, they are studied often independently.[12,13] CO<sub>2</sub> is captured with adequate agents, such as amines or alkaline solutions, isolated while regenerating the capture medium, and compressed to be supplied to a conversion system.[14] This last occurs in a pure, gaseous form, as a derivate (such as carbonate and carbamate) or sequestered in a material.[15–17] The captured

form will also determine how easy is to convert it afterwards and the overall CCU efficiency (e.g., carbamates require >100 °C to release CO<sub>2</sub>).

For CO<sub>2</sub> conversion several technologies have been proposed, being the most significant summarized in Table 1.1. From these conversion strategies, the electrocatalytic conversion of CO<sub>2</sub> (eCO<sub>2</sub>R) is gaining increasing interest in the scientific community since it allows more flexible use of electricity (i.e., demand side management), presents a one-step conversion of CO<sub>2</sub> to C<sub>1</sub>, C<sub>2</sub> and even C<sub>2+</sub> products and potentially allows the production of a wide range of molecules (see Table 1.1).[18–20] Both CO<sub>2</sub> capture and conversion will be discussed in the next chapters (1.2 and 1.3) separately.

**Table 1.1.** Some technologies proposed to convert CO<sub>2</sub>. [21]

Technology	Energy input	Main product(s)	TRL	References
<b>Thermocatalysis</b>	Heat and pressure	Methanol, methane, urea	Methanol: 5-9 Methane: 8-9 Urea: 9	[22]
<b>Mineralisation</b>	Chemical (reaction with metal cations)	Carbonate salts	Concrete ingredients: 4-8 Concrete curing: 7-8	[23]
<b>Electrocatalytic</b>	Electricity	CO/syngas, formic acid, other C <sub>1</sub> and C <sub>2+</sub>	CO/syngas/formic acid: 4-8 C <sub>2+</sub> : 1-3	[24,25]
<b>Bioelectrocatalytic</b>	Electricity	Methane	4-7	[26]
<b>Photo(electro)catalysis</b>	Solar with or without electricity	Methanol, methane	1-3	[27,28]
<b>Plasmacatalytic</b>	Weak-ionised plasma	CO, methanol, ethylene, other C <sub>2+</sub> products	1-3	[29]

## 1.2 CO<sub>2</sub> Capture

CO<sub>2</sub> can be captured from the air, namely Direct Air Capture (DAC), or industrial waste stream, namely flue gas capture.[30,31] To separate CO<sub>2</sub> from the gaseous media, firstly a reactive absorbent solution (like amines or alkaline solutions) is used. Then, CO<sub>2</sub> is stripped from the absorbent and stored as a high pressurised, pure gas (>99.9%). However, depending on which source is the CO<sub>2</sub> captured (air or flue gas), the process varies since the concentration of CO<sub>2</sub> and composition of the source is different (i.e., %CO<sub>2</sub> in flue gas lies between 1-10% while it is 0.04% in air).

A typical DAC concept is shown in Figure 1.4. By using a ventilator system, the air is directed at a certain flow rate through the contactor module where it reacts with the capture solution, i.e., NaOH, which is separated from the air via a membrane contactor (see *Annex A.1.1*). The atmospheric CO<sub>2</sub> reacts with NaOH to form Na<sub>2</sub>CO<sub>3</sub>. To separate the Na<sub>2</sub>CO<sub>3</sub> from the aqueous solution, a causticization with Ca(OH)<sub>2</sub> is performed, converting the Na<sub>2</sub>CO<sub>3</sub> to CaCO<sub>3</sub>. Since CaCO<sub>3</sub> is insoluble in water (0.013 g L<sup>-1</sup>), it precipitates as a solid and can be separated from the rest of the solution. In this step, the NaOH is recycled, too. Finally, the CaCO<sub>3</sub> is calcinated to extract the CO<sub>2</sub> and, by Lime hydration, is regenerated back to Ca(OH)<sub>2</sub>. The CO<sub>2</sub> is compressed and stored.

On the other hand, a process to capture CO<sub>2</sub> from flue gas is shown in Figure 1.5. Since the concentration of CO<sub>2</sub> in flue gas is much higher than in air (1-10% vs 0.04%) the process is less energy intensive. As will be discussed in *Chapter 4*, this technology is already applied on industrial scale. The flue gas is collected from the industrial point source and enters an absorber module where the liquid absorbent, an aqueous amine solution, is sprayed in the scrubber. The amine in the small droplets reacts with the CO<sub>2</sub> to form carbamate. Afterwards, the carbamate solution is thermally treated in a stripper and the amine and CO<sub>2</sub> are isolated and stored in a pure form.

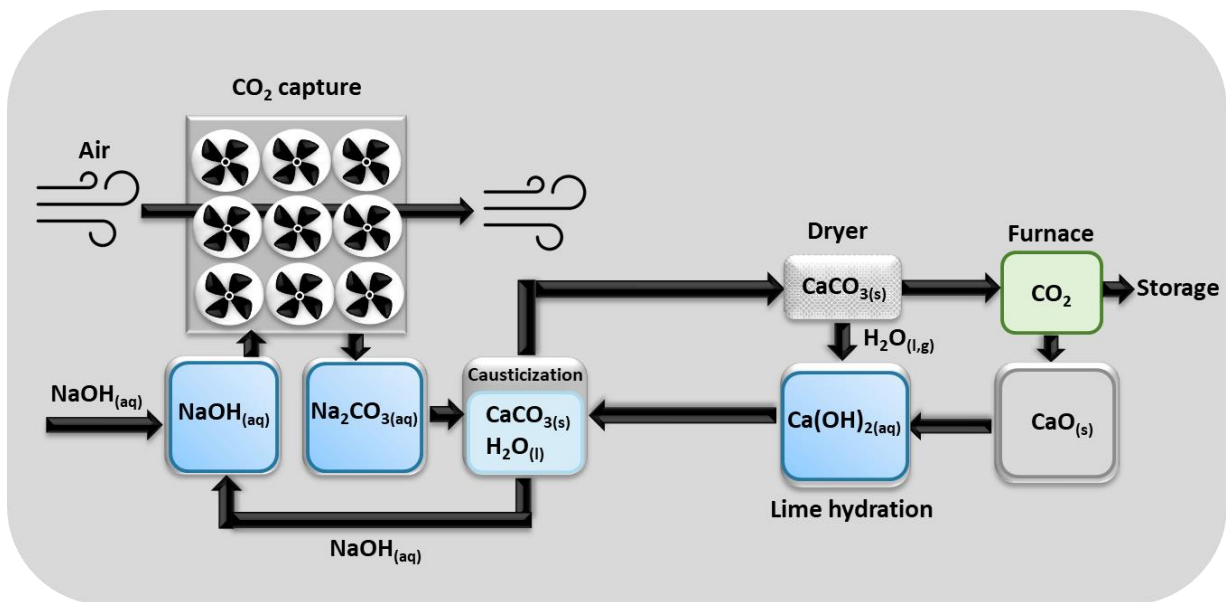


**Figure 1.4.** DAC Process using sodium hydroxide as the absorbent and including a solvent regeneration step. Re-drawn from [32]

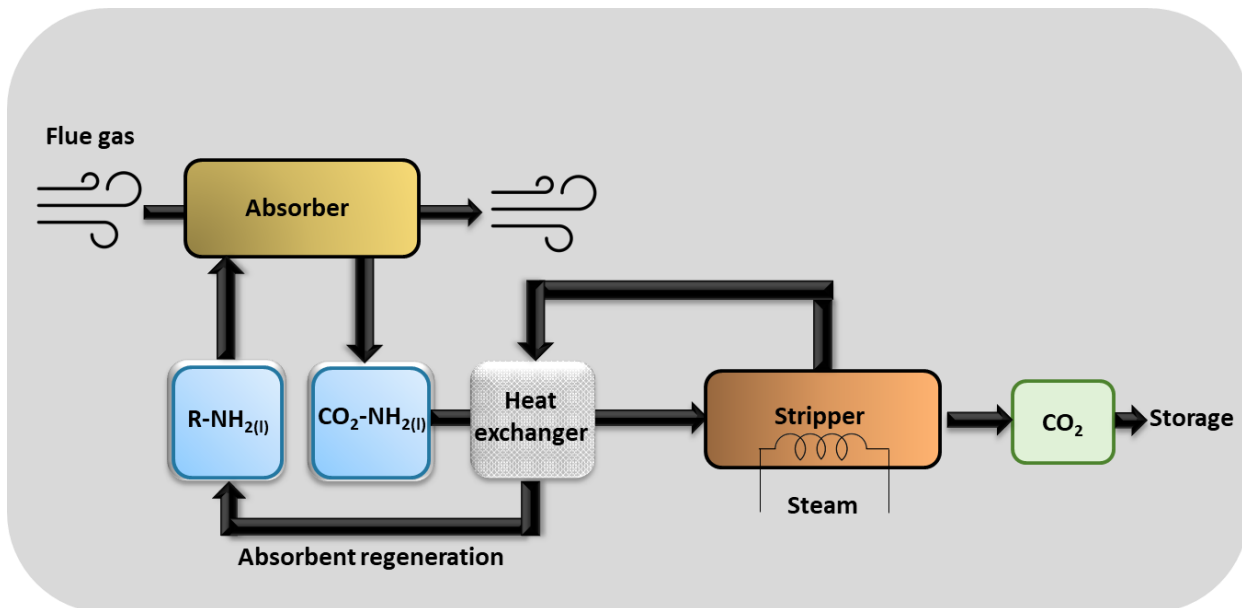


**Figure 1.5.** CO<sub>2</sub> capture from flue gas by using an amine solution as an absorber and regenerating the solvent in the stripper. Re-drawn from [33]



### 1.3 Electrochemical CO<sub>2</sub> conversion

Once CO<sub>2</sub> is captured, compressed, and stored with high purity, it is converted into valuable products, such as plastics, syngas or fuels, by applying energy. As mentioned earlier, electrocatalysis is a promising conversion method and is selected for elaboration in this thesis. The electrocatalytic, or in other words, the electrochemical CO<sub>2</sub> conversion is a reaction where the CO<sub>2</sub> is converted, by applying electricity as energy source, to a species with a lower oxidation state, and thus electrochemically reduced. For this reason, the electrochemical CO<sub>2</sub> conversion is more commonly named electrochemical CO<sub>2</sub> reduction (eCO<sub>2</sub>R).

A variety of eCO<sub>2</sub>R products exist and it is important to evaluate the economic viability of the corresponding process within a given value chain by a techno-economic analysis (TEA). Each product requires a different catalyst system, reaction pathway (Figure 1.6) and amount of CO<sub>2</sub> feedstock and energy to be produced, showing a different market value range. The system can be evaluated mainly by two means: high volume production and/or high value of the product. From the list of products shown in Table 1.2, formic acid (HCOOH) and CO are posed as two of the most promising products for the applicability of the CCU technology. Formic acid is a bulk chemical of high interest in energy storage (formic acid fuel cell) and as a precursor building block for the chemical industry.[34,35] On the other hand, CO is used for syngas production when mixed with H<sub>2</sub> and as a chemical building block, too.[36,37] Nevertheless, C<sub>2</sub> and C<sub>3</sub> products show the highest valorization potential, like ethanol, due to their direct application as fuels and their potential higher (premium) price.

As observed in Table 1.2, CO and formic acid, although the market price is lower than other products such as methanol and ethanol, have the highest market price per electron spent, thus being firm candidates for the development of CCU technologies. In this

context, some pilot plants for the electrochemical conversion of CO<sub>2</sub> to formic acid and CO are already running, which will be discussed in *Chapter 4*.

In this doctoral thesis, formic acid was selected as the target product for the eCO<sub>2</sub>R, as an ‘easy’, low-risk molecule, for R&D purposes. Since eCO<sub>2</sub>R systems are, usually, based on (mild)alkaline electrolytes, formate will be the species formed. To obtain formate from CO<sub>2</sub>, Sn-based electrocatalyst was used based on their outperforming properties (cheap in cost, abundant, non-toxic, widely studied and highly selective).[38] Eventually, for the upscaling studies, CO was targeted, too, using, a Ag-based catalyst.

**Table 1.2.** Market price and yearly global production of some eCO<sub>2</sub>R products (2018). Some electrocatalysts able to convert CO<sub>2</sub> to specific products. [39,40]

eCO <sub>2</sub> R Product	n <sup>o</sup> electrons	Market price (\$/kg)	Normalized price (\$/e <sup>-</sup> ) × 10 <sup>3</sup>	Yearly production (Mt)	Electrocatalyst	References
CO (syngas)	2	0.06	0.8	150	Ag, Au, Cu	[41–45]
CO	2	0.60	8.0	-		
HCOOH	2	0.70	16	0.60	Pb, Sn, Pd	[38,46,47]
CH <sub>3</sub> OH	6	0.60	3.1	110	Cu/CuO <sub>x</sub>	[48,49]
CH <sub>4</sub>	8	0.18	0.4	250	Cu/CuO <sub>x</sub>	[50,51]
CH <sub>3</sub> CH <sub>2</sub> OH	12	1.00	3.8	77	Cu/CuO <sub>x</sub>	[52,53]

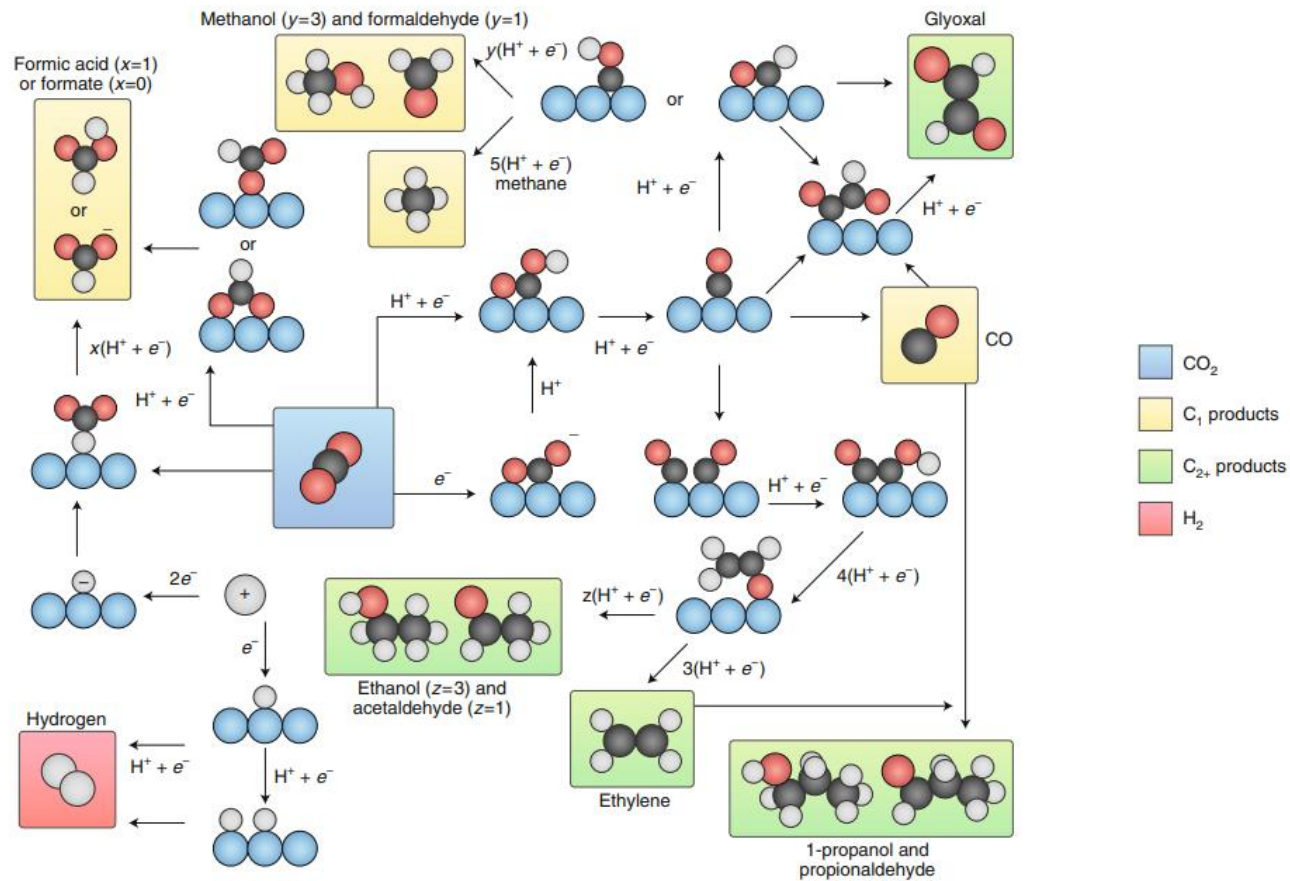


**Figure 1.6.** Overview of reaction pathways for eCO<sub>2</sub>R towards different products. Reproduced with the permission of [39]

## 1.4 Integrating the capture and the conversion of CO<sub>2</sub>

The capture and the electrochemical conversion steps have been well defined and studied separately. There exist already pilot plants for both DAC and eCO<sub>2</sub>R systems (see *Chapter 4* and *3*, respectively). Furthermore, some industries (i.e., petrochemical) have installed flue gas capture systems in their waste stream to decrease the carbon print their processes leave. Although these systems are at high Technology Readiness Level (TRL), technological feasibility is not yet reached when evaluating the overall CCU process as a combined system. The efforts to reach this feasibility lay on optimizing even further the capture or the conversion step, as separate steps. Nevertheless, high energy (see *Chapter 1.5*) is spent in the minor steps that connect the capture and the conversion step, often neglected in research. For instance, one-third of the costs in capturing CO<sub>2</sub> lay in regenerating and compressing the CO<sub>2</sub> after it has been captured, since most of the conversion technology in the state-of-the-art requires pure, high concentrated CO<sub>2</sub> to operate. Therefore, if these steps are avoided, the capital and operational costs of technology decrease, as will be discussed in the techno-economic assessment (TEA) of *Chapter 1.5*.

An integrated capture and electrochemical CO<sub>2</sub> conversion system is proposed (Figure 1.7), where CO<sub>2</sub> is captured from the air by DAC, however, this time, less concentrated KOH is used as capture solution instead of concentrated NaOH solution. This choice is two-folded: Firstly, since the CO<sub>2</sub> must be captured in form of an aqueous (bi)carbonate solution, the final concentration of the salt must lay below the solubility point (between 2 and 3 M, depending on the temperature and pressure). Secondly, K<sup>+</sup> is preferred over Na<sup>+</sup> in the conversion step since the conductivity is higher (less ohmic drop). This time, the causticization step is avoided since there is no interest in separating the CO<sub>2</sub> as a solid carbonate. The post-capture solution, composed of potassium bicarbonate (KHCO<sub>3</sub>, to simplify is mentioned just as bicarbonate in this thesis), is directly supplied to the electrochemical cell. There, potassium bicarbonate has both the role of electrolyte and

CO<sub>2</sub> source, delivering CO<sub>2</sub>, that comes from the equilibrium with water, to the surface of the electrode, where it is converted. The post-conversion solution leaves the electrolyser and enters a downstream process (DSP) where the carbon product is separated from the rest of the solution, KOH an bicarbonate, which is recirculated to the capture step to start the procedure again.[54,55]

In the next section, a TEA is performed, where the integrated strategy (CO<sub>2</sub> is captured and supplied as bicarbonate to the electrolyser) is compared to the conventional two-step route (CO<sub>2</sub> is compressed and regenerated before being supplied to the electrolyser). The aim is to deliver a context for the integrated concept, as well as identify the advantages and limitations of the strategy compared to the state-of-the-art two-step route.

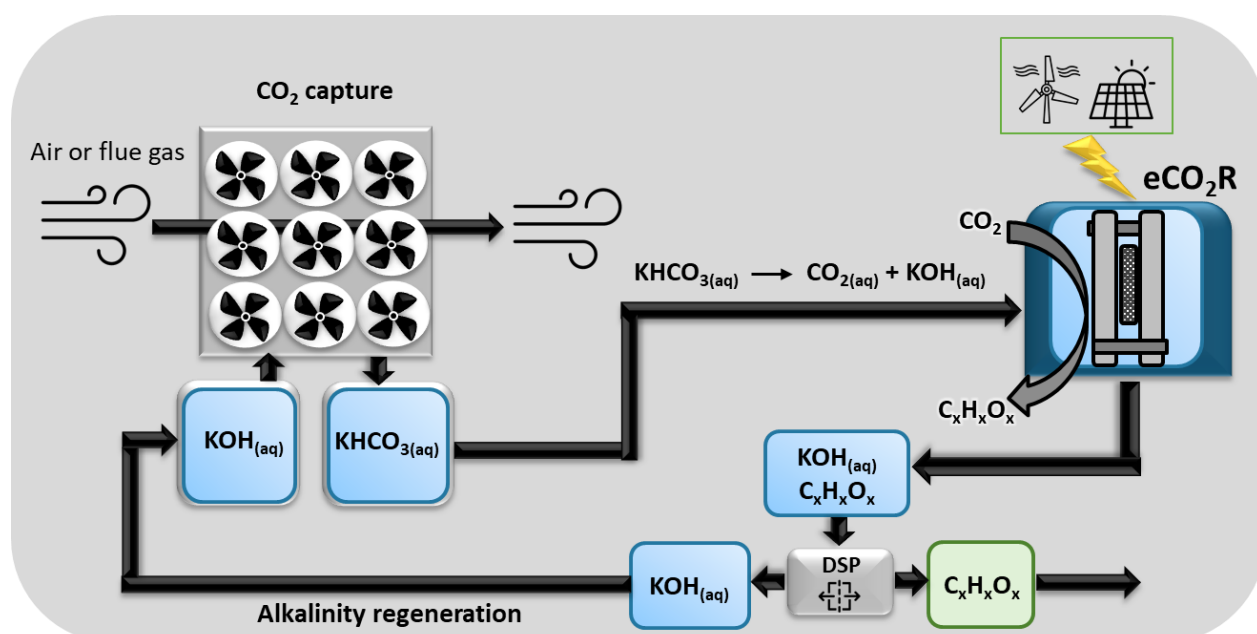


**Figure 1.7.** Schematic representation of an integrated CO<sub>2</sub> capture and electrochemical conversion system involving KOH as capture solution.

## 1.5 Techno-economic assessment: Integrated vs. Two-step route

This section aims to evaluate and validate the economic feasibility of integrated CO<sub>2</sub> capture and conversion. More concretely, CO<sub>2</sub> captured from air using an alkaline solvent (KOH in water) is considered, after which the resulting (bi)carbonate stream is sent to an electrochemical cell, where the CO<sub>2</sub> is released again and directly converted into a valuable product. This novel route is compared with the conventional approach, whereby CO<sub>2</sub> capture and electrochemical conversion are done in two distinct steps.

DAC is assumed to be a technology that delivers the CO<sub>2</sub> feedstock in the present work. More specifically, the technology developed by the Canadian company Carbon Engineering is considered.[32] The carbon engineering process has been described in detail by Keith *et al.* (2018). This article constitutes the basis for the mass and energy balances of the CO<sub>2</sub> capture step in the present work. Interestingly, the article provides energy consumption data for each of the main unit operations separately, too. This allows for studying the novel route, which only uses the air contactor step, and benchmarking it with the conventional approach. This technology consists of four main unit operations. First, the air is brought into contact with a capture solution containing KOH. During this process, CO<sub>2</sub> is absorbed in the form of potassium (bi)carbonate, while other gases flow through the contactor without reacting. The subsequent unit operations (pellet reactor, calcination and slaker) serve to release the CO<sub>2</sub> in a pure form and to recover the capture solution so that it can be re-used. Data about the electrochemical conversion of pure CO<sub>2</sub> and (bi)carbonate have been obtained from the work of Verma *et al.* (2017) and Li *et al.* (2019) respectively.[56,57] CO has been considered the target product since for this product there is substantial data for both routes available. This TEA is scalable to other products, however sensitive differences must be considered such as the selectivity of the reaction (<20 % for C<sub>2+</sub> products) or the valorisation of co-reactions (i.e., HER is valorised in the integrated route when CO is targeted since it will be further used for syngas production)

Table 1.3 summarizes the main mass and energy-related parameters for the two-step (conventional) and integrated route. The overall trade-off between the two options is clear: the integrated route allows to avoid most of the energy consumption in CO<sub>2</sub> capture and its efficient use in the electrochemical conversion step. However, the integrated route faces higher energy consumption in the electrochemical conversion step due to the less energy-efficient electrolysis (carbonate electrolysis presents lower FE than conventional eCO<sub>2</sub>R). In addition, Faradaic efficiency (FE) is lower.

**Table 1.3.** Comparison of the process performance of the two-step and integrated route. Cell potentials at which industrially relevant current densities (> 200 mA cm<sup>-2</sup>) have been achieved are chosen.

Parameter	Two-step route	Integrated route
<b>CO<sub>2</sub> capture</b>		
<b>CO<sub>2</sub> regeneration energy consumption (MWh tCO<sub>2</sub><sup>-1</sup>)</b>	1.46	0
<b>Auxiliary system energy consumption (MWh tCO<sub>2</sub><sup>-1</sup>)</b>	0.40	0.08
<b>Electrochemical conversion</b>		
<b>Cell potential (V)</b>	2.3	3.5
<b>Faradaic efficiency</b>	90%	30%
<b>CO<sub>2</sub> utilisation - single pass</b>	10%	100%
<b>CO<sub>2</sub> utilisation - incl. recycling of exit CO<sub>2</sub></b>	60%	100%
<b>Reference</b>	[56]	[57]

A single pass CO<sub>2</sub> utilisation is assumed in the study of Li *et al.* (2019) (integrated route) as 100% of the captured CO<sub>2</sub> is stored as carbonate in the carbon pool, and therefore not lost, eventually being reduced in the cyclic technology. A crucial feature of the proposed

integrated route is the ability to regenerate the capture solvent (KOH) during the electrochemical conversion step, so that afterwards it can be recycled to the CO<sub>2</sub> capture step, closing the loop. However, this can only be assumed if the capture efficiency stays at 100%, i.e., if KOH is 100% recovered and not lost in the process (for example, by salt precipitation). This is highly unlikely, and these energy losses were not considered in the approach of Li *et al.* Nevertheless, we decided to use this assumption for the TEA to simplify the model, although for future, more detailed models, an accurate value for the single pass CO<sub>2</sub> utilization must be used.

Concerning the importance of FE when producing CO, it needs to be kept in mind that in industrial applications CO is only an intermediate of methanation ( $\text{CO} + 3\text{H}_2 \rightarrow \text{CH}_4 + \text{H}_2\text{O}$ ), and is often used in conjunction with H<sub>2</sub> which is the main by-product of the electrochemical conversion step. Fischer-Tropsch (F-T) based conversion of syngas requires an H<sub>2</sub>/CO molar ratio of about 2, implying that a FE of 33% would already be sufficient if the remainder of the current is spent for H<sub>2</sub> production. For that reason, we consider the FE of the integrated pathway high enough and a scenario with FE = 33% for both cases. This ratio would allow the production of different synthetic fuel types, e.g., for aviation, through the F-T process.

As said, the assumptions for the CO<sub>2</sub> capture step are all based on the work of Keith *et al.* (2018). As for operational and maintenance costs (OPEX), the integrated route was assumed to have one-fourth of the cost of the two-step route, since only one out of four-unit operations remains in place (= the air contactor). This assumption is an approximation since every process presents different OPEX, therefore results might slightly differ (increasing or decreasing the costs) if the OPEX costs are accurately calculated for the integrated route. The electrolyser cost data are all based on information about conventional water electrolysers (see Mayyas *et al.* 2019).[58] A critical assumption here is that the CO<sub>2</sub> electrolyser would achieve stable operations over a prolonged period (multiple years), which is required to bring down the CAPEX to an acceptable level. It is



also assumed that, after electrolysis, unreacted CO<sub>2</sub> would be separated from CO and H<sub>2</sub> so that it can be recycled. A separation cost of 40 € t<sup>-1</sup> is maintained based on Ramdin *et al.* (2019).[59] Since for the integrated route full CO<sub>2</sub> utilization has been reported, this cost is not applicable there. Table 1.4 summarizes the economic assumptions made in the TEA.

**Table 1.4.** Economic assumptions as described by Keith *et al.* (2018).[32]

Parameter	Two-step route	Integrated route
	<i>CO<sub>2</sub> capture</i>	
Capture plant CAPEX (€ tCO <sub>2</sub> <sup>-1</sup> year <sup>-1</sup> )	796	250
Operational and maintenance costs (€ tCO <sub>2</sub> <sup>-1</sup> )	42	10.5
Capture plant lifetime (year)		20
	<i>Electrochemical conversion</i>	
Electrolyser CAPEX (€ kW <sup>-1</sup> )		1000
Stack lifetime (h)		40000*
Balance of plant lifetime (year)		20
Operational and maintenance cost (%CAPEX year <sup>-1</sup> )		1.75
Downstream processing (CO <sub>2</sub> separation from syngas) (€ tCO <sub>2</sub> <sup>-1</sup> )	40	n.a.
	<i>General</i>	
Electricity cost (€ MWh <sup>-1</sup> )		50
WACC (%)		7.5
Operating hours (h year <sup>-1</sup> )		8000

\*Recently, Sargent *et al.*, proposed a lifetime of 80000 h as desirable, based on values reached by industrial water electrolyzers.[60] Nevertheless, the data proposed by Keith *et al.* (2019), was used in the TEA since a more detailed model was delivered.

Based on the assumptions listed in Table 1.3 and Table 1.4, the syngas production cost was derived (assuming that both CO and H<sub>2</sub> would be valorised). This reflects the minimum syngas price that would need to be obtained to cover all expenses over the project lifetime and offer investors their required return on capital. Electricity is assumed to be the sole source of energy for all process steps. The original Carbon Engineering approach envisages natural gas as an energy source for the thermally driven process steps (whereby also these emissions are captured), however, we assume that this cannot be a long-term solution due to the fossil source energy input. As can be observed, the integrated route offers a major cost reduction at the level of the CO<sub>2</sub> capture step (Figure 1.8). While the conventional CO<sub>2</sub> capture approach leads to a cost of >200 € t<sup>-1</sup>, this would rather be <50 € t<sup>-1</sup> in the integrated route. A strong cost reduction is observed across all main categories: CAPEX, electricity cost and operational and maintenance cost. This result is intuitive since the integrated route allows for a major process simplification of the CO<sub>2</sub> capture step (only the air contactor is required).

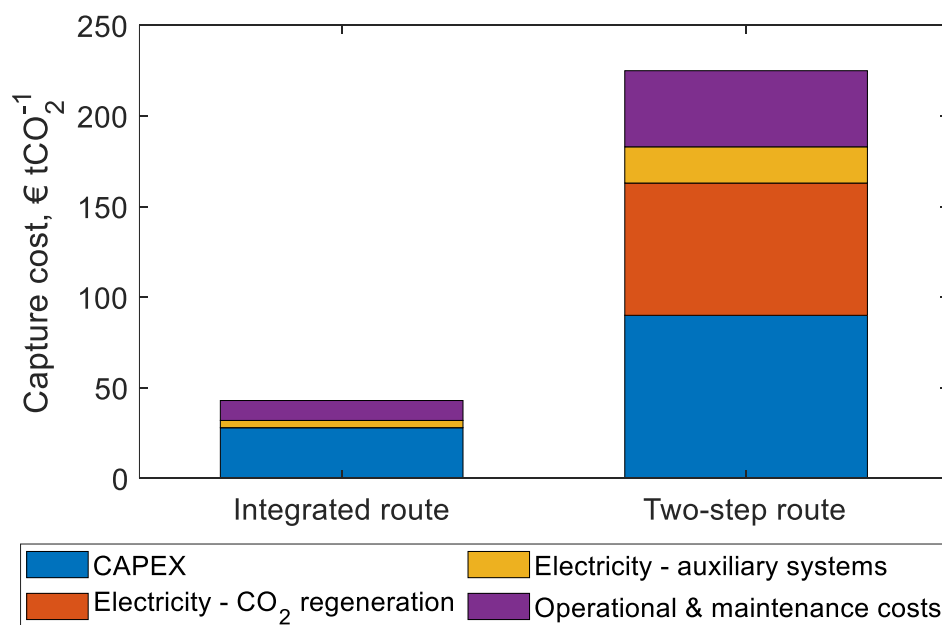


**Figure 1.8.** Comparison of the CO<sub>2</sub> capture cost of the integrated and two-step route

However, as indicated previously, the direct use of (bi)carbonate solutions instead of pure CO<sub>2</sub> has a downside in that the energy efficiency (EE) of the electrochemical conversion step is lower. To evaluate which of the two effects prevails, the total syngas production cost was calculated for both the integrated and two-step route (Figure 1.9). It is for (bi)carbonate found that, despite the high cell potential of the integrated route, this option is more economical than the two-step approach. The gains in terms of CO<sub>2</sub> capture costs seem to outweigh the extra electricity consumption. If the cell potential of the integrated route would be 4 V instead of 3.5 V as assumed here, the cost of both routes would be roughly equal.

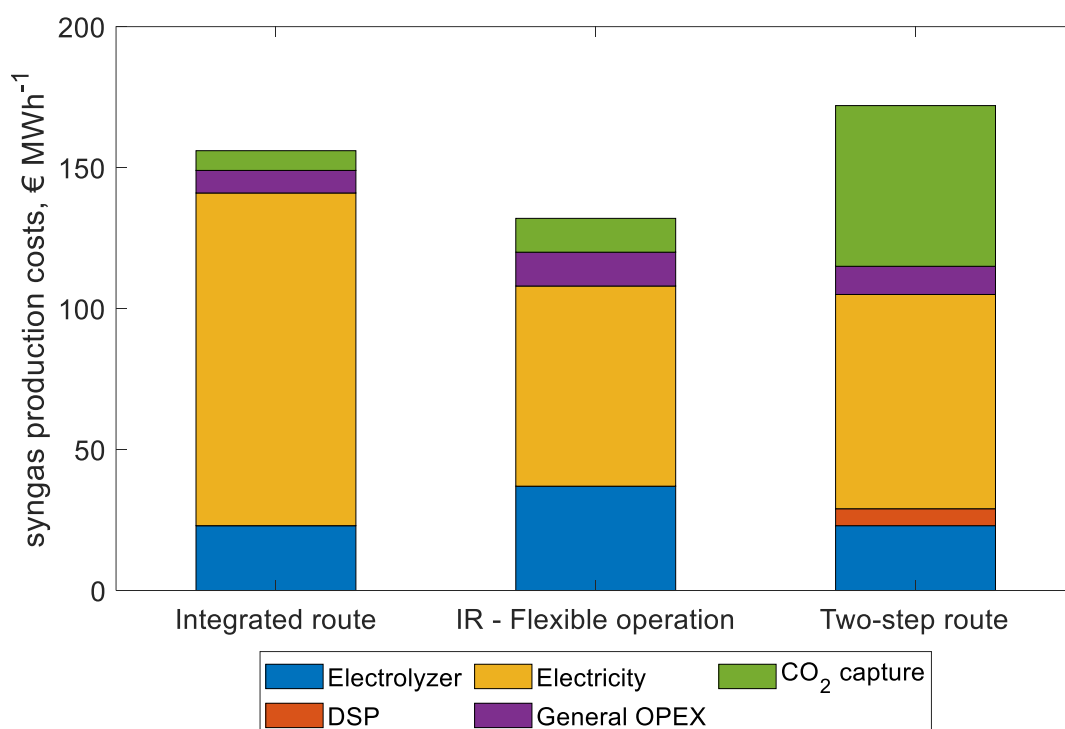


**Figure 1.9.** Comparison of syngas production cost of the two-step and integrated routes (IR)

The analysis has assumed baseload operation (8000 hours year<sup>-1</sup>) at 50 € MWh<sup>-1</sup>, which is the historical electricity price for large industrial consumers in the EU. However, since in the integrated route CO<sub>2</sub> can be easily stored in a liquid form, intermittent operation with

a direct connection and renewable power source can be envisaged. This comes at the expense of fewer operating hours, but avoids grid tariffs, taxes, etc. related to baseload operation. Using an example, we consider a scenario with 4000 operating hours and 30 € MWh<sup>-1</sup> (e.g., through a combination of solar PV and onshore wind). This provides an avenue for further cost reductions in the (bi)carbonate route (Figure 1.9 – flexible operation).

Whereas a significant cost reduction appears possible concerning the two-step approach, it needs to be noted that all production costs obtained here remain elevated (> 100 € MWh<sup>-1</sup>). For reference, the current (high) prices of oil (100 € barrel<sup>-1</sup>) correspond to about 60 € MWh<sup>-1</sup>. Ideally, further cost reductions would be achieved, for example in the form of lower cell potential through improved bipolar membranes as well as lower electrolyser cost. Additionally, the results presented in this TEA are highly sensitive to parameters such as the loss of electrolyte, the cell potential or the (unreacted) exit CO<sub>2</sub>. Therefore, a sensitivity analysis was performed.

As for future research, it is important to further validate the alkalinity regeneration principle, since losses in alkalinity of the capture agent would quickly erode the benefit compared to the two-step approach (Figure 1.10). A loss of about 5% of the molar amount of KOH required to capture 1 mol of CO<sub>2</sub> during each cycle is sufficient to make the two-step route more economical. Higher losses drastically increase the production cost.

Another critical parameter to consider is the cell potential of the integrated route. Since electricity cost represents more than half of the total cost of this route, any deviation in terms of cell potential has a very measurable impact. At around 3.75 V, the integrated and two-step route perform equal, while improvements can lead to a significant cost reduction, and vice versa (Figure 1.11).

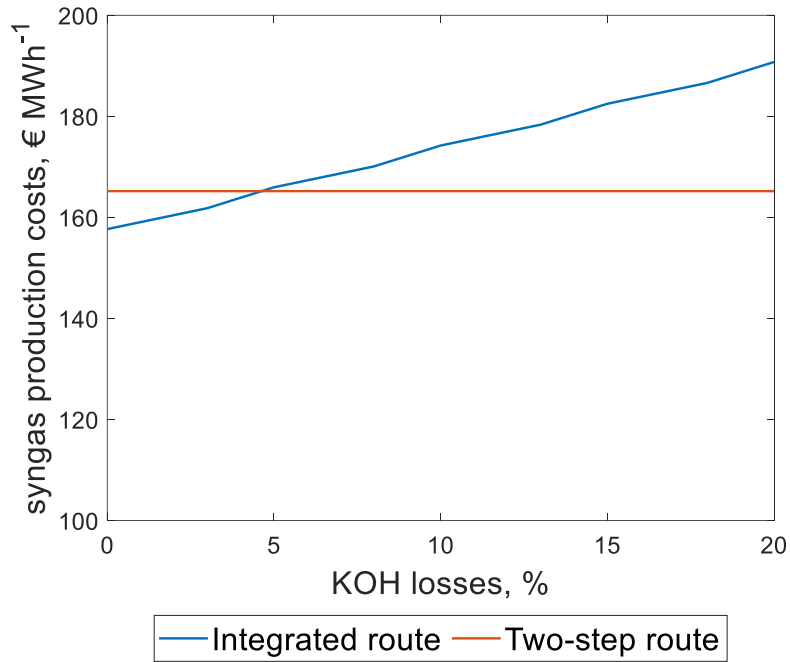


**Figure 1.10.** Impact of electrolyte losses in the integrated route on syngas production cost.

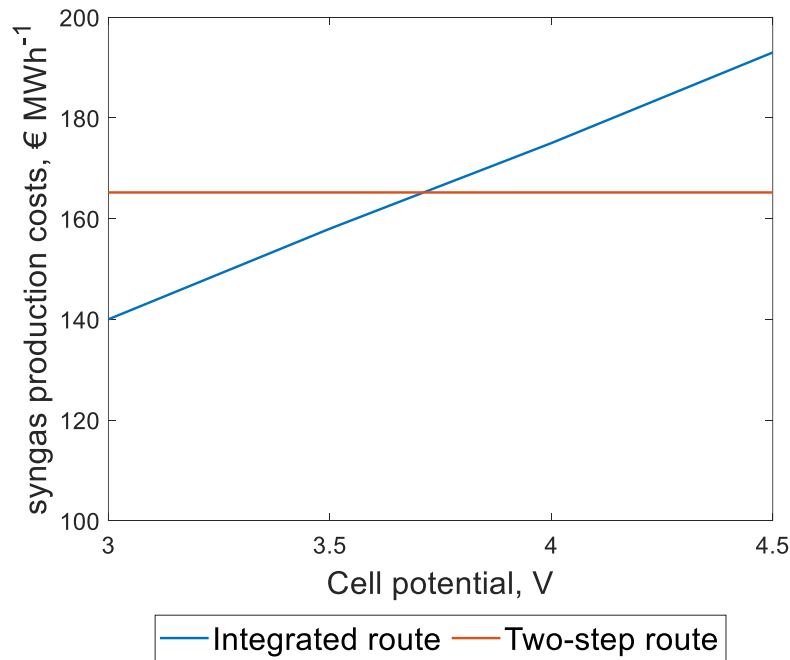


**Figure 1.11.** Impact of the cell potential of the integrated route on syngas production cost.

A third parameter considered is the amount of exit (unreacted) CO<sub>2</sub> found in the syngas after reaction. While Li *et al.* (2019) have not found any exit CO<sub>2</sub> in the syngas stream, other articles on bicarbonate electrolysis have done so. Therefore, the impact of varying the amount of exit CO<sub>2</sub> is shown in Figure 1.12, for two different CO<sub>2</sub> separation costs. While low levels of exit CO<sub>2</sub> (<10%) have little effect on the production cost, higher rates are found to have a measurable impact on the production cost.

It should be noted that here it is assumed that CO<sub>2</sub> separated from syngas can be recycled again to the electrochemical conversion step. Considering that there are commercial technologies available to separate CO<sub>2</sub> from CO/H<sub>2</sub> mixtures, such as pressure swing adsorption (PSA), this seems like a plausible assumption. However, Li *et al.* (2019) have noted that this recycling has not yet been demonstrated experimentally.

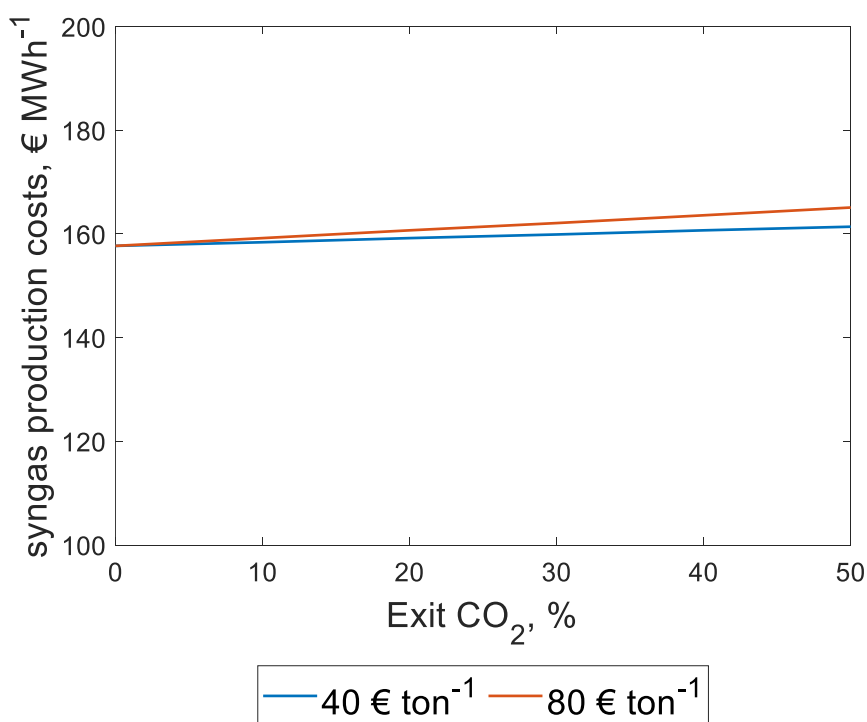


**Figure 1.12.** Impact of the amount of exist CO<sub>2</sub> and DSP cost on syngas production cost (integrated route only).

It is clearly shown how, in the integrated concept, the costs are decreased compared to the conventional two-step strategy. However, to reach this economic feasibility, first bicarbonate electrolysis must be properly understood, as the reports are almost non-existent and the mechanism is not clear. Additionally, a proper method to deliver DAC solutions (with enough bicarbonate) to the electrolyser is needed as, up to day, only synthetic bicarbonate solutions were used as a CO<sub>2</sub> source (for fundamental research). By the end of this thesis, we want to propose a commercialization strategy of the integration route by improving the metrics of bicarbonate electrolysis (i.e., FE>30%) and successfully delivering highly concentrated bicarbonate solutions (>0.5 M) to the electrolyzer. It is essential that the conversion parameters shown in Table 1.3 (FE 30% at 200 mA cm<sup>-2</sup>) are taken as reference for the realization of this thesis. Based on these premises, the scope and outline are developed, which are discussed in the following chapter.





# **CHAPTER 2**

## **Scope and outline**

THE OVERALL SCOPE, OUTLINE AND GOALS OF THIS DOCTORAL THESIS WILL BE EXPLAINED IN THIS CHAPTER, ENABLING THE READERS TO COMPREHEND THE STRUCTURE AND FLOW OF THE WORK.

## 2.1 Scope

From the TEA of section 1.5, it is concluded that integrating the CO<sub>2</sub> capture and the electrochemical reduction of CO<sub>2</sub> is a promising strategy to reduce the costs of such CCU technology. In this context, although for eCO<sub>2</sub>R these products have been widely reported, converting (bi)carbonate into useful chemicals (like formate or CO) selectively and efficiently (i.e., FE>30%) remains a major challenge. At the start of this work, bicarbonate reduction was almost non existing in literature, even at the most fundamental level. It was even discussed within the scientific community if the reaction was feasible at the usual operating conditions of eCO<sub>2</sub>R. From that point, the challenge was clear: how can we make (bi)carbonate electrolysis work? To unravel this, first, a more fundamental question had to be asked: What is the mechanism of the electrochemical (bi)carbonate reduction? Literature was not very concise on the reaction pathway, being debated within two schools of thought: the bicarbonate anion is directly reduced, or it provides CO<sub>2</sub> which is later reduced. Only after understanding the mechanism of (bi)carbonate reduction, the engineering aspects of the reactor could be properly studied. Different parameters, such as the temperature, flow of catholyte or catalyst configuration affect the reaction efficiency in different ways such as thermodynamically (e.g., electrochemical potential) or kinetically (e.g., mass transfer of reactants). Lastly, after obtaining the know-how and proving that (bi)carbonate can be electrolyzed at relevant current densities (10-400 mA cm<sup>-2</sup>), (bi)carbonate solutions, this time obtained by capturing CO<sub>2</sub> from the air, were electrolyzed

The goal of this doctoral thesis is to deliver a proof of concept and provide know-how on the integration of capture and electrochemical CO<sub>2</sub> conversion, therefore upscaling from TRL 1 (fundamental research) to TRL 4 (proof of concept). Only by proving that a bicarbonate electrolyzer can convert post CO<sub>2</sub> capture solutions, a proper commercialization strategy can be proposed towards TRL 8-9. This strategy should include the optimization of the capture system and the direct integration of the electrolyzer to

the capture process (TRL 4-6) finally leading to a pilot plant (TRL 7) (Figure 2.1). Our target is that with the results obtained in this thesis, the industrialization of an integrated CO<sub>2</sub> capture and conversion system is closer to reality.

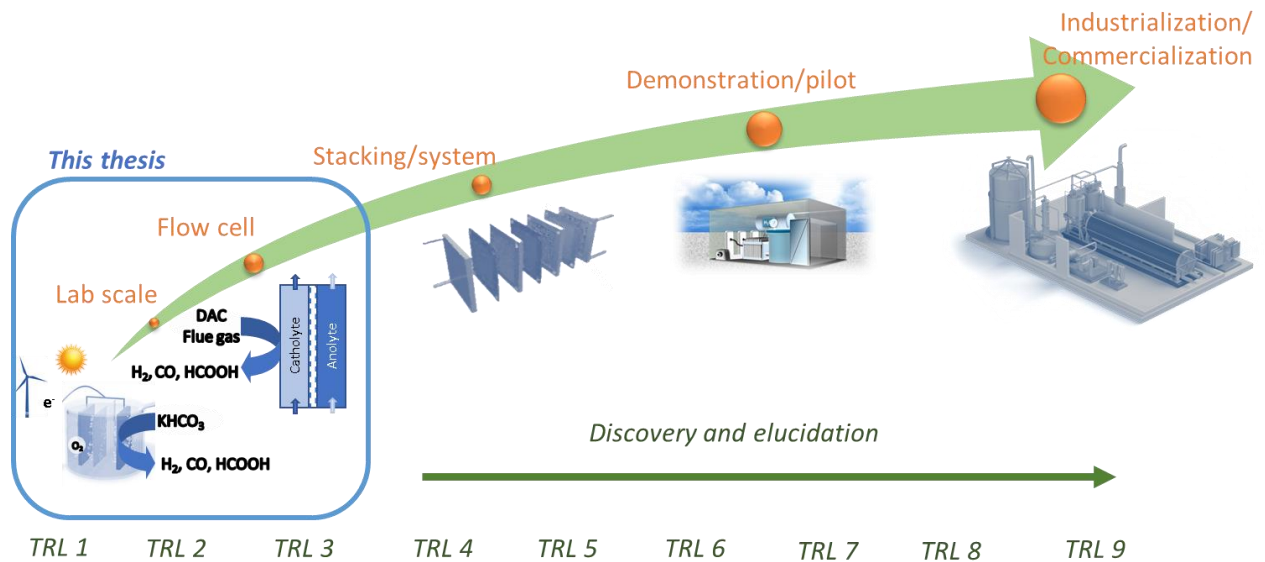


**Figure 2.1.** TRL scale of eCO<sub>2</sub>R technologies

## 2.2 Strategy

The strategy of the research performed in this thesis is based on three major pillars: literature review, fundamental research, and reactor engineering.

Firstly, a revision of the state-of-the-art of eCO<sub>2</sub>R technology is performed, both in the frame of upscaling towards industrialization and the integrating concept. This is crucial to understand the implementation status, as well as to identify the challenges and bottlenecks.

Secondly, a more fundamental approach is applied, i.e., the mechanism of bicarbonate electrochemical reduction is unravelled. An understanding of the role of bicarbonate as substrate in eCO<sub>2</sub>R is necessary to propose a pathway towards upscaling.

Finally, the last step was to design and fine-tune a bicarbonate electrolyser. To deliver an electrochemical system with high currents and thus high productivity, flow reactors with high electrocatalyst surface area are proposed. Different parameters affect the performance of flow reactors, such as the use of a given separator membrane, the reactor temperature, the electrocatalyst, the electrolyte flow rate, etc. The target is the identification of these parameters' impact on the energy efficiency of the bicarbonate electrolyser and the optimal conditions for its design and operation.

By covering these topics, the thesis' aim is to propose a system (or more than one) where CO<sub>2</sub> is captured and converted electrochemically in one and a single system, as a proof of concept to validate the technology and set a benchmark in the integrated capture and eCO<sub>2</sub>R strategy.

## 2.3 Outline

The outline of this doctoral thesis consists of ten chapters subdivided into five parts. A schematic overview is depicted in Figure 2.2.

*Chapters 1, 2* and the *Annex* provide an insight into the main topics of this doctoral thesis. Here the problem related to the increase in the levels of atmospheric CO<sub>2</sub> leading to Earth's global warming and the necessity of proposing an (cost-)efficient CCU technology is discussed. Next, an introduction to CO<sub>2</sub> capture and electrochemical conversion and the potential value of integrating both steps are provided, including a TEA analysis performed as an initial approach and validation of the strategy. Lastly, an overview of the theoretical background of the aspects discussed in this thesis.

*Chapters 3* and *4* are extensive literature reviews on eCO<sub>2</sub>R from the industrial point of view. The most recent advances in upscaling eCO<sub>2</sub>R technologies, including pilot plants and ongoing projects, are provided, as well as a deep discussion on the advantages and

drawbacks of the different components currently used in upscaled electrolyzers. Then the state-of-the-art on technologies to capture CO<sub>2</sub> from the air and industrial point sources are explained, as well as the current strategies to convert electrochemically post-capture CO<sub>2</sub> solutions.

*Chapters 5-7* are studies that focus on the mechanism of electrochemical bicarbonate conversion. Here the role of the bicarbonate anion and the effective reaction's substrate is identified. Based on these findings, a strategy to convert bicarbonate solutions more efficiently is proposed.

*Chapters 8 and 9* are upscaling studies of bicarbonate electrolysis. Firstly, a bicarbonate flow electrolyser is built with a bipolar membrane as a separator and in a zero-gap configuration. This configuration is chosen to promote acidification of the catholyte and thus liberation and supply of CO<sub>2</sub> to the electrode surface. Then, different engineering aspects that affect the energy efficiency of the system are studied to, finally, propose the conditions to obtain the most efficient bicarbonate electrolyser configuration. In parallel, a DAC system is built to capture CO<sub>2</sub> in the form of bicarbonate and, by using the zero-gap electrolyser, convert CO<sub>2</sub> from the air to formate and CO, serving as a proof of concept and as a validation of the feasibility of the technology.

Finally, the thesis is concluded with in *Chapter 10*. In this chapter the findings of the thesis and the future next steps are discussed.

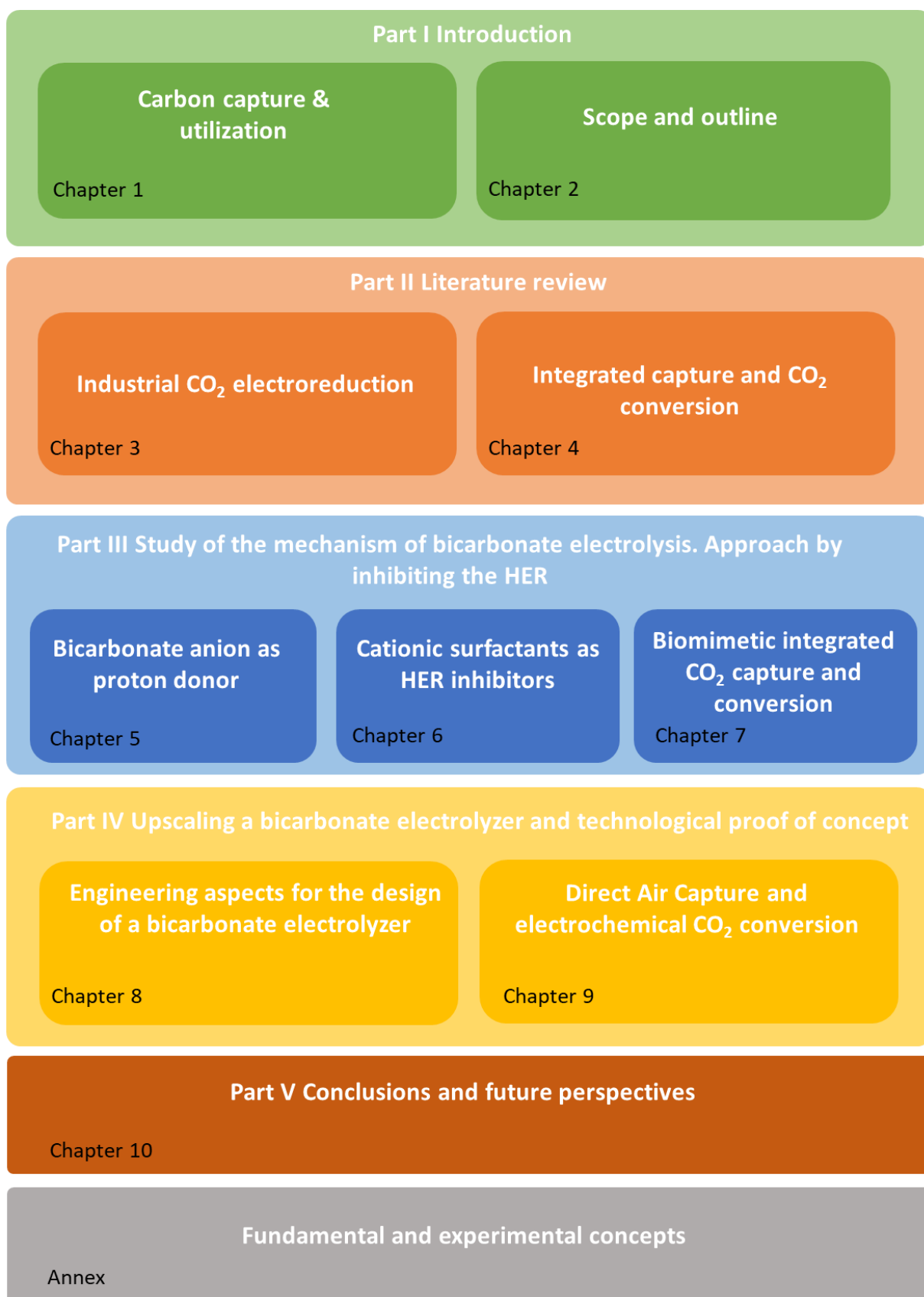


**Figure 2.2.** Schematic outline of this doctoral thesis

# **Part II**

**Literature review on the state-of-the-art of  
upscaling CO<sub>2</sub> capture and electrochemical  
conversion systems**





# CHAPTER 3

## Recent advances in industrial CO<sub>2</sub> electroreduction

UPSCALING TOWARDS APPLICABILITY IS ALWAYS THE MAIN TARGET OF AN EMERGING TECHNOLOGY. THE INDUSTRIALIZATION OF THE ELECTROCHEMICAL CO<sub>2</sub> REDUCTION IS STILL ON EARLY STAGE; HOWEVER, SEVERAL ADVANCES HAVE BEEN DONE ON THE LAST FEW YEARS. IN THIS CHAPTER, WE REVIEW THE CURRENT STATE OF THE CO<sub>2</sub> ELECTROREDUCTION TECHNOLOGIES CLOSEST TO INDUSTRIAL SCALE.

This chapter is a shared contribution of both O. Gutierrez-Sanchez and Dr. Y. Y. Birdja and is published as: O. Gutierrez-Sanchez, Y.Y. Birdja, M. Bulut, J. Vaes, T. Breugelmans and D. Pant, Recent advances in industrial CO<sub>2</sub> electroreduction, *Current Opinion in Green and Sustainable Chemistry*, 2019, 16, 47-56

### 3.1 Introduction

It is well-known that the selectivity, activity and stability are key parameters which impede the implementation of CO<sub>2</sub>R in industry.[61] Each of these parameters has been investigated and are being improved by focusing on the nature of the electrocatalyst, the morphology of the electrocatalyst, the electrolyte composition and process conditions.[39,62] From an industrial point of view, a TEA plays an important role as well, which indicate favorable output products, specific industrial routes or specific requirements of the reactor.[63–68] Based on these recent TEA studies, the electrosynthesis of the 2-electron transfer products, formic acid and carbon monoxide, as preferred products that could be competitive with current (non-electrochemical) production methods, whereas higher-order products are usually not economically viable. Although electrification of the chemical industry may be challenging to compete economically with the non-electrochemical routes or fossil fuel-based industry, we believe that the development of large-scale electrochemical technologies (e.g., for eCO<sub>2</sub>R) powered by zero-emission electricity is necessary in view of the enormous environmental impact and unavoidable CO<sub>2</sub> emission costs in the future. The economic viability of eCO<sub>2</sub>R processes depends not only on its technology-readiness but also on future decision-making, incentives for green production routes and carbon tax policies.

In this chapter, we cover advances towards industrial applications of eCO<sub>2</sub>R technologies. Very recent literature and examples of (pre-)commercial CO<sub>2</sub>R industries are reviewed and discussed from an integrated and future industrial perspective to point out important breakthroughs and hurdles. Compared to most available review articles in the field of CO<sub>2</sub>R, looking from an industrial perspective to the CO<sub>2</sub>R highlights different aspects and explores different routes for research and development of this technology. We mainly focus on direct eCO<sub>2</sub>R reduction technologies where special attention is given to reactor design, electrode structure, membranes and anode reaction, while we avoid in-depth

discussion of catalyst related or mechanistic aspects and TEAs. Pre- and post-conversion technologies such as CO<sub>2</sub> capture, product separation and purification are not covered in this chapter. Unless mentioned explicitly, we discuss eCO<sub>2</sub>R in aqueous electrolytes, which is more favorable in terms of large-scale application compared to non-aqueous electrolytes.

### 3.2 Status quo of industrial CO<sub>2</sub>R technologies

Commercially available eCO<sub>2</sub>R technologies are almost non-existing. The main challenge for the industrial electro-conversion of CO<sub>2</sub> to chemicals lies in upscaling, which is related to optimization of the process to make it profitable and competitive. The few existing large-scale eCO<sub>2</sub>R demonstrators are mainly in the pre-commercial stage. In 2011, Det Norske Veritas (DNV) assembled a demonstration reactor (ECFORM) for the electrochemical reduction of 1 kg CO<sub>2</sub> day<sup>-1</sup> to formate/formic acid.[69] The device consisted of 600 cm<sup>2</sup> of electrodes with electrodeposited Sn as electrocatalyst and was powered by photovoltaics. Around the same time, Mantra Energy (currently not in existence) developed a pilot plant with 100 kg CO<sub>2</sub> day<sup>-1</sup> capacity by a similar process with the reactor based on prototypes and patents by Oloman and Li.[70] Nowadays, other companies are developing technologies for eCO<sub>2</sub>R aimed at upscaling to a pilot plant. Carbon Recycling International and Mitsui Chemical Inc. are mature industries converting captured CO<sub>2</sub> to methanol. [71,72] However, these processes do not electrochemically reduce CO<sub>2</sub>, but utilize electrochemically produced H<sub>2</sub> for CO<sub>2</sub> hydrogenation on a ZnO-Cu/Alumina catalyst. A similar technology is followed by Air Company, where the CO<sub>2</sub> is captured from fermentation plants and then reacts with electrochemically produced H<sub>2</sub> to produce ethanol and methanol.[73] Dioxide Materials developed a commercial lab-scale electrolyser (an integrated lab-scale process) that converts CO<sub>2</sub> to formic acid in the cathodic compartment using a nanostructured Sn catalyst on a gas diffusion electrode (GDE), and H<sub>2</sub>O to O<sub>2</sub> in the anodic compartment containing an IrO<sub>2</sub> catalyst.[74] Siemens

and Evonik have launched the Rheticus project in 2018 (currently finished), which aims at technology development for electrochemical reduction of CO<sub>2</sub> and H<sub>2</sub>O to syngas, followed by fermentation and upscaling to pilot level.[75] Carbon Electrocatalytic Recycling Toronto is another company working on upscaling their technology, which has reached a micro-pilot scale for the production of CO for syngas applications.[76,77] More recently (2021), Twelve (Opus 12) did notable advances in upscaling CO<sub>2</sub> electrolyzers for the production of fuels and building block chemicals, aiming to increase the production from CO<sub>2</sub> from 5 kg day<sup>-1</sup> to 150-1000+ tons day<sup>-1</sup>. [78] Because of the importance of this topic, many projects have been initiated recently, involving institutes, universities and companies from different countries aiming at developing an efficient and optimized process for CO<sub>2</sub> capture and (bio)electro-conversion. Some of the relevant projects in Europe, recently finished or still on-going, are shown in Table 3.1.

The main approach of the industries discussed before and most of the projects shown in Table 3.1 is to scale-up an efficient reactor or process, working under environmental relevant conditions, to realize a meaningful productivity. This step is the key factor to upgrade the electrocatalytic manufacturing into one of the top technologies in chemical and process CCU industries. On the other hand, these technologies are contributing directly to the objective of environmental decarbonization (through atmospheric CO<sub>2</sub> consumption) while at the same time the rate of carbon resources used in chemical industries is getting reduced, making them sustainable and high valued nowadays and in close/midterm future.

In the following paragraphs, we zoom in on individual components which play an important role in the upscaling and commercialization of the eCO<sub>2</sub>R technology.

**Table 3.1.** Some representative electrochemical CO<sub>2</sub> reduction projects (updated on June 2022).

<b>Project name</b>	<i>Project lead (Country)</i>	<i>Target product</i>	<i>Description of the technology &amp; Achievements/Objectives</i>	<i>Project website</i>
<b>eCO2Fuel</b>	<b>DLR (Germany)</b>	Liquid e-fuels	Aims to design, manufacture, operate and validate the worldwide first low-temperature 1MW direct, electrochemical CO <sub>2</sub> conversion system to produce economic and sustainable liquid e-fuel.	eco2fuel-project.eu
<b>Take-Off</b>	<b>TNO (Netherlands)</b>	Light olefins	Aims to deliver a highly innovative process that produces Sustainable Aviation Fuels at low costs and high energy efficiency by capturing CO <sub>2</sub> from flue gas or DAC which reacts with electrochemically obtained H <sub>2</sub>	takeoff-project.eu
<b>VALCO2 II</b>	<b>Solvay (Belgium)</b>	Formic acid and methanol	Aims to develop large-scale CO <sub>2</sub> conversion processes for various chemical and energy markets and to set up an observatory to identify available sources of industrial CO <sub>2</sub> in France.	axelera.org
<b>BioRECO2VER</b>	<b>VITO (Belgium)</b>	Lactate and Isobutene	Aims to develop a process including enzymatic CO <sub>2</sub> capture and bio-electrochemical systems, in-situ generated H <sub>2</sub> and renewable CO <sub>2</sub> conversion. Along with a fermentation design, it validates the most promising isobutene and lactate production route.	bioreco2ver.eu

## Integrated capture and electrochemical conversion of CO<sub>2</sub>

<b>Kopernikus Power-to-X</b>	<b>Forschungszentrum Jülich</b> (Germany)	Liquid fuels, H <sub>2</sub> , syngas and CO <sub>2</sub> -based polymers	Electrochemical obtention of H <sub>2</sub> and CO. These resources are stored, distributed and converted into the end-product. The project consists of six research clusters, three related to electrolysis and three to the conversion of syngas into fuels and chemicals via heterogeneous catalytic synthesis.	kopernikus-projekte.de
<b>Select CO<sub>2</sub></b>	<b>DTU</b> (Denmark)	CO, ethanol and ethylene	Development of highly selective and efficient devices for the very high selective eCO <sub>2</sub> R to high value products at low temperature and pressure.	selectco2.eu
<b>Condor</b>	<b>University of Bologna</b> (Italy)	Methanol/DME	Laboratory-scale prototype that couples photoelectrochemical production of H <sub>2</sub> and CO, and photocatalytic conversion of syngas to DME with an efficiency of 4.5% (O <sub>2</sub> or Cl <sub>2</sub> evolution) or 6% (biomass oxidation).	condor-h2020.eu
<b>eForFuel</b>	<b>Max Plank Institute of Molecular Plant Biology</b> (Germany)	Propane and isobutene	Aims to develop an integrated electro-bioreactor to produce hydrocarbons. Includes the electrocatalytic conversion of CO <sub>2</sub> to formic acid and the bacterial conversion of formate towards hydrocarbons.	eforfuel.eu
<b>OCEAN</b>	<b>European Research Ins. of Catalysis</b> (Belgium)	Formic acid and oxalic acid. Other C <sub>2</sub> compounds and polymers.	Process to produce oxalic acid from formate, obtained electrochemically from CO <sub>2</sub> . One step from commercialization, converting 250 gCO <sub>2</sub> h <sup>-1</sup> at 1.5 kA m <sup>-2</sup> . Energy efficiency will be improved by coupling the oxidation of glucose at the anode.	spire2030.eu/ocean

<b>Recode</b>	<b>Fondazione IIT</b> <i>(Italy)</i>	Formic acid, oxalic acid and glycine	CO <sub>2</sub> from the flue gases produced by the cement industry is re-used within plant to produce related products in a circular-economy technology. CO <sub>2</sub> emissions reduction (20%) and production of high value products achieved upon upscaling.	<a href="https://www.recodetech2020.eu">recodetech2020.eu</a>
<b>CLUE</b>	<b>VITO</b> <i>(Belgium)</i>	Ethylene	Development of an efficient electrolyzer for durable eCO <sub>2</sub> R to ethylene using realistic and industrially relevant CO <sub>2</sub> streams and highly stable and efficiency electrodes based on mono- and bimetallic deposited clusters.	<a href="https://www.clue-project.be">clue-project.be</a>
<b>CAPTIN-2</b>	<b>Catalisti</b> <i>(Belgium)</i>	Syngas, methanol	Intensification of the CO <sub>2</sub> capture by a multi-angled approach, focusing on adsorption and absorption. Integration of the capture and conversion steps by using alkali-mediated capture combined with eCO <sub>2</sub> R.	<a href="https://www.moonshotflanders.be/mot3-captin">moonshotflanders.be/mot3-captin</a>

### 3.3 Reactor configuration

Fundamental research on eCO<sub>2</sub>R has mainly been carried out in batch-type, two-compartment electrochemical cells (H-cells), whereas for industrial application these cells are not convenient due to mass transport limitations, high IR losses and low current densities. Continuous-flow reactors have potential for the electrochemical CO<sub>2</sub> reduction on industrial scale.[79–81] The reactors in use for low temperature eCO<sub>2</sub>R can be categorized in membrane reactors or microfluidic reactors. At high temperatures (500–1000 °C), a solid-oxide electrolyser can be employed. The typical configurations of the various reactors are depicted in Figure 3.1.

Membrane reactors are the most-utilized electrochemical cells in eCO<sub>2</sub>R and show great potential for industrialization. Recently, Merino-Garcia *et al.* reviewed membrane reactors for CO<sub>2</sub> utilization.[82] This reactor consists of an ion-exchange membrane which separates the anode and cathode, leading to improved product separation, and avoiding re-oxidation of reaction products. The catalyst is usually incorporated in a gas diffusion layer (GDL) to enhance mass transport and increase the electrochemical active surface area. Another possibility is to coat the catalyst directly on the membrane (catalyst coated membrane). These two reactor components, (gas diffusion) electrode and membrane, will be discussed in *Chapter 3.4* and *3.6* respectively. A subdivision into gas-gas, gas-liquid or liquid-liquid membrane reactors can be made based on the electrolyte state (Figure 3.1, B-D).[115] Introducing CO<sub>2</sub> as (humidified) gas is attractive, since it allows to circumvent the solubility issues, to avoid the HER by controlling the water content and to suppress CO<sub>2</sub> transport limitations. Masel *et al.*, introduced a novel 3-compartment reactor for eCO<sub>2</sub>R to formic acid, and reported improved eCO<sub>2</sub>R performance (stability of 500 hours, cell voltage of 3.5 V, current density of 140 mA cm<sup>-2</sup> and FE up to 94%).[79] In this configuration, a centre compartment separated by a cation- and anion exchange membrane at respectively the anode and cathode side, has the ability to utilize protons produced at the anode to acidify formate ions produced at the cathode to obtain the



more valuable formic acid. Such a configuration can circumvent expensive separation/purification downstream processes.

In terms of upscaling, inspiration can be sought from the state-of-the-art large-scale membrane reactors such as chlor-alkali and hydrogen electrolyzers. A possible configuration for a future CO<sub>2</sub> electro-refinery which aims to create an industrial (bio)electrochemical production platform to convert waste CO<sub>2</sub> to building block chemicals as well as higher organic compounds was proposed recently. To reach this level, VITO targets to improve the overall energy efficiency by developing high selective CO<sub>2</sub> capture and conversion processes, more efficient purification technologies, and robust catalyst systems.

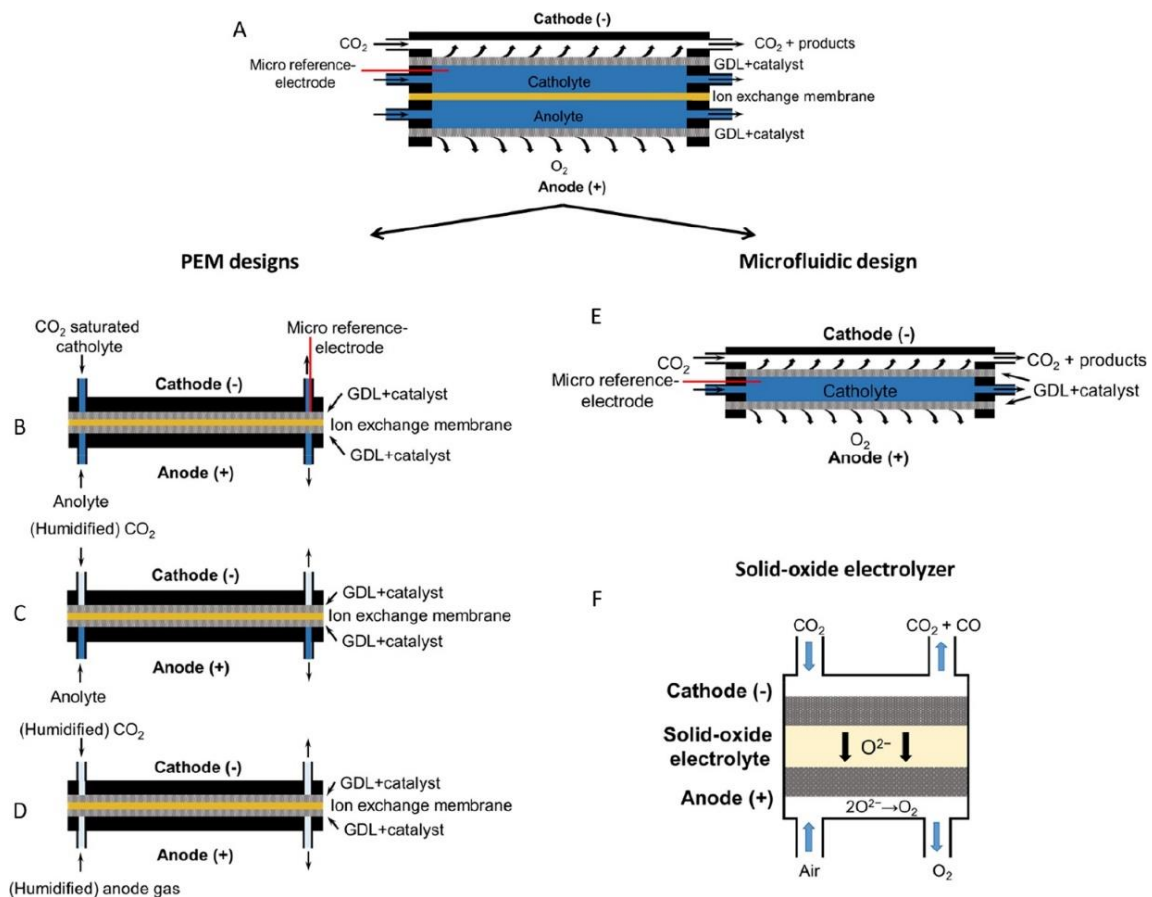


**Figure 3.1.** Various configurations for electrochemical flow reactors. (A) general design; (B-D) membrane reactors depending on the state of catholyte and anolyte; (E) classical microfluidic reactor; (F) Solid-oxide electrolyser. This figure is reproduced with permission from reference.[81].

Microfluidic reactors for eCO<sub>2</sub>R were introduced by the Kenis group.[83] In this configuration a membrane is not needed to separate anode and cathode, and the separation is established by the flowing electrolyte within a <1 mm channel. Better control of flooding and dry-out phenomena at the electrodes (electrode wetting) and mixed-media operation are reported to be the advantages of this configuration.[84] However, pressurization and scale-up is generally more difficult compared to a membrane reactor. eCO<sub>2</sub>R studies in microfluidic reactors have been limited to the screening of different electrocatalysts and operating conditions.

CO<sub>2</sub> reduction in a solid oxide electrolyser (SOE) has been studied since the previous decade.[85] Recently more attention has been given to this type of reactor for eCO<sub>2</sub>R due to its operation under high temperature, longer operation times, and co-electrolysis of CO<sub>2</sub> and H<sub>2</sub>O for the production of syngas.[86,87] However, since a TEA has not been reported for CO<sub>2</sub> reduction in a SOE, it is difficult to assess the economic viability of industrial eCO<sub>2</sub>R in a SOE. Additionally, the flexibility of the process in terms of components using a SOE is relatively poor since the electrode has to be very specialized (usually Ni-YSZ, Lanthanum Strontium Manganite-YSZ, LSM-YSZ, electrodes), leading to a specific product distribution besides the intrinsic weaknesses of high temperature operation (thermal stress, diffusion, non-equilibrated anion conducting membrane). We therefore believe that the membrane and microfluidic reactors have a higher potential to be utilized in large scale eCO<sub>2</sub>R processes compared to a SOE. The main advantages and disadvantages of the various reactor designs are shown in Table 3.2.

### **3.4 Electrode structure**

In this section, we focus on the configuration and composition of the cathode and highlight recent advances leading to the improvement of eCO<sub>2</sub>R performance. Aiming at a CO<sub>2</sub> electrolyser operating at industrial scale, gas diffusion electrodes (GDEs) have been suggested, because of lower mass transfer resistance and larger availability of active sites per unit area compared to planar-electrode systems.[88] GDEs have been employed for

a variety of catalysts, ranging from metals, metal-free catalysts, molecular catalysts, enzymes and microbes.[88–90] As shown in Figure 3.2, a GDE is generally composed of a catalyst layer (CL), a GDL and current collector. The GDL is a porous medium that facilitates transport of reactants and products to and from the CL and consists of a macroporous layer either with or without a microporous layer (MPL). A wide variety of GDL parameters have been investigated to enhance electrolyser or fuel cell performance.[89] However, optimization of GDEs for eCO<sub>2</sub>R has been given little attention.

Weng *et al.* developed a GDE consisting of Ag for eCO<sub>2</sub>R to CO, which provides a quantitative basis for the effects of different parameters.[91] They showed that the performance depends on the local environment of the CL and interaction between kinetics and transport. The influence of wettability, catalyst loading, flowrate and porosity was discussed, and it was concluded that flooding of the CL leads to an inhomogeneous CO<sub>2</sub> distribution and poor catalyst utilization. Such a model provides guidelines on how to design a GDEs for improved performance. Han *et al.* demonstrated the important role of the flow on the eCO<sub>2</sub>R performance.[92] They reported enhanced activity and selectivity of CO<sub>2</sub> reduction to C<sub>2</sub>H<sub>4</sub> on a Cu GDE in a flow-through configuration compared to a flow-by configuration. The differences are explained by a low diffusion constant and solubility in the latter configuration and are expected to play a role in eCO<sub>2</sub>R as well. There are several technologies for the preparation of GDEs. Wet deposition is time-consuming, while a dry pressing method is relatively simple and easily up-scalable.[93] The deposition methodology of the CL has been reported to ultimately affect the reaction performance. Jhong *et al.* showed that a fully automated air-brushing method of CL deposition leads to significant higher partial current density for CO on silver GDEs compared to hand-painting and screen-printing techniques.[94]

**Table 3.2.** Main advantages and drawbacks of eCO<sub>2</sub>R reactor configurations.

Reactor configuration		Advantages	Drawbacks
Batch reactors	<b>1-compartment</b>	<ul style="list-style-type: none"> <li>• Simple design</li> <li>• Convenient for small scale experiments</li> </ul>	<ul style="list-style-type: none"> <li>• Poor mass transfer</li> <li>• Poor mixing</li> <li>• Re-oxidation of reaction products at anode</li> <li>• Contamination of working electrode more likely</li> </ul>
	<b>2-compartment (H-cell)</b>	<ul style="list-style-type: none"> <li>• Convenient to study half-cell reactions</li> <li>• Convenient for small scale experiments</li> <li>• Avoid product cross-over and re-oxidation</li> </ul>	<ul style="list-style-type: none"> <li>• Poor mass transfer</li> <li>• Poor mixing</li> <li>• Additional losses due to membrane resistance</li> </ul>
Continuous-flow reactors	<b>Membrane reactor</b>	<ul style="list-style-type: none"> <li>• Different configurations possible and easy upscaling</li> <li>• Pressurization relatively easy</li> <li>• Existing know-how, due to similarities with water electrolyzers</li> <li>• Straightforward stack construction</li> </ul>	<ul style="list-style-type: none"> <li>• Little knowledge on effects of membranes</li> <li>• Membrane may lead to additional resistance or product cross-over</li> <li>• Membrane cost and stability issues</li> </ul>
	<b>Microfluidic reactor</b>	<ul style="list-style-type: none"> <li>• No membrane included</li> <li>• Fast screening of catalysts</li> <li>• Better control of flooding</li> </ul>	<ul style="list-style-type: none"> <li>• Less effective separation of products</li> <li>• Difficult to pressurize</li> <li>• Difficult upscaling</li> </ul>
	<b>Solid oxide electrolyser (SOE)</b>	<ul style="list-style-type: none"> <li>• Decrease in overpotentials</li> <li>• Increase in charge transfer</li> <li>• Long term CO<sub>2</sub> electrolysis feasible (~500 h)</li> </ul>	<ul style="list-style-type: none"> <li>• Extreme conditions required</li> <li>• Impurities in gas stream may lead to electrode passivation</li> <li>• Techno-economic feasibility for CO<sub>2</sub> reduction unknown</li> <li>• Specialized electrode needed</li> </ul>

This enhancement is attributed to an increase in homogeneity and a decrease of agglomeration in the CL. Another strategy to enhance the performance of the silver-based CL for eCO<sub>2</sub>R to CO is the incorporation of multi-walled carbon nanotubes (MWCNT) leading to enhanced current densities which is partly due to a decreased charge-transfer resistance.[95] Moreover, uniform mixing of Ag nanoparticles with MWCNT shows better results compared to an Ag layer on top of a MWCNT layer. Recently, Dinh *et al.* reported on the increased stability and selectivity of eCO<sub>2</sub>R to C<sub>2</sub>H<sub>4</sub> on an “abrupt reaction interface” in highly alkaline media.[96] In this configuration, the Cu catalyst was embedded between a hydrophobic polytetrafluoroethylene (PTFE or Teflon) layer and conductive carbon nanoparticles, which maintains the hydrophobicity of the GDL and consequently prevents flooding.

The GDL may contain a MPL which improves electrical conductivity and water management. The Kenis group investigated several properties of the MPL with respect to eCO<sub>2</sub>R performance in a microfluidic flow cell. They found that the presence of a MPL enhances eCO<sub>2</sub>R towards CO with tenfold higher activity, due to the increased electronic conductivity, the ability to prevent flooding of the CL and catalyst loss from the CL.[97] Another parameter that is investigated is the amount of PTFE-binder in the MPL. The PTFE content determines the hydrophobicity of the MPL which ideally prevents the electrolyte flow from CL through the MPL but decreases the electronic conductivity. Due to counteracting influences of these parameters, there is usually an optimum of PTFE content for the MPL and CL.[97,98] A qualitative overview of the effects of different parameters is summarized in Figure 3.2. Wang *et al.* reported a membrane that functions as a GDE without the need of a binder, exhibiting less ohmic losses, increased stability, large number of active sites and hence enhanced eCO<sub>2</sub>R activity.[99] Such catalyst coated membranes have been observed before with a molecular catalyst for eCO<sub>2</sub>R and for the Oxygen Evolution Reaction (OER).[100,101] We believe that the optimization of this type of catalyst configuration can play an important role in the industrialization of the eCO<sub>2</sub>R process.

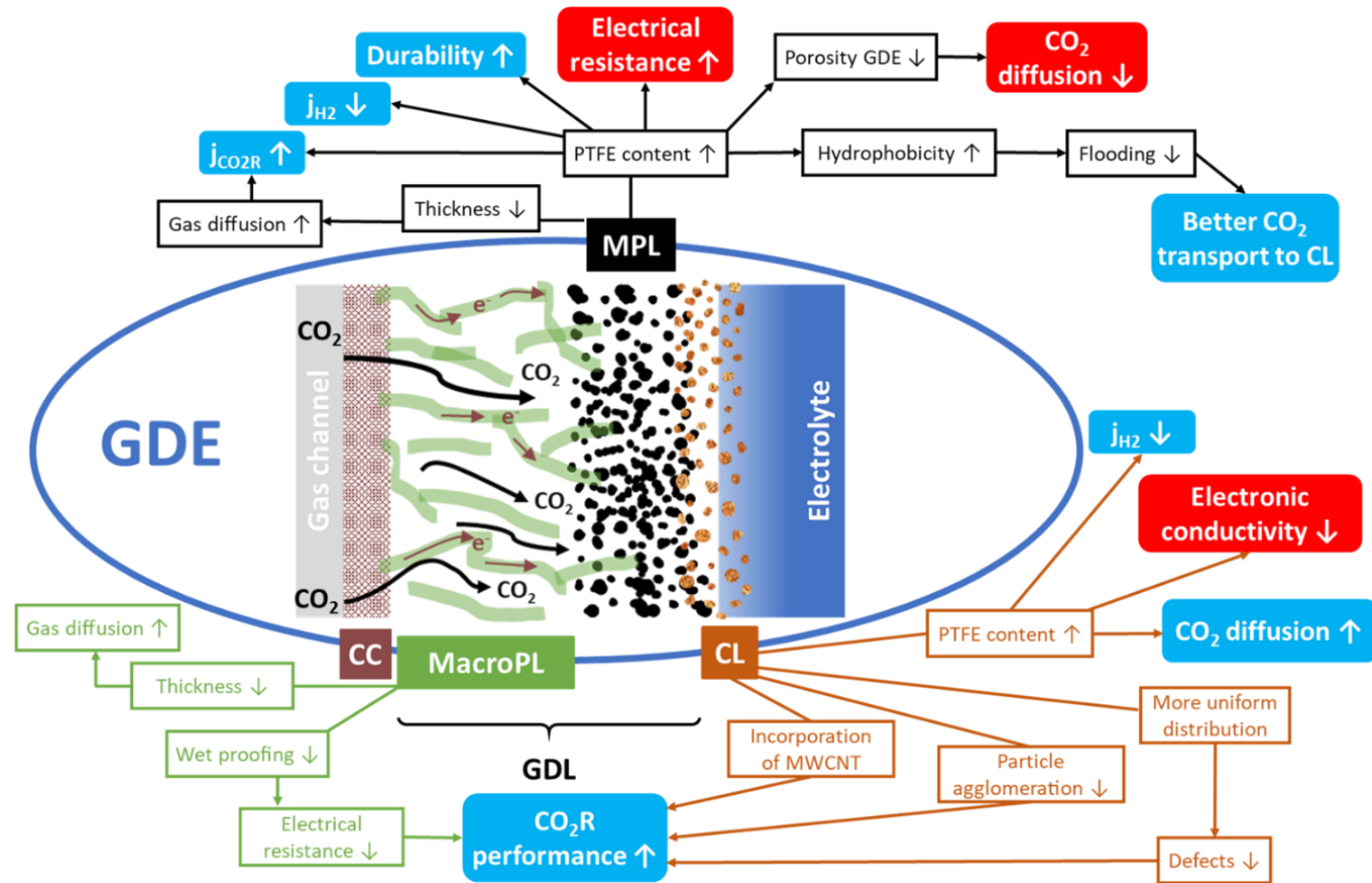


**Figure 3.2.** Schematic of a gas diffusion electrode including interrelated effects of the GDL and CL design parameters. Parameters shown in the black, brown, and green boxes refer to the microporous layer, catalyst layer and macro-porous layer respectively. Positive effects are shown in blue and negative effects in red colored boxes.

### 3.5 Anode reaction

For the operation of a CO<sub>2</sub> electrolyser, an electro-oxidation process at the anode must occur simultaneously with eCO<sub>2</sub>R at the cathode. Since the majority of eCO<sub>2</sub>R research has focused solely on the cathode reaction, the anode reaction is often not closely looked into as part of the complete system. The OER as half reaction has been under study for a century and has been optimized over the last few decades. It is important to improve the anode reaction as part of the complete eCO<sub>2</sub>R system, since it has been shown that lowering the overpotential of the anode reaction significantly benefits the total cell energy efficiency, and consequently the electrical requirements of a CO<sub>2</sub> electrolyser.[102] Usually water splitting (OER) is the reaction taking place at the anode, producing O<sub>2</sub> from H<sub>2</sub>O at high overpotentials. Here we highlight eCO<sub>2</sub>R studies that considered the anode reaction, instead of specific research on the OER as half reaction. Luc *et al.* reported that titanium-based materials are ideal catalyst supports for OER catalysts compatible with near-neutral operation conditions of eCO<sub>2</sub>R in aqueous media.[101] Moreover, Ti coated with Ir have shown excellent stability and OER activity. Other Ir-based anode materials have been reported to have a beneficial effect on the overall performance of the integrated system.[103,104] From an economical perspective, the use of Ir-based catalysts is undoubtedly less attractive.[105] However, it is still the catalyst of choice because of stability/performance. Cheaper alternatives (lower loading, effect of support) are also being sought after including non-PGM materials, but there is a lack of upscaling strategies. Another strategy to improve the anode reaction is to step away from the OER. Other anode reactions have been studied such as the oxidation of chloride ions to Cl<sub>2</sub>, and the oxidation of alcohols to ketones/aldehydes/carboxylic acids, leading to an additional benefit of producing value-added products at both electrodes.[102,106,107] For a large-scale operation, the anode reactions apart from OER still need to be optimized for continuous operation, and included in techno-economic analyses.

### 3.6 Membranes

Apart from the cathode and anode which can positively impact the energetic efficiency of a CO<sub>2</sub> electrolyser by decreasing the respective overpotential, another measure to obtain lower energy requirements is to lower the IR drop between anode and cathode. The majority of eCO<sub>2</sub>R research utilized PEM viz. Nafion.[81,108] However, recently AEM BPM have received increased interest for eCO<sub>2</sub>R.[109–112] The difference of using these membranes lies in the transport of ionic species from anode to cathode and vice versa. In case of a BPM, water is dissociated into H<sup>+</sup> and OH<sup>-</sup>, which is driven toward the cathode and anode respectively leading to similar pH on both sides of the membrane, allowing for different compositions of anolyte and catholyte. In all cases thinner membranes are generally better performing because of a lower resistance but bring along sealing and cross contamination issues.

Product crossover is an important aspect of membranes. Recently, this issue was investigated for AEMs and BPMs.[113–115] It was found that through AEMs the rate of product crossover is proportional to the current density, and even neutral alcohols experience crossover, as is the case for AEM fuel cells. Additionally, BPMs were found to inhibit charged and neutral product crossover due to the outward fluxes of generated H<sup>+</sup> and OH<sup>-</sup> species, leading to enhanced performance.

Dioxide Materials has developed ion exchange Sustainion<sup>®</sup> membranes that contain imidazolium functional groups, which were found to improve the performance and steer the selectivity towards CO<sub>2</sub> reduction products. [116,117] Aeshala *et al.* highlighted the improved eCO<sub>2</sub>R efficiency of quaternary ammonium groups in anionic solid polymer electrolytes.[118] Recently, it was reported that encapsulation of the catalyst in different types of polymers may have a significant influence on the eCO<sub>2</sub>R selectivity and stability, depending on the nature of the polymer.[119] The design and tuning of the membranes can therefore be an attractive strategy toward enhancement of eCO<sub>2</sub>R performance in membrane-type reactors needed for large-scale implementation.



### 3.7 Conclusions

Industrial CO<sub>2</sub> reduction may not be economically competitive compared to fossil fuel-based alternatives for the chemical industry and energy storage. However, from an environmental and sustainability perspective, it is needed to realize this technology on large scale via pilot plants or demonstrator electrolyser. Prospected carbon taxes in the future for CO<sub>2</sub> emissions, together with the need for intrinsically flexible production methods using renewable power as energy input, will also pave the way for this approach, especially when imposed on a global scale. Despite breakthroughs in the individual components on small scale, the key bottleneck towards industrialization of the electrochemical CO<sub>2</sub> reduction process is system integration and system-level optimization. Solely focusing on either high selectivity, activity, stability, cost or scalability would not be effective; a tradeoff between all the parameters is ultimately required. Hence, research and demonstration activities are needed, studying the interactions between the individual technological aspects to come to the optimization of an eCO<sub>2</sub>R electrolyser as a complete system. The next steps would be to emphasize on reactor design for enhanced mass transport, as well as on the robustness of the catalysts and electrode structures under various operational regimes.



## CHAPTER 4

### State-of-the-Art on Integrated CO<sub>2</sub> Capture and Electrochemical Conversion Systems

THE INTEGRATED CONCEPT IS PROMISING BUT ALSO A CHALLENGING CCU STRATEGY. TO PROPERLY INTEGRATE BOTH TECHNOLOGIES, IT IS CRUCIAL TO KNOW WHAT IS THE SITUATION ON THE CAPTURE OF CO<sub>2</sub> AT INDUSTRIAL SCALE AND THE STATE-OF-THE-ART OF THE CONVERSION OF POST-CAPTURE CO<sub>2</sub> SOLUTIONS. IN THIS CHAPTER, WE REVIEW AND DISCUSS THE CURRENT STATUS OF THE INTEGRATED STRATEGY.

This chapter is published as: O. Gutierrez-Sanchez, B. Bohlen, N. Daems, M. Bulut, D. Pant and T. Breugelmans, A State-of-the-Art Update on Integrated CO<sub>2</sub> Capture and Electrochemical Conversion Systems, ChemElectroChem, 2022, 9 (5), e202101540

## 4.1 Introduction

In this chapter, we review the most recent advances towards the integration of CO<sub>2</sub> capture and eCO<sub>2</sub>R technologies, specifically by covering the most important studies in CO<sub>2</sub> capture and very recent literature in eCO<sub>2</sub>R using CO<sub>2</sub> captured solutions (2018-2021). The elaboration of this literature study was motivated by the fact that crucial strategies to integrate CO<sub>2</sub> capture and eCO<sub>2</sub>R (such as an efficient procedure to directly reduce carbamate or (bi)carbonate solutions which were, until recently, almost unreported and experimentally unfeasible) have been published in the last couple of years, thus unlocking one of the limitations the technology had: using the CO<sub>2</sub> that is chemically bound to the capture solution. A broader compilation of these new studies is needed to understand the current status on integrating CO<sub>2</sub> capture and eCO<sub>2</sub>R as much ground has been covered in this field since, to the best of our knowledge, only a (mini-) review touching this topic was published.[120] Compared with the majority of other available review articles in the field of eCO<sub>2</sub>R, where they mainly target more fundamental aspects (such as catalyst configuration or reaction mechanism),[13,54] we look more from an industrial point of view, exploring the aspects that can contribute to upscaling the technology and in optimizing the energy efficiency of the overall CCU process. We focus on CO<sub>2</sub> capture technologies (giving special attention to the source of CO<sub>2</sub>, the capturing agent and what kind of solution is delivered afterwards) and on eCO<sub>2</sub>R systems where the source of CO<sub>2</sub> is a (real or mimicked) CO<sub>2</sub> captured solution (looking at the reactor design, used membranes and catholyte composition). Finally, we provide a glimpse of what the new emerging technologies represent for the integration of both systems.

## 4.2 CO<sub>2</sub> source: Capture and delivery technologies

### 4.2.1 CO<sub>2</sub> from the air: Direct Air Capture

DAC is a type of negative emission technology, able to retrieve CO<sub>2</sub> directly from the atmosphere, where CO<sub>2</sub> is present in low concentrations (i.e., 400-420 ppm).[121] This

makes the technology challenging since a high volume of air is needed to obtain usable amounts of CO<sub>2</sub>. The main technology proposed for DAC uses concentrated alkaline solutions, such as KOH, to react with CO<sub>2</sub>, generating carbonate. To recover CO<sub>2</sub> in the form of a high purity concentrated gas, carbonate is typically precipitated with calcium hydroxide and the calcium carbonate is calcined at elevated temperatures to generate calcium oxide and CO<sub>2</sub> (detailedly described in *Chapter 1.2*).[32] An alternative to concentrated alkaline bases is the use of a solid sorbent (such as zeolites, supported amines or porous carbon), which requires less energy for the desorption of CO<sub>2</sub> but is impossible to use as a feed for CO<sub>2</sub> electrolysis.[122] The DAC process, however, has two major disadvantages. On the one hand, it is highly energy-intensive (huge amounts of air need to be processed to capture significant amounts of CO, which needs to be subsequently released and compressed, further adding to the energy cost) and, on the other hand, it typically also results in water evaporation, especially when the air is dry. [123] Sanz-Pérez *et al.* published a thorough review on the direct capture of CO<sub>2</sub> from the air and presented new materials that could be used in this technology such as alkali carbonates, amine-supported materials or metal-organic frameworks (MOFs).[124]

Although it is a costly technology (typically ranging from 100 to 1000 US\$ t<sup>-1</sup>),[125] according to the International Energy Agency (IEA), there are currently 19 DAC (pilot) plants operating in Europe, the United States and Canada, capturing more than 9000 tCO<sub>2</sub> year<sup>-1</sup> (Table 4.1).[30] However, most of these plants are still on small scale and the CO<sub>2</sub> captured cannot be delivered in significant quantities, limiting its applicability. Nevertheless, Carbon Engineering in partnership with Occidental Petroleum is developing a large-scale DAC plant able to capture 1 MtCO<sub>2</sub> year<sup>-1</sup> and it is planned to be operational in 2023. Furthermore, Climeworks, in partnership with Carbfix has recently launched Orca, a plant that can capture up to 4000 tCO<sub>2</sub> year<sup>-1</sup>, almost half the amount of the total CO<sub>2</sub> captured by the 19 DAC plants worldwide currently operating.

**Table 4.1.** Some of the current operational DAC (pilot) plants in Europe, the United States and Canada.

<b>Company (Country)</b>	<b>Location</b>	<b>CO<sub>2</sub> removed</b>	<b>Technology</b>	<b>Reference</b>
<b>Climeworks (Switzerland)</b>	Zurich	900 t year <sup>-1</sup>	Solid sorbent	[126]
<b>Climeworks + Carbfix (Iceland)</b>	Iceland	4000 t year <sup>-1</sup>	Solid sorbent	[127]
<b>Carbon Engineering (Canada)</b>	British Columbia, Canada	1 t day <sup>-1</sup>	Liquid sorbent (KOH)	[128]
<b>Global Thermostat (USA)</b>	Huntsville, Alabama	Project: up to 40 Kt year <sup>-1</sup>	Liquid (amine-based)	[129]
<b>Carbon Engineering (Canada)</b>	USA	Planned for 2024: Up to 1 Mt year <sup>-1</sup>	Liquid sorbent	[130]
<b>Prometheus Fuels (USA)</b>	USA	Planned for 2022: 4450 t year <sup>-1</sup>	Combines DAC with eCO <sub>2</sub> R	[131]

#### 4.2.2 CO<sub>2</sub> from flue gas

Considering flue gas as the source of CO<sub>2</sub>, the most utilized applied capture technology is from post-combustion gases, mainly because of the ease of installing this end-stage technology in the existing plants.[132]

Various processes for the post-combustion capture have been used to this date, for example, membranes, solid adsorbents or solvent-based absorption.[133] Among the

different absorption solvents, amine scrubbing is the most dominant technology used for post-combustion CO<sub>2</sub> capture (detailedly described in *Chapter 1.2*), due to its maturity: the process was already patented in the 1930s and first evaluated at scale in 1991.[134] Different amines can be used as absorbent molecules and the choice of amine depends on factors such as the capacity of absorbing CO<sub>2</sub>, absorption rate and heat of absorption.[135] MEA is a primary amine and the most used in the industrial amine scrubbing process at concentrations up to 30 wt.%, due to its low cost, availability and the combination of important CO<sub>2</sub> absorption factors, such as ideal viscosity and high CO absorption capacity. [136,137] The drawbacks of this process are the high energy consumption for the regeneration of the amine, possible thermal degradation, large freshwater consumption and the generation of toxic waste and corrosive fumes during the process.[138,139]

Amine scrubbing is usually associated with the regeneration of the solvent and desorption of CO<sub>2</sub>, which is then compressed and stored in geological sites. However, the safety and the consequences of pumping CO<sub>2</sub> into the soil are not fully understood until today, thus requiring other solutions (like the combined technology under investigation here).[132,140] Besides, the regeneration of the amine is an energy-consuming process, since it requires the heating of the capture solution to cleave the C-N bond.[141] According to the literature, the energy consumption of the CO<sub>2</sub> desorption from MEA-H<sub>2</sub>O solutions is up to 3.8 GJ t<sup>-1</sup> CO<sub>2</sub> and 70% of the total operating costs of the process are due to this desorption and regeneration step.[142,143]

Several studies have been carried out to decrease the energy consumption associated with the amine scrubbing process, in an attempt to decrease and/or completely avoid the necessity of heating for regeneration. In this respect, ionic liquid solutions have been studied as an alternative to the aqueous 30 wt.% amine solution as they require almost 40% less energy.[143] Another alternative is the use of phase change adsorbent where Li *et al.* studied the combination of five different amines and three alcohols to investigate their behavior after CO<sub>2</sub> absorption. Blends constituted by the mixture of

amine/alcohol/water have the characteristic of forming distinct phases after CO<sub>2</sub> absorption and, with that, only the CO<sub>2</sub>-rich phase needs to be heated, decreasing the amount of energy required.[142] A final alternative is promoting the electrochemically mediated amine regeneration, where heating is no longer required. The latter is discussed in more detail later in *Chapter 4.3.1*. [144,145]

### 4.2.3 Catalytic CO<sub>2</sub> capture: improving capture rates

In this case, the capture solution has the role to react with the CO<sub>2</sub> and form a stable product, such as carbamate or carbonate, to be treated and delivered afterwards. However, due to the low concentration of CO<sub>2</sub> present in the gas mixtures used as CO<sub>2</sub> carriers (especially in air), the energy required for the capturing process is high.[124] Decreasing the time needed to capture a certain quantity of CO<sub>2</sub> is directly translated as decreasing the costs of the technology, since the amount of kWh used per ton of CO<sub>2</sub> captured will decrease. For this reason, several studies have focused on how to increase the kinetic rate of the reaction between the CO<sub>2</sub> and the capture agent, specifically with KOH but possibly to be extrapolated to amines.[146]

Most of the studies that focused on increasing the rate constant of the reaction between CO<sub>2</sub> and OH<sup>-</sup> to form bicarbonate are inspired by the enzymatic reaction found in nature which is catalyzed by the enzyme carbonic anhydrase (CAH).[147,148] The co-factor of CAH is Zn<sup>2+</sup> that forms a metal complex to three histidine terminals from the enzyme. This structure can easily bind water molecules and decrease to a great extent its  $pK_a$  (i.e., from 14 to 6.9), promoting its deprotonation and the formation of a fixed activated OH<sup>-</sup> structure which then binds CO<sub>2</sub> to form bicarbonate (Figure 4.1).[149] The reader is referred to *Chapter 7.1* for a more detailed explanation. The rate constant of the CO<sub>2</sub> hydration in CAH is at least  $10^6 \text{ M}^{-1} \text{ s}^{-1}$ , thus there is interest in integrating these systems in current CO<sub>2</sub> capture technologies as this could significantly enhance the capture rate.[150,151] One of the strategies is to integrate the biomimetic system in components such as membranes or porous materials. This increases the reusability of the enzyme as



well as the mechanical resistance of the capturing material. Wen *et al.* synthesized a reusable membrane for converting CO<sub>2</sub> to bicarbonate based on a bimetal (Zn<sup>2+</sup> and Cu<sup>2+</sup>)-protein hybrid hydrogel.[152] This material presented a recovery activity of 70% compared to analogous control experiments where the activity was 35% (Zn-based support) and 10% (Cu-based support). On the other hand, Jin *et al.* developed a re-usable, stable, MOF with structural similarities to the Zn-coordination complex in CAH to improve CO<sub>2</sub> absorption kinetics and proposed a model to convert CO<sub>2</sub>. [153] They evaluated the material by investigating the hydrolysis of para-nitrophenyl acetate, usually used to evaluate the performance of the CAH enzyme, probing the biomimetic properties of the material. Other research exploited the engineering challenges of the technology, such as finding durable support for the immobilization of the CAH onto surfaces. Kim *et al.* explored the stability of the CAH immobilized onto the renewable support material diatom bio-silica.[154] This biomaterial showed high reusability and no enzyme leakage even at elevated temperature conditions (>100 °C). Molina-Fernandez *et al.* recently reviewed further strategies to immobilize CAH in surfaces for industrial implementation.[155] Another approach exploited is to use the CAH or the biomimetic material directly suspended in the capturing solution. Sivanesan *et al.* evaluated a series of Zn-coordinated metal complexes in a tertiary amine medium by calculating the rate constant of the CO<sub>2</sub> hydration in each case scenario for its implementation in CO<sub>2</sub> capture from industrial gas waste. [156] In a similar strategy, Hanunsch *et al.* studied the performance of a metal-free pyrrolizidine catalyst for DAC and CO<sub>2</sub> conversion applications.[157]

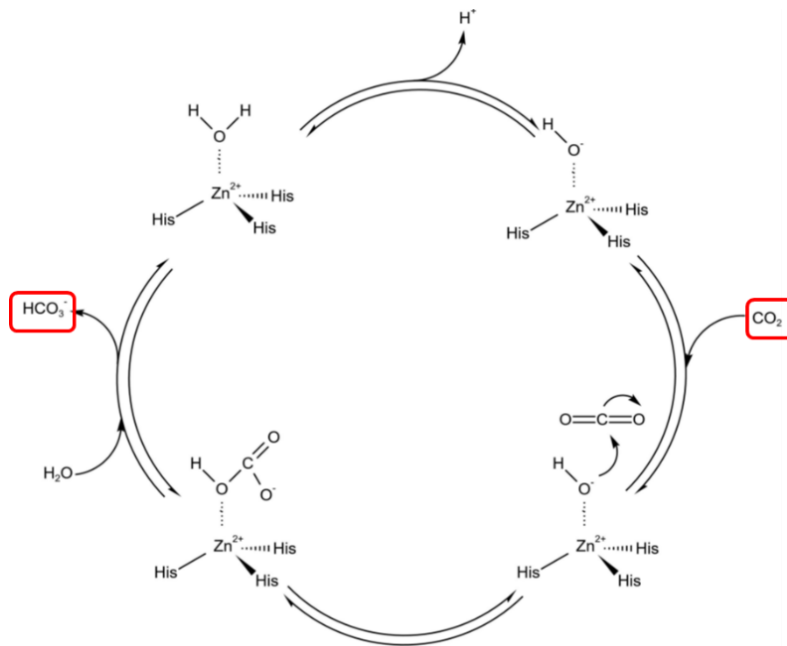


**Figure 4.1.** Mechanism of the hydration of CO<sub>2</sub> in the metal cofactor of the enzyme CAH.

Using materials that mimic the enzymatic reaction of CAH is an interesting approach to decrease the costs of capturing CO<sub>2</sub>. However, there still exist some drawbacks and challenges to consider before applying this technology in an upscaled system. For instance, for materials involving the immobilization of the enzyme, the stability of the enzyme is an issue. Flue gas streams use to be at elevated temperatures in the range of 150-1200 °C. At this temperature range, CAH degrades.[158] On the other hand, using an enzymatic suspension in the capture solution could be suboptimal if we consider that the solution will be later used as the electrolyte in the electrochemical cell. A separation and recovery step should be needed, increasing the costs of the technology. The most optimal route seems to be synthesizing thermoresistant materials (such as carbon-based or MOFs) that bio-mimic the enzymatic reaction of the CAH without the necessity of integrating the enzyme, acting as heterogeneous catalysts. These materials would be easily removed from the solution without the necessity of adding extra steps to the capturing process.

## 4.3 Post-capture electrochemical CO<sub>2</sub> conversion

### 4.3.1 CO<sub>2</sub> conversion from carbamate

The use of CO<sub>2</sub> directly from the amine (in form of carbamate) capture solution presents an added advantage, apart from avoiding the thermal solvent regeneration process, which is evading the sequestration of CO<sub>2</sub> into geological sites and the generation of chemicals of industrial interest, such as fuels and syngas.[136,142,159] Chen *et al.* published the first report on the direct electrochemical reduction of CO<sub>2</sub> from amine capture solutions. Different metal catalysts were tested for the generation of products such as CO and formate and two techniques were applied to improve the performance towards CO<sub>2</sub> reduction: increase of the catalyst surface area and the addition of a surfactant; a FE for formate of up to 60.8% was reached with a porous Pb electrode in the presence of the surfactant.[136] Lee *et al.* presented more recently a study on the effect of the addition of cations on the direct electrochemical CO<sub>2</sub> reduction of the amine scrubbing medium. Cations were added to the MEA solution to modify the electrochemical double layer and improve the reduction reaction. A FE of 72% for CO was achieved by using an Ag catalyst, at a current density of 50 mA cm<sup>-2</sup> by using 2 M KCl as salt.[140] Adding alkali salts to promote CO<sub>2</sub> conversion from amines was also explored in the same year by Khurram *et al.* In their study, they investigate the role of individual electrolyte salt constituents across multiple cations and anions in dimethyl sulfoxide electrolytes to clearly understand the role of these salts in the performance of the reaction. They concluded that although the anion appears to have a minor effect, the cation is found to strongly modulate the thermochemistry of the amine–CO<sub>2</sub> adducts through electrostatic interactions. Pérez-Gallent *et al.* evaluated the performance of an amine-based capture solvent as electrolyte for CO<sub>2</sub> conversion achieving up to 50% FE for formate and up to 45% for CO with carbon conversion of 30%. They promoted the reaction rate by a factor of 10 by increasing the temperature up to 75 °C.[160]

It is clear that based on the studies published in recent years and discussed in this chapter, reducing CO<sub>2</sub> that has been previously captured by an amine holds promise but there is still room for improvement as compared to the typical gaseous CO<sub>2</sub> electrolyzers in terms of FE and current density. However, thanks to the advancement in understanding how to dissociate the CO<sub>2</sub> from the amine in the electrochemical reactor, the next studies can focus on optimizing engineering aspects of the reactor to achieve higher overall energy efficiency.

#### **4.3.2 CO<sub>2</sub> conversion from bicarbonate**

CO<sub>2</sub> is captured in the form of bicarbonate when strong bases like KOH are used as capture solutions. Bicarbonate can be easily stored and delivered to the electrochemical reactor. However, its feasibility as a substrate for the direct electrochemical bicarbonate reduction reaction has been discussed within the community for a long time since extremely low FE towards carbon products (i.e., <10%) has been observed when bicarbonate electrolytes that have not been previously purged or saturated with CO<sub>2</sub> are used, with H<sub>2</sub> being the main product.[161]

The role of bicarbonate as CO<sub>2</sub> supplier in the eCO<sub>2</sub>R is discussed in *Annex A.3.1*. The reader is referred there to understand the concept. In addition to the CO<sub>2</sub> supplier ability of bicarbonate, Ooka *et al.* identified that when the concentration of bicarbonate is higher (>1 M), bicarbonate acts as a proton donor instead of a carbon donor, promoting to a great extent the HER, in accordance with the experimental observations done up to date.[162] This effect will be confirmed and discussed later in the *Chapter 5* of this thesis.[161,163]

Based on the proton donor ability of bicarbonate, the research on developing an electrochemical bicarbonate reduction reactor has drifted towards promoting the carbon donor ability instead, to increase the in-situ concentration of CO<sub>2</sub> at the surface of the electrode and thus increase the FE and partial current density towards carbon products.

The main strategy followed nowadays to perform the electrochemical bicarbonate reduction reaction is to build the set up in a zero-gap flow electrolyser, using a BPM as a separator. In a zero-gap configuration, as mentioned in *Annex A.5.2*, the protons formed in the BPM from the water dissociation heavily influence the catholyte next to the electrode surface and the performance of the reaction.[164] The protons formed from the BPM react with the bicarbonate to form water and dissolved CO<sub>2</sub>, which will then be the substrate of the electrochemical reaction (Figure 4.2). Li *et al.* used a zero-gap flow electrolyser and a BPM to develop an electrochemical reactor that reduces bicarbonate from a 3 M bicarbonate electrolyte to CO with a FE of 81% at 25 mA cm<sup>-2</sup> and 37% at 100 mA cm<sup>-2</sup>. [165] Lees *et al.* further explored the electrochemical reduction of bicarbonate to CO by performing an optimization study of the working electrode. [166] They concluded that commonly used components that improve the performance of GDE for CO<sub>2</sub> reduction, such as PTFE and microporous layers, are not beneficial for the performance of the electrochemical bicarbonate reduction. Since CO<sub>2</sub> is diffused from bicarbonate, gas-diffusion layers are no longer needed and they could limit the performance of the electrode. Later on, they also reduced bicarbonate to formate in a similar set up achieving a FE of 60% at 100 mA cm<sup>-2</sup> but using Bi as an electrocatalyst. [167] In *Chapter 8* of this thesis, the bicarbonate zero-gap flow electrolyser is further optimized to convert bicarbonate to formate, reaching relatively high FE (>30%) at industrially relevant current densities (400 mA cm<sup>-2</sup>). [168] The reader is referred there for a detailed discussion of the results.

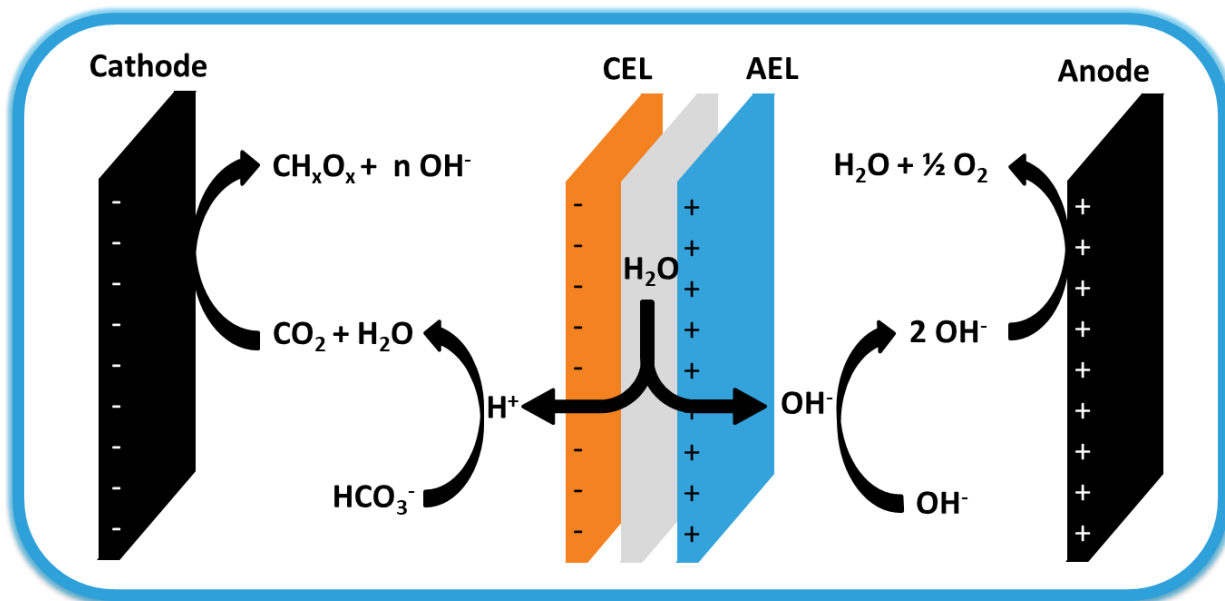


**Figure 4.2.** Schematic representation of the mechanism of bicarbonate electrochemical reduction in reactors involving a BPM.

Thanks to the understanding of how the electrochemical reduction of bicarbonate works achieved in recent years (2019-2021), electrolyzers that involve bicarbonate as the single carbon donor species can now compete in terms of FE and partial current density with state-of-the-art gaseous CO<sub>2</sub> electrolyzers. However, the technology remains a step below in terms of optimization. To make it feasible, either additives in the electrolyser (usually undesired in terms of downstream processing) or the necessity to use a BPM (high cell voltage at current densities >200 mA cm<sup>-2</sup>) is currently needed. Despite these drawbacks, being able to convert directly a CO<sub>2</sub> captured solution adds a higher value to the valorization of the whole CCU process. Overstepping costly CO<sub>2</sub> treatment steps before the delivery to the electrochemical cell might compensate for the higher energy requirements for the conversion step. Thus, further optimization of the reactor and the components directly influencing the reaction (such as the BPM and the electrocatalyst) is needed to increase the overall energy efficiency and finally achieve a positive capture-conversion energy balance.

## 4.4 Emerging technologies: CO<sub>2</sub> capture and conversion from ionic liquids and covalent organic frameworks

Besides the well-established processes based on amine and alkaline media, different sorbents have been investigated as agents for CO<sub>2</sub> capture.[169] Among these, two types are prominent, whose directed design leads to a wide range of application directed materials: ionic liquids (IL), a type of liquid sorbent, previously mentioned as an alternative for the amine scrubbing solution, and metallic/covalent organic frameworks (MOFs and COFs), solid sorbents.[54,170] Changing the combination of cations and anions of ILs or the organic precursors of the MOFs and COFs, their characteristics can be tuned, for example for an increased selectivity towards CO<sub>2</sub>, which is important for the capture from sources with a low concentration of CO<sub>2</sub> or a mixture of gases.[171,172] Both technologies are in the conceptual phase of industrial readiness, nonetheless, they are promising techniques with efficient capture potential.

In addition to the advantageous use as capture agents, ILs are interesting electrolytes for the eCO<sub>2</sub>R because these are not aqueous solutions, so the competing HER is suppressed and the efficiency of the eCO<sub>2</sub>R increased. Besides, the CO<sub>2</sub> molecule captured by the IL has a bent structure, which leads to smaller overpotentials required for the reduction reaction. Lu *et al.* present a type of IL as capture solution and electrolyte for the photoelectrochemical conversion of CO<sub>2</sub> to formate with a FE of 94.1%.[173] COFs present a high affinity towards CO<sub>2</sub>, which poses an advantage of their use as capture agents and is one characteristic that encouraged the investigation of these materials as catalysts for the eCO<sub>2</sub>R. This is a solid sorbent, thus the combination with the electrochemical process will be different than for the liquid absorbents, its capability of being used as a catalyst for the eCO<sub>2</sub>R may lead to the development of one-step capture and conversion processes. Ozdemir *et al.* present a series of different studies that utilized COF as catalysts for the eCO<sub>2</sub>R.[171] Liu *et al.* present an amine COF as a catalyst on a

silver electrode for the eCO<sub>2</sub>R to CO, with notably enhanced performance and chemical stability.[174]

Studies presenting the use of these capture agents in the eCO<sub>2</sub>R demonstrate the feasibility of the combination of capture and conversion.[175] Increasing investments and research in this topic will lead to the development of the technologies, decreasing the associated cost and increasing the competitiveness to the state-of-the-art processes.

## **4.5 Conclusions**

Integrating CO<sub>2</sub> capture and electrochemical conversion remains a challenge due to the high energy requirements in capturing the CO<sub>2</sub> (specifically from the air) and the difficulty to valorize the CO<sub>2</sub> afterwards. However, thanks to the recent advances in converting CO<sub>2</sub> directly from the capturing solution (in form of carbamate and bicarbonate), the technology is now approaching feasibility in terms of total energy and carbon balance, since previously one of the most cost-intensive steps was the compression and purification of CO<sub>2</sub> from the capturing solution. Nevertheless, the energy efficiency of the electrochemical reaction is still too low for industrial applicability. CO<sub>2</sub> conversion from carbamates showed promising results, but the current density is still too low for upscaling (in the range of 50 mA cm<sup>-2</sup>) and most of the systems still involve heating and thus an extra energy cost. On the other hand, CO<sub>2</sub> conversion from bicarbonate solutions showed satisfactory results in terms of current density (more than 300 mA cm<sup>-2</sup> in some studies) and FE (more than 50%) but using a BPM (high ohmic drop) and a zero-gap configuration (limited applicability) is required. Further research in optimizing these reactors is needed to valorize the high energy requirements of capturing CO<sub>2</sub> from the air or flue gas. For instance, parameters such as the morphology of the catalyst material, the flow rate of the electrolyte or the configuration of the BPM might influence the performance of the reactor. Another interesting approach could be to use of real DAC or flue gas captured samples as electrolyte for the eCO<sub>2</sub>R since now it is experimentally proven that the captured solution (although artificially prepared) can be converted.



The coupling of capture solution and CO<sub>2</sub> valorization based on renewable energy can be a future sustainable approach to restrain the advance of CO<sub>2</sub> emissions and fossil fuel usage and tackle the consequences of anthropogenic actions in the environment. For that, many improvements can be made in the direct electrochemical CO<sub>2</sub> reduction from capture medium, especially focusing on enhanced performance, if investments are directed to this increasing field of research.



# **Part III**

**Study of the mechanism of bicarbonate electrolysis. Role of the bicarbonate anion, co-reactions, and proposed approach**



## CHAPTER 5

### **The role of the bicarbonate anion as proton donor in CO<sub>2</sub> reduction systems: a strategy to increase the Faradaic efficiency of bicarbonate electrolysis**

THIS CHAPTER GIVES AN INSIGHT INTO THE MECHANISM OF THE ELECTROCHEMICAL BICARBONATE REDUCTION. THE REAL SUBSTRATE OF THE REACTION IS UNRAVELLED AND A STRATEGY TO INHIBIT THE MAIN CO-REACTION, THE HYDROGEN EVOLUTION REACTION, IS PROPOSED

This chapter is published as: O. Gutierrez-Sanchez, W. Offermans, N. Daems, Y.Y Birdja, M. Bulut, D. Pant and T. Breugelmans. The inhibition of the proton donor ability of bicarbonate promotes the electrochemical conversion of CO<sub>2</sub> from bicarbonate solutions, *Journal of CO<sub>2</sub> Utilization*, 2021, 48, 101521

## 5.1 Introduction

Even though the relative abundance of CO<sub>2</sub> in bicarbonate solutions is low, in concentrated bicarbonate solutions the concentration of CO<sub>2</sub> should be high enough to be comparable to saturated CO<sub>2</sub> solutions (Figure A.8) and should thus allow for a successful competition with the HER. Unfortunately, the FE towards carbon products of electrolysis in a saturated CO<sub>2</sub> solution is substantially higher compared to a bicarbonate solution, where most of the FE goes to HER. This must mean that other parameters are at play impeding the eCO<sub>2</sub>R in concentrated bicarbonate electrolytes. An explanation for the high HER obtained in bicarbonate electrolytes can be given by studies done on HER. It is reported that bicarbonate has a role as proton donor similar to water in the catalytic mechanism of HER via supplying H<sup>+</sup> to a previously electrochemically reduced weak acid like water or carbonic acid in a Volmer-Heyrovsky reaction pathway (Figure 5.1).[162,176,177] However, Dunwell *et al.* presented evidence that in CO<sub>2</sub> saturated electrolytes, at a controlled acidic pH, low concentrations of bicarbonate act as a CO<sub>2</sub> donor instead of as a proton donor.[178] It appears that the pH and the concentration of bicarbonate are key parameters to determine the role of bicarbonate in certain systems.

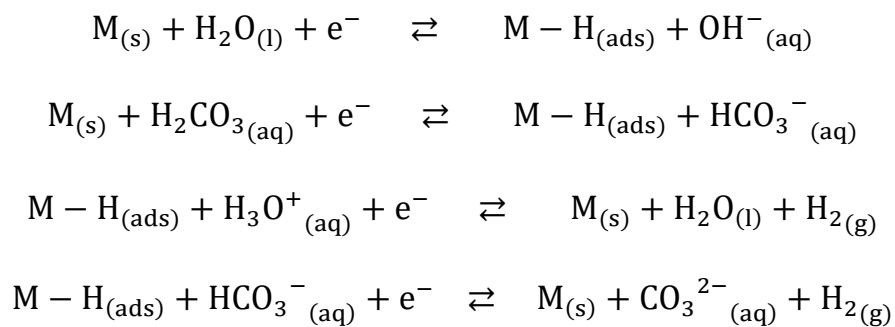


**Figure 5.1.** Volmer-Heyrovsky mechanism of HER involving water and bicarbonate.

The main cause of the inefficiency of the bicarbonate electrolysis thus might be the strong competition with the HER, the main side reaction, leading to a significant decrease of the FE towards carbon products. In CO<sub>2</sub>-saturated electrolytes, the inhibition of HER has been

studied in detail, mostly involving surfactants as additives of the electrolyte or deposited on top of the surface of the electrode. For example, Banerjee *et al.* used the cationic surfactant cetyltrimethylammonium bromide (CTAB) to modify the OHP by displacing the cations during electrolysis, inhibiting HER.[179,180] Zhong *et al.* studied the interfacial interactions of different cationic surfactants in CO<sub>2</sub>R proposing a mechanism where CO<sub>2</sub> reduction is promoted while HER is inhibited by the formation of a CO<sub>2</sub>-permeable coating.[181] On the other hand, Wakerley *et al.* made a hydrophobic electrode by treating Cu dendrites with 1-octadecanethiol, avoiding the penetration of water molecules while allowing CO<sub>2</sub> to reach the surface of the electrode, increasing its local concentration.[182] This strategy could also be applied for bicarbonate electrolysis. If, for instance, HER is inhibited while the FE towards carbon products is maintained, there is a direct proof that bicarbonate anion is not reduced directly but it is instead CO<sub>2</sub> the substrate of the reaction.

In this chapter, HER is inhibited in bicarbonate electrolysis and, by doing it, both the reaction mechanism proposed (and unconfirmed in literature) in *Annex A.3.1* and the role of bicarbonate as proton donor are confirmed. Parallely, a method to obtain high FE from the conversion of CO<sub>2</sub> to formate from different concentrations of bicarbonate electrolytes by inhibiting the proton donor ability of bicarbonate and water and, thus, inhibiting HER, is proposed. This method is benchmarked as procedure to study bicarbonate electrolysis from batch set-up and obtain relevant FE. This allows broader number of strategies to be considered when reducing CO<sub>2</sub> from bicarbonate solutions. However, the pathway proposed can also be complementary to the strategies currently in the state-of-the-art, such as the use of flow reactors, to even reach higher performance.

## 5.2 Experimental

### 5.2.1 Materials and solutions

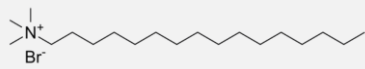
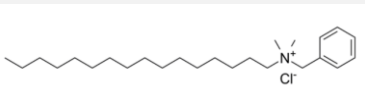
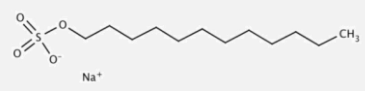
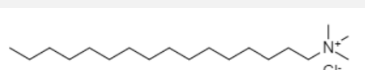
All the chemicals were obtained from commercial sources and used without purification unless stated otherwise. KHCO<sub>3</sub> solutions used as catholyte were prepared by dissolving the corresponding amount of 0.1, 0.5, 1 and 2 M of potassium hydrogen carbonate 99.5% (Chem-Lab) in Ultra-Pure water (MilliQ, 18.2 MΩcm). The saturated CO<sub>2</sub> solution was prepared by bubbling a 0.5 M KHCO<sub>3</sub> solution with gaseous CO<sub>2</sub> (purchased from Nippon, 99,9985%) for 45 minutes prior to the corresponding electrochemical experiment. A pH-meter was used to control and identify saturation. The anolyte was prepared by dissolving the corresponding amount of 1 M of potassium hydroxide pellets (Chem-Lab) in Ultra-Pure water. Each surfactant solution was prepared by dissolving the corresponding amount of hexadecyl trimethylammonium bromide, 98%+ (Chem-Lab); benzyl dimethyl hexadecyl ammonium chloride, 95%+ (Alfa Aesar); sodium dodecyl sulphate, 98%+ (Chem-Lab); or hexadecyl trimethylammonium chloride, 98% (Sigma Aldrich) in a previously prepared KHCO<sub>3</sub> solution. The solutions were sonicated for 10 minutes at room temperature. The structure and the abbreviation of the surfactants are shown in Table 5.1. Metallic Sn 99.9985% (2.0 mm dia., Alfa Aesar); Sn rotating disc electrode, RDE, (Good Fellow, polycrystalline, 99.999+%) and Cu RDE (Good Fellow, polycrystalline, 99.99+%) were used as working electrode. The surface was polished with alumina (particle size: 1 μm) and then sonicated in HPLC-grade acetonitrile (Chem-Lab) and Ultra-Pure water separately for 10 minutes. Nafion 117 CEM was used in the electrochemical H-Cell for chronoamperometric studies. The pre-treatment procedure of the Nafion 117 membranes was: 1 h in 0.5 M H<sub>2</sub>SO<sub>4</sub> at 80 °C, followed by 1 h in MilliQ water at 80 °C, then 1h in 0.5 M H<sub>2</sub>O<sub>2</sub> at 80 °C and finally 1 h in MilliQ water at 80 °C.



### 5.2.2 Instruments

The CA experiments were performed with a Biologic potentiostat and the LSV experiments with an Autolab potentiostat. The software EC-Lab (Biologic) and Nova (Autolab) were used for setting the electrochemical conditions up. For product analysis, Waters 2695 Separation module High-Performance Liquid Chromatography (HPLC) and RSpak KC-811 8×300 column was used to separate the products and Waters 2996 Photodiode Array Detector to detect and quantify formate in the form of formic acid. The samples were previously acidified with HClO<sub>4</sub> and filtered to avoid bubble formation and obstruction in the column. HClO<sub>4</sub> 0.1% was used as mobile phase.

**Table 5.1.** Structure and properties of the surfactants tested.

Surfactant	Abbreviation	Charge	Ion	Structure
Hexadecyl trimethylammonium bromide	CTAB	+	Br <sup>-</sup>	
Benzyl dimethyl hexadecylammonium chloride	CKC	+	Cl <sup>-</sup>	
Sodium dodecyl sulfate	SDS	-	Na <sup>+</sup>	
Hexadecyl trimethylammonium chloride	CTAC	+	Cl <sup>-</sup>	

### 5.2.3 Experimental set up and procedure

Two types of working electrodes were used depending on the performed electrochemical experiment. For LSV experiments, a Sn RDE of 0.22 cm<sup>2</sup> and a Cu RDE of 0.28 cm<sup>2</sup> were used to provide better electroanalytical control while for CA experiments a Sn wire electrode of 2 cm<sup>2</sup> (immersed length: 3.15 cm) was used in order to obtain higher concentration of formate and ensure analytical detection. A Pt mesh was used as counter electrode and Ag/AgCl 3 M was used as reference electrode. A voltammetry cell in a Faradaic cage was used for LSV experiments and a jacketed H-Cell was used for chronoamperometric experiments (Figure A.14). To separate the anolyte and the catholyte in the H-Cell and avoid product re-oxidation but ensure conductivity, a Nafion 117 membrane was used. For LSV experiments, 50 mL of electrolyte were previously purged with N<sub>2</sub> for 10 minutes to remove the diluted O<sub>2</sub> and the air-liquid interface was gassed with N<sub>2</sub> during the experiment to avoid diffusion of O<sub>2</sub> from the air. However, in experiments involving dissolved CO<sub>2</sub>, the solution was purged with CO<sub>2</sub> instead. The Sn RDE working electrode was electrochemically preconditioned by cycling from -0.5 V to -1.5 V<sub>RHE</sub> 10 times at 100 mV s<sup>-1</sup> prior to the experiment. To perform LSV experiments, the current was measured from -0.55 to -1.3 V<sub>RHE</sub> at 1 mV s<sup>-1</sup>. For CA experiments the Sn working electrode was electrochemically preconditioned by cycling from -0.5 to -1.5 V<sub>RHE</sub> 10 times at 100 mV s<sup>-1</sup> prior to the experiment, too. After the electrochemical precondition, 140 mL of electrolyte (70 mL of catholyte and 70 mL of anolyte) were electrolyzed at a fixed potential for one hour. The solution was continuously stirred with a magnetic stirrer at 300 rpm. All the experiments were performed at standard conditions (thermostatic at 25 °C and 1 atm). The difference of experimental potential (vs. Ag/AgCl 3 M and pH 8.3) and RHE is calculated and fixed at 0.7 V (e.g., applied potential of -1.6 V corresponds to -0.9 V<sub>RHE</sub>). After one hour, 0.5 mL of the solution was sampled and analyzed in the HPLC. After analysis, the concentration of formate in the electrolyte was obtained and the FE and partial current densities were calculated (Eq. A.11). Since only liquid analysis was performed, only the FE towards formate was quantified. Thus, in this

study, the rest of the current is approximated to go towards HER, supported by the high selectivity of Sn electrocatalyst towards formate as carbon product.[38] Each CA experiment was repeated three times unless stated otherwise. The FE shown in the manuscript belongs to the average value of three experiments and the error bars correspond to the standard deviation.

### 5.3 Results and discussion

The role of bicarbonate anion in bicarbonate electrolysis was studied by performing LSV and CA experiments in different bicarbonate solutions. Within the reduction current, eCO<sub>2</sub>R and HER occur simultaneously.[177] FE should increase with the concentration of bicarbonate, since the concentration of CO<sub>2</sub> is higher. However, results show that the current density corresponding to HER/CO<sub>2</sub>R increases significantly with the concentration of bicarbonate, as expected due to the higher conductivity of the solution (Figure 5.2), but the FE towards formate barely improves. Instead, even though the concentration of CO<sub>2</sub> is higher as the concentration of bicarbonate increases, most of the FE, and therefore the current, goes to HER (~90%). This indicates that a high concentration of bicarbonate must promote HER over eCO<sub>2</sub>R and confirms the role of bicarbonate in highly concentrated bicarbonate solutions as a proton donor species, inevitably giving high HER rates and low eCO<sub>2</sub>R FE's, in accordance with previous literature. Therefore, the process becomes highly inefficient.

Unlike in CO<sub>2</sub>-saturated systems, in concentrated bicarbonate electrolytes, the addition of cationic surfactants does not only impact the inhibition of HER by inhibiting the reaction step between an adsorbed hydrogen and water, but also interrupts the proton donation of bicarbonate in a similar way it does this for water molecules. This effect is achieved after negatively polarizing the electrode and covering the surface of the electrode by a hydrophobic layer where charged and polar molecules (bicarbonate and water) are partially repelled and non-polar and small molecules/ions (CO<sub>2</sub>, H<sup>+</sup>) can

trespass, allowing CO<sub>2</sub> hydrogenation and inhibiting HER. This may sound contradictory since the trespassing of H<sup>+</sup> should thus promote HER. However, it is known that to allow HER, a second water molecule must cross the EDL to supply a H<sup>+</sup> to the already adsorbed H<sup>+</sup>, forming H<sub>2</sub>. Therefore, it still goes in accordance with the mechanism proposed. Nevertheless, the exact HER inhibition may then be more complex than just the hydrophobic effect of cationic surfactants and it is, then, an interesting objective of research in future studies.

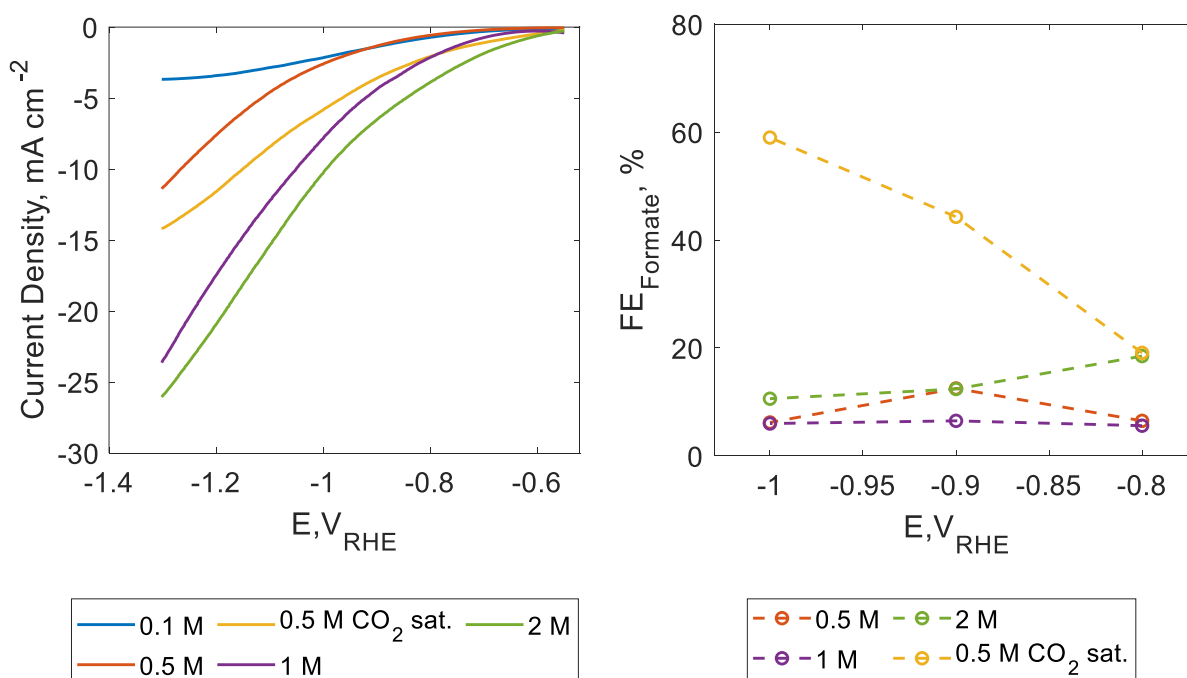


**Figure 5.2:** LSV voltammograms of a Sn electrode in different KHCO<sub>3</sub> solutions (left) at scan rate 1 mV s<sup>-1</sup>. FE<sub>Formate</sub> after 1 h electrolysis at different potentials in various KHCO<sub>3</sub> solutions (right).

The composition of the surfactant can also influence the overall effectiveness of this HER inhibition. It has been reported that cationic surfactants with aromatic groups in the polar head give higher hydrophobic properties to the surface compared to those without such groups, although the exact mechanism was still unknown.[183]

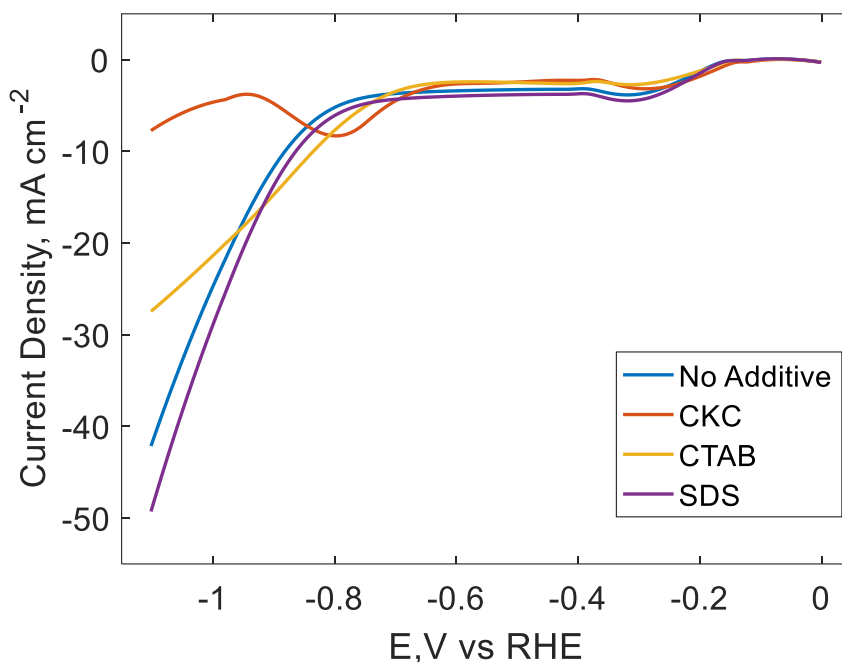


**Figure 5.3.** LSV voltammograms of a Sn electrode in KHCO<sub>3</sub> 2 M electrolytes at scan rate 1 mV s<sup>-1</sup> in presence and in the absence of 1000 μM of surfactants of different nature.

Based on the observations above, CKC was proposed as the most promising functional cationic surfactant to inhibit HER, and thus achieve the highest FE, in bicarbonate electrolytes. CKC is a cationic surfactant that has a 16-carbon alkyl chain and a tertiary amine as polar head functionalized with a benzyl group. HER is expected to be inhibited when CKC is present following a similar mechanism as CTAB was reported to do in CO<sub>2</sub> saturated electrolytes.[180] However, we expect a higher inhibition with CKC compared to CTAB because of the presence of the aromatic group, hypothetically increasing the hydrophobicity and CO<sub>2</sub>-philicity of the surfactant layer (unconfirmed up to this point). To identify HER inhibition, the electrochemical behavior of the working electrode when it is negatively polarized in a 2 M potassium bicarbonate solution in presence and in the absence of different surfactants was studied. LSV showed that a reduction peak, starting at -0.7 V<sub>RHE</sub>, appeared only in presence of CKC (Figure 5.3). At more negative potentials (< -0.9 V<sub>RHE</sub>), lower currents are achieved than in the absence of CKC, indicating that the HER is inhibited as it generally takes up the most significant fraction of the current at these

more negative potentials.[184] The nature of this cathodic peak and if it has a role on the mechanism of HER inhibition, and thus the reason why the inhibition is promoted in presence of CKC, was not yet reported on literature and was still not clear.

There are hints indicating that the interaction between surfactant and the metastable oxide layer of Sn at cathodic currents might play a role since such reduction peak is not observed in electrodes of different nature like Cu (Figure 5.4). However, a deep electrochemical study is needed to define and confirm the precise mechanism and the electrochemical reduction process of the phenomena observed when a cathodic current is applied to Sn surfaces in presence of CKC. For this reason, a separate chapter (*Chapter 6*) was elaborated solely to cover this topic.

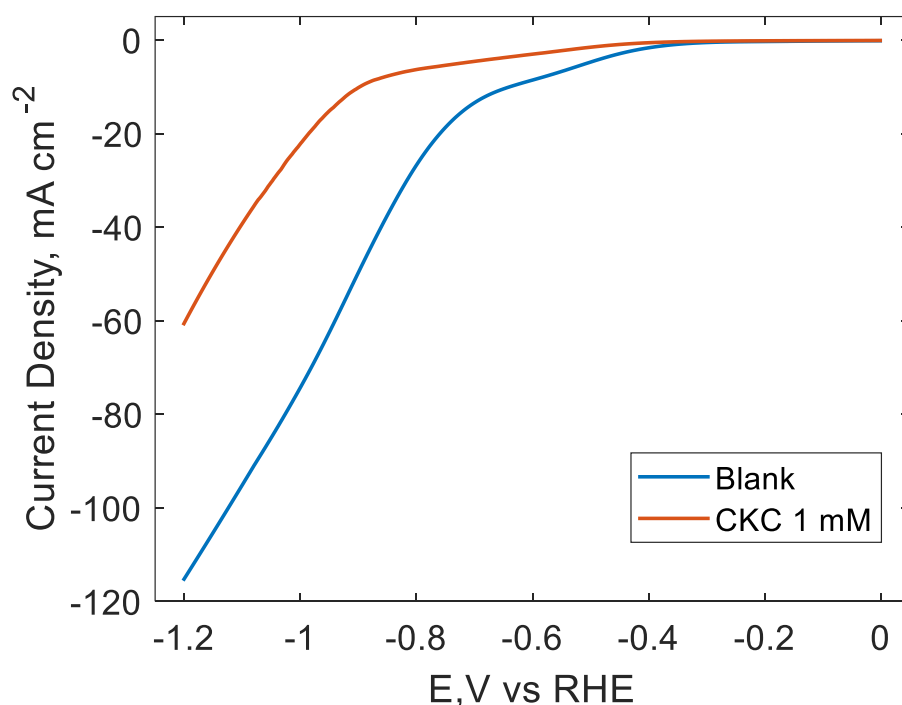


**Figure 5.4.** LSV of a Cu electrode in KHCO<sub>3</sub> 2 M electrolytes at scan rate 1 mV s<sup>-1</sup> in presence and in the absence of 1000 μM of CKC.

Other parameters like the charge of the surfactant and the nature of the counter ion have been already studied in other electrochemical studies involving CO<sub>2</sub> and surfactants.[183]

To confirm that the mentioned parameters have a similar effect on bicarbonate electrolytes, we briefly evaluated the impact on the decrease of the current, which is directly related to HER inhibition, of surfactants of different nature on bicarbonate electrolytes (Figure 5.3). LSV experiments showed that only cationic surfactants inhibit HER. Anionic surfactants (SDS) had little effect compared to control experiments. In presence of CTAB and CTAC the HER inhibition is lower than CKC, confirming previous work and our hypothesis that the presence of the aromatic group amine group is beneficial for the performance. Looking at CTAB and CTAC voltammograms, we can say that the difference when using Cl<sup>-</sup> or Br<sup>-</sup> as counter ions of the surfactants is not significant in this system, in accordance with literature (Figure 5.5).

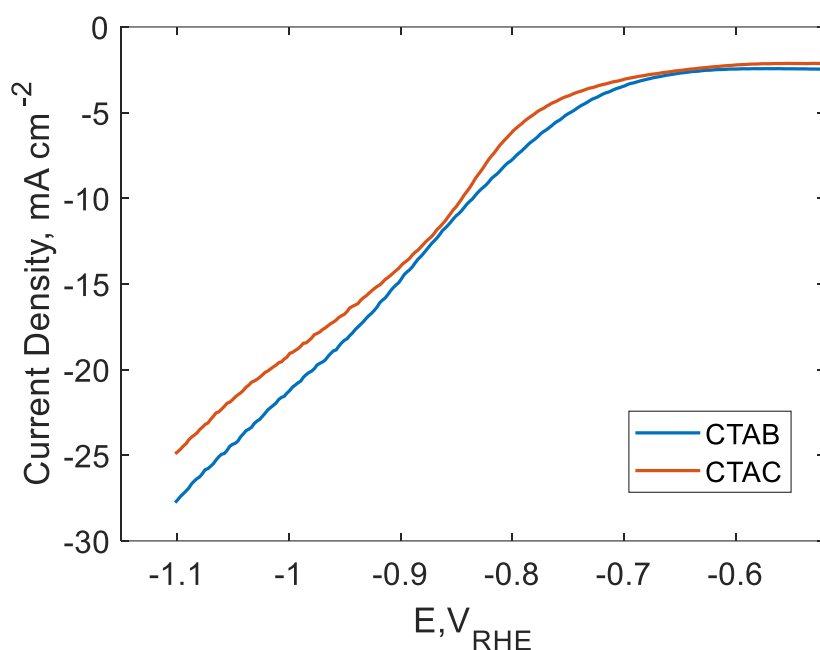


**Figure 5.5.** LSV of a Sn electrode in KHCO<sub>3</sub> 2 M at scan rate 1 mV s<sup>-1</sup> in presence and in the absence of 1000 μM of CTAB and CTAC.

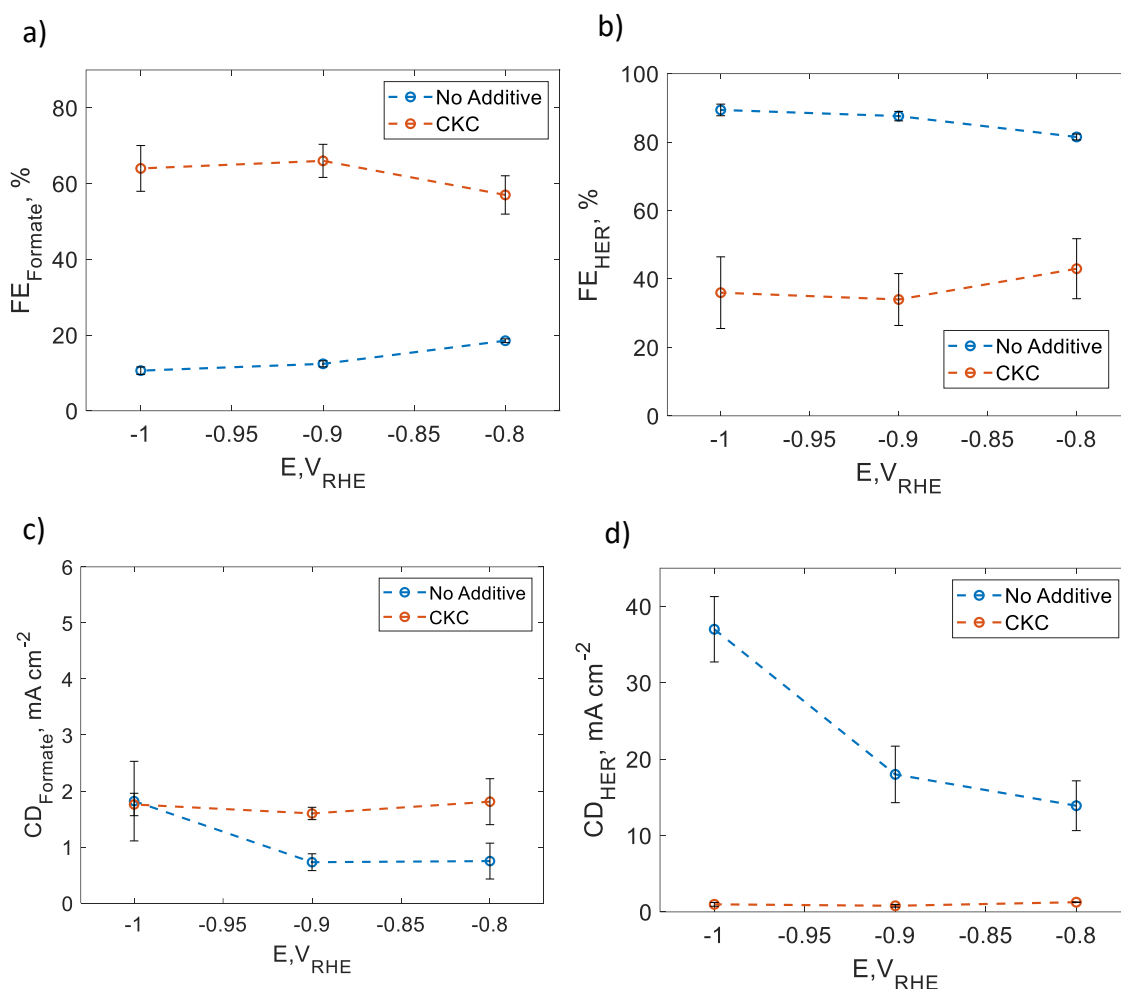


**Figure 5.6.** a)  $FE_{Formate}$  after 1 h electrolysis at different applied potential in  $KHCO_3$  2 M in presence and in the absence of CKC. b) Corresponding  $FE_{HER}$  c) Partial current density towards formate; d) partial current density towards HER.

We evaluated the performance of CKC on inhibiting HER by electrolyzing a 2 M bicarbonate solution for one hour with a Sn electrode in presence of 1000  $\mu M$  of CKC at different potentials and comparing the results to analogous control experiments in the absence of a cationic surfactant. In Figure 5.6 it is observed how the  $FE_{Formate}$  increases substantially upon addition of CKC. For instance, 66% FE is obtained in presence of CKC compared to 12% in surfactant-free electrolyte at  $-0.9 V_{RHE}$ , an increase of 54%. Analogous experiments involving CTAB (Figure 5.9) confirmed that CKC has higher impact than CTAB on HER inhibition ( $\sim 20\%$  addition in FE) due to the presence of aromatic groups. In



agreement with previous literature on CO<sub>2</sub>-saturated electrolytes, the presence of a cationic surfactant results in a decrease of the total current density in proportion with the increase of FE towards eCO<sub>2</sub>R products and a decrease of FE<sub>HER</sub>.<sup>[179]</sup> This decrease in the total current density is related to HER as the partial current density of HER is diminished while the eCO<sub>2</sub>R remains almost unaffected (Figure 5.6c, 5.6d). Then, the overall decrease of the current density is not negatively affecting the performance when reducing CO<sub>2</sub>, since it only affects the HER. The FE remained rather constant when increasing the concentration of CKC proving that once a critical micellar concentration is reached (CMC, 500 μM) further increasing the concentration doesn't result in further increase in performance (Figure 5.7, left). We observed closer this effect by performing LSV experiments with different concentrations of CKC (Figure 5.7, right). By comparing the total current density, from the CMC, the efficiency of HER inhibition does not differ much when the concentration of CKC is increased (6-9 mA cm<sup>-2</sup> at -1.1 V<sub>RHE</sub>). This may indicate that once the surfactant starts forming micelles, HER inhibition is not further improved.

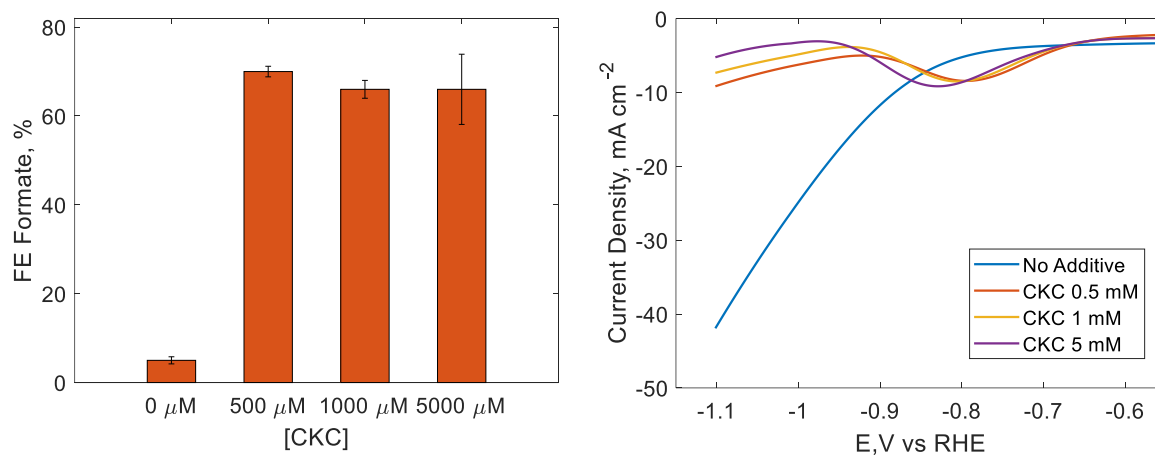


**Figure 5.7:** FE<sub>Formate</sub> after 1 h electrolysis at -0.9 V<sub>RHE</sub> in 2 M KHCO<sub>3</sub> in presence and in the absence of different concentrations of CKC (left) LSV voltammograms of a Sn electrode in KHCO<sub>3</sub> 2 M in presence and in the absence of different concentrations of CKC.

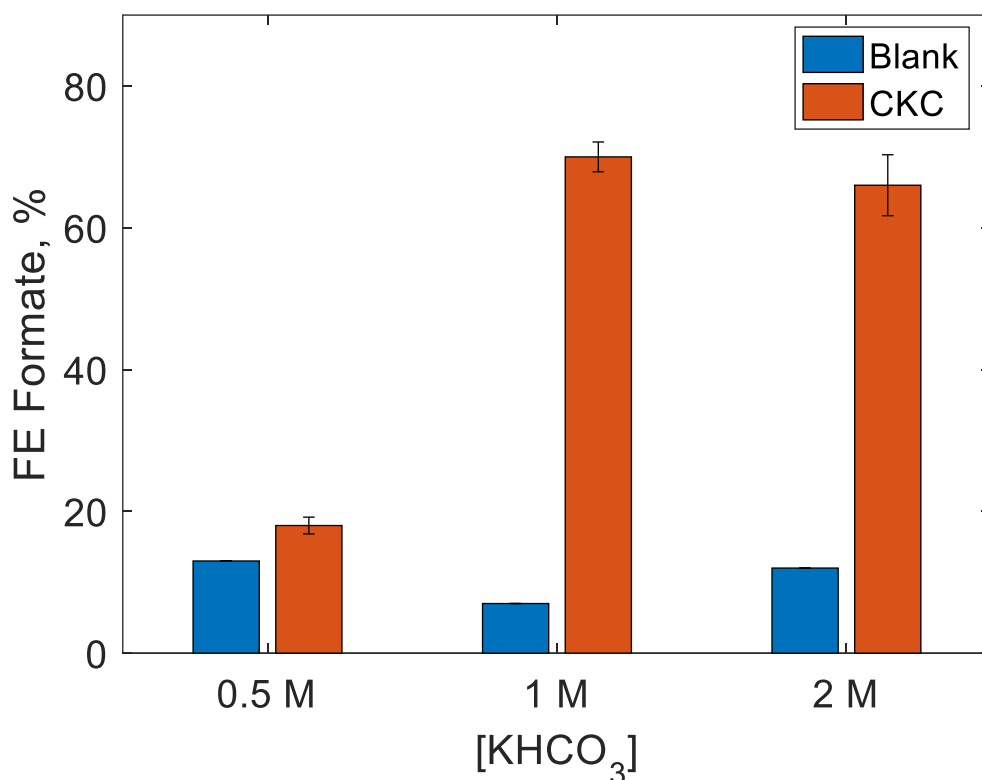


**Figure 5.8.**  $FE_{\text{Formate}}$  after 1 h electrolysis at  $-0.9 V_{\text{RHE}}$  in different concentrations of  $\text{KHCO}_3$  electrolytes in presence and in the absence of  $1000 \mu\text{M}$  of CKC.

Additional experiments were carried out varying the concentration of potassium bicarbonate and fixing the applied potential to  $-0.9 V_{\text{RHE}}$ . In contrast with the results shown in Figure 5.2, where the  $FE_{\text{Formate}}$  barely changes with the concentration of bicarbonate, in presence of CKC the  $FE_{\text{Formate}}$  increases considerably when the concentration of bicarbonate goes from 0.5 M to 1 and 2 M (Figure 5.8). Between 1 and 2 M,  $FE_{\text{Formate}}$  lies within the same range (71 and 66%, respectively). The FE in 0.5 M bicarbonate with CKC slightly increases compared to the control test (19 and 13%, respectively), which is believed to be due to the very low  $\text{CO}_2$  concentration (0.006 M). The concentration of potassium bicarbonate thus clearly matters as higher concentrations result in more  $\text{CO}_2$  being transported to the surface of the electrode and converted. This finding is very significant since a target of using bicarbonate as a substrate instead of gaseous  $\text{CO}_2$  feeds is to provide a system where  $\text{CO}_2$  can be continuously and

efficiently converted from a liquid phase. Nevertheless, we must take into account the effect of the concentration of the cation, K<sup>+</sup>, as it is known that high concentrations of this inhibit the HER, too.[185] However, we didn't see an effect of K<sup>+</sup> in systems in the absence of surfactant (Figure 5.2, right). Then, if there is a HER inhibition effect of the cation in bicarbonate electrolysis, the proton donor ability of bicarbonate is competing with it. Therefore, future research should be performed with an as high as possible bicarbonate concentration to run an as efficient as possible process from capture to conversion.

## 5.4 Conclusions

In summary, by identifying the role of the bicarbonate anion in the bicarbonate electrolysis the electrochemical reduction mechanism is unraveled in this chapter. Bicarbonate anion acts as a proton donor species promoting HER over eCO<sub>2</sub>R, which is inefficient from a practical point of view. By using cationic surfactant, this trait was efficiently inhibited and the mechanism where CO<sub>2</sub> is the actual substrate of the reaction is confirmed. In addition, a new approach to obtain high FE towards carbon products from bicarbonate electrolysis is benchmarked. CO<sub>2</sub> was efficiently converted to formate from a bicarbonate electrolyte that was not previously purged with CO<sub>2</sub> by inhibiting the proton donor ability of bicarbonate, and thus the HER, with the cationic surfactant CKC. High FE<sub>Formate</sub> from bicarbonate electrolytes (>70%) were obtained in this chapter. As shown, with the presence of the cationic surfactant CKC in the bicarbonate electrolyte, the surface of the electrode becomes hydrophobic enabling non-polar molecules, like the CO<sub>2</sub> derived from the equilibrium with bicarbonate, to diffuse to the surface of the electrode and preventing polar molecules like bicarbonate and water to promote HER. This way, bicarbonate acts as a CO<sub>2</sub> source instead of as a proton donor. Through this mechanism, a bicarbonate solution becomes a high loaded carbon pool enabling CO<sub>2</sub> to be captured and stored up to saturation levels of bicarbonate (~2 M) and then converted to valuable products in an electrochemical cell, avoiding the necessity of using a pure CO<sub>2</sub> gas inlet and thus the separation and storage costs. The mechanism proposed in this manuscript

and the results shown enable new strategies for the electrochemical conversion of CO<sub>2</sub> from bicarbonate, which in many cases, although industrially very attractive, its practical use has been limited within the community due to high obtained HER rates. Since such disadvantage is tackled in this chapter and high FE<sub>Formate</sub> is obtained (thereby low HER rates), further fundamentals on the reaction mechanism (such as the buffering effect of bicarbonate, the kinetics or the product selectivity) will be studied in detail and the strategy of electrochemically converting CO<sub>2</sub> from bicarbonate becomes more promising and closer to applicability. Up to day, only the electrocatalytic conversion of CO<sub>2</sub> from bicarbonate to CO and formate has been reported in literature, opening a wide window of research where other CO<sub>2</sub>R valued products (like CH<sub>3</sub>OH, CH<sub>4</sub> or CH<sub>3</sub>CH<sub>2</sub>OH) can be targeted by modulating cell parameters such as the catalyst choice. Although the presence of surfactant should affect the selectivity of the reaction (since the electrochemical double layer is altered), the HER inhibition mechanism proposed in this chapter should behave in a similar way whatever catalyst is used, since it is apparently dependent on the electrolyte.

## 5.5 Supporting information

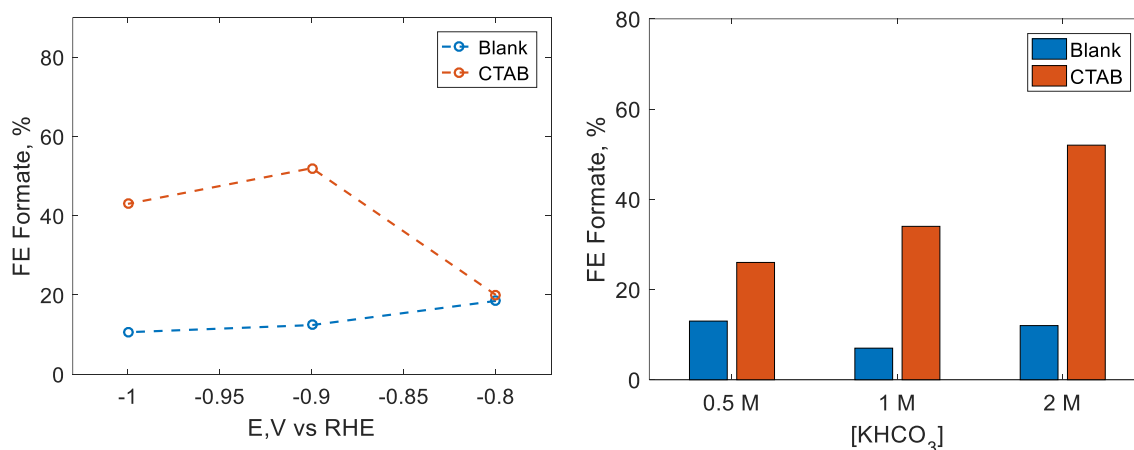


**Figure 5.9.** FE<sub>Formate</sub> after 1 h electrolysis at different potentials in KHCO<sub>3</sub> 2 M with and without 1000 μM of CTAB (left). FE<sub>Formate</sub> after 1 h electrolysis at -0.9 V<sub>RHE</sub> in different concentrations of KHCO<sub>3</sub> with and without 1000 μM of CTAB (right).

## CHAPTER 6

### **A deep study on the HER inhibition mechanism of cationic surfactants during bicarbonate electrolysis**

AS SEEN IN CHAPTER 6, CATIONIC SURFACTANTS INHIBIT TO A GREAT EXTENT THE HYDROGEN EVOLUTION REACTION IN BICARBONATE ELECTROLYSIS. IN THIS CHAPTER, WE GIVE MORE INSIGHT ON THE INHIBITION MECHANISM AND THE EFFECTS OF THE CATIONIC SURFACTANT TO THE SURFACE OF THE ELECTRODE.

This chapter is published as: O. Gutierrez-Sanchez, N. Daems, M. Bulut, D. Pant and T. Breugelmans. Effects of benzyl functionalized cationic surfactants on the inhibition of the hydrogen evolution reaction in CO<sub>2</sub> reduction systems, *ACS Applied Materials & Interfaces*, 2021, 13, 47, 56205–56216

## 6.1 Introduction

In *Chapter 5* it was proven how the properties of the electrolyte and the species that are close to the electrocatalyst may benefit CO<sub>2</sub>R over HER. This field is, in fact, gaining interest in eCO<sub>2</sub>R when saturated CO<sub>2</sub> or bicarbonate solutions are used as electrolyte and as CO<sub>2</sub> donor.[186] It is well known that the solubility of CO<sub>2</sub> is substantially affected by the presence of other salt species, which is shown by it being significantly lower in seawater. Though this interaction between CO<sub>2</sub> conversion and electrolyte has been investigated in several studies, this has been mainly done from the perspective where gaseous CO<sub>2</sub> is usually continuously bubbled through the electrolyte.[187] However, the effect of the ionic species and additives present in the electrolyte when a bicarbonate solution is used as a carbon source instead of gaseous CO<sub>2</sub> remains rather an unexplored domain. This includes using cationic surfactants as HER inhibitors for bicarbonate electrolysis applications.

In eCO<sub>2</sub>R, these cationic surfactants are part of the cationic species present in the electrochemical double layer when the potential is applied (Figure A.6) and due to the amphiphilic properties of the surfactants, the positively charged polar head of the molecule will orientate towards the surface of the cathode while the hydrophobic tail is orientated towards the bulk electrolyte, forming a non-polar layer (Figure 6.1).[181] In a CO<sub>2</sub> containing electrolyte the main substrate for the competing HER is H<sub>2</sub>O and since the surface of the electrode is partially hydrophobic after adding cationic surfactants to the electrolyte, H<sub>2</sub>O is partially repelled, making it difficult to reach the surface and react, thus inhibiting the HER. On the other hand, since CO<sub>2</sub> is a non-polar molecule, the eCO<sub>2</sub>R reaction remains unaffected resulting in an increase in the FE towards the carbon products.[161] This effect was first shown in bicarbonate electrolysis while investigating the reaction mechanism in *Chapter 6*. The inhibition effect appears to be independent of the nature and design of the electrode used since it has been reported on Au, Sn and Cu

electrodes, being thus instead an effect derived of the properties of the electrochemical double layer.[180]

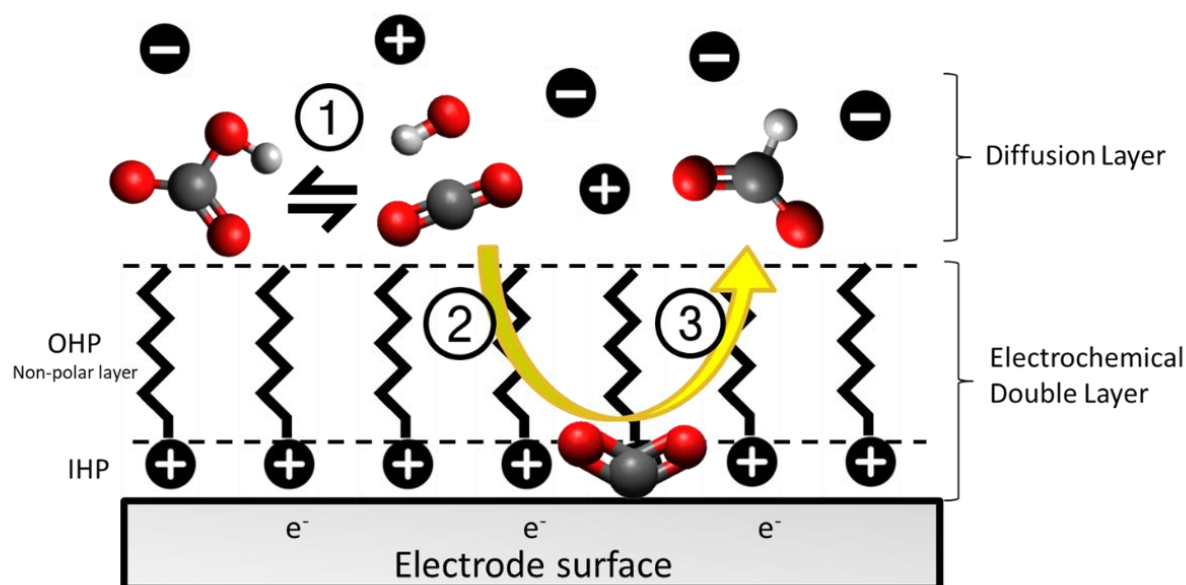


**Figure 6.1.** Schematic interpretation of the eCO<sub>2</sub>R to formate when using bicarbonate as a carbon source. A cationic surfactant is used and a non-polar layer is formed close to the surface of the cathode, promoting the reaction. 1) CO<sub>2</sub> is formed from the equilibrium with bicarbonate with water. 2) CO<sub>2</sub> (non-polar) diffuses through the non-polar layer and reaches the surface of the electrode. 3) CO<sub>2</sub> is reduced to formate.

Due to the proton donor ability of bicarbonate anion, bicarbonate electrolytes do not only act as a carbon source but also as a promotor of the HER more than in analogous saturated CO<sub>2</sub> electrolytes, where water is the only proton donor species present.[176] In the previous chapter, the inhibiting mechanism of cationic surfactants was confirmed also in bicarbonate electrolytes and it was proven that they play a similar role (but with higher impact) in inhibiting the HER in this type of bicarbonate electrolytes compared to its CO<sub>2</sub> saturated analogues. Since bicarbonate is a polar molecule, it is also partially repelled after the non-polar layer is formed, thereby limiting its role to proton supplier as it can no longer reach the active sites as such but it can still liberate CO<sub>2</sub> first which can then travel through the non-polar channels to the active zone (Figure 6.1). Its role as proton

donor for the HER is thereby inhibited as this would need it to reach the active sites intact. In this chapter, we continue utilizing this approach with saturated bicarbonate solutions as an electrolyte because of the high industrial interest in using saturated bicarbonate as CO<sub>2</sub> supply instead of saturated CO<sub>2</sub> solutions (*Chapter 1.4*). Moreover, because the HER inhibition ability of cationic surfactants is more accentuated in bicarbonate-based electrolytes as it forms a better case study to investigate the role of the surfactant in more detail.

In most cases, the cationic surfactants used to inhibit HER during eCO<sub>2</sub>R are from the family of the trimethyl-ammonium N-alkyl bromide, with the most common one being CTAB.[180] The high stability of the quaternary amine ensures that the surfactant is not reduced when the working potential is applied and the long alkyl chain ensures the formation of the desired hydrophobic layer. Although the properties of the electrochemical double layer in presence and in the absence of CTAB during eCO<sub>2</sub>R have been extensively studied over the last two years,[179–181] little research has been done on how a modification of the surfactant may affect the functionality of the cationic surfactant, the catalytic surface and the overall efficiency of the process. For instance, substituting the methyl groups of the quaternary amine of CTAB for specific functional groups that could promote the amphiphilic function of the surfactant or the affinity towards a specific substrate have been mentioned and preliminary tests were performed but a specific study investigating the mechanism behind these other functionalities in surfactants is to the best of our knowledge still missing and is the focus of this work.[183]

In the previous chapter it was observed how the addition of benzyl groups to the quaternary amine of CTAB increased the rate of HER inhibition, further increasing the FE towards carbon products compared to analogous experiments using CTAB but without a clear understanding of the underlying mechanism. In addition, some till now unexplainable changes in the electrochemical behavior of the Sn electrode (used as electrocatalyst) were also observed. These include a subsequent decrease in the partial



current density towards HER and the apparition of an electrochemical reduction reaction non-existing in control and CTAB experiments (Figure 5.3). Sn is a metal with a PZC of 0.1  $V_{RHE}$  in bicarbonate electrolytes (with pH 8.3), meaning that at working potentials below this value (which is the case for the complete potential range under investigation here), cationic species adsorb and the electrochemical double layer is formed.[188] Then, the changes observed in the behavior of the Sn electrode might thus come from the direct interaction of agents present in the electrolyte with the surface of the electrode. For this reason, the effects of the benzyl-functionalized cationic surfactant, CKC, on the electrochemistry of the Sn electrocatalyst after the electrochemical double layer is formed are worth of an in-depth investigation. In this chapter, a variety of electrochemical techniques were utilized to evaluate the changes of the Sn electrode after the addition of CKC and compared it to analogous experiment using CTAB and the anionic surfactant SDS. This allowed the identification of the underlying phenomena occurring on the surface of the electrode and proposed a mechanism where the benzyl group acted like a second hydrophobic agent of the cationic surfactant in the electrochemical double layer thus promoting the impermeability of the electrode.

## 6.2 Experimental

### 6.2.1 Materials and solutions

All the chemicals were obtained from commercial sources and used without purification unless stated otherwise. The  $KHCO_3$  electrolytes and the CTAB, CKC and SDS surfactant solutions were prepared following the same procedure as in *Chapter 5.2.1*. Each benzyl-derived solution was prepared by dissolving the corresponding amount of benzyl trimethylammonium bromide, 98+% (Alfa Aesar); acetophenone, 99+% (Chem-Lab); benzaldehyde, 99+% (Chem-Lab); benzoic acid, 99.9+% (Chem-Lab); or benzyl bromide, 98% (Sigma Aldrich) in a previously prepared  $KHCO_3$  solution. The Sn wire, Sn RDE and Cu RDE electrodes used as working electrodes are the same as the ones used in *Chapter 5*.

Nafion 117® PEM was used in the electrochemical H-Cell (Figure A.14) for electrolysis studies. The membrane was preconditioned following the same procedure as *Chapter 5.2.1*.

## 6.2.2 Experimental set up and procedure

Two types of working electrodes were used depending on the performed electrochemical experiment. For LSV and EIS experiments, a Sn RDE of 0.22 cm<sup>2</sup> and a Cu RDE of 0.28 cm<sup>2</sup> were used to provide better electroanalytical control while for CA experiments a Sn wire electrode of 2 cm<sup>2</sup> (immersed length: 3.15 cm) was used in order to obtain higher concentrations of formate and ensure analytical detection. A Pt mesh was used as counter electrode and Ag/AgCl 3 M was used as reference electrode. All three electrodes were immersed in an electrochemical cell placed in a Faradaic cage for LSV and EIS experiments and in a jacketed H-Cell for CA experiment. To separate the anolyte and the catholyte in the H-Cell and to avoid product re-oxidation while ensuring conductivity, a Nafion 117® membrane was used. For LSV and EIS experiments, 50 mL of KHCO<sub>3</sub> 2 M electrolyte were previously purged with N<sub>2</sub> for 10 minutes to remove the diluted O<sub>2</sub> and the air-liquid interface was gassed with N<sub>2</sub> during the experiment to avoid diffusion of O<sub>2</sub> from the air. All types of working electrodes were electrochemically preconditioned by following the same procedure as in *Chapter 5.2.3*. To perform LSV experiments, the current was measured from 0 V to -1.1 V<sub>RHE</sub> at 1 or 10 mV s<sup>-1</sup> unless stated otherwise. For EIS experiments, the impedance was measured at a fixed potential from 1 to 20,000 Hz. Two types of equivalent circuits were used to fit the experimental data, which are discussed in detail later in the chapter. For CA experiments, the same electrochemical preconditioning and procedure than in *Chapter 5* were followed. All the experiments were performed at standard conditions (thermostatic at 25 °C and 1 atm). The difference of experimental potential (vs. Ag/AgCl 3 M and pH 8.3) and RHE is calculated and fixed at 0.7 V (e.g., applied potential of -1.6 V corresponds to -0.9 V<sub>RHE</sub>). After one hour, 0.5 mL of the solution was sampled and analyzed in the HPLC. After analysis, the concentration of

formate in the electrolyte was obtained and the FE was calculated (Eq. A.11). Since we only performed liquid analysis (formate), we can only quantify the FE towards formate. Thus, in this study, we simply consider that the remaining current goes towards HER, although a small but significant fraction of the FE is expected to go to CO formation, as well. However, the evaluation and conclusions made in this work were not affected by this assumption. Each CA and EIS experiment were repeated three times. The FE and the DL-Capacitance shown in the manuscript belong to the average value of three experiments and the error bars correspond to the standard error.

### 6.2.3 Analytical techniques

The CA experiments were performed with a Biologic potentiostat (Model VMP3) and the LSV and the EIS experiments with an Autolab potentiostat (Model PGSTAT302N). The software EC-Lab (Biologic) and Nova (Autolab) were used for setting the electrochemical conditions. For RDE experiments an RDE probe (Hach Lange, Radiometer Analytical) was used. For EIS simulations, EIS Spectrum Analyzer software was used. For product analysis, Waters 2695 Separation module (HPLC and RSpak KC-811 8×300 column) was used to separate the products and Waters 2996 Photodiode Array Detector to detect and quantify formate in the form of formic acid. The samples were previously acidified with HClO<sub>4</sub> and filtered to avoid bubble formation and obstruction in the column, respectively. HClO<sub>4</sub> 0.1% was used as a mobile phase. For the analysis of the impurities, Waters Acquity (Model Arc) Liquid Chromatography – Mass Spectrometry (LC-MS) was used. For computational calculations of the electronic orbitals, ORCA program package was used (see input script in *Chapter 6.5*).

## 6.3 Results and discussion

### 6.3.1 Electrocatalytic reduction of CO<sub>2</sub> in presence of surfactants

First, the behavior of the Sn electrode when it is negatively polarized up to  $-1.1 V_{RHE}$  by performing LSV in saturated KHCO<sub>3</sub> solutions in presence and in the absence (control experiment) of surfactants was evaluated. These surfactants can affect the electrochemical double layer and thus the performance of the eCO<sub>2</sub>R and HER. Additionally, LSV in KHCO<sub>3</sub> electrolyte saturated with N<sub>2</sub> or with CO<sub>2</sub> were performed. This confirmed that the changes saw in the electrochemical response of the system are negligible since the concentration of CO<sub>2</sub> in a saturated KHCO<sub>3</sub> solution is close to the solubility of CO<sub>2</sub> in water were performed (Figure 6.1). Therefore, in a 2 M KHCO<sub>3</sub> solution, bubbling CO<sub>2</sub> is comparable to saturating the solution with an inert gas like N<sub>2</sub>. A drop in the current density is expected when certain surfactants are added to the electrolyte, as surfactants are known to inhibit the HER without affecting the eCO<sub>2</sub>R thereby resulting in lower currents.[182] Those surfactants that decrease the current density in the potential range of eCO<sub>2</sub>R + HER are then considered as HER inhibitors.

When the electrolyte had no additive (KHCO<sub>3</sub> 2 M) two phenomena were observed: a reduction peak from  $-0.2$  to  $-0.4 V_{RHE}$  and an increasing reduction process starting around  $-0.8 V_{RHE}$ . We attribute the first reduction peak to the reduction reaction of the passivated Sn oxide layer that is typically formed when the electrode is in contact with an alkaline solution and the second reduction process to the combined eCO<sub>2</sub>R + HER (Figure 5.3).[189] When the anionic surfactant, SDS, is added to the electrolyte, a similar behavior is observed as the current density remained similar compared to the control electrolyte (49 and 42 mA cm<sup>-2</sup> at  $-1.1 V_{RHE}$  respectively), indicating that anionic surfactants did not migrate to the surface of the cathode when the negative potential was applied due to charge repulsion. For this reason, surfactants bearing the same charge as the electrode will have no significant effect on the composition of the electrochemical double layer and

the performance of the reactions on the surface of the electrode. However, when a cationic surfactant, CTAB, is added, no changes were observed in the reduction peak of Sn oxide but the current density of the  $e\text{CO}_2\text{R} + \text{HER}$  decreased abruptly from 49 to 27  $\text{mA cm}^{-2}$  at  $-1.1 V_{\text{RHE}}$ , confirming the alteration of the electrochemical double layer and the successful HER inhibition. This effect was even more pronounced when the cationic surfactant CKC is added to the electrolyte, decreasing the current density even further to 8  $\text{mA cm}^{-2}$ . However, in the presence of CKC a new reduction peak is observed from  $-0.7$  to  $-0.9 V_{\text{RHE}}$ , which was still unreported in literature.

To confirm that the decrease in current density is ascribed to an inhibition of the HER, one-hour CA experiments were performed at  $-0.9 V_{\text{RHE}}$  and the  $\text{FE}_{\text{Formate}}$  and the partial current density were determined. After the results obtained in the previous chapter, a working potential of  $-0.9 V_{\text{RHE}}$ , the best performance, was chosen. The effect of shifting the potential on the  $\text{FE}_{\text{Formate}}$  and the current density were the same in electrolytes containing surfactants or in their absence (increasing the potential leads to an increase of the current density and a decrease in the  $\text{FE}_{\text{Formate}}$ ). Therefore, the working potential at the frame of study was concluded to not have a significant impact in the performance of the surfactant in our system.

The results obtained showed a clear increase in  $\text{FE}_{\text{Formate}}$  and a drastic decrease in the partial current density of HER ( $\text{CD}_{\text{HER}}$ ) upon addition of CTAB and CKC confirming the HER inhibition (Figure 6.2). The higher HER inhibition ability of CKC over CTAB was also confirmed ( $\text{FE}_{\text{Formate}}$  was 66 and 39% and  $\text{CD}_{\text{HER}}$  was 2.40 and 3.95  $\text{mA cm}^{-2}$ , respectively). In addition, the lack of impact of SDS on the performance was observed as well ( $\text{FE}_{\text{Formate}}$  was 5% for both SDS and control experiment). On the other hand, the partial current density of the  $e\text{CO}_2\text{R}$  to formate ( $\text{CD}_{\text{Formate}}$ ) remained similar (or even increased) in every experiment proving that the inhibition effect is selective for the HER. Since the main difference between CTAB and CKC is the benzyl functionalization of the quaternary amine, it is subsequently deduced that the higher HER inhibition observed in presence of CKC

comes from the direct effect of the benzyl groups in the electrochemical double layer or it is a consequence of the apparition of the CKC exclusive reduction peak. However, up until now, both the effect of benzyl groups to inhibit HER and the nature of the previously mentioned reduction peak were unknown and unreported in literature. Thus, it was still unconfirmed if the presence of the extra reduction process observed in CKC was linked with HER inhibition or if it was a consequence of the benzyl functionalization of the cationic surfactant (less likely). To further explain these effects a study on both the nature of the characteristic reduction process and the effect of benzyl groups on HER inhibition was performed.

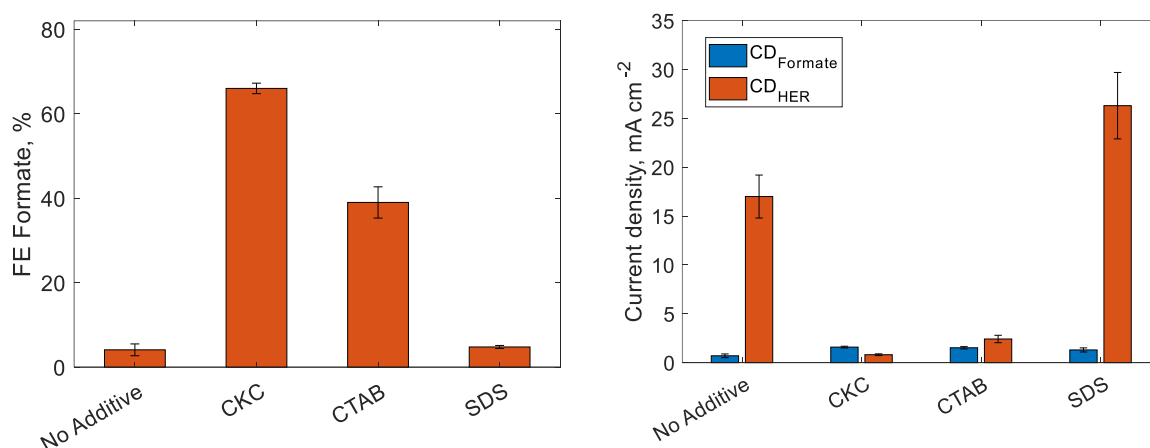


**Figure 6.2.** LSV at  $10 \text{ mV s}^{-1}$  of a Sn electrode in  $\text{KHCO}_3$  2 M in presence or in the absence of different surfactants (left)  $\text{FE}_{\text{Formate}}$  after 1 h electrolysis and c) Partial current density for formate and  $\text{H}_2$  production after one hour CA of a Sn electrode in  $\text{KHCO}_3$  2 M in presence and in the absence of 1 mM of different surfactants (right).

### 6.3.2 Study of the surfactant-electrode interface by Linear Sweep Voltammetry

It is not straightforward to determine what species was being reduced or which mechanism is taking place in the presence of CKC at  $-0.7 \text{ V}_{\text{RHE}}$ , especially because the peak did not occur in the presence of CTAB and CKC is known to be a very stable molecule. For this reason, it is hypothesized that neither any methyl from the 16-alkyl chain nor the

quaternary amine of the polar head were reduced at this potential. Then, only the benzyl group or some undetermined impurity product of the synthesis of CKC (up to 5% of the product, 50  $\mu\text{M}$  when using 1 mM of CKC) not present in CTAB is the species that is being reduced. To unravel the nature of this reduction peak, first the impact of a change in concentration of CKC present in the electrolyte was investigated. We observed that although the reduction process corresponding to  $\text{eCO}_2\text{R} + \text{HER}$  was sensitive to the concentration of CKC (the current density slightly decreased as the concentration of CKC increased), the unknown reduction reaction had a similar charge for each concentration of CKC used (Figure 5.5). This should thus mean that there was a saturation of reactant even at low concentration of CKC (0.5 mM) or that the formed product was not desorbed from the surface, and rather saturating it and preventing new reactants to be adsorbed and to react. This product might then have stayed or be desorbed at higher potentials, in both cases allowing  $\text{eCO}_2\text{R}$  and HER to occur at their typical (lower) potential (i.e.,  $-0.9 V_{\text{RHE}}$ ).

To investigate the impact of the nature of the electrode material on this peak, we then used a different electrocatalyst, namely Cu, and evaluated its performance in presence and absence of CKC or CTAB in the electrolyte. It was observed that, when using Cu as cathode and CKC as surfactant, two main changes occurred in the experiment. First, the passivation reduction peak present in Sn electrodes was not visible for Cu electrodes, indicating that if there was a passivation layer formed after the surface was in contact with the alkaline solution, it was thin enough to be reduced immediately after applying the potential. Secondly, the CKC characteristic reduction peak was not present (Figure 6.3). The decrease in current density on the other hand, was present when using Cu electrodes either when using CTAB or CKC at different concentrations, thus indicating that HER inhibition occurs in a similar way as when Sn was used as the cathode. Indeed, the current density dropped from 97 to 67  $\text{mA cm}^{-2}$  and 40  $\text{mA cm}^{-2}$  at  $-1.0 V_{\text{RHE}}$  when using CTAB and CKC, respectively.

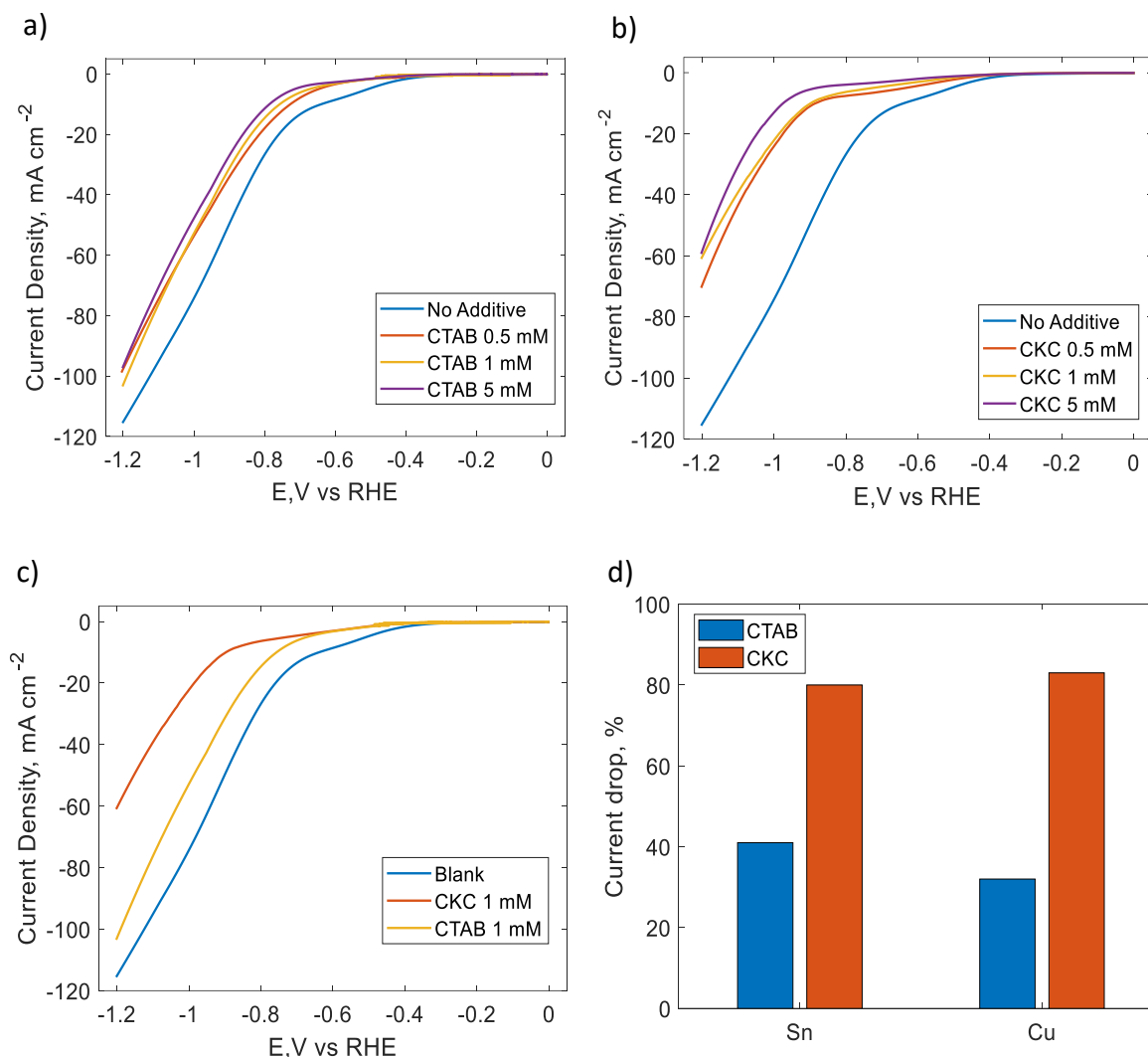


**Figure 6.3.** LSV at 10 mV s<sup>-1</sup> of a Cu electrode in KHCO<sub>3</sub> 2 M in presence and in the absence of a) CTAB and b) CKC. c) LSV at 10 mV s<sup>-1</sup> of a Cu electrode in KHCO<sub>3</sub> 2 M in presence and in the absence of 1 mM of CTAB and CKC. d) Current drop observed at -1.0 V<sub>RHE</sub> when adding CTAB or CKC in a LSV experiment using Sn or Cu as cathode.

We can therefore conclude that the cationic surfactants were also taking part in the electrochemical double layer like they did for Sn. The HER inhibition even followed the same trend when varying the concentration of cationic surfactant (Figure 6.3a and 6.3b). In fact, if we compare the current drop (directly related to HER) at a fixed potential when using Sn or Cu as cathode (setting the current



density at  $-0.9 V_{RHE}$  in the experiment without any additive at 100%) we can observe how it is identical for both electrodes ( $\sim 40$  and  $\sim 80\%$  for CTAB and CKC respectively at  $-0.9 V_{RHE}$ , Figure 6.3d). Based on these observations, we can conclude that: 1) the formation of the characteristic reduction peak of CKC is not generalized for every electrode and it might come then from the intrinsic properties of the Sn electrode and 2) the formation of the characteristic reduction peak of CKC in Sn electrodes is not the main reason of the high HER inhibition properties of the cationic surfactant CKC since HER inhibition is apparently equally effective for Cu electrodes either by using CTAB or CKC.

We then turned back our attention to the role of the passivation layer (present for Sn in alkaline solutions) in the presence of the unknown reduction reaction at  $-0.7 V_{RHE}$ . It has been reported that metallic Sn is not highly active for  $eCO_2R$ , although presenting  $FE_{Formate}$  over 90% in many reports.[190–192] Instead, a metastable oxide layer (in the form of Sn(II) oxyhydroxide) is formed during the reduction process, activating the electrode and acting as an active site for the  $CO_2$  electrochemical reduction to formate.[193,194] In our system, the Sn oxide metastable layer must have therefore been present as well after the reduction of the passivation layer at  $-0.2 V_{RHE}$ .

To confirm the presence of this metastable layer all along the potential range we performed LSV of a Sn electrode in  $KHCO_3$  (2 M) but this time when rotating the electrode at different speeds. If the Sn oxyhydroxide layer was metastable, then reducing the size of the diffusion layer by increasing rotation speed would have allowed fresh alkaline electrolyte to better reach the surface and passivate the Sn again at the same time as it was being reduced due to the negative potential, thereby increasing the reduction peak of the passivation layer and forming a plateau right after the maximum of the peak. As observed in Figure 6.4, the reduction peak related to the passivation layer increased as the rotation speed

increased and the plateau was formed, indicating that Sn oxide was formed and reduced at the same time. Hence, we can assume that during every experiment using Sn and all along the potential range, there was a metastable oxyhydroxide layer between the metallic Sn and the bulk electrolyte as the alkaline electrolyte is ever present and will keep passivating the surface. The species that interacted with the surface (H<sub>2</sub>O, CO<sub>2</sub> or the surfactant) they thus did it with the oxyhydroxide layer instead of with the metallic Sn surface. We could also observe how the current density at eCO<sub>2</sub>R + HER reduction potentials increased as the rotating speed increased (from 25 to 37 mA cm<sup>-2</sup>), confirming that HER is a mass transfer limited reaction as has been reported previously.[162]

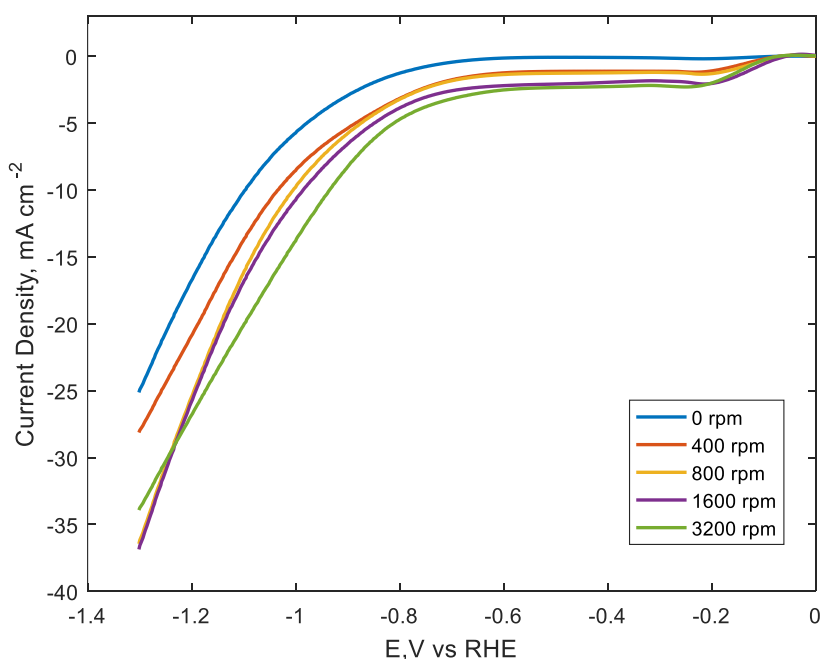


**Figure 6.4.** LSV at 1 mV s<sup>-1</sup> of a Sn RDE electrode in KHCO<sub>3</sub> 2 M while rotating the electrode at different speeds (0 – 3200 rpm).

Afterwards, CKC was added to the electrolyte and the experiment was repeated at the same conditions and rotation speeds. We observed that, this time, the current density of the CKC characteristic reduction peak increased substantially when the

rotation speed went from 0 to 400 and 800 rpm, increasing from  $2 \text{ mA cm}^{-2}$  to 17 and  $18 \text{ mA cm}^{-2}$  respectively. The current density at 1600 and 3200 rpm was also increased ( $16$  and  $12 \text{ mA cm}^{-2}$ , respectively) but less than when rotating at 400 or 800 rpm (Figure 6.5, left). When half the amount of CKC was used, the same effects were observed (Figure 6.5, right) and the same current density/rotation speed patterns were followed (higher increase in current with 400 and 800 rpm, smaller current increase with 1600 and 3200 rpm) although this time, the increase of the current of the reduction peak was halved as compared to the previous experiment ( $9$  and  $18 \text{ mA cm}^{-2}$  at 800 rpm with  $0.5$  and  $1 \text{ mM}$  of CKC respectively) (Figure 6.6).

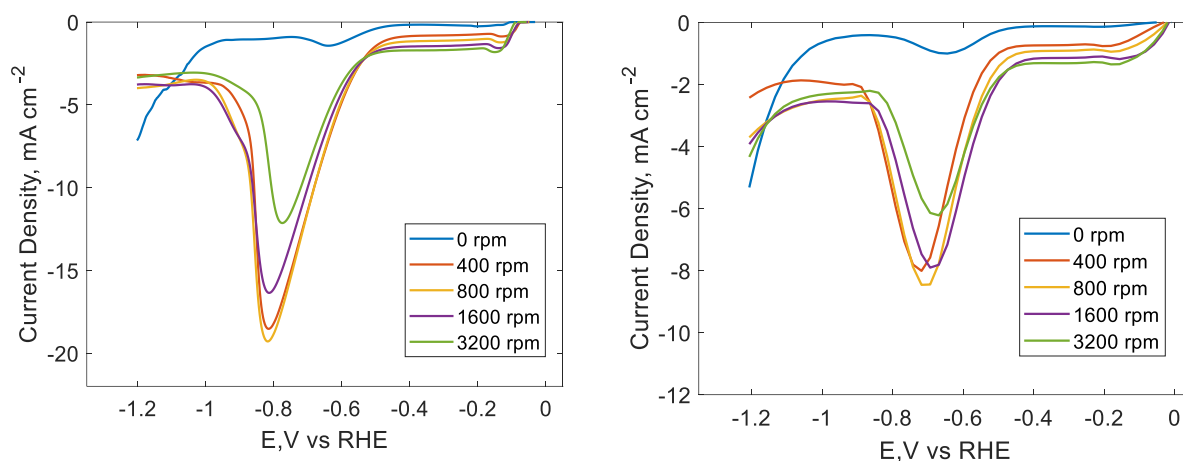


**Figure 6.5.** LSV at  $1 \text{ mV s}^{-1}$  of a Sn RDE electrode in  $\text{KHCO}_3$   $2 \text{ M}$  while rotating the electrode at different speeds in presence of  $1 \text{ mM}$  CKC (left) and  $0.5 \text{ mM}$  CKC (right).

We could confirm that the overall increase in the current density of the reduction peak was caused by the decrease of the diffusion boundary layer thickness and therefore concluded that the reduction process occurring at  $-0.7V_{\text{RHE}}$  is diffusion limited. However, the fact that a maximum current density is achieved at intermediate rotation speeds (800 rpm) indicates that once the rotation speed becomes too high, the reactant does not have enough time to adsorb and gets dragged away from the surface, thereby suggesting a rate limiting adsorption step and confirming that the occurring reduction requires an adsorption step. At 400

and 800 rpm, the diffusion layer was thinner allowing more reactant to reach the surface and the rotating speed was low enough to avoid the reactant from being carried away from the surface prior to adsorption. This conclusion is also supported by the following: we only observed the effect of increasing CKC concentrations on the increase of current density of the characteristic reduction peak when we rotate the electrode (current density for both 1 mM and 0.5 mM of CKC at 0 rpm was 2 mA cm<sup>-2</sup>), supporting both statements for the diffusion limited reaction and the irreversible chemisorption of the reactant. The reduction reaction mechanism must have thus been initiated by the irreversible chemisorption of the reactant to the passivated Sn surface, which was then electrochemically reduced and remained on the surface.

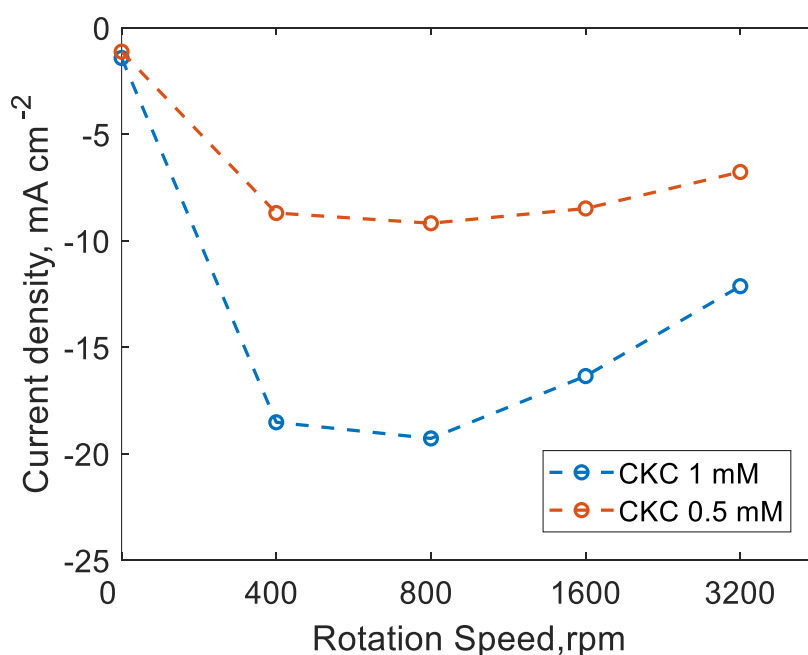


**Figure 6.6.** Comparison of the highest current density reached for the CKC characteristic reduction peak between 1 mM and 0.5 mM CKC when rotating at different speeds.

### 6.3.3 Determination of the hydrophobicity of the electrode by electrochemical impedance spectroscopy

We were able to confirm the formation of a partial coating made of the adsorbed product and the changes made to the electrochemical double layer after the surfactants were added to the electrolyte by performing EIS in systems in the presence and in the absence of surfactants within the potential range where the characteristic reduction reaction of CKC appeared. For an electrolyte in the absence of a surfactant, in presence of CTAB and in presence of SDS, the equivalent electrical circuit model used to fit the experimental data is shown in Figure A.7. This model is usually applied in systems where there is a formation of a single electrochemical double layer between the charged electrode and the bulk electrolyte (see *Annex A.2.4*), thus showing a single capacitor (shown as CPE). This model was suitable to fit the experimental data for the whole potential range and for all cases in presence and absence of a surfactant (Figure 6.15-17). The measured impedance and the calculated phase shift values (Figure 6.7) showed that CTAB was taking part in the electrochemical double layer since the phase shift decreased from one system to another (from 25 to 5 degrees at  $-1.0 V_{RHE}$ ). On the other hand, little changes in the phase shift were observed when SDS was present proving once more that SDS did not take part in the IHP. However, the phase shift did decrease slightly (from 28 to 20 degrees at  $-1.0 V_{RHE}$ ) suggesting that SDS took part of the OHP only because of its nature as an anionic species, thus changing the capacitor properties.

When CKC was in the system, the equivalent electrical circuit model shown in Figure A.7 was not valid anymore, which is in accordance with the conclusions made up to this point as to the different mechanism through which CKC interacts with the electrode. We propose a model where a coating was partially formed (due to the adsorption product which is formed in presence of CKC and is irreversibly adsorbed) on the surface thus acting as a second capacitor ( $C_c$ ) in parallel to the capacitor formed after the arrangement of the electrochemical double layer (Figure 6.8). The model was only valid for the points

measured at -0.6, -0.7 and -0.8 V<sub>RHE</sub>, coinciding with the potentials where the reduction starts (-0.6 V<sub>RHE</sub>), is charged transfer limited (-0.7 V<sub>RHE</sub>) and reaches the diffusion or, as we concluded earlier, the saturation of the surface (-0.8 V<sub>RHE</sub>). From -0.8 V<sub>RHE</sub> onwards, the equivalent electric circuit model shown in Figure A.7 was valid again, indicating either the complete coating of the surface by the adsorbed product or the detachment of the partial coating, therefore turning the system back to one capacitor (C<sub>c</sub> or CPE) (Figure 6.18).

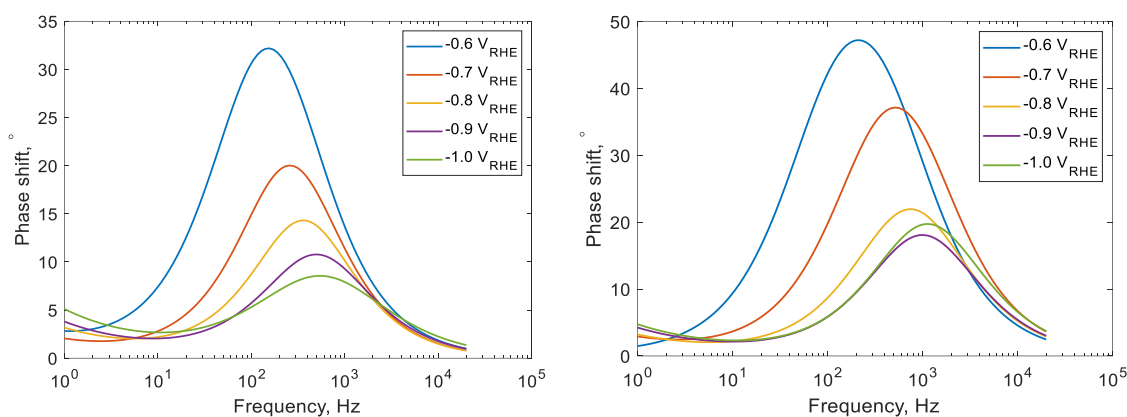


**Figure 6.7.** Phase shift at different frequencies extracted from the EIS of a Sn electrode in KHCO<sub>3</sub> 2 M in presence of 1 mM of CTAB (left) or SDS (right).

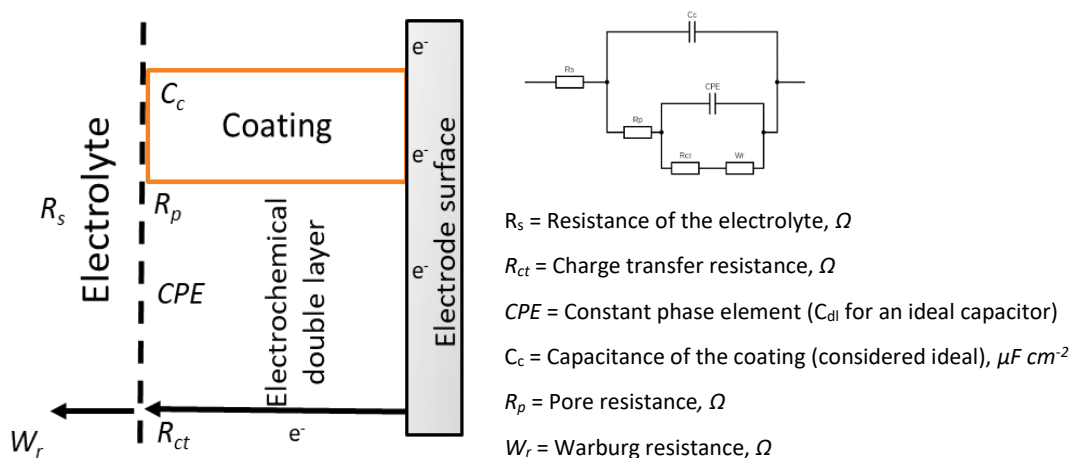


**Figure 6.8.** Equivalent electrical circuit model used for the EIS simulations to fit the experimental data of systems in presence of CKC. A Warburg resistor was added after  $R_{ct}$  at potentials -0.9 and -1.0 V<sub>RHE</sub>.

The phase shift calculations showed a second peak forming at high frequencies starting from  $-0.6 V_{RHE}$ , indicating the formation of a new capacitor ( $C_c$ ). The peak increased as the potential increased, while the corresponding peak for the capacitor of the initial electrochemical double layer formed (CPE) decreased. At  $-0.9$  and  $-1.0 V_{RHE}$ , only the second peak formed (formerly  $C_c$ , now CPE) corresponding to the coating, appeared in the system indicating that the surface was completely coated and the main capacitor of the system was then  $C_c$  (Figure 6.9). The Nyquist plots generally indicate higher resistance in the presence of cationic surfactants than in the absence. This is particularly visible at high negative potentials (vs RHE). This confirms the successful formation of the hydrophobic layer of the electrode, but it also means an increase in the overpotential of the reaction (Ohm's law). However, the gain in the  $FE_{Formate}$  while using surfactants (66% compared to 5% in control experiments) is larger than the increase in overpotential and thus warrants the use of surfactants in this current system.

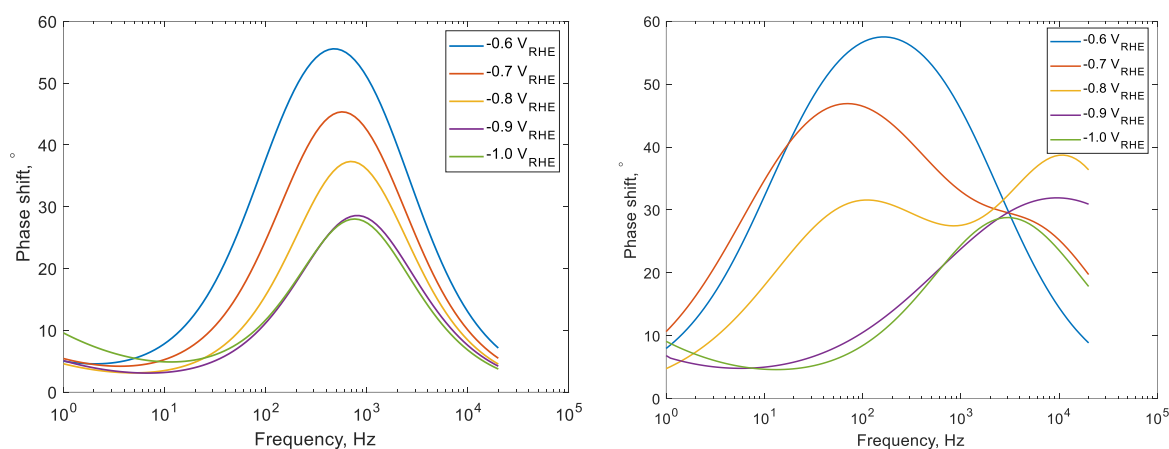


**Figure 6.9.** Phase shift at different frequencies extracted from the EIS of a Sn electrode in  $KHCO_3$  2 M in the absence of surfactant (left) and in presence of 1 mM of CKC (right).

Calculating the DL-capacitance from the EIS data allowed to evaluate the effect of each surfactant on the hydrophobicity of the electrode surface. A high hydrophobic surface presents a lower capacitance, since it becomes less permeable, and is thus more suitable for  $eCO_2R$  and less active for HER since it is harder for polar molecules such as  $H_2O$  and  $HCO_3^-$  to reach the surface of the electrode. As expected, CTAB and CKC decreased the

DL-capacitance while SDS had little effect on it (Figure 6.10). This agrees with the HER inhibition properties observed for each surfactant. CKC presented the lowest DL-capacitance and highest HER inhibition ( $3 \mu\text{F cm}^{-2}$  and 34%  $\text{FE}_{\text{HER}}$  at  $-0.9 V_{\text{RHE}}$ , respectively) followed by CTAB ( $14 \mu\text{F cm}^{-2}$  and 61%  $\text{FE}_{\text{HER}}$  at  $-0.9 V_{\text{RHE}}$ , respectively). SDS slightly increased the DL-capacitance ( $27 \mu\text{F cm}^{-2}$  compared to  $23 \mu\text{F cm}^{-2}$  of control electrolyte at  $-0.9 V_{\text{RHE}}$ ) but had no effect on HER inhibition (95%  $\text{FE}_{\text{HER}}$  both for SDS and control electrolyte). From  $-0.6$  to  $-0.8 V_{\text{RHE}}$ , CKC presented an increase in the DL-capacitance due to the ongoing reduction process at these potentials. As a control experiment, EIS experiments were also performed on Cu and the DL-capacitance was calculated. This time, regardless of the applied potential, the equivalent circuit model shown in Figure A.7 was used to fit the experimental data since a capacitor corresponding to the formation of a coating ( $C_c$ ) was not observed (Figure 6.11) in accordance with previous observations (absence of extra reduction peak in presence of CKC). This was further confirmed by the calculated DL-capacitance as it did not show an increase in capacitance with respect to the blank electrolyte (as was the case for Sn) and therefore confirms that no coating was formed. The DL-capacitance when using CKC however is lower than when using CTAB ( $21$  and  $63 \mu\text{F cm}^{-2}$  at  $-0.9 V_{\text{RHE}}$  respectively), following the same trend as the Sn electrodes, meaning that the formation of the coating might then not be essential towards obtaining a highly hydrophobic layer on the electrode in the presence of CKC and thus in the HER inhibition properties of CKC.

Since the formation of the coating was specific for the Sn electrodes but the high hydrophobic properties of CKC were observable both in Sn and Cu electrodes, the promoted properties of CKC might thus come from the interaction of the benzyl group with the electrochemical double layer. On the other hand, the presence of a reduction reaction when using Sn electrodes might come from one of the untagged impurities present in CKC that are not present in CTAB. This impurity must be electrochemically active and potentially reactive to the Sn oxyhydroxide layer. Both claims will be investigated further in what follows.



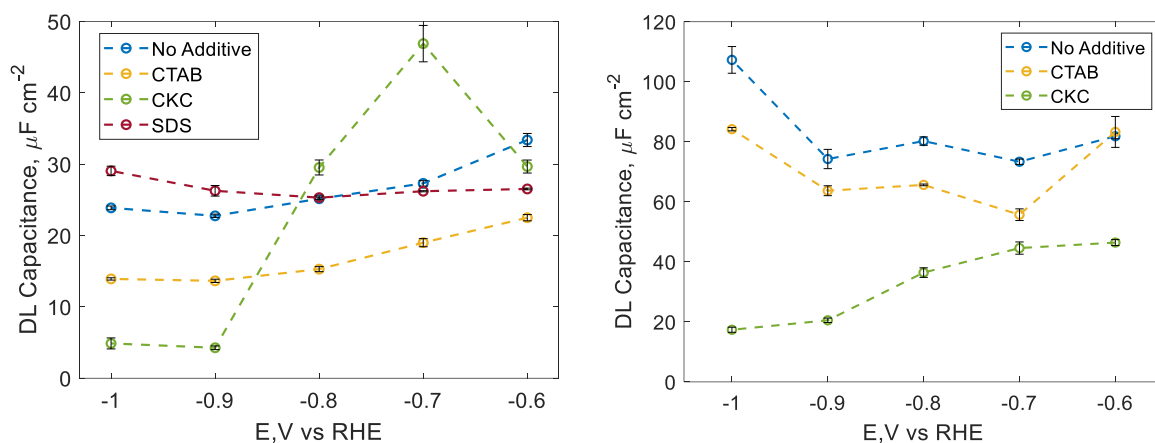


**Figure 6.10.** Double-layer Capacitance extracted by modelling EIS of a Sn electrode (left) and Cu electrode (right) in  $\text{KHCO}_3$  2 M solutions in presence and in the absence of 1 mM of different surfactants.

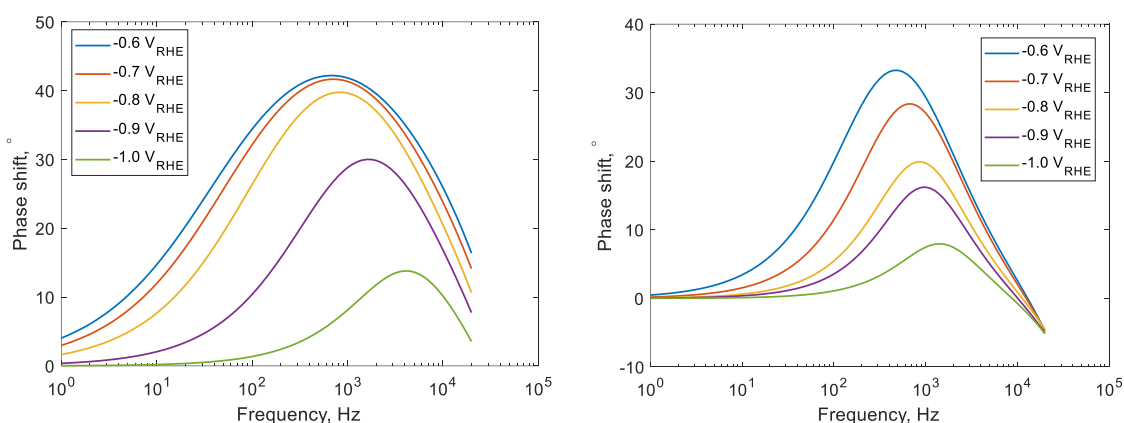


**Figure 6.11.** Phase shift at different frequencies extracted from the EIS of a Cu electrode in  $\text{KHCO}_3$  2 M in the absence (left) and in presence of 1 mM of CKC (right).

### 6.3.4 Benzyl functional groups as HER inhibitor promoters

We first evaluated if benzyl groups themselves can partially inhibit the HER in a similar way cationic surfactant does by comparing the current density drop when the electrolyte contained CKC or benzyl trimethylammonium chloride (BTAC). BTAC has the same structure as CKC, but the alkyl chain is substituted by a methyl group. If the benzyl group would not be active, we could therefore expect that the HER inhibition effects are not

present anymore for BTAC since the hydrophobic alkyl layer would no longer extend to the OHP. LSV experiments however showed how BTAC was able to decrease the current density to a great extent compared to control experiments without surfactant but not as much as CKC (17, 43 and 9 mA cm<sup>-2</sup> at -1.0 V<sub>RHE</sub>, respectively), meaning that the surface was partially hydrophobic when BTAC was present in the electrolyte (Figure 6.12). Since we did not observe the characteristic reduction peak of CKC at -0.7 V<sub>RHE</sub>, we could once again confirm that the benzyl group of CKC is not being reduced, as supported by the previous statements. The explanation behind the observed inhibition in presence of benzyl groups can be found in literature. Indeed, it has been reported that benzene has hydrophobic properties and can interact with cationic species (for instance, the ones present in the IHP or the positively charged amine from the surfactant) to form firm hydrophobic films on top of the surface of the electrode.[195] We confirmed this statement by performing LSV experiments with electrolytes containing acetophenone, benzaldehyde and benzyl bromide, which all contain a benzyl group.

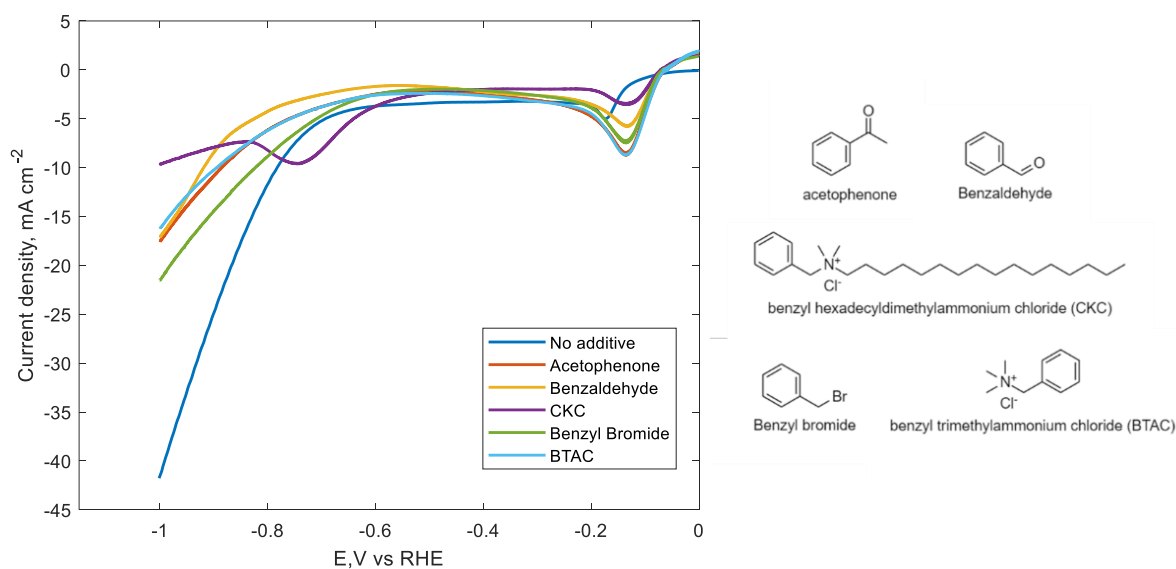


**Figure 6.12.** LSV at 10 mV s<sup>-1</sup> of a Sn electrode in KHCO<sub>3</sub> 2 M in presence and in the absence of 1 mM of benzyl-functionalized substances (left) and structure of the benzyl-functionalized species used (right).

All of them presented a clear decrease in the current density (from 43 to 17, 17 and 22 mA cm<sup>-2</sup> at -1.0 V<sub>RHE</sub>, respectively) proving the hydrophobic effect of benzyl containing substances. It can thus be concluded that the high hydrophobic property of CKC came both from the rearrangement of the alkyl chain in the OHP (also observable in CTAB) and the intrinsic ability of benzyl groups to form hydrophobic layers on top of the negatively polarized electrode (also observable in benzyl-functionalized molecules), explaining why CKC has a higher HER inhibition ability compared to CTAB and benzyl-containing molecules.

### 6.3.5 Impurities in surfactants: analysis and electrochemical consequences

Since we concluded that (1) the HER inhibition ability of CKC came from the intrinsic hydrophobic properties of the rearrangement of the surfactant in the electrochemical double layer and not due to the formation of the coating after the reduction process observed at -0.7 V<sub>RHE</sub>, and (2) the functional groups present in CKC are electrochemically inactive (benzyl group, quaternary amine and alkyl chain), it thus suggests that the reduction process in presence of CKC over Sn might have come from one of the impurities present in a CKC solution. CKC is currently delivered with a 95% purity, the remaining 5% being water and untagged impurities derived from the synthesis of the surfactant. To find the electrochemical active impurity, present in a CKC solution we performed LC-MS (see analytical data in the supportive information). Three major impurities were found: N-benzyl dodecan-1-amine, benzyl dimethyldodecylammonium and N-benzylhexadecan-1-amine. On the other hand, CTAB presents a purity of 98% and two major impurities were found: heptadecyltrimethylammonium and octadecyl trimethylammonium (Figure 6.13).

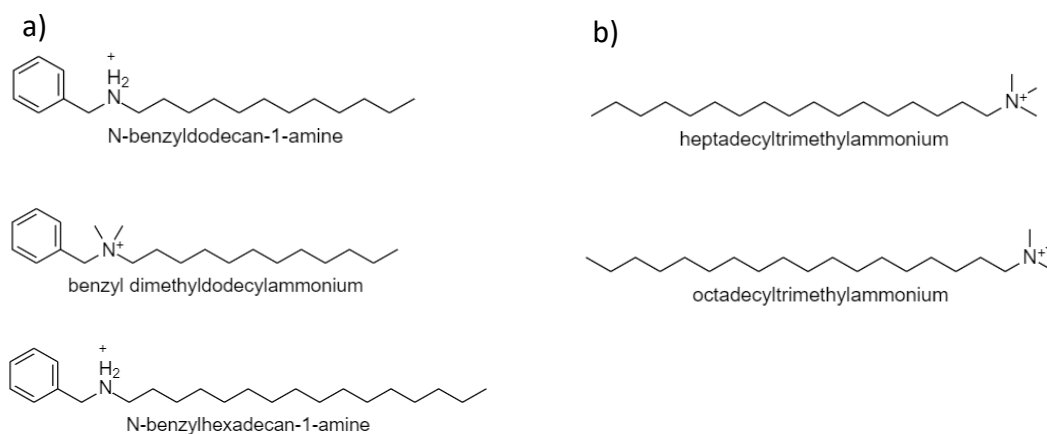


**Figure 6.13.** Structure and identity of the impurities found in (a) CKC and (b) CTAB.

Thus, the electrochemical active impurity from CKC must be one of the secondary amines, or both, since they are not present in CTAB and present a potential reactive site, namely the charged amine. This charged amine would selectively react with the oxyhydroxide surface of Sn, thus giving the corresponding reduction peak.

**Table 6.1.** LUMO energy of CKC, CTAB and the impurities found.

Surfactant	LUMO Energy (eV)
<b>Benzyl dimethylhexadecylammonium (CKC)</b>	-0.200
<b>Hexadecyltrimethylammonium (CTAB)</b>	0.083
<b>N-benzyl dodecan-1-amine</b>	3.726
<b>N-benzylhexadecan-1-amine</b>	3.728
<b>Benzyl dimethyldodecylammonium</b>	-0.203
<b>Heptadecyl trimethylammonium</b>	0.083
<b>Octadecyl trimethylammonium</b>	0.084

Unfortunately, both of the molecules are hardly available in the market to be tested independently and, since the main objective of this manuscript was to evaluate the effect of benzyl groups in cationic surfactants, we only looked at the electron affinity of each

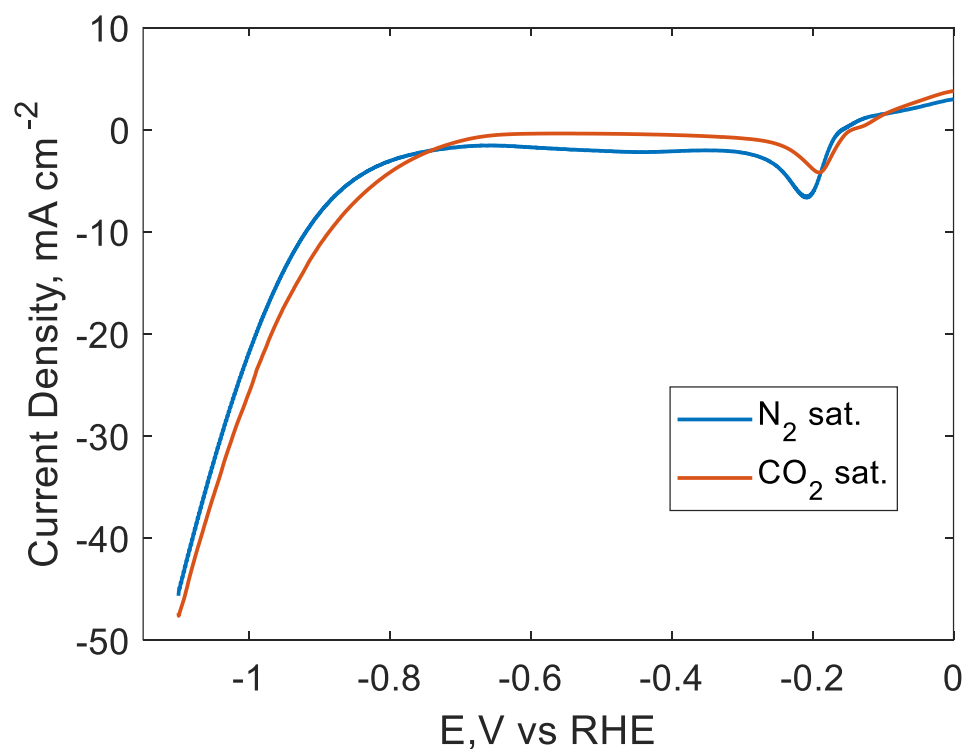
molecule by calculating the energy of the Lowest Unoccupied Molecular Orbital (LUMO), which, although it cannot be used to calculate reduction potentials it gives an approximation of which molecules are more prone to reduce compared to others under the same conditions.[196] A table of the calculated LUMO energies is shown in Table 6.1. These calculations confirm that the amines are more likely to be reduced (i.e., higher LUMO energy) and thus are firm candidates to be the molecules that were reduced in systems involving CKC. Nevertheless, the exact reduction mechanism is still unclear (for instance, the electron transfer mechanism or the product formation) and further study probably involving spectroscopic techniques is needed to determine exactly the mechanism undergoing when the oxyhydroxide layer reacts with the secondary amine present in solution. Nevertheless, although these amines are strong candidates to be the responsible of the electrochemical behavior observed in the data, there are other scenarios to be considered other than the reduction of these impurities. For instance, not the electrochemical reduction but the re-organization of the surfactant layer on the surface of the electrode could be the responsible for such observations. Further experimentation is needed (and worth for future work) to determine the role of these impurities in electrochemical systems.

## 6.4 Conclusions

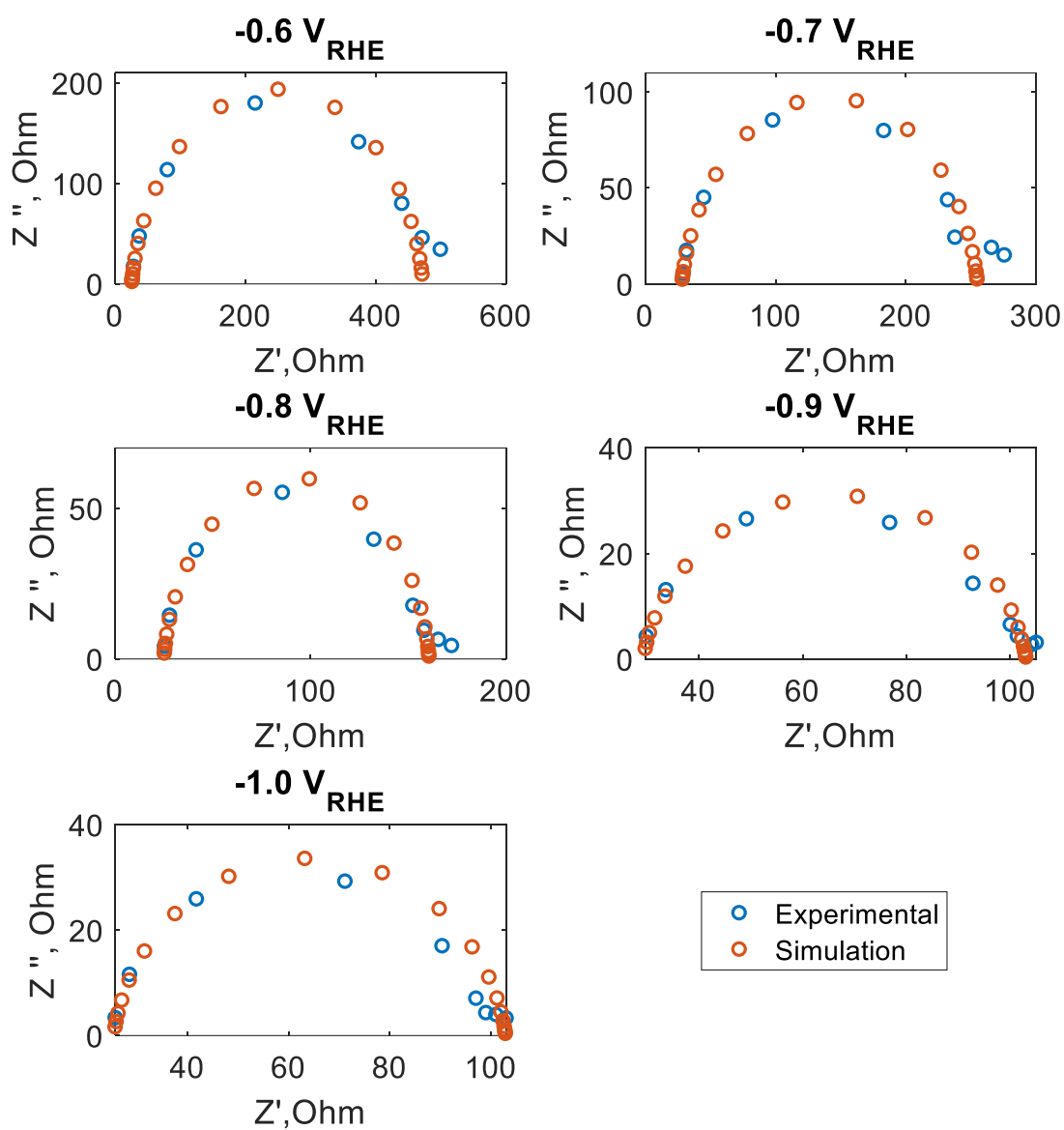
Cationic surfactants, mainly CTAB, are widely used in electrocatalysis to make the surface hydrophobic and inhibit the HER to promote targeted electrocatalytic reactions like  $e\text{CO}_2\text{R}$ . For instance, the use of CTAB for this application has been extensively reported within the last years. However, little research was done on its modification. We proved how, by substituting one of the methyl groups from the quaternary amine of CTAB for a benzyl group, the hydrophobicity of the surface of the electrode increased even more than when using CTAB, thus promoting the  $e\text{CO}_2\text{R}$  over HER to a greater extent (partial current density towards HER is drastically decreased and  $\text{FE}_{\text{Formate}}$  is increased from 39 to 66% in  $\text{KHCO}_3$  electrolytes). By studying the electrochemical properties of the surface of

the electrode in presence of this cationic surfactant, CKC, we observed how the benzyl group acted in a similar way as the 16-carbon chain did. For instance, the DL-capacitance of a CKC containing electrolyte is lower than a CTAB containing electrolyte ( $3 \mu\text{F cm}^{-2}$  and  $14 \mu\text{F cm}^{-2}$  at  $-0.9 V_{\text{RHE}}$ , respectively), proving the increased impermeability of the electrode when exposed to CKC. Nevertheless, we must also consider the effects of adding additional functional groups to the surfactant such as steric effects, hindrance, ionic interactions.... (e.g., the EDL disposition changes with the composition of the surfactant and thus change the electrochemical activity of the system). For future work it is important to do further research in surface analysis to elaborate a proper theory on the effect of these additional functional groups to the structure of the EDL. We also showed how impurities, commonly present in many commercial surfactants, even at low percentage, can affect the evaluation of a system and that they must be considered when working with surfactants, especially in highly sensitive systems like electrochemical systems. In the experiments shown in this manuscript, one of the impurities of CKC (N-benzyl-N-alkyl-1-amine) influenced the early evaluation of the results but the later evaluation and characterization of the impurity showed that it had no effect on the functionality of the CKC and the characteristic hydrophobic properties of it.

## 6.5 Supporting information

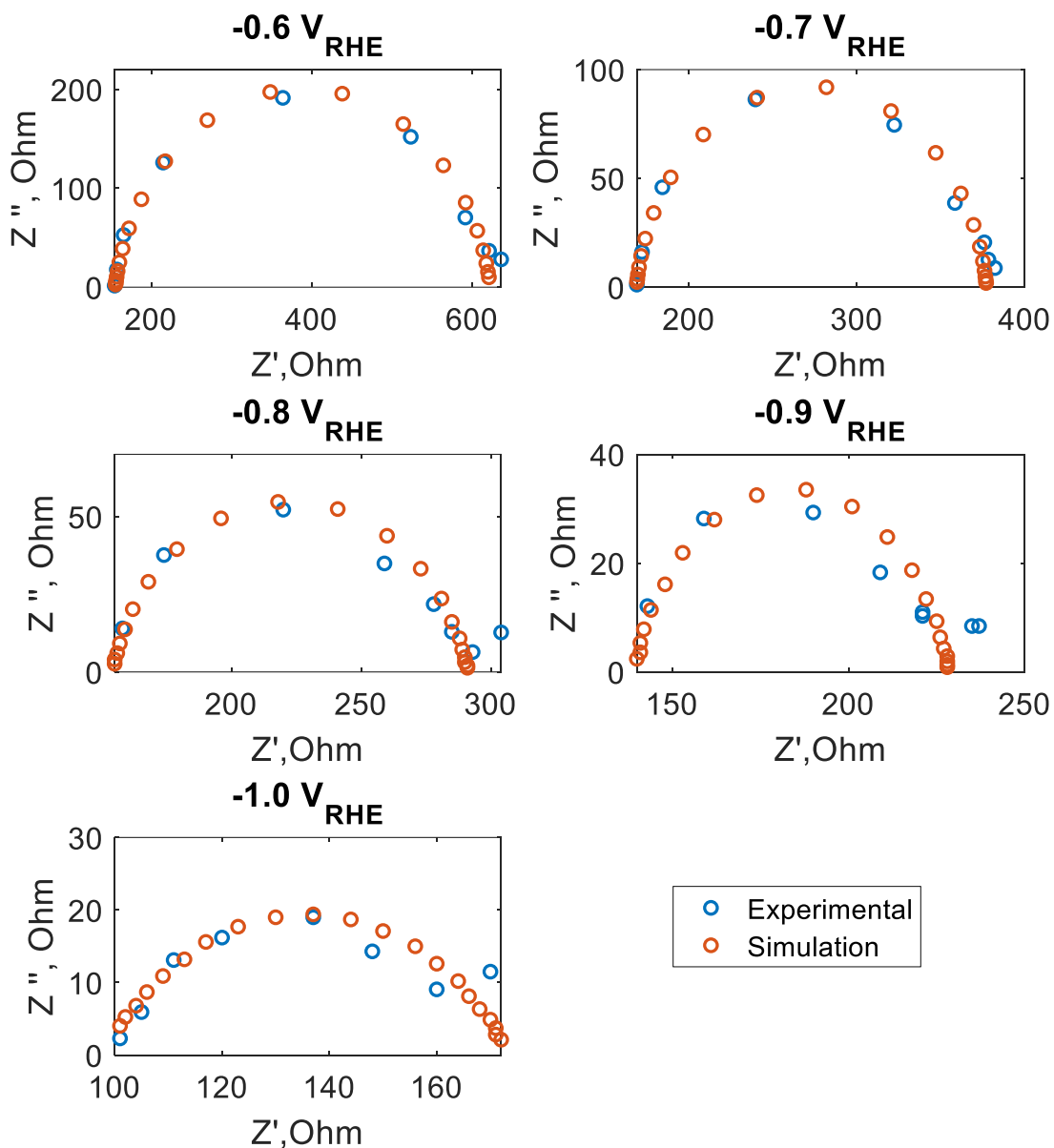


**Figure 6.14.** LSV at  $10 \text{ mV s}^{-1}$  of a Sn RDE electrode in  $\text{KHCO}_3$  2 M previously saturated with  $\text{N}_2$  (blue) or  $\text{CO}_2$  (orange).

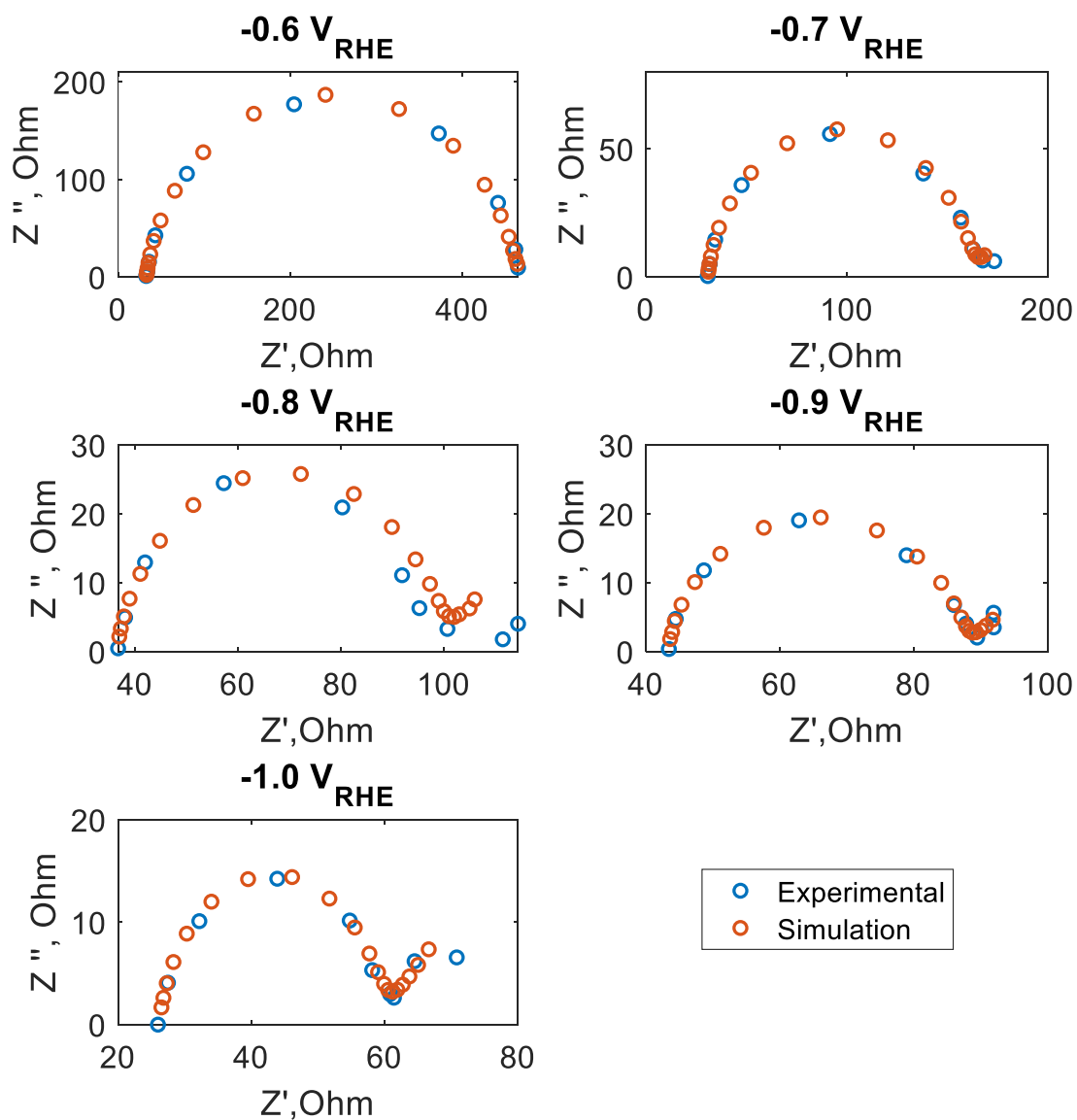


**Figure 6.15.** Nyquist plot (experimental and simulation) for EIS experiments carried out in  $\text{KHCO}_3$  2 M electrolyte and using a Sn electrode in the absence of surfactants.

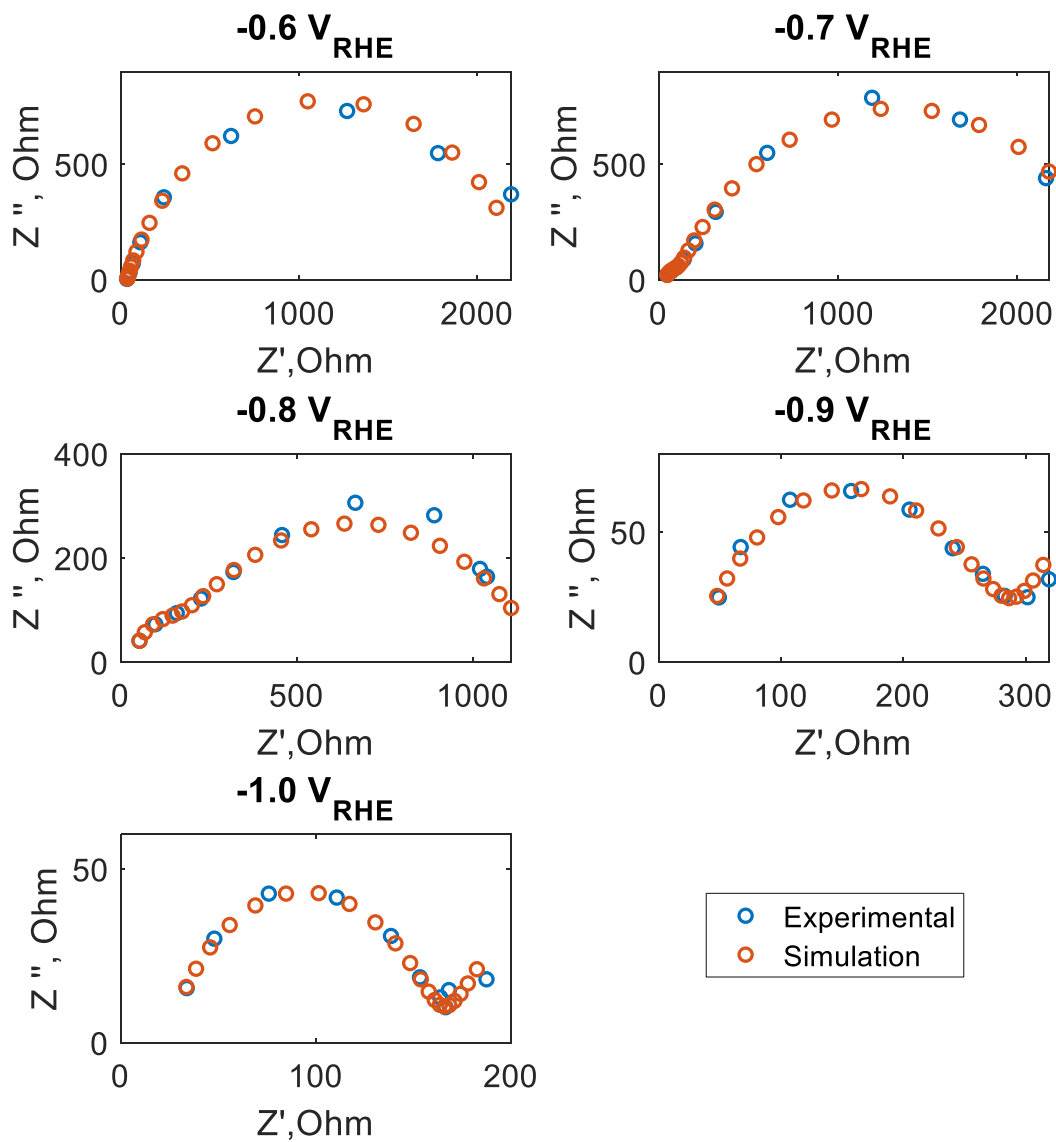




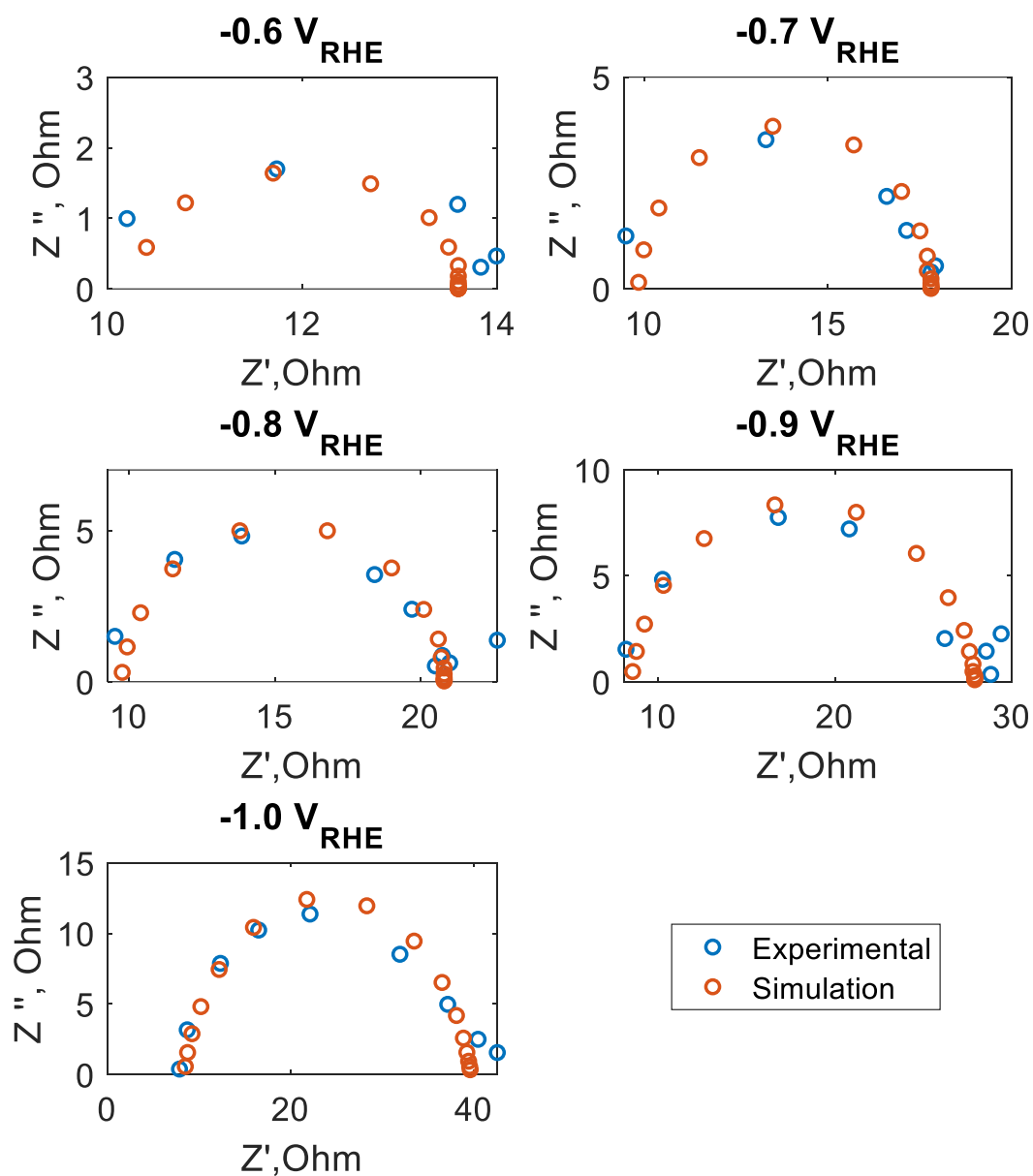
**Figure 6.16.** Nyquist plot (experimental and simulation) for EIS experiments carried out in  $KHCO_3$  2 M electrolyte and using a Sn electrode in presence of 1 mM CTAB.



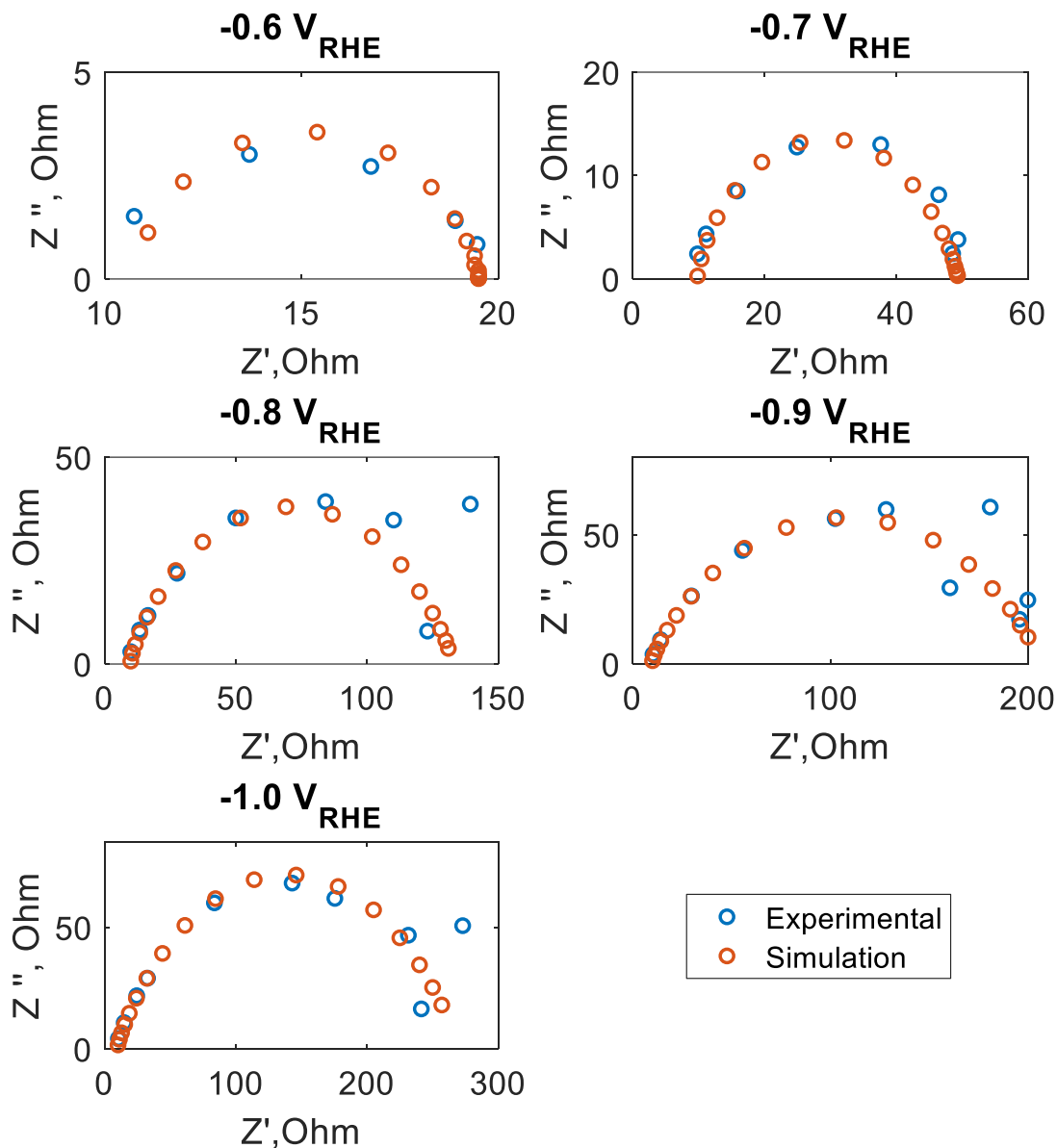
**Figure 6.17.** Nyquist plot (experimental and simulation) for EIS experiments carried out in  $\text{KHCO}_3$  2 M electrolyte and using a Sn electrode in presence of 1 mM SDS.



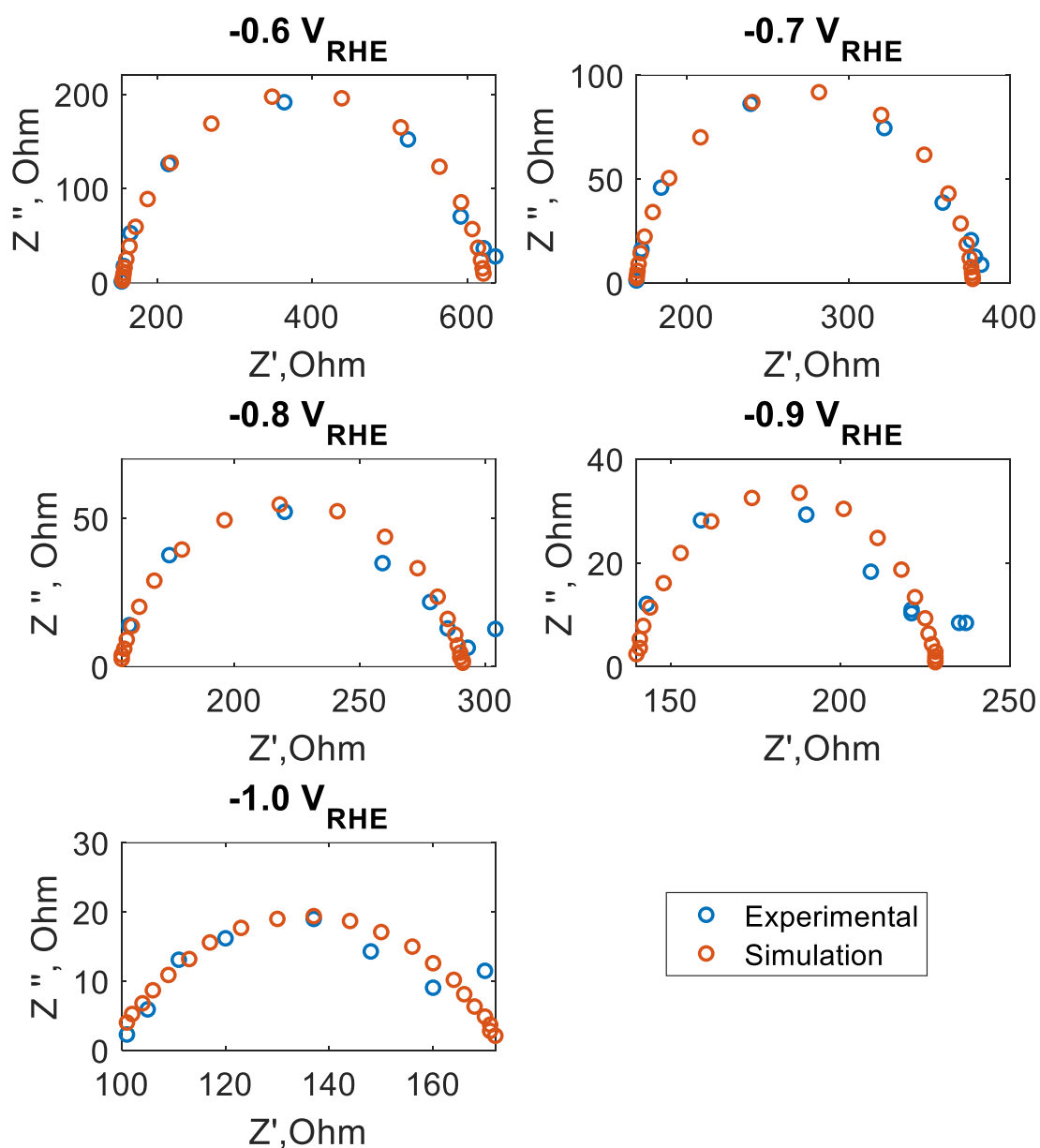
**Figure 6.18.** Nyquist plot (experimental and simulation) for EIS experiments carried out in  $KHCO_3$  2 M electrolyte and using a Sn electrode in presence of 1 mM CKC.



**Figure 6.19.** Nyquist plot (experimental and simulation) for EIS experiments carried out in  $\text{KHCO}_3$  2 M electrolyte and using a Cu electrode in the absence of surfactants.



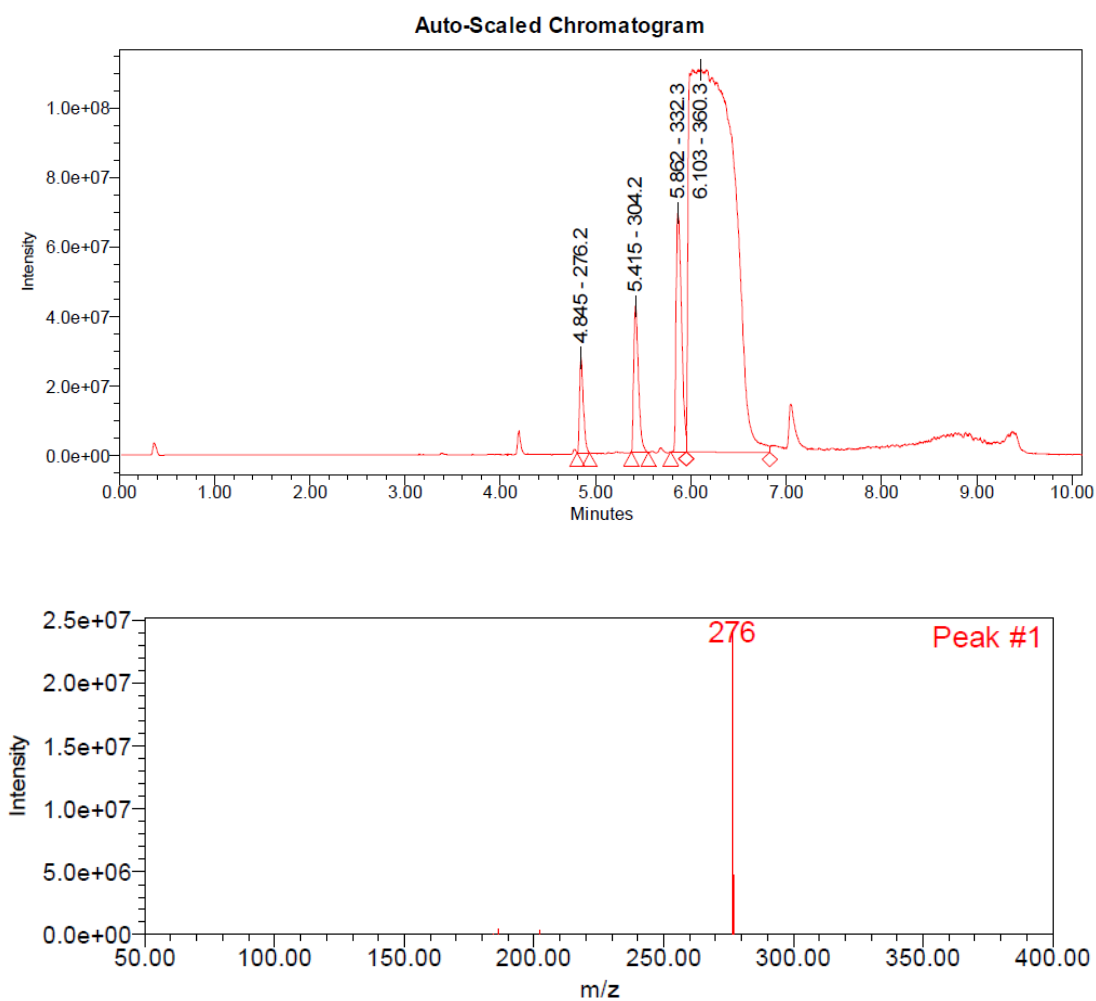
**Figure 6.20.** Nyquist plot (experimental and simulation) for EIS experiments carried out in  $\text{KHCO}_3$  2 M electrolyte and using a Cu electrode in presence of 1 mM CKC.

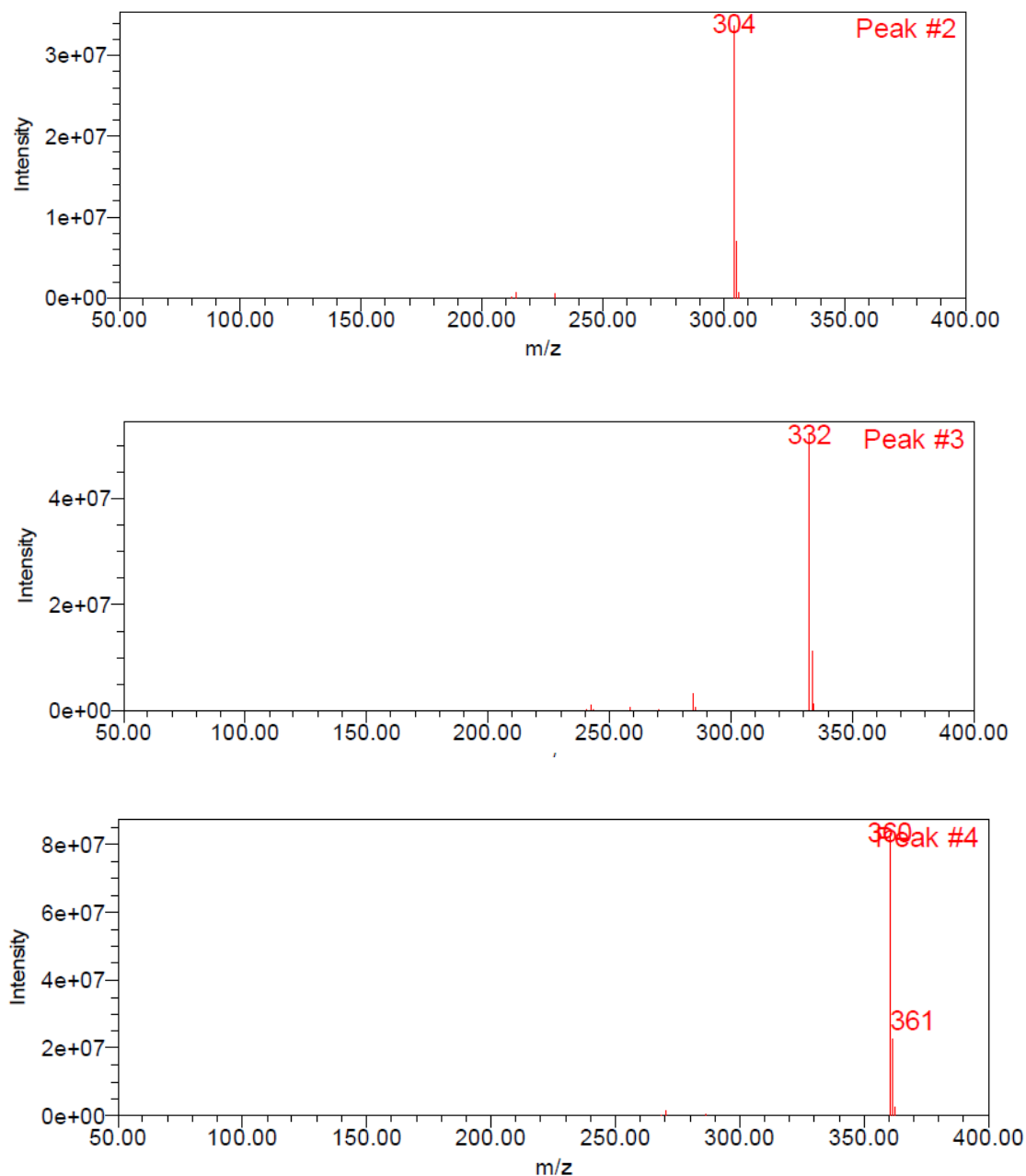


**Figure 6.21.** Nyquist plot (experimental and simulation) for EIS experiments carried out in KHCO<sub>3</sub> 2 M electrolyte and using a Cu electrode in presence of 1 mM CTAB.

## LC-MS analysis

The LC-MS separated the main product (CKC) at retention time (RT) 6.103 min with a mass of 360 m/z, corresponding to benzyl dimethyl hexadecylammonium from three major impurities at RT 4.845, 5.415 and 5.862 min with masses of 276, 304 and 332 m/z, respectively (Figure 6.22). These RT and masses belong to N-benzyl dodecan-1-amine, benzyl dimethyldodecylammonium and N-benzylhexadecan-1-amine, respectively.

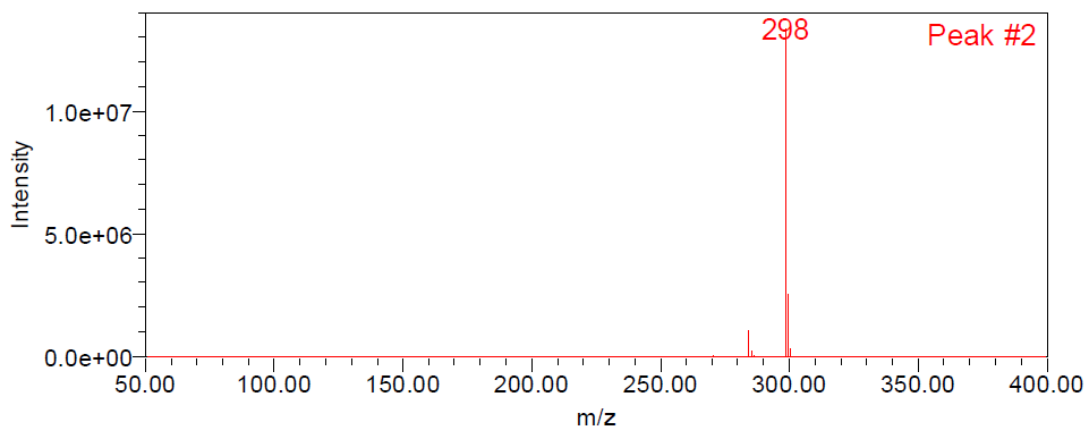
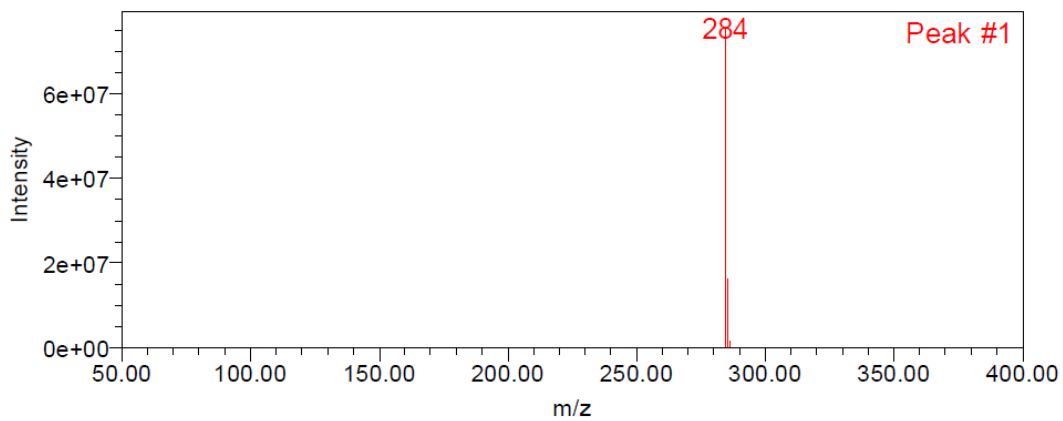
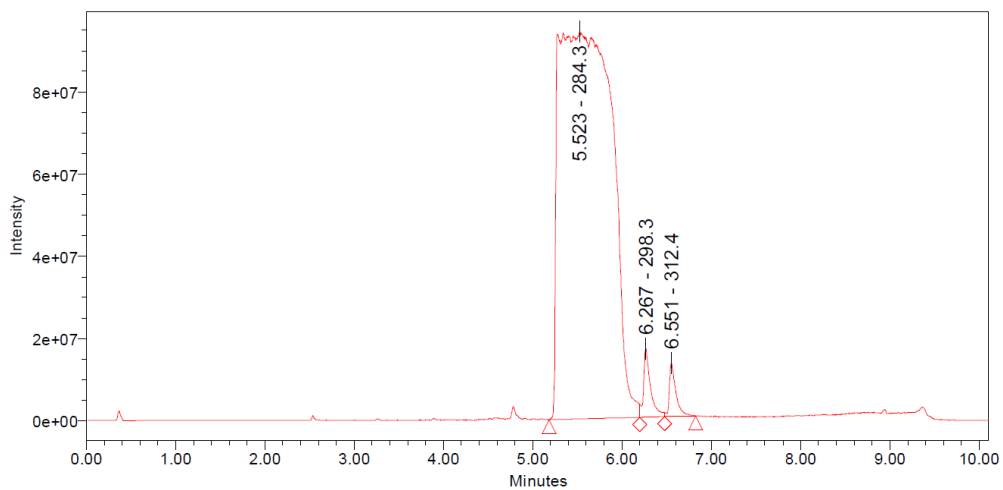




**Figure 6.22.** LC Chromatogram of a CKC solution and MS spectra of the species detected.

The LC-MS separated the main product (CTAB) at RT 5.523 min with a mass of 284 m/z corresponding to hexadecyl trimethylammonium and two major impurities at RT 6.267 and 6.551 min with masses of 298 and 312 m/z corresponding to heptadecyl trimethylammonium and octadecyl trimethylammonium, respectively.





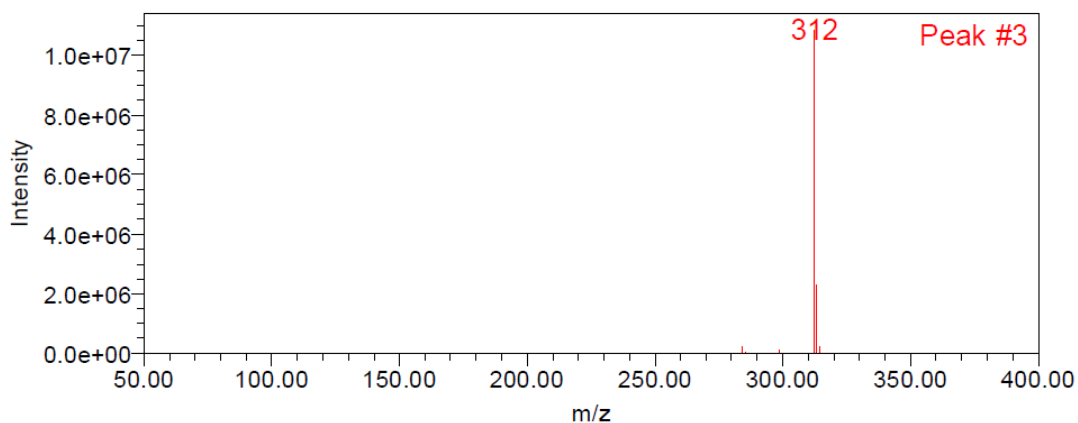


**Figure 6.23.** LC Chromatogram of a CTAB solution and MS spectra of the species detected.

### Input for ORCA ab initio calculations

```
# avogadro generated ORCA input file
```

```
# Basic Mode
```

```
#
```

```
! RHF SP def2-SVP
```

```
%output
```

```
Print[ P_Basis ] 2
```

```
Print[ P_MOs ] 1
```

```
*Atomic coordinates*
```

```
End
```

## CHAPTER 7

### **Development of a biomimetic bifunctional catalyst for the integrated capture and electrochemical conversion of CO<sub>2</sub>**

THANKS TO THE KNOWLEDGE GAINED IN CHAPTERS 5 AND 6, WE SYNTHETIZED AN ARTIFICIAL ENZYME ABLE TO BOTH CAPTURE FASTER THE CO<sub>2</sub> AND INHIBIT THE HYDROGEN EVOLUTION REACTION. IN THIS CHAPTER, THIS NEW MATERIAL, FUNCTIONAL FOR BOTH THE CAPTURE AND CONVERSION STEPS, IS DEEPLY INVESTIGATED FOR THE INTEGRATED STRATEGY.

This chapter is currently under review to be published as: O. Gutierrez-Sanchez, H. Y. Vincent Ching, N. Daems, M. Bulut, D. Pant and T. Breugelmans, Bifunctional Artificial Carbonic Anhydrase for the Integrated Capture and Electrochemical Conversion of CO<sub>2</sub>, 2022.

## 7.1 Introduction

There is increasing interest in optimizing the combined capture and CO<sub>2</sub> conversion process to make it industrially feasible.[168] For instance, a promising option to optimize the capture step is to decrease the operational time to capture a certain amount of CO<sub>2</sub> (g CO<sub>2</sub> h<sup>-1</sup>) in the form of bicarbonate.[197] On the other hand, a strategy to increase the energy efficiency of the bicarbonate electrolyser is to inhibit the proton donor ability of bicarbonate and the undesired HER.[161] However, these two strategies have only been investigated as separate processes. Studies showed how the CO<sub>2</sub> capture is catalysed by using certain bio-inspired strategies, while the HER inhibition in eCO<sub>2</sub>R has been investigated continuously in the last decade, in addition to the eCO<sub>2</sub>R from bicarbonate electrolytes studied in the previous chapters.[162,163,198]

In nature there are certain enzymes called CAH that promotes the conversion of CO<sub>2</sub> to bicarbonate (7.1), and often considered an ultra-fast enzyme for the catalysis of this reaction, as it was already mentioned in *Chapter 4.2.3*.[199] The active site of the enzyme is formed by a Zn<sup>2+</sup> co-factor coordinated to three histidines in a tetrahedral geometry, leaving a fourth coordination site vacant (Figure 7.1). Due to this specific structure, Zn<sup>2+</sup> can coordinate with and fixate H<sub>2</sub>O (7.2). The electro-positivity of the metal centre draws electro-negativity away from the oxygen atom of the aqua ligand, and in turn greatly decreasing the pK<sub>a</sub> of aqua ligand from 14 to ≈7, i.e., becoming more acidic (7.3). In the presence of CO<sub>2</sub>, the aqua ligand deprotonates and binds CO<sub>2</sub> to forms a bicarbonate ligand (7.4), which ligand exchanges with a new H<sub>2</sub>O molecule (7.5 → 7.2).[200,201]

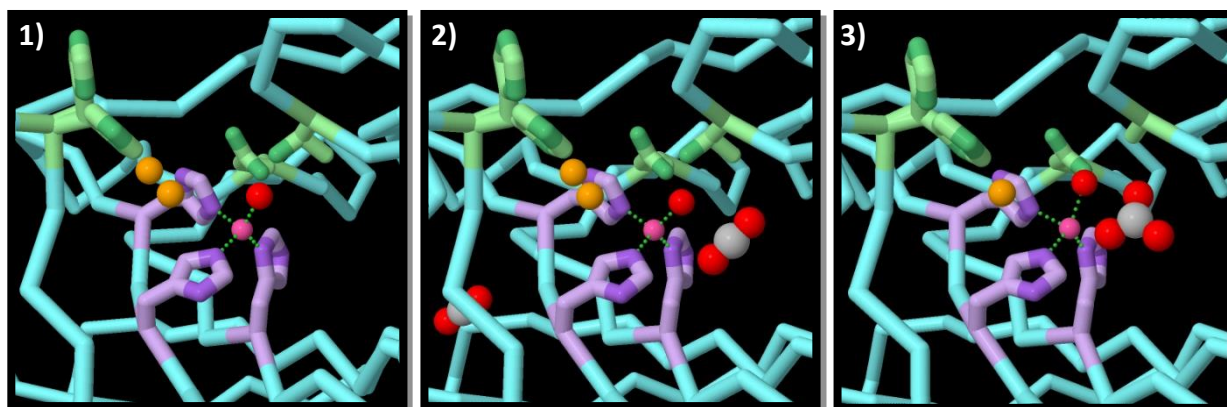
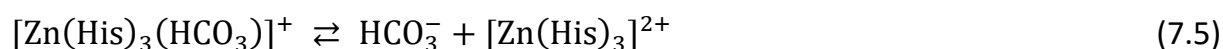
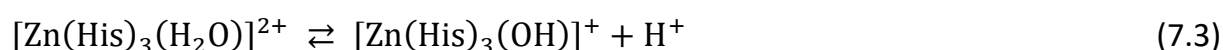
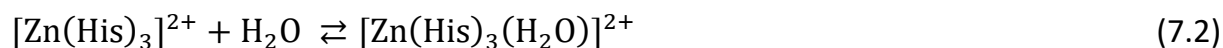


**Figure 7.1.** Schematic representation of the catalytic mechanism of the conversion of CO<sub>2</sub> to bicarbonate in the metal co-factor of CAH (hydrogen atoms are not displayed). 1) H<sub>2</sub>O coordination to the unoccupied position of the tetrahedral structure; 2) Reaction between CO<sub>2</sub> and coordinated OH<sup>-</sup> and; 3) formation of bicarbonate and substitution with a new H<sub>2</sub>O molecule. [202]



Because of the above-mentioned properties to convert CO<sub>2</sub> to bicarbonate, CAH has been studied for several years in the field of carbon sequestration.[147,203,204] However, the high price and the low stability of the enzyme in the harsh conditions (very alkaline media and high temperature) of CO<sub>2</sub> capture technologies made it difficult to implement it in the currently available integrated capture and electrochemical conversion strategies. Nevertheless, promising advances in improving the enzyme stability have been achieved.

For instance, Alvizo *et al.*, indentified CAH that tolerated up to 107 °C in the presence of solvent of pH > 10.[205] However, for CO<sub>2</sub> capture applications, the entire natural enzyme is not needed. The catalytic reaction of the CAH can also be achieved without using the natural enzyme if the active site is mimicked synthetically yielding an artificial enzyme.[206] In some cases, artificial enzymes can outperform natural enzymes in their role as catalysts.[207] Different ligands and metals have been used to synthesize artificial CAH to study the kinetic properties of the enzyme CAH or to immobilize it on a surface for carbon sequestration. Most of these ligands are similar to the ones found in CAH and are ligands that typically form tetrahedral geometries with metal cations after coordination.[208,209] However, there are no studies on using these artificial CAH enzymes to study the CO<sub>2</sub> capture for integrated CCU technologies as no artificial CAH has yet been found to be compatible with the integrated CO<sub>2</sub> capture and conversion strategy. To be compatible, 1) it must be stable in highly alkaline conditions (pH > 14); 2) it must increase the rate of the conversion of CO<sub>2</sub> to bicarbonate; and 3) it must be inert under the electrochemical conditions of eCO<sub>2</sub>R. Additionally to these functions, since in an integrated CCU strategy the artificial CAH will still be part of the electrolyte in the eCO<sub>2</sub>R step, it is interesting to investigate if there could be a role for the artificial CAH during the electrolysis step, specifically in promoting the efficiency of the reaction.

As mentioned earlier, the efficiency of the bicarbonate electrochemical reduction is low compared to conventional gas-fed CO<sub>2</sub> electrolyzers, mainly due to the high proton donor ability of bicarbonate, promoting HER. In the previous chapters we managed to inhibit the HER in bicarbonate electrolysis by using cationic surfactants,.[163,180,181] The concept of using superhydrophobic surfaces to promote the eCO<sub>2</sub>R is inspired by similar effects found in nature, such as the cell membrane interface, the lotus effect found in leaves or the structure of gas-trapping cuticles on subaquatic spiders, as has been recently mentioned by Wakerley *et al.* during their study on HER inhibition for eCO<sub>2</sub>R systems.[182] This amphiphilic structure typical of cationic surfactants (i.e., CTAB and KKC, see *Chapter 5* and *6*) is identified in certain artificial CAH's as well. Indeed, the Zn<sup>2+</sup>

acts as the hydrophilic head and the ligands (usually heterocycles or long carbon chains) act as the hydrophobic tail. Thus if a proper ligand could be chosen it might not only speed up the conversion of CO<sub>2</sub> to bicarbonate but it could also form a coordination complex able to inhibit HER and promote the eCO<sub>2</sub>R in bicarbonate systems.

For this reason, we selected three potential ligands that led to the desired artificial CAH being able to fulfil both bio-inspired functions (Figure 7.2) and could thus make the integrated capture and conversion more efficient. Histidine was selected because it is the amino acid coordinated to the Zn<sup>2+</sup> centre CAH. Imidazole was selected as a simplified version of histidine as it only contains the nitrogen donor heterocycle of the amino acid. Finally, cyclen was selected because it is a tetradentate chelator that offer extra ligand-metal binding affinity (Figure 7.2). Indeed, the [Zn(cyclen)]<sup>2+</sup> complex has performed favourably in previous CAH activity kinetic studied, therefore it was suitable for being tested in present work.[210] Other parameters such as the effect of the concentration of artificial CAH and the temperature of the capture solution were studied here as well in order to optimize the capture step. As a result, we could identify the optimal conditions for capturing CO<sub>2</sub> with artificial CAH's. The most optimal ligand (being cyclen), in terms of catalytic performance and stability was selected and further evaluated as HER inhibitor during eCO<sub>2</sub>R using the capture solution directly as carbon substrate. In summary, we propose a biomimetic homogeneous catalyst that is both able to catalyze the capture of CO<sub>2</sub> in a 2 M KOH solution and then promote the electrochemical conversion of CO<sub>2</sub> to formate in a 2 M bicarbonate solution, thus outperforming both catalyst that can only be used to speed up the capture of CO<sub>2</sub> or that inhibit HER during eCO<sub>2</sub>R. The artificial CAH [Zn(cyclen)]<sup>2+</sup> increased the rate of capturing CO<sub>2</sub> by 84% compared to control experiments and inhibited the HER (partial current density is diminished from 18 mA cm<sup>-2</sup> in control experiments to 0.7 mA cm<sup>-2</sup>) during the eCO<sub>2</sub>R step. To the best of our knowledge, this is the first ever report of a the strategy using an artificial CAH for integrated capture and conversion of CO<sub>2</sub>.

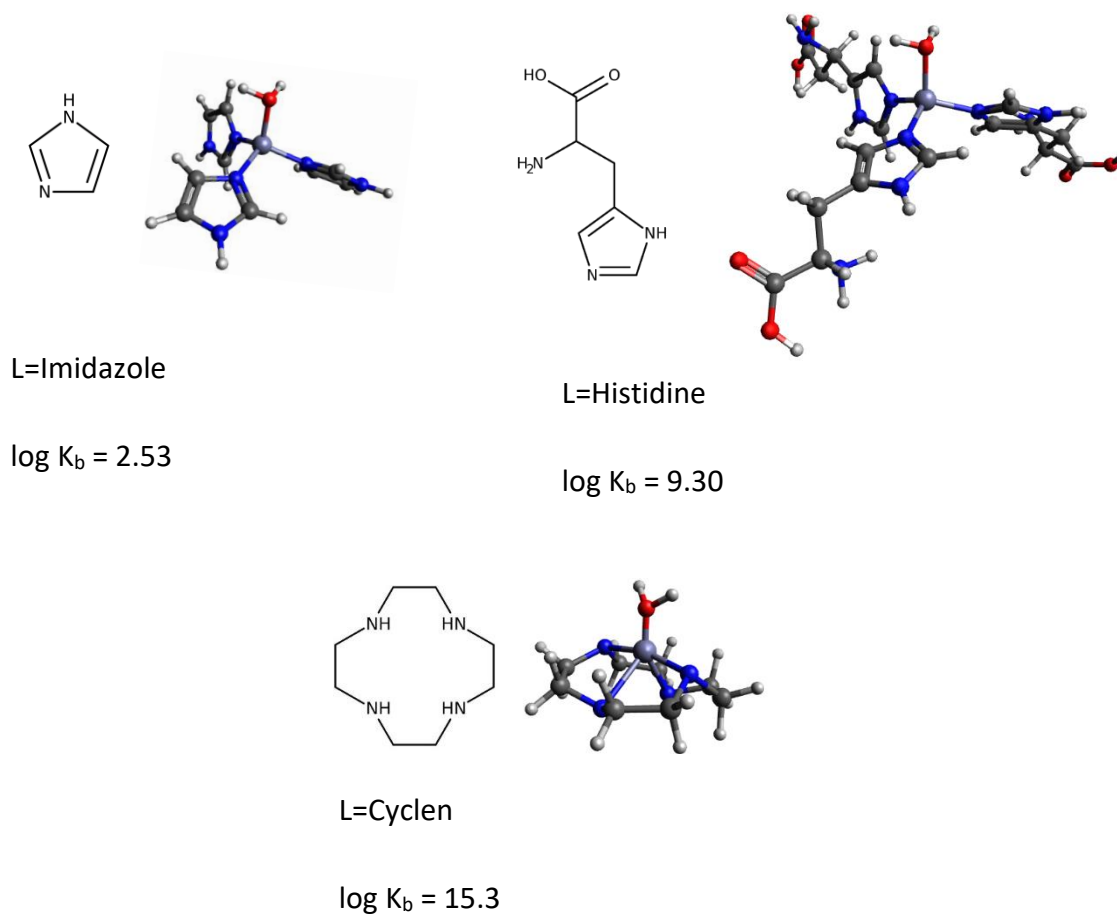


**Figure 7.2.** Potential ligands chosen to form the artificial CAH. Log  $k_b$  refer to the binding constant  $Zn^{2+}$ -L. The  $pK_a$  corresponds to the H<sub>2</sub>O after being fixated to the complex.[210–214]

## 7.2 Experimental

### 7.2.1 Materials and solutions

All the chemicals were obtained from commercial sources and used without purification unless stated otherwise. Every solution is prepared in Ultra-Pure water (MilliQ, 18.2 MΩcm). Each solution was sonicated for 10 minutes at room temperature to ensure homogeneity before experimentation. The potassium hydroxide pellets were purchased from Chem-Lab. The ligands imidazole 99+%, L-histidine 98+% and Cyclen 99+% were



obtained from Chem-Lab, Alfa Aesar and Chematech, respectively. ZnBr<sub>2</sub> anhydrous 98+% was obtained from Chem-Lab. CO<sub>2</sub> (99.998%) was purchased from Nippon Gas. Benzyltrimethylhexadecylammonium chloride 95+% (CKC) was obtained from Alfa Aesar. The Pt mesh (99.9%) and the Sn wire (99.9985%, 2 mm dia.) were obtained from Goodfellow and Alfa Aesar, respectively. The reference electrode Ag/AgCl 3M KCl and the pH-electrode were purchased from Metrohm. The Nafion 117<sup>®</sup> CEM was obtained from FuelCell store. The CEM was pre-treated as follows: 1 h in 0.5 M H<sub>2</sub>SO<sub>4</sub> at 80 °C, followed by 1 h in MilliQ water at 80 °C, then 1 h in 0.5 M H<sub>2</sub>O<sub>2</sub> at 80 °C and finally 1 h in MilliQ water at 80 °C.

### 7.2.2 CO<sub>2</sub> capture set-up and procedure

The set-up used for the CO<sub>2</sub> capture experiments is shown in Figure A.12. A sealed jacketed electrochemical half-cell was filled with 70 mL of the capture solution: 2 M KOH. The concentration of KOH was chosen based on the solubility of bicarbonate (2.2 M). The solution was thermostated at 25 °C (unless stated otherwise) with a Julabo thermostat. A gas sparger connected to a gas flow controller was used to flush CO<sub>2</sub> from the gas bottle to the solution at a fixed flow rate of 10 mL min<sup>-1</sup>. The solution was homogenized at all times with a magnetic stirrer rotating at 300 rpm. The pH of the solution was digitally monitored and registered using the Adafruit IO pH meter. The upper limit of detection of the digital pH-meter was 14, thus the first seconds of reaction (pH>14) were not monitored. This did not affect the outcome of the experiment since this range of pH was not used in this study. The concentration of the [Zn(L)<sub>x</sub>]<sup>2+</sup> used as artificial CAH for the CO<sub>2</sub> capture catalysis was benchmarked to 2 mM (unless stated otherwise). To properly synthesize the coordination complex, 140 μL of a 1 M ZnBr<sub>2</sub> solution and 150 μL of a 3 M (histidine and imidazole) or 1 M (cyclen) solution were added drop-wise at the same time to the 2 M KOH capture solution while homogenizing the solution at all time with a magnetic stirrer (6). The amount of ligand added was stoichiometrically slightly higher than needed to ensure at least a 3:1 ratio (histidine and imidazole) or a 1:1 ratio (cyclen)

of coordination. This was crucial to avoid the formation of insoluble Zn(OH)<sub>2</sub> and thus the loss of catalyst.

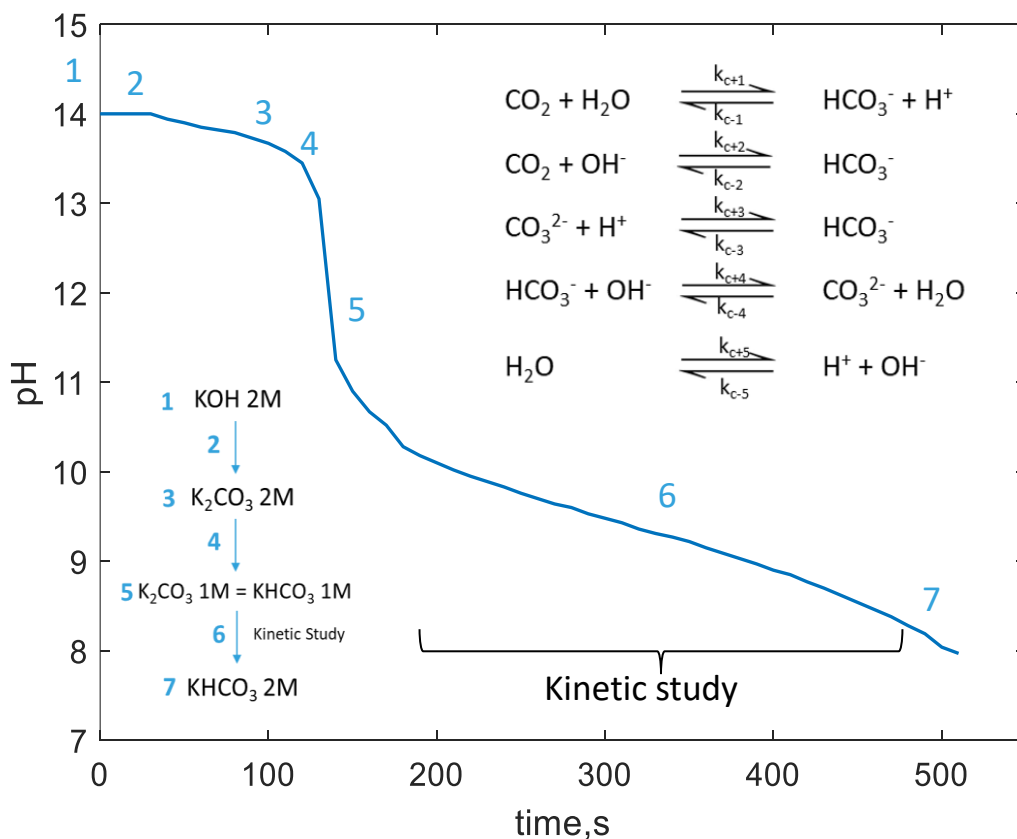
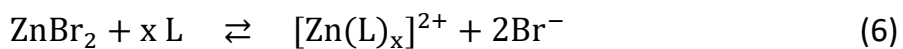


**Figure 7.3.** Evolution of pH and equilibrium reactions of the species present when saturating a 2 M KOH solution with gaseous CO<sub>2</sub>.



The procedure of CO<sub>2</sub> capture and reactions of CO<sub>2</sub> with the capture solution KOH are detailedly described in *Annex A.4*. The final pH when the solution is saturated is 8. At this pH all the KOH is fully converted to carbonate and then the carbonate is fully converted to bicarbonate. However, some free CO<sub>2</sub> remains in solution as the maximum solubility of bicarbonate (i.e., 2.2 M) was reached at pH = 8.3 (or the pH at which the maximum relative abundance of bicarbonate is found, see Bjerrum plot as Figure A.8). This small portion of dissolved CO<sub>2</sub> goes at the cost of a portion of bicarbonate, therefore, to obtain

the maximum amount of bicarbonate and maximize CO<sub>2</sub> capture efficiency, either the capture experiment is stopped at pH 8.3 or the initial concentration of KOH is increased to 2.2 M. To avoid precipitation of salts due to concentration gradients within the solution and the reactor, the first option was more appropriate for the experiments and was therefore selected. During the capture of CO<sub>2</sub>, several equilibria and buffer reactions are occurring during the titration of KOH with CO<sub>2</sub>. These reactions are compiled in Figure 7.3. The concentration of each species at a given time is described by the following rate equations.[215]

$$\frac{d[CO_2]}{dt} = k_{c-1}[H^+][HCO_3^-] + k_{c-2}[HCO_3^-] - k_{c+1}[CO_2] - k_{c+2}[OH^-]$$

$$\begin{aligned} \frac{d[HCO_3^-]}{dt} = & k_{c+1}[CO_2] + k_{c+2}[CO_2][OH^-] + k_{c+3}[CO_3^{2-}][H^+] + k_{c-4}[CO_3^{2-}] - k_{c-1}[HCO_3^-][H^+] - k_{c-2}[HCO_3^-] \\ & - k_{c-3}[HCO_3^-] - k_{c+4}[HCO_3^-][OH^-] \end{aligned}$$

$$\frac{d[CO_3^{2-}]}{dt} = k_{c-3}[HCO_3^-] + k_{c+4}[CO_2][OH^-] - k_{c+3}[CO_3^{2-}][H^+] - k_{c-4}[CO_3^{2-}]$$

$$\frac{d[H^+]}{dt} = k_{c+1}[CO_2] + k_{c-3}[HCO_3^-] + k_{c+5} - k_{c-1}[HCO_3^-][H^+] - k_{c+3}[CO_3^{2-}][H^+] - k_{c-5}[OH^-][H^+]$$

$$\frac{d[OH^-]}{dt} = k_{c-2}[HCO_3^-] + k_{c-4}[CO_3^{2-}] + k_{c+5} - k_{c+2}[CO_2][OH^-] - k_{c+4}[CO_2][OH^-] - k_{c-5}[OH^-][H^+]$$

To elaborate a detailed kinetic model and determine the accurate, independent, rate constant ( $k_c$ ) of the capture of CO<sub>2</sub>, every differential equation had to be taken into consideration. However, we could elaborate a model based on the evolution of pH over time, which is directly related to the consumption of CO<sub>2</sub> and thus the CO<sub>2</sub> capture rate. As observed in Figure 7.3, the pH decreases during the CO<sub>2</sub> capture, thus the concentration of H<sup>+</sup> increases over time, allowing us to calculate a (pseudo)rate constant ( $K_c^*$ ) based on the (pseudo)first-order rate equation of the production of H<sup>+</sup> (Eq. 7.1).

$$\frac{+d[H^+]}{dt} = K_c^*[H^+] \quad (\text{Eq. 7.1})$$

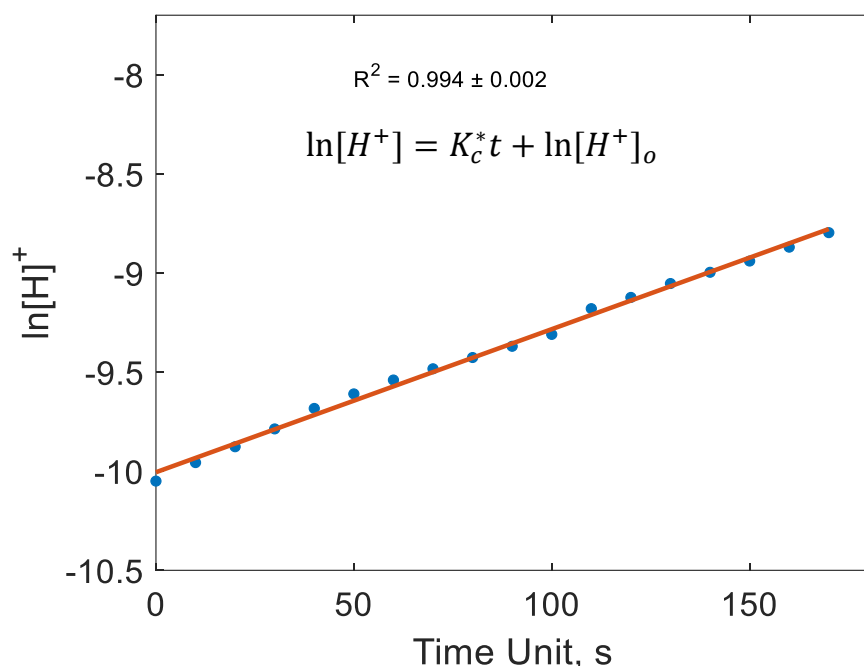


**Figure 7.4.** Linear regression fitting of the evolution of pH when saturating 2 M KOH solutions with gaseous CO<sub>2</sub>. The time range chosen belongs to the conversion of carbonate to bicarbonate.

As such, we obtain a rate equation that only depends on the concentration of H<sup>+</sup> at a given time, which is calculated from the measured pH of the solution. This approximation is experimentally proven by using the linear regression fitting method. In a (pseudo)first-order kinetic equation,  $\ln[X]$  has linear regression with time ( $R^2 > 0.95$ ). This is indeed observed in our system. For instance, when evaluating the pH evolution during the step where carbonate is converted to bicarbonate in a CO<sub>2</sub> capture experiment using 2 M KOH as capture solution, a linear regression was obtained (Figure 7.4). We can then confirm that this rate equation and model is valid for studying the evolution of H<sup>+</sup> overtime during the CO<sub>2</sub> capture and thus to calculate  $K_c^*$  for each case scenario (ligand, concentration and temperature screening). The  $K_c^*$  is directly related to the efficiency of the capture solution (KOH + artificial CAH) to convert CO<sub>2</sub> to bicarbonate, the larger the faster the capture step.

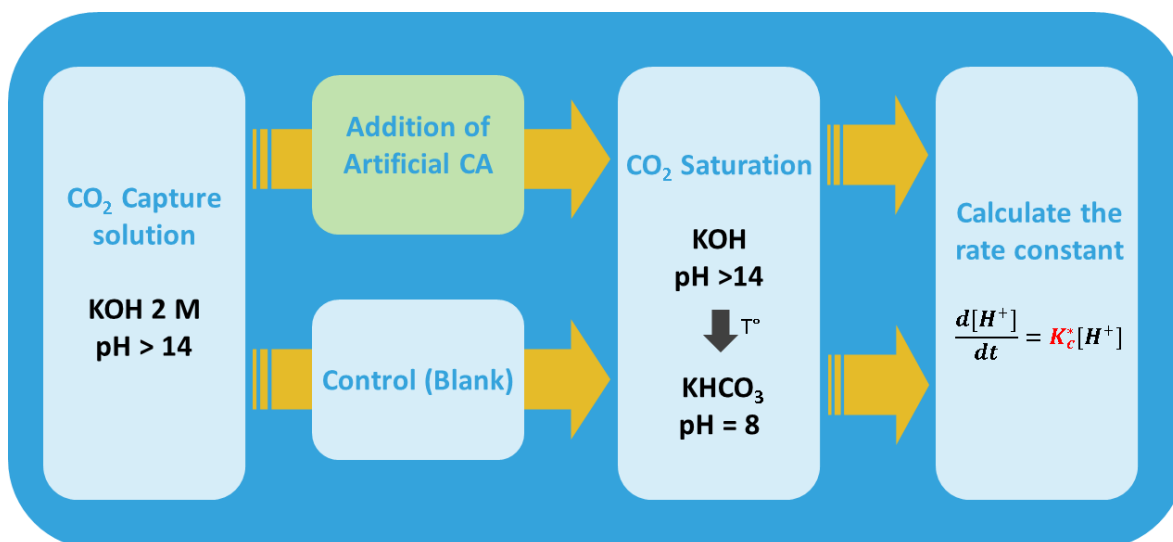


**Figure 7.5.** Scheme of the experimental procedure to evaluate the effectiveness of the bio-mimetic catalyst and the conditions of the CO<sub>2</sub> capture in a 2 M KOH media.

The procedure to evaluate each artificial CAH and system is displayed in Figure 7.5. The capture solution (2 M KOH) was purged with CO<sub>2</sub> in the presence and the absence of the artificial CAH. The nature of the ligand, the concentration of the catalyst and the temperature of the solution varied throughout the study. The pH was measured from the starting point (pH>14) to the saturation point (when pH remains constant). For conventional systems, the experiment finished at pH 8. The  $K_c^*$  was calculated using the data that belonged to the conversion of carbonate to bicarbonate (pH 10 → pH 8.3) to avoid the lack of data at the beginning of the experiment (pH>14) and the half-neutralization point (pH 13 → 10). The pH range of the study varied ± 0.3 depending on the variables of the study. A higher  $K_c^*$  determined a faster rate of the conversion of CO<sub>2</sub> to bicarbonate. Three tests per set of experiments were performed and are displayed as average. The error bars correspond to the standard deviation.

### 7.2.3 Bicarbonate electrolysis: set-up and procedure

The set-up for electrochemically converting bicarbonate (i.e., the capture solution) to formate is shown in Figure A.14. A tailored jacketed H-cell was filled with 140 mL of

electrolyte: 70 mL of catholyte and 70 mL of anolyte. The catholyte was the 2 M potassium bicarbonate solution obtained from the CO<sub>2</sub> capture step (in the presence or the absence of additives) and the anolyte was a 1 M KOH solution. To obtain a 2 M bicarbonate solution, the CO<sub>2</sub> capture step had to be stopped at pH 8.3. Both half-cells were separated by a CEM to ensure ionic conductivity (charge balance) and avoid product crossover. The system was thermostatic at 25 °C unless stated otherwise. All the experiments were performed at standard pressure (1 atm). A Sn wire (0.2 cm<sup>2</sup>) was used as an electrocatalyst to convert CO<sub>2</sub> to formate, an Ag/AgCl 3 M KCl electrode was used as a reference electrode and a Pt mesh was used as a counter electrode in the three-electrode system. A Sn electrocatalyst was selected due to its high selectivity towards formate, which we could quantify by liquid analysis and thus allowed a proper evaluation of our model.[93,190] With a Biologic potentiostat (model VMP3), one-hour chronoamperometry experiments at the fixed potential of -0.9 V<sub>RHE</sub> was performed to electrochemically convert the bicarbonate solution. The working potential was chosen based on the bicarbonate electrolysis potential screening performed in *Chapter 5*. The preconditioning of the working electrode followed the same procedure as in *Chapter 5*, too (i.e., cleaning and electrochemical surface stabilization). The solution was homogenized with a magnetic stirrer at 300 rpm throughout the experiment. After electrolysis, 0.5 mL of the solution was sampled and analysed in an Agilent 1200 HPLC using an Agilent Hi-Plex H 7.7×300 mm column. The samples were previously diluted in MilliQ water and acidified with H<sub>2</sub>SO<sub>4</sub> to avoid bubble formation and obstruction in the column. H<sub>2</sub>SO<sub>4</sub> 0.01 M was used as the mobile phase. The results of the electrolysis are presented in the form of the FE (Eq. A.11). The FE<sub>Formate</sub> is quantified by liquid analysis while the rest of the FE is considered to go towards HER, although this is an approximation based on the high selectivity of Sn electrocatalyst towards formate. Gas analysis was performed in preliminary studies where saturated CO<sub>2</sub> solutions were used instead of bicarbonate solutions in the same conditions as this study and a neglectable fraction of FE went to CO (less than 1%), allowing this approximation. Three tests per set of experiments were performed and displayed as average. The error bars correspond to the

standard deviation. The difference of experimental potential (vs. Ag/AgCl 3 M and pH 8.3) and RHE is calculated and fixed at 0.7 V (e.g., applied potential of -1.6 V corresponds to -0.9 V<sub>RHE</sub>).

To study the effects of the additives on the electrochemical performance of the electrolyte, LSV and EIS were performed in an Autolab potentiostat (model PGSTAT302N). For LSV experiments, the CD was measured in the potential range of -0.3 to -1.3 V<sub>RHE</sub> at 5 mV s<sup>-1</sup>. For EIS experiments, the impedance was measured at the fixed potential of -0.9 V<sub>RHE</sub> from 1 to 20,000 Hz. The details on the equivalent circuit model are shown in Figure A.7 and the Nyquist plot fitting are shown in the supportive information (Figure 7.13). The results are displayed in the form of DL-Capacitance.

## 7.3 Results and discussion: Biomimetic catalysis of the CO<sub>2</sub> capture

### 7.3.1 Effect of the nature of the ligand

The first investigated parameter was the nature of the ligand that forms the coordination complex with Zn<sup>2+</sup>. The nature of the ligand affected the system in, at least, two ways: 1) it modified the electron density during the re-arrangement of the d orbitals after [Zn(L)<sub>x</sub>]<sup>2+</sup> was formed;<sup>[216]</sup> and 2) the binding constant (*k<sub>b</sub>*) of the ligand towards Zn<sup>2+</sup>, which determines how stable the complex is and how it competed with the formation of insoluble Zn(OH)<sub>2</sub> and ZnCO<sub>3</sub>. There was interest in having the electron-affinity (electropositivity) region of the coordination complex concentrated on the position where H<sub>2</sub>O was binding. A stronger [Zn(L)<sub>x</sub>(H<sub>2</sub>O)]<sup>2+</sup> bond made H<sub>2</sub>O more acidic and thus increased *K<sub>c</sub><sup>\*</sup>*. As shown in Figure 7.6, the *K<sub>c</sub><sup>\*</sup>* increased in the presence of the artificial CAH, [Zn(L)<sub>x</sub>]<sup>2+</sup>, independently of the ligand used. In the absence of the catalyst (No ligand), the value of the *K<sub>c</sub><sup>\*</sup>* was 7.7 × 10<sup>-3</sup> s<sup>-1</sup> while in the presence of histidine, imidazole and cyclen the value was 8.9 × 10<sup>-3</sup>, 10.6 × 10<sup>-3</sup> and 11.1 × 10<sup>-3</sup> s<sup>-1</sup>, respectively. The best performance was thus obtained by using imidazole and cyclen as ligand, the latter being slightly more effective (+37 and +41%, respectively). Although histidine is the amino acid that forms

the coordination complex in the enzyme CAH, in this set of experiments it was the least effective catalyst (+15%). We can attribute this effect to the amine and carboxylic acid groups of histidine, which in the enzyme are not present because they form the peptide bonds, are interfering with the formation of the tetrahedral Zn<sup>2+</sup> complexes and/or the binding of H<sub>2</sub>O and consequently also the annexing of CO<sub>2</sub>. Coordination complexes with simpler ligands (imidazole) and ligands with a fixed structure (cyclen) appeared to be more efficient in binding and fixing H<sub>2</sub>O for the catalysis of the reaction of CO<sub>2</sub> to bicarbonate.

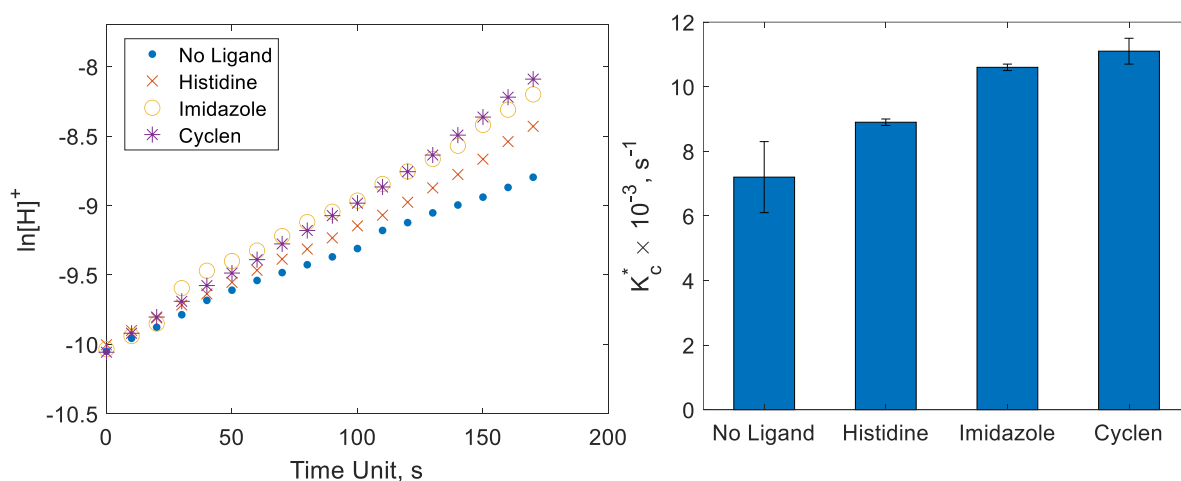
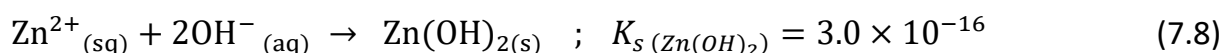
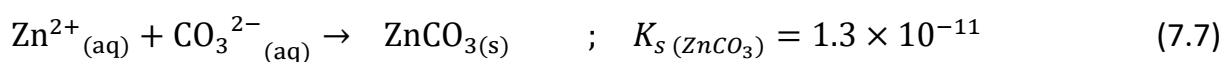


**Figure 7.6.** Evolution of  $\ln[H^+]$  over time (left) and  $K_c^*$  calculated (right) from the corresponding linear regression equation (Figure 7.14) of a CO<sub>2</sub> capture solution in the presence and in the absence of  $[Zn(L)_x]^{2+}$ , where L are different ligands tested (histidine, imidazole and cyclen).

Based on the calculation of  $K_c^*$ , it can then be assumed that both imidazole and cyclen were almost equally effective as ligands in  $[Zn(L)_x]^{2+}$  for the catalytic capture of CO<sub>2</sub>. However, during the experiment, we observed that in the presence of imidazole, the solution became colloidal and finally a sediment was formed, which was not observed when histidine and cyclen were used as ligands. After further evaluation, we reached the conclusion that the sediment formed was ZnCO<sub>3</sub> and Zn(OH)<sub>2</sub> based on the fact that imidazole has a significantly lower equilibrium constant for the coordination of the Zn<sup>2+</sup>



metal cation and the ligands ( $k_b$ ) of 2.53 as compared to those of histidine (9.30) and cyclen (15.3). Therefore, since the  $k_b$  of imidazole to form  $[\text{Zn}(\text{imidazole})_3]^{2+}$  is low, the coordination complex was easily dissociated to the metal cation and the ligands (7.6). In the first steps of the experiment (pH >14  $\rightarrow$  pH 10.5) the concentration of OH<sup>-</sup> was high and the CO<sub>2</sub> was captured mostly in the form of carbonate. Since the Zn<sup>2+</sup> was easily dissociated from  $[\text{Zn}(\text{imidazole})_3]^{2+}$ , it reacted with OH<sup>-</sup> and the carbonate, leading to the water insoluble compounds ZnCO<sub>3</sub> and Zn(OH)<sub>2</sub> (7.7 and 7.8).



As OH<sup>-</sup> was being consumed in the form of Zn(OH)<sub>2</sub> and ZnCO<sub>3</sub>, alkalinity was lost during the capture step. Consequently, although the model proposed to calculate  $K_c^*$  when imidazole was used as a ligand was still valid, it couldn't be used anymore for comparison to the other systems. Indeed, to be able to compare the effectiveness of each ligand, we assumed that the concentration of Dissolved Inorganic Carbon (DIC) at the end of the capture step was 2 M. If alkalinity, and thus carbonate was lost, then the final concentration of bicarbonate was lower than 2 M and thus lower than for the cyclen and histidine systems. This would also imply that the total time spent to convert the carbonate to bicarbonate was lower than the one recorded and consequently the value for  $K_c^*$  was mistakenly found to be higher. For this reason, imidazole was excluded for further study.

Cyclen showed the best effectiveness as a ligand in coordinating Zn<sup>2+</sup> to form an artificial CAH for capturing CO<sub>2</sub>. It outperformed histidine in terms of catalytic activity ( $K_c^* = 11.1 \times 10^{-3} \text{ s}^{-1}$ ) and imidazole in terms of stability. Therefore, for the following two sets of experiments (effects of the concentration of catalyst and temperature of the solution), cyclen was benchmarked as the ligand for the synthesis of artificial CAH.

### 7.3.2 Effect of the concentration of catalyst

The next parameter to study was the effect of the concentration of the artificial CAH present in the capture solution. We expected that by increasing the concentration, the performance of the catalyst would increase due to the presence of a higher number of catalytic sites in the capture solution. The concentration of [Zn(cyclen)]<sup>2+</sup> was increased from 0 to 50 mM and the  $K_c^*$  was calculated for each concentration (Figure 7.7). As expected, the catalytic performance did indeed increase with the concentration of [Zn(cyclen)]<sup>2+</sup>. The most significant increase in  $K_c^*$  was from  $7.7 \times 10^{-3}$  to  $11.1 \times 10^{-3} \text{ s}^{-1}$  (+41%) with a change in concentration from 0 to 2 mM. Upon further increase of the concentration, the value of the  $K_c^*$  increased to  $12 \times 10^{-3}$  (+56%) at 10 mM,  $12.9 \times 10^{-3}$  (+68%) at 20 mM and  $14.7 \times 10^{-3} \text{ s}^{-1}$  (+91%) at 50 mM. We attributed the abrupt increase of the catalytic performance from 0 to 2 mM to the effect of the addition of the homogeneous catalyst. Later, the increase of the  $K_c^*$  is less pronounced since the concentration of CO<sub>2</sub> is not high enough to occupy all the active sites present in the solution. We must consider that although the kinetic study relates to the conversion of carbonate to bicarbonate, CO<sub>2</sub> must first be dissolved in the solution ( $\text{CO}_{2(g)} \rightarrow \text{CO}_{2(l)}$ ) to start the catalytic reaction. The solubility of CO<sub>2</sub> is very low in aqueous solutions (33 mM). Very fast conversion to bicarbonate due to the presence of the artificial CAH is thus limited by the concentration of diluted CO<sub>2</sub>. In this scenario, where the concentration of catalyst is high and that of the substrate (CO<sub>2</sub>) is low, the effect of adding additional artificial CAH is further diminished since it also catalyzes the reverse reaction (conversion of bicarbonate back to CO<sub>2</sub>).

Further increasing the concentration above 50 mM was not considered since the solution became slightly colloidal during the experiment with 50 mM of artificial CAH. This is attributed to the same effect as observed when imidazole was the ligand of the coordination complex. When the concentration was 50 mM, either the concentration of Zn<sup>2+</sup> derived from the equilibrium with [Zn(cyclen)]<sup>2+</sup> is high enough to react with OH<sup>-</sup> and carbonate and start forming the insoluble salts (affecting the evaluation and effectiveness

of the system) or the solubility limit of the metal complex in water is reached. As was the case for imidazole in *Chapter 7.3.1*, we cannot assume that the  $K_c^*$  obtained at 50 mM is valid (most likely overestimation). Therefore, 20 mM is chosen as the optimal concentration of [Zn(cyclen)]<sup>2+</sup> to capture CO<sub>2</sub> using 2 M KOH as capture solution (a +68% faster capture is achieved). This concentration of artificial CAH was used in the following studies, both for the evaluation of the impact of temperature on the capture step and for the bicarbonate electrolysis experiments.

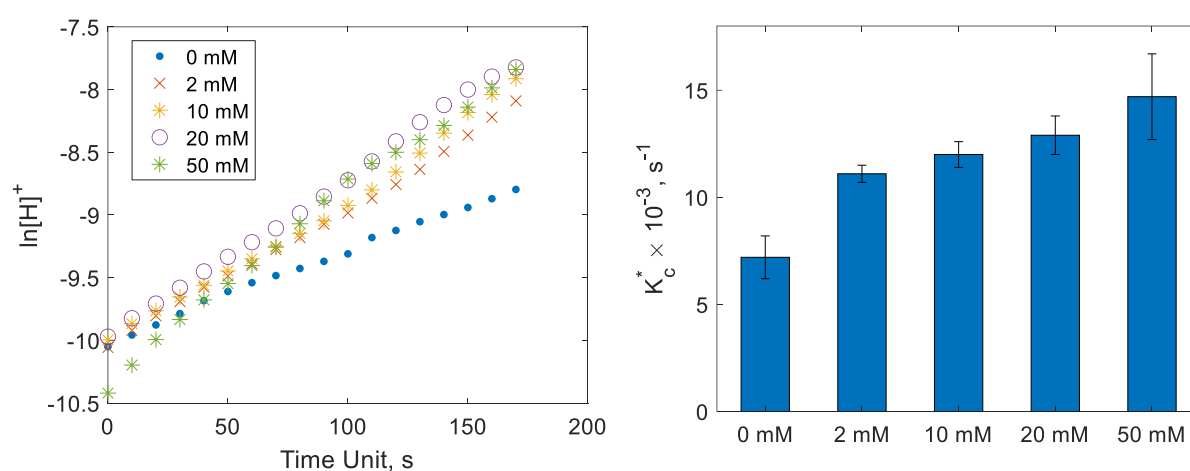


**Figure 7.7.** Evolution of  $\ln[H]^+$  over time (left) and  $K_c^*$  calculated (right) from the corresponding linear regression equation (Figure 7.15) of a CO<sub>2</sub> capture solution in the presence and the absence of [Zn(cyclen)]<sup>2+</sup> at different concentrations.

### 7.3.3 Effect of the temperature of the solution

Finally, the last studied parameter was the temperature of the capture solution. As with any catalytic system, temperature plays an important role. Rate and catalytic constants are temperature dependent, as defined by the Arrhenius equation, and thus  $K_c^*$  will also change with temperature. Nevertheless, given the Arrhenius equation and enzymes natural working temperature, we can assume that  $K_c^*$  will increase with temperature. However, we must also take into account that as the temperature of the solution changes, the solubility and equilibrium constants of the species and reactions involved in the

catalytic route (CO<sub>2</sub>, bicarbonate and carbonate equilibrium and coordination stability) are affected, as well. An increase in temperature decreases the solubility of CO<sub>2</sub>, which is undesirable, while on the other hand the solubility of bicarbonate and carbonate increases, which is desirable. Thus, several factors play a role and were taken into consideration when evaluating each system.

The temperature of the capture solution was increased from room temperature (25 °C) to 40 and 60 °C (Figure 7.8). From 25 to 40 °C, the  $K_c^*$  increased significantly from  $12.9 \times 10^{-3}$  to  $14.2 \times 10^{-3} \text{ s}^{-1}$  (+68% and +84%, respectively). This behaviour could be explained by the Arrhenius equation, being an exponential function, the rate constant thus increases rapidly with the temperature. However, this equation could not explain why from 40 to 60 °C, the  $K_c^*$  barely increased to  $14.3 \times 10^{-3} \text{ s}^{-1}$  (+85%). Therefore, the increase in the temperature, and thus the kinetic rate must have been counteracted by the instability of the artificial CAH, which is also observed in natural enzymes.[217] Since the formation of  $[\text{Zn}(\text{cyclen})]^{2+}$  is an exothermic reaction, the stability of the coordination complex decreases with the increase in temperature, weakening the coordination bond and thus deactivating the artificial CAH.

To obtain information on the system when it is cooled, we also evaluated it at lower temperatures (i.e., 10°C). As expected, the  $K_c^*$  decreased to  $9.3 \times 10^{-3} \text{ s}^{-1}$ . Nevertheless, the  $K_c^*$  was still higher than in a capture solution at 25°C in the absence of artificial CAH (+20%). In addition, although it took more time to reach saturation, the final pH, 7.4, was lower than at 25 °C, meaning that more CO<sub>2</sub> was captured at the end of the experiment (Figure 7.17), in accordance with the increase of the solubility of CO<sub>2</sub> at lower temperatures.

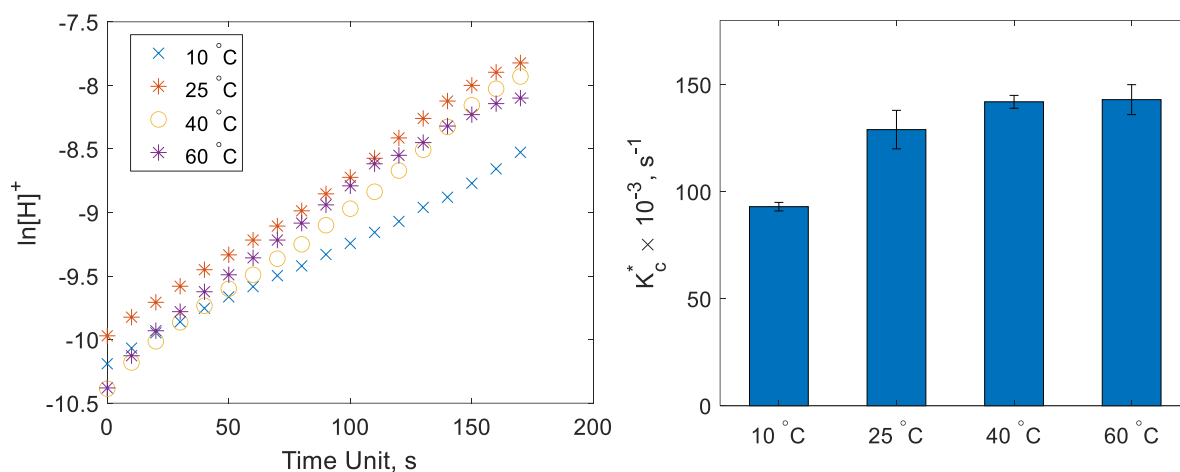


**Figure 7.8.** Evolution of  $\ln[H]^+$  over time (left) and calculated  $K_c^*$  (right) from the corresponding linear regression equation (Figure 7.16) of a CO<sub>2</sub> capture solution at different temperatures (10, 25, 40 and 60 °C) in the presence and the absence of 20 mM of  $[Zn(cyclen)]^{2+}$ .

Based on the results obtained, increasing the temperature up to 40 °C is beneficial for obtaining a faster CO<sub>2</sub> capture rate, however, increasing the temperature further leads to the deactivation of the artificial CAH and is, thus, detrimental for the technology. Capturing CO<sub>2</sub> at lower temperatures may be attractive in terms of total DIC captured, but the rate constant is significantly decreased.

## 7.4 Results and discussion: Promoted bicarbonate electrolysis

Here we describe the effect of the presence of the artificial CAH during eCO<sub>2</sub>R. The most optimal conditions for capturing CO<sub>2</sub> in a 2 M KOH solution found in the previous section (cyclen as ligand and 20 mM as the concentration of artificial CAH) were selected. After the CO<sub>2</sub> capture step, the resulting solution contained 2 M KHCO<sub>3</sub> in the presence of 20 mM of  $[Zn(cyclen)]^{2+}$  and will be the electrolyte of the electrochemical cell in further experiments. The FE obtained from the electrolysis experiments were compared to analogous experiments in the absence of artificial CAH (no additive), in presence of 20 mM of cyclen (but in the absence of Zn<sup>2+</sup>) or in the presence of 1 mM of the cationic

surfactant CKC (known HER inhibitor as it was shown in *Chapter 5* and *6*).[163] As can be observed in Figure 7.9, the  $FE_{\text{Formate}}$  is very low (4.1%) in pure bicarbonate electrolytes (no additive), which is in accordance with what it was observed in *Chapter 5*. [161] In bicarbonate electrolytes in the presence of uncoordinated cyclen, the  $FE_{\text{Formate}}$  was in the same range as in pure bicarbonate electrolytes (4.6 %). The presence of cyclen did not affect the selectivity of the reaction. However, it can be observed how the total current density significantly increased (from 19 to 32 mA cm<sup>-2</sup>) compared to the pure bicarbonate electrolyte (Figure 7.10). It is known that some additives can inhibit the corrosion of a metal surface under an applied potential increasing the effective active surface area, which explains the increase in the total current density.[218] On the other hand, in the presence of [Zn(cyclen)]<sup>2+</sup> or CKC, the  $FE_{\text{Formate}}$  increased substantially from 4.6 to 55%. Furthermore, the partial current density towards is substantially and selectively decreased from 18 to 0.7 mA cm<sup>-2</sup>, while the current density towards formate remained similar compared to control experiments (from 0.7 to 0.8 mA cm<sup>-2</sup>, meaning that HER is being inhibited. This effect is also observed when the HER inhibitor CKC is present ( $FE_{\text{Formate}}$  of 64% and partial current density towards HER of 0.8 mA cm<sup>-2</sup>). We thus assume that the artificial CAH [Zn(cyclen)]<sup>2+</sup> and the HER inhibitor CKC play a similar role in inhibiting HER in eCO<sub>2</sub>R in bicarbonate electrolytes.

To gain further insights into how the [Zn(cyclen)]<sup>2+</sup> inhibits HER, we further evaluated the role of the artificial CAH by studying specifically the changes on the surface of the electrode. LSV experiments showed how the total current density increases substantially in the presence of cyclen (reinforcing the previously explained observation), but decreases also substantially in the presence of [Zn(cyclen)]<sup>2+</sup>, which is also in accordance with the electrolysis experiments (Figure 7.11).

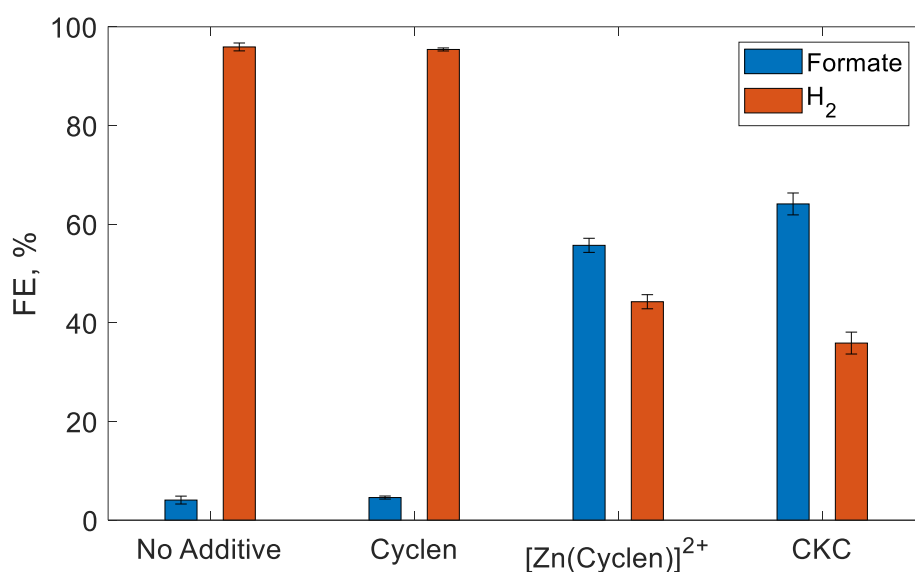


**Figure 7.9.** FE<sub>formate</sub> (measured) and H<sub>2</sub> (approximated) of the electrolysis of a 2 M KHCO<sub>3</sub> solution (prepared from a 2 M KOH capture solution) in the presence and the absence of 20 mM of cyclen, 20 mM of [Zn(cyclen)]<sup>2+</sup> or 1 mM of CKC.

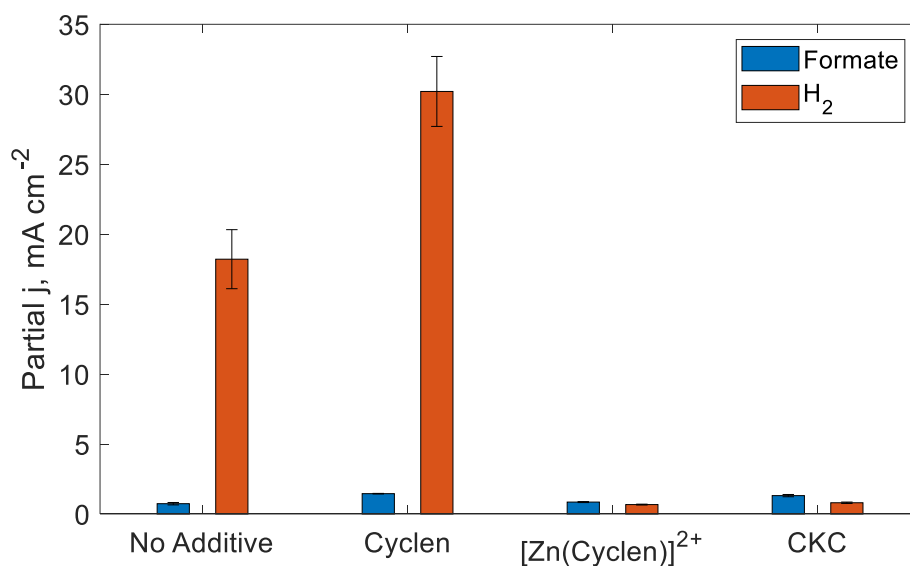


**Figure 7.10.** Partial CD towards formate and H<sub>2</sub> (approximated) of the electrolysis of a 2 M KHCO<sub>3</sub> solution (prepared from a 2 M KOH capture solution) in the presence and the absence of 20 mM of cyclen, 20 mM of [Zn(cyclen)]<sup>2+</sup> or 1 mM of CKC.

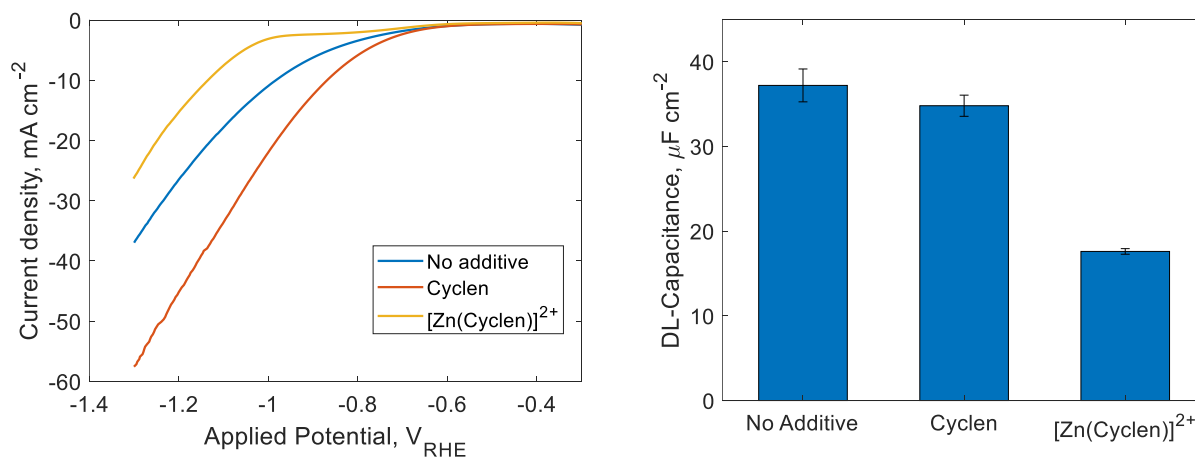


**Figure 7.11.** LSV (left) and DL-Capacitance (right) of 2 M KHCO<sub>3</sub> solutions in the presence and the absence of cyclen and [Zn(cyclen)]<sup>2+</sup>

At the electrolysis working potential (i.e., -0.9 V<sub>RHE</sub>) a small shoulder was observed in the LSV plots, which can be attributed to the reduction of CO<sub>2</sub> or, on the other hand, to the reduction of Zn<sup>2+</sup> to metallic Zn ( $E^{\circ}_{\text{red}} = -0.76 \text{ V}_{\text{RHE}}$ ), which would mean that the coordination complex is not stable under the working potential. We performed an additional analogous experiment involving [Zn(imidazole)<sub>3</sub>]<sup>2+</sup> as artificial CAH to verify this. Due to the low  $k_b$ , the coordination complex was easily dissociated and thus Zn<sup>2+</sup> was present more often as a free cation in the electrolyte. For this experiment, 2 mM [Zn(imidazole)<sub>3</sub>]<sup>2+</sup> had to be used instead of 20 mM since the solution became very colloidal at these high concentrations. Even at this low concentration, the FE<sub>Formate</sub> was 1.2%, which is low even in comparison with the 4.1% of the control experiment and much lower than the 55% of [Zn(cyclen)]<sup>2+</sup> experiment. The HER inhibition effect is lost as the coordination complex is unstable but more importantly, the FE<sub>Formate</sub> dropped by 3% as compared to the control experiment, which was attributed to the current that was spent for the reduction of Zn<sup>2+</sup> to metallic Zn. Additionally, after one hour of electrolysis, the surface of the Sn electrode was completely covered with a black coating, corresponding to the metallic Zn, which is not observed when [Zn(cyclen)]<sup>2+</sup> was used (Figure 7.18). We can therefore assume that [Zn(cyclen)]<sup>2+</sup> is stable in the working conditions (1 h electrolysis and -0.9 V<sub>RHE</sub>) and the shoulder can thus most likely be entirely assigned to



CO<sub>2</sub> reduction. Even if part of the current of the observed small shoulder in the LSV corresponded to the reduction of Zn<sup>2+</sup>, the effect was negligible to be considered as a drawback as no Zn deposits were discovered on the Sn wire in this case.

To further evaluate the surface effects due to the presence of [Zn(cyclen)]<sup>2+</sup>, we performed EIS and calculated the DL-Capacitance for three scenarios (Figure 7.11, no additive, cyclen addition only and CAH addition). From our previous work it is known that the DL-capacitance of the EDL formed between the working electrode and the electrolyte is typically lower in the presence of HER inhibitors such as CKC, directly linked to an increase in hydrophobicity of the surface. This was observed in our current system as well when [Zn(cyclen)]<sup>2+</sup> is added to the electrolyte. Indeed, the DL-Capacitance dropped from 37 to 18 μF cm<sup>-2</sup>. When cyclen alone was present, the DL-Capacitance remained similar (35 μF cm<sup>-2</sup>). Since [Zn(cyclen)]<sup>2+</sup> is a cationic species, once the working potential, i.e., -0.9 V<sub>RHE</sub>, is applied, it migrated towards the cathode, taking part of the inner layer of the EDL (Figure 7.12), similar to the mechanism found when cationic surfactants were used as HER inhibitors. Without the presence of Zn<sup>2+</sup>, cyclen can't migrate towards the surface of the electrode and take part directly in the EDL, thus the expected hydrophobic layer cannot form and as such the DL-Capacitance didn't increase because of a lower surface that would have been available otherwise. With these results, we can confirm that [Zn(cyclen)]<sup>2+</sup> has the function of a HER inhibitor during eCO<sub>2</sub>R and has the same effect on the surface of the electrode as conventional cationic surfactants such as CKC during the inhibition of HER but with the added advantage that it also aids capturing as compared to CKC which does not fulfil this role.

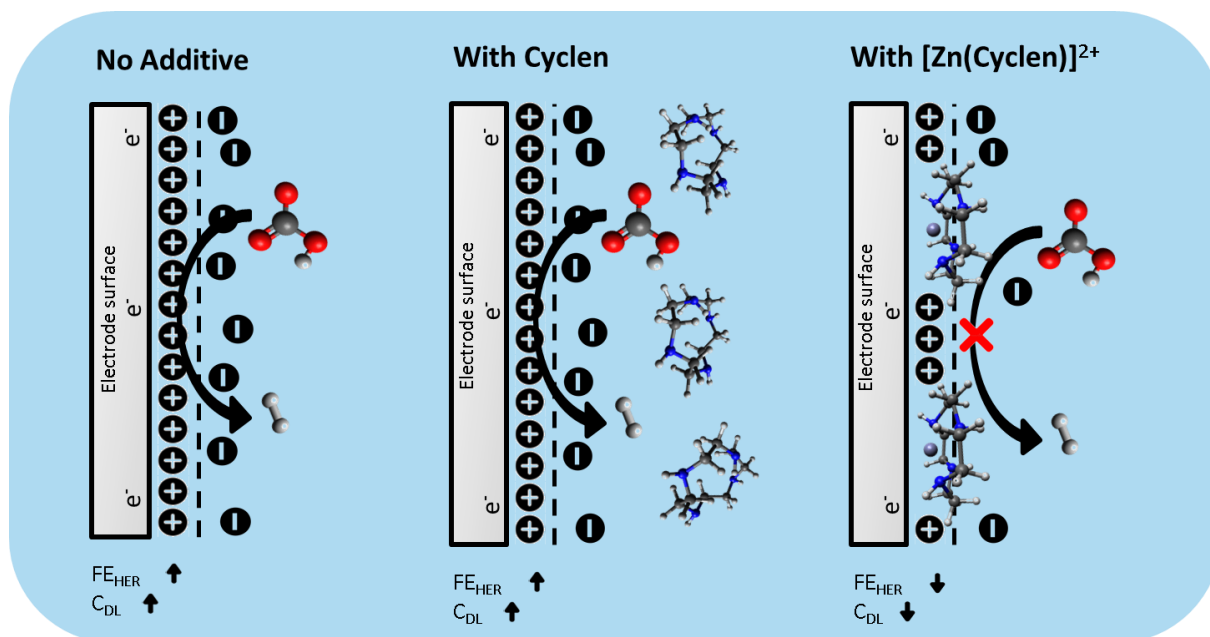


**Figure 7.12.** EDL representation for each case scenario (absence of artificial CA, presence of cyclen and presence of  $[\text{Zn}(\text{cyclen})]^{2+}$ ) and HER inhibition model proposed.

## 7.5 Conclusions

Integrating the capture and the electrochemical conversion of CO<sub>2</sub> is a challenging technology that requires the most optimal operational conditions for both the capture and the conversion steps to be proposed as a potential technology in the field of CCU. However, until now, the capture and the conversion steps were investigated mostly as separated processes, limiting the up-scalability of the integrated concept. In the field of CO<sub>2</sub> sequestration, artificial CAH has been investigated to promote the conversion of CO<sub>2</sub> to bicarbonate and the addition of cationic surfactants to the electrolyte has been investigated to promote bicarbonate electrolysis. In our work, after an optimization study, we proposed the bio-inspired coordination complex  $[\text{Zn}(\text{cyclen})]^{2+}$  as an additive able to fulfil the two functions. An increase of the rate of the conversion of CO<sub>2</sub> to bicarbonate of 84% was obtained when using 20 mM  $[\text{Zn}(\text{cyclen})]^{2+}$  in a 2 M KOH solution at 40 °C. The resulting bicarbonate solution was further used as an electrolyte in the eCO<sub>2</sub>R, where the coordination complex fulfilled the role of HER inhibitor. After one hour

of electrolysis, the  $FE_{\text{Formate}}$  increased from 4.1 (in absence of CA) to 55%. We have proven how, by studying at the same time the capture and the conversion steps, new possibilities appear such as the addition of new agents able to have a significant role in each of the two steps.

## 7.6 Supporting information

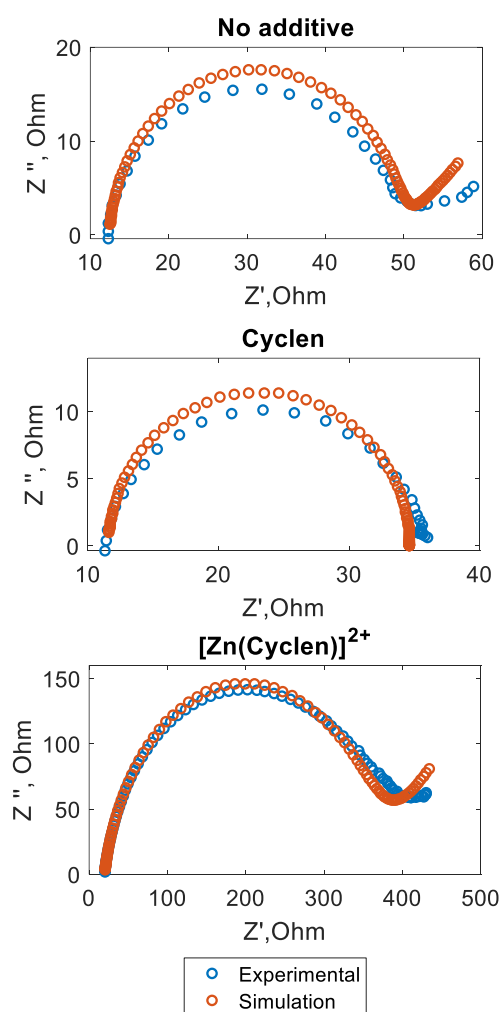


**Figure 7.13.** Nyquist plots (experimental and simulation) for EIS experiments carried out in the chapter.

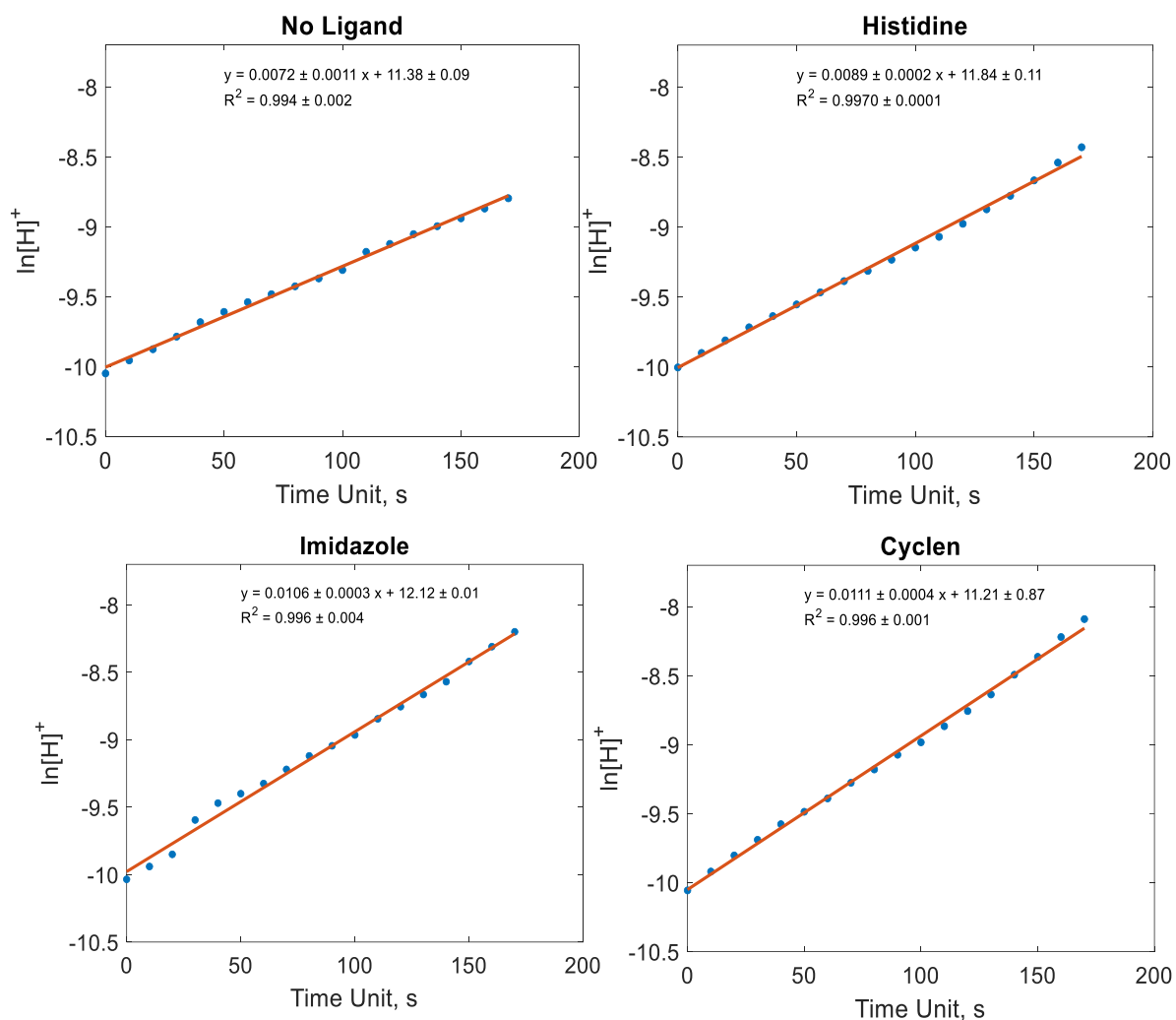


**Figure 7.14.** Linear regression fitting of the evolution of pH when saturating 2 M KOH solutions with gaseous CO<sub>2</sub> in presence and in the absence of  $[Zn(L)_x]^{2+}$ , where L are different ligands tested (histidine, imidazole and cyclen).

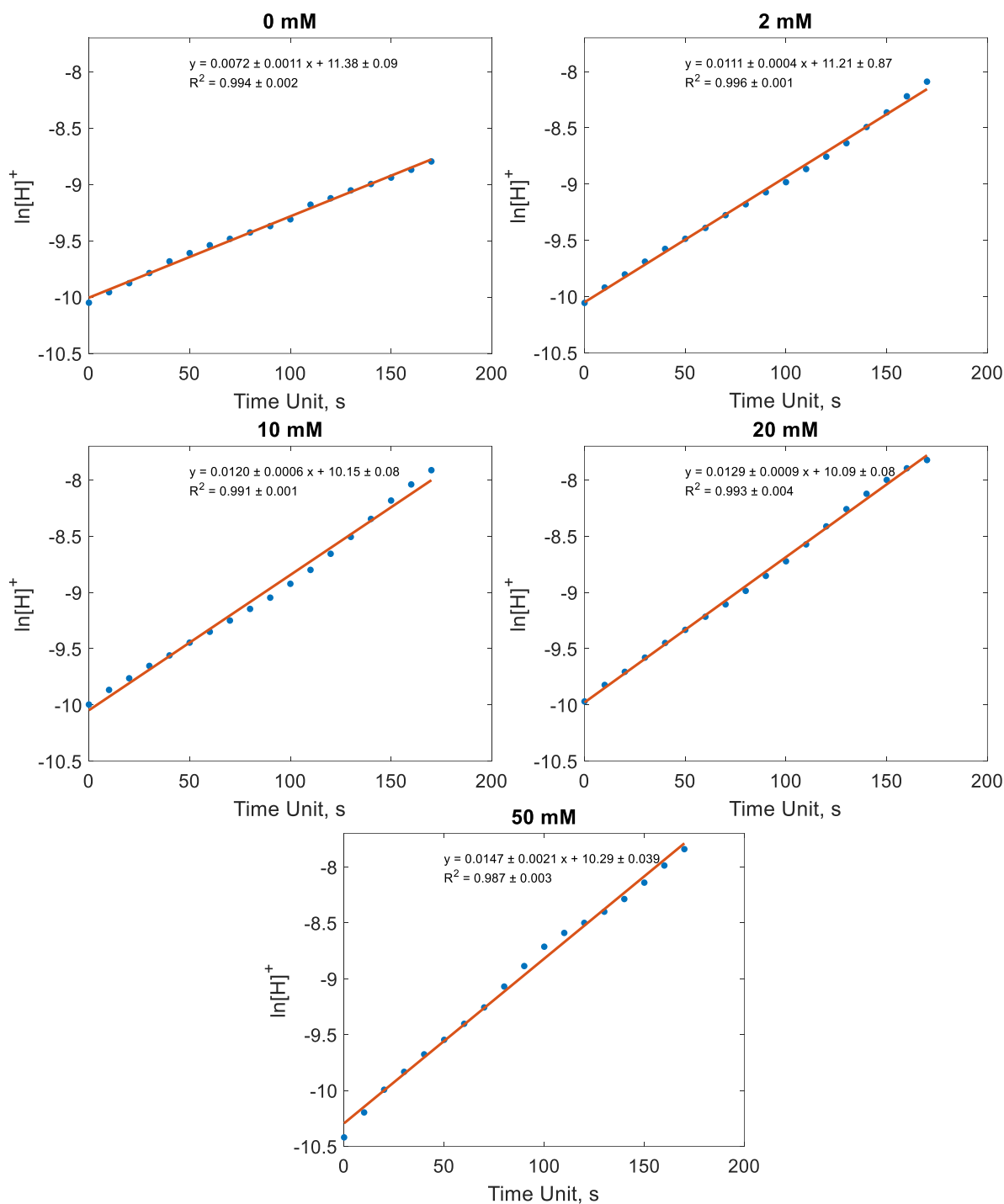


**Figure 7.15.** Linear regression fitting of the evolution of pH when saturating 2 M KOH solutions with gaseous CO<sub>2</sub> in presence and in the absence of [Zn(cyclen)]<sup>2+</sup> at different concentrations.

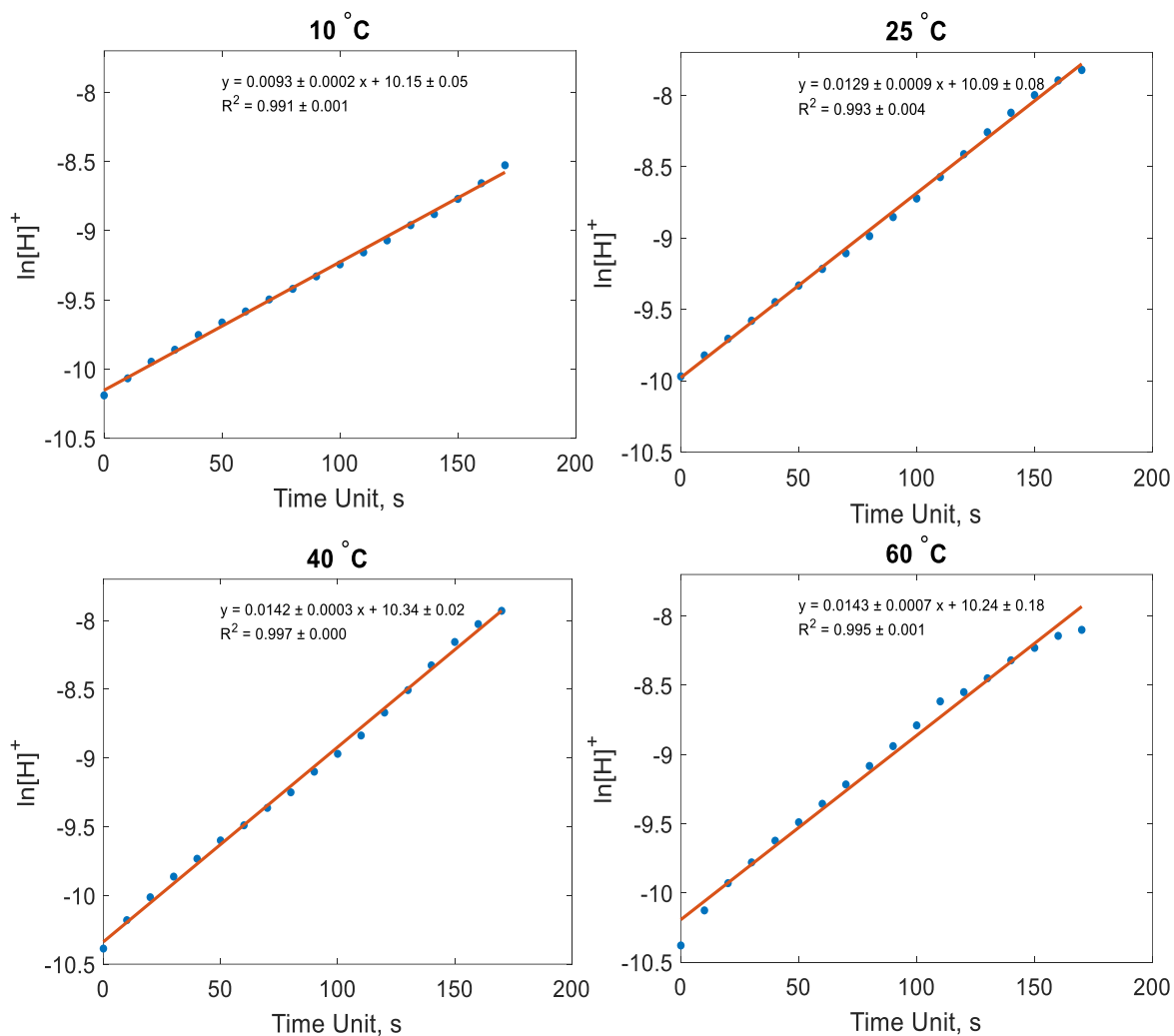


**Figure 7.16.** Linear regression fitting of the evolution of pH when saturating 2 M KOH solutions at different temperature with gaseous CO<sub>2</sub> in presence and in the absence of 20 mM [Zn(cyclen)]<sup>2+</sup>.

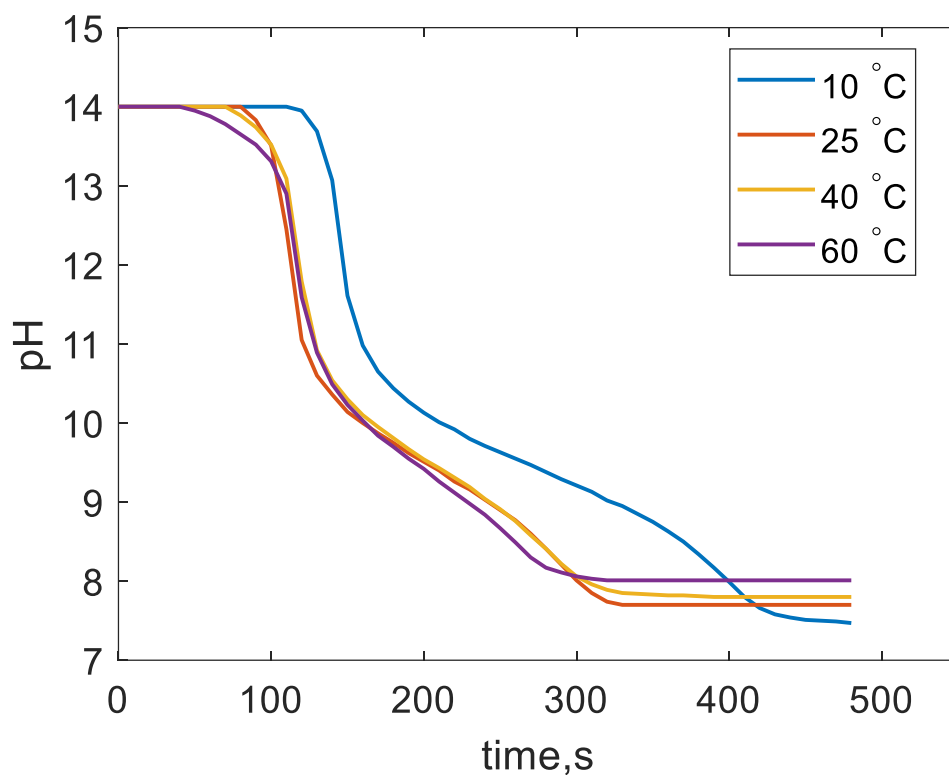


**Figure 7.17.** Evolution of pH when saturating a 2 M KOH solution with gaseous CO<sub>2</sub> at different temperature in the presence of 20 mM of [Zn(cyclen)]<sup>2+</sup>.



**Figure 7.18.** Sn working electrode after 1 h electrolysis in KHCO<sub>3</sub> 2 M in presence of 20 mM of [Zn(cyclen)]<sup>2+</sup> (left) and 2 mM of [Zn(imidazole)<sub>3</sub>]<sup>2+</sup> (right).





# **Part IV**

**Upscaling a bicarbonate electrolyser:  
Engineering approach and technological  
proof of concept**



## CHAPTER 8

### Engineering aspects for the design of a bicarbonate zero-gap flow electrolyser

BICARBONATE ZERO-GAP FLOW ELECTROLYSERS INVOLVING A BIPOLAR MEMBRANE AS A SEPARATOR ARE PROPOSED AS THE MOST PROMISING REACTORS FOR BICARBONATE ELECTROLYSIS APPLICATIONS. IN THIS CHAPTER WE INVESTIGATE THE INFLUENCE OF A VARIETY OF PROCESS PARAMETERS ON THE PERFORMANCE OF THE ELECTROLYSER.

This chapter is a shared contribution of both O. Gutierrez-Sanchez (who provided the fundamental knowledge regarding bicarbonate electrolysis) and B. De Mot (who provided the insights in the engineering aspects of the system). The findings of this chapter are published as: O. Gutierrez-Sanchez, B. De Mot, M. Bulut, D. Pant and T. Breugelmans, Engineering Aspects for the Design of a Bicarbonate Zero-Gap Flow Electrolyser for the Conversion of CO<sub>2</sub> to Formate, ACS Applied Materials & Interfaces, 2022 (in press)

## 8.1 Introduction

In part III of this thesis, the role of bicarbonate anion in bicarbonate electrolysis was unraveled. In addition, a strategy to increase the FE of bicarbonate electrolysis by inhibiting the HER using cationic surfactants was proposed, reaching FE<sub>Formate</sub> up to 70% when using bicarbonate electrolyte as CO<sub>2</sub> source and CKC or [Zn(cyclen)]<sup>2+</sup> as HER inhibitors. However, although the concept is promising, low partial CD was obtained (1-3 mA cm<sup>-2</sup>), limiting the up-scalability towards industrially relevant parameters (CD > 50 mA cm<sup>-2</sup>). Therefore, further research is needed to improve the viability of this technology. For this reason, in this thesis, we also explored the other main strategy to improve the bicarbonate electrolysis, which is to promote the carbon donor ability of bicarbonate instead of inhibiting the proton donor ability.

Recently, some studies explored how to improve the carbon donor ability of bicarbonate by acidifying in situ the catholyte (and thus releasing more CO<sub>2</sub> from bicarbonate) by using a BPM as a separator in a zero-gap flow electrolyser, depleting water to H<sup>+</sup> (towards the catholyte) and OH<sup>-</sup> (towards the anolyte) upon the polarization of the electrodes (Figure 8.1). The results obtained by using this strategy were promising, specifically in terms of partial CD (50-150 mA cm<sup>-2</sup>), and good FE towards formate or CO were obtained (40-60%).[165,167] However, since a BPM has a three-membrane layer configuration, the ohmic drop between the two electrodes is very high. In addition, an overpotential for water dissociation is added to the system thus becoming more inefficient in terms of EE of the electrochemical cell than in analogous systems involving CO<sub>2</sub> gas and ionomeric membranes (because of the increase in the cell voltage, V<sub>Cell</sub>).[112,114,115,164] Nevertheless, due to its special role in bicarbonate electrolysis, the use of BPM is benchmarked for the design of bicarbonate (zero gap) electrolysers.

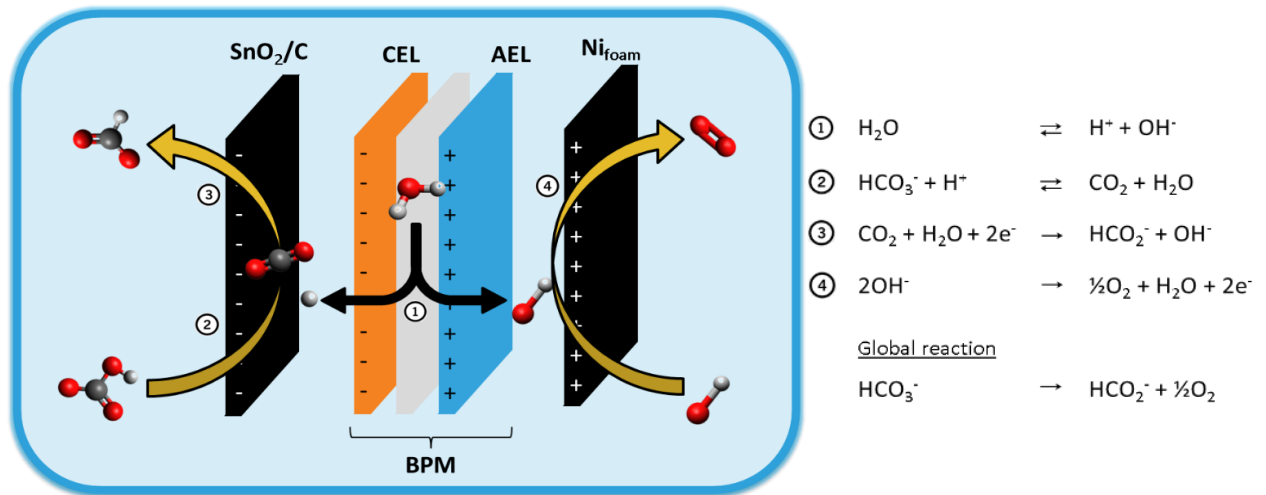


**Figure 8.1.** Schematic representation of the mechanism of bicarbonate electrochemical reduction to formate in reactors involving a BPM (CEL: Cation Exchange Layer. AEL: Anion Exchange Layer).

As the most promising strategy, there is interest in optimizing the performance of the bicarbonate zero-gap electrolyser involving BPM as a separator. The first approach was to find the most optimal configuration of the electrocatalyst to achieve the highest FE and partial CD towards carbon products. Most eCO<sub>2</sub>R flow electrolyzers involve GDE to avoid flooding of the electrode while the CO<sub>2</sub> is provided from the gas phase.[219] To achieve these functions, the GDEs are generally formed of carbon support, a MPL and a hydrophobic PTFE layer. Since in bicarbonate electrolyzers the CO<sub>2</sub> is delivered from the bicarbonate electrolyte, this electrocatalyst configuration was suboptimal. Lees *et al.* (2020) investigated the effect of the different layers present in a GDE for bicarbonate electrolysis. They proposed an optimal configuration of the electrocatalyst where the MPL and PTFE layers are removed from the GDE. The increase in the hydrophobicity of the electrode was detrimental for the diffusion of CO<sub>2</sub> from bicarbonate (partial flooding of the electrode is of interest in bicarbonate electrolyzers), thus decreasing the FE and partial CD.[166]

Other than investigating the configuration of the electrode, there is a lack of detailed research on other engineering aspects for bicarbonate electrolysis. Therefore, there is still

room for improvement on the optimization of a bicarbonate zero-gap flow electrolyser. For this reason, we have investigated how operational parameters such as the temperature of the reactor, the inlet flow rate of the electrolyte and the concentration of carbon load affect the performance of a bicarbonate zero-gap flow electrolyser involving a BPM. In addition, we have complemented the study on the optimization of the electrocatalyst done by Lees *et al.* (2020), by investigating the effect of the binder material used in the composition of the electrocatalyst ink on the performance of the system. Formate is targeted as a product as it allowed us to analyse and quantify it with high precision and therefore a Sn-based electrocatalyst was selected to convert bicarbonate since it is one of the most selective materials for the production of formate.[38] In addition, Sn has never been tested before in bicarbonate zero-gap flow electrolyzers, adding extra value to the study (only Bi has been reported).[220] Nevertheless, the conclusions of the results obtained in this study can be easily extrapolated to other targeted products, such as CO, since the same reactor configuration is currently used.

The  $FE_{\text{Formate}}$ , the formate concentration, the  $V_{\text{Cell}}$  and the EE were used to evaluate and compare the performance of the electrolyser in each case scenario for a broad range of current densities (10-400 mA cm<sup>-2</sup>). The formulas used are found in *Annex A.2.5* and the assumptions made to calculate the EE as the most accurate possible are found in the supporting information (*Chapter 9.5*). The FE allowed us to evaluate the selectivity of the electrolysis, the formate concentration allowed us to evaluate the profitability of the product solution for downstream processing, the  $V_{\text{Cell}}$  allowed us to evaluate the CE of the electrolyser and finally, the EE allowed us to evaluate the overall efficiency of the electrolysis (for upscaling prospects). For the evaluation of the effect of the binder material in the configuration of the electrode, only the FE was evaluated. At the end of this chapter, the most optimal configuration(s) are proposed for benchmarking high-efficient engineering aspects for the design of a bicarbonate zero-gap flow electrolyser.

## 8.2 Materials and methods

### 8.2.1 Materials and solutions

All the chemicals were obtained from commercial sources and used without purification unless stated otherwise.  $\text{KHCO}_3$  solutions used as catholyte were prepared by dissolving the corresponding amount of 3 M (unless stated otherwise) potassium hydrogen carbonate 99.5% (Chem-Lab) in Ultra-Pure water (MilliQ, 18.2 M $\Omega$  cm). The KOH solutions used as anolyte were prepared by dissolving the corresponding amount of 1 M of potassium hydroxide pellets (Chem-Lab) in Ultra-Pure water. Tin nanoparticles, particle size <150 nm (Sigma-Aldrich) and tin (IV) oxide nanoparticles (Sigma-Aldrich), particle size  $\leq$ 100 nm were used as the catalyst and porous carbon paper AvCarb MGL 190 (Fuel Cell Store) was used as catalyst support. Nafion D-520 dispersion (Alfa Aesar) and Sustanion<sup>®</sup> XA-9 (Dioxide Materials) were used as binder ionomer during electrode manufacturing. For the counter electrode, Ni foam (Nanografi) was used. To separate the catholyte and the anolyte, a BPM (FumaSep) was used.

### 8.2.2 Working electrode manufacturing

Adding complexity to the electrocatalyst material has been questioned due to the unrealistic upscaling capabilities even though the electrochemical response in lab-scale is proficient. For instance, complex electrodes that consists of multiple components such as nano-scaled arrangements, binders or additives present a huge variety of properties (conductivity, active sites, stability...) that, as a result, make the chemistry/structure of the surface almost impossible to correlate. Akbashev (2022) pointed out the necessity to benchmark and standardize patterns in electrocatalysis since the hard reproducibility of published reports have become a worrisome blockage to develop the technology, such as  $\text{eCO}_2\text{R}$ . [221] To benchmark our experimental procedure and to focus specifically on the engineering parameters of the reactor mentioned, commercial Sn (or  $\text{SnO}_2$ ) nanoparticles of particle size <150 nm are used. Del Castillo *et al.* demonstrated an optimal reduction

of CO<sub>2</sub> to formate on by using these Sn particles with a particle size of 150 nm.[222] We used this procedure in previous eCO<sub>2</sub>R engineering studies and it allowed a proper evaluation of the results obtained as well as good reproducibility.[223] Parallely, we used SnO<sub>2</sub> particles, too, as high performance has been observed in recent studies.[224,225]

Working electrodes were manufactured by spray coating a catalyst ink on top of a 4x4 cm<sub>2</sub> porous carbon paper. For the preparation of this ink, the nanoparticles (Sn or SnO<sub>2</sub>) were mixed with a 50/50 isopropanol/water solution. Optionally a binder ionomer was added to the mixture following the procedure benchmarked in our previous research (mass ratio of 70/30 nanoparticles/binder and concentration of 3 wt.%).[226] Next, a sonication probe (SinapTec NexTgen Lab 120) was used for 30 minutes to disperse the nanoparticles in the solution and create a homogenous ink. After the sonication procedure, the homogenous ink is deposited on the porous carbon substrate by airbrushing with argon as carrier gas. During the airbrushing procedure, the electrode was placed on a hotplate where the temperature was maintained at 60 °C to promote the evaporation of the solvent. Finally, the finished electrode is dried under atmospheric conditions and weighed to calculate the loading of the catalyst particles. All electrodes used in the experiments had a final loading of  $2.0 \pm 0.2$  mg cm<sup>-2</sup> nanoparticles.

### **8.2.3 Electrolysis**

The electrochemical screening is performed in a custom build bicarbonate electrolyser, of which a schematic presentation and details are shown in Figure A.16 and the whole set-up is shown in Figure 8.2. The electrolyte was not previously purged with an inert gas to mimic as better as possible a CO<sub>2</sub> capture solution. Then, O<sub>2</sub> reduction is assumed as an artefact of the process and as a contributor to the total FE. The bicarbonate enters the electrolyser from the bottom, where it flows through the graphite flow channel to the top of the electrolyser. The graphite flow channel has an interdigitated design, thereby the bicarbonate is convectively forced in the pores of the working electrode which is pressed against the graphite plate. This flow design thereby optimizes the mass transfer of



bicarbonate towards the catalyst surface. On top of the electrode, a BPM is placed. This BPM serves multiple purposes. 1) It separates the cathode from the anode region and thereby prevents product crossover; 2) allows the movement of ions in between the two electrodes and 3) provides the protons to the catholyte. The last purpose is essential for the good operation of the cell as the protons will dissociate the bicarbonate in water and  $\text{CO}_2$ . The anode side of the electrolyser is like the previously described cathode side. However, here a nickel foam was used as an electrode and potassium hydroxide as an anolyte. Copper current collectors are fitted against the backs of the graphite flow channels and are used to connect the potentiostat (Autolab PGSTAT302N) to the system. Finally, the electrolyser is assembled using two aluminium backplates and Viton gaskets to provide sealing.

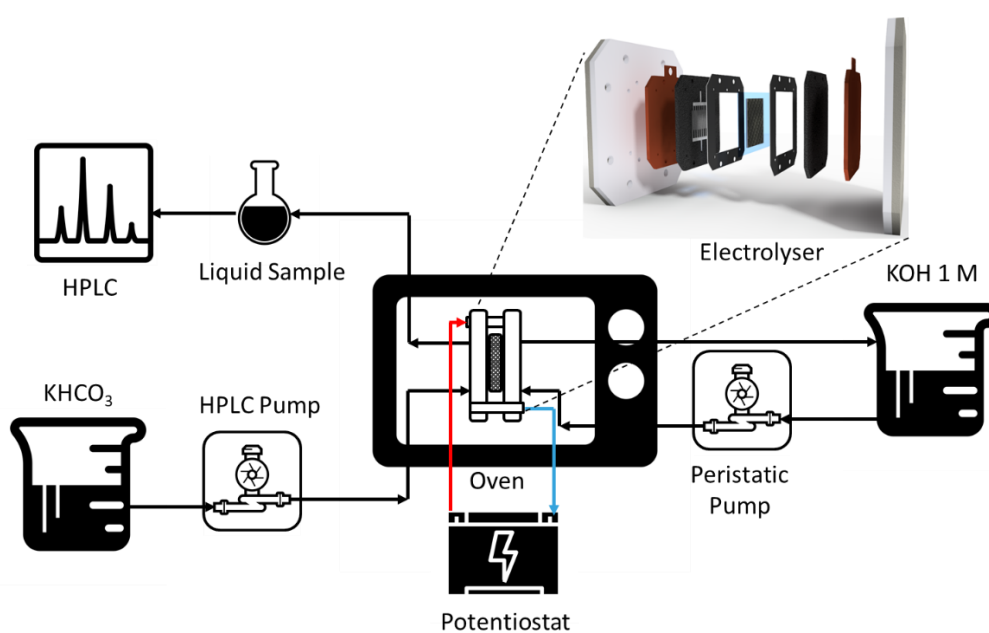


**Figure 8.2.** Schematic representation of the experimental set-up of the zero-gap electrolyser for bicarbonate electrochemical reduction.

The bicarbonate solution was fed in single-pass mode to the cathode side of the electrolyser using a HPLC pump which allowed for accurate control of the flowrate. At the outlet of the electrolyser, a liquid/gas separator was used to separate the different phases of the flow exiting the reactor and samples were taken for product analysis. On the anode

side, a peristaltic pump was used to recirculate 1000 mL of 1 M potassium hydroxide at a flow rate of 20 mL min<sup>-1</sup>. The complete electrolyser was placed in an oven (Binder Oven) to control the temperature of the system at multiple values (25, 40 and 60 °C). All the experiments were performed at 1 atm.

#### 8.2.4 Product analysis

For product analysis, Agilent 1200 HPLC with Agilent Hi-Plex H 7.7×300 mm column was used to separate the product and Agilent 1260 RID detector to detect and quantify formate in the form of formic acid. The samples were previously diluted with water and acidified with H<sub>2</sub>SO<sub>4</sub> to avoid bubble formation and obstruction in the column. H<sub>2</sub>SO<sub>4</sub> 0.01 M was used as the mobile phase. Two tests per set of experiments are performed and displayed as the average of FE, the concentration of formate, V<sub>Cell</sub> and EE. The error bars correspond to the standard deviation.

### 8.3 Results and Discussion

#### 8.3.1 Catalyst configuration: binder material and oxidation state

Tin-based catalysts are already well established among the preferred catalyst for the eCO<sub>2</sub>R towards formate. Recently it was shown that oxidized (IV) tin performed even better.[193,194,227] To analyse if this behaviour remains in a bicarbonate electrolyser, we have performed experiments with porous carbon on which either Sn or SnO<sub>2</sub> nanoparticles were deposited. The results displayed in Figure 8.3 (left) show that at low current densities (10 mA cm<sup>-2</sup>) the FE<sub>Formate</sub> is slightly better on Sn (38%) versus SnO<sub>2</sub> (33%). However, by increasing the CD a drop in FE<sub>Formate</sub> on Sn was observed, while on SnO<sub>2</sub> drastically increased. At 25 mA cm<sup>-2</sup>, the FE<sub>Formate</sub> on SnO<sub>2</sub> nanoparticles reached a peak at 51% after which it linearly decreased to 31% at 100 mA cm<sup>-2</sup>. On Sn nanoparticles, the FE<sub>Formate</sub> drops 29% at 25 mA cm<sup>-2</sup>. Further increase of the current had little effect as

the  $FE_{\text{Formate}}$  stabilized at 30%. From these results, in analogy to  $e\text{CO}_2\text{R}$  electrolyzers,  $\text{SnO}_2$  outperforms Sn.

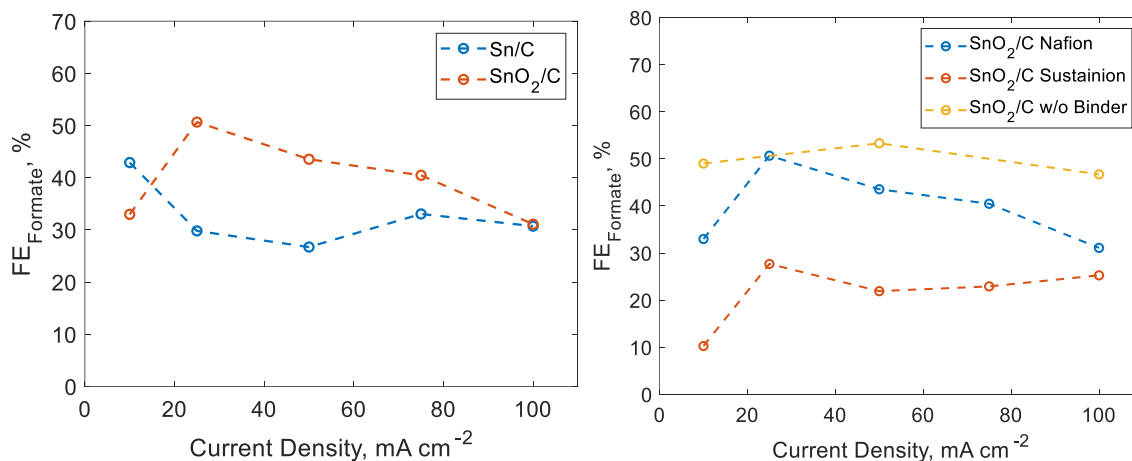


**Figure 8.3.**  $FE_{\text{Formate}}$  when using Sn or  $\text{SnO}_2$  nanoparticles as electrocatalysts on top of a porous carbon substrate (left).  $FE_{\text{Formate}}$  when using a  $\text{SnO}_2/\text{C}$  catalyst with a Nafion binder, a Sustainion® binder or without a binder (right).

Since in bicarbonate electrolyzers there is high competition with HER, we also evaluated the effect of the binder material used in the manufacturing of the working electrodes. The binder may have an impact on the performance of the reactor, caused by the high proton activity at the catalyst surface due to the high rate of protons generated at the BPM surface, in combination with the binder effect. A proton exchange binder such as Nafion promotes the transfer of  $\text{H}^+$  to the catalytic surface, promoting HER, while an anion exchange binder like Sustainion® promotes the transfer of bicarbonate ions (also a good proton donor) promoting HER as well. Overall, these phenomena promote HER and thereby lower the FE and partial CD towards formate. The data shown in Figure 8.3 (right) further confirms that the performance of the bicarbonate electrolyser was altered when different binder materials were used during the production process of the CL. Here the data is presented for porous carbon coated with  $\text{SnO}_2$  catalyst and either Nafion, Sustainion® or no binder present. Both the Nafion® and Sustainion® binders show similar behaviour. At low CD the  $FE_{\text{Formate}}$  is low. Then increasing the CD leads to a peak  $FE_{\text{Formate}}$

at 25 mA cm<sup>-2</sup> (27% and 51% for Sustainion® and Nafion respectively) and a further increase of CD results in the stabilization of FE<sub>Formate</sub>. Nevertheless, Nafion outperforms Sustainion® since the concentration of bicarbonate anions is substantially higher than protons. Again, the performance of the electrolyser in terms of FE<sub>Formate</sub> was severely limited due to the favouring of HER. When no binder was used, the FE<sub>Formate</sub> remained constant around 50%, increasing slightly to 54% at 50 mA cm<sup>-2</sup>, in contrast to the experiments with a binder, where a decrease in performance when the CD increased occurred.

Based on these experimental results and due to this study is not focused on the stability of the electrocatalyst, we decided to avoid using a binder as part of the ink for electrode manufacturing. We understand that, by not incorporating the binder, the stability of the electrode is compromised (as will be discussed further). However, obtaining higher FE (and thus higher absolute values) facilitated the evaluation and comparison of the different experimental results obtained in this study. It is worth mentioning that the results obtained in this section adds further knowledge in the field of developing electrocatalyst for bicarbonate reduction, and complements the studies done so far, as mentioned previously. Therefore, SnO<sub>2</sub> coated electrodes without binder were used during the experiment as it was shown that this is the optimal composition for the conversion of bicarbonate to formate.

### 8.3.2 Effect of the inlet flow rate

While research has shown that catalyst material and electrode composition are crucial in the optimization of reactor performance, it is also important to investigate the influence of process parameters, which is currently lacking in the literature. In the first set of experiments the bicarbonate flowrate is varied between 0.5 mL min<sup>-1</sup>, 1 mL min<sup>-1</sup> and 5 mL min<sup>-1</sup> while the CD is increased from 10 mA cm<sup>-2</sup> to 400 mA cm<sup>-2</sup>. The performance of the reactor (in terms of FE) is plotted versus the applied current density in Figure 8.4a for the different flow rates. The overall behaviour of the evolution of FE represented with the

different flow rates is very similar. At low current densities, when overpotential is low, the  $FE_{\text{Formate}}$  is between 41 and 18 % depending on the flow rate. These results are very similar to literature, where this behaviour is ascribed to the more preferred CO formation (one of the co-products often found when using Sn catalyst) at low overpotentials leading to a decrease of FE towards other carbon products such as formate, which is what we propose as an explanation of this observation.[228,229] However, gas phase analysis, which was not performed in this study, is needed to confirm this effect and give an exact value of FE towards CO and H<sub>2</sub>, as well as the possible energy losses present during the electrolysis. When the CD is increased towards 50 and 100 mA cm<sup>-2</sup> a sharp increase in  $FE_{\text{Formate}}$  can be noted. A maximum  $FE_{\text{Formate}}$  of 58 % was achieved at 5 mL min<sup>-1</sup> and 100 mA cm<sup>-2</sup>. A further increase of the CD led to a linear decrease of the  $FE_{\text{Formate}}$ , again this is like literature where the co-reaction HER starts dominating at increased overpotentials.[162]

When evaluating the effect of the flow rate in eCO<sub>2</sub>R, one of the most interesting parameters to study is the concentration of formate at the outlet of the catholyte. A lower flow rate increases the retention time of the catholyte in the electrolyser so the final concentration of formate at the outlet flow will be higher. The cost of the downstream processing to separate the formate from the rest of the solution and valorise it depends directly on its concentration. A higher concentration of formate decreases the operational costs of the DSP. Former studies on the processing of products for conventional gas-fed CO<sub>2</sub> electrolyzers stated that, to be technologically feasible, the concentration of formate must be at least 45 g L<sup>-1</sup>. [230] Although this concentration is calculated based on the processing of gas-fed CO<sub>2</sub> electrolyzers, it can serve as a reference for bicarbonate electrolyzers, too. In Figure 8.4b, the concentration of formate at the outlet catholyte for each case scenario is displayed. As observed, the concentration increases significantly when the flow rate decreases, as expected. For instance, at 100 mA cm<sup>-2</sup>, it increased from 2.1 to 10 and 27 g L<sup>-1</sup> when the flow rate was 5, 1 and 0.5 mL min<sup>-1</sup>, respectively.

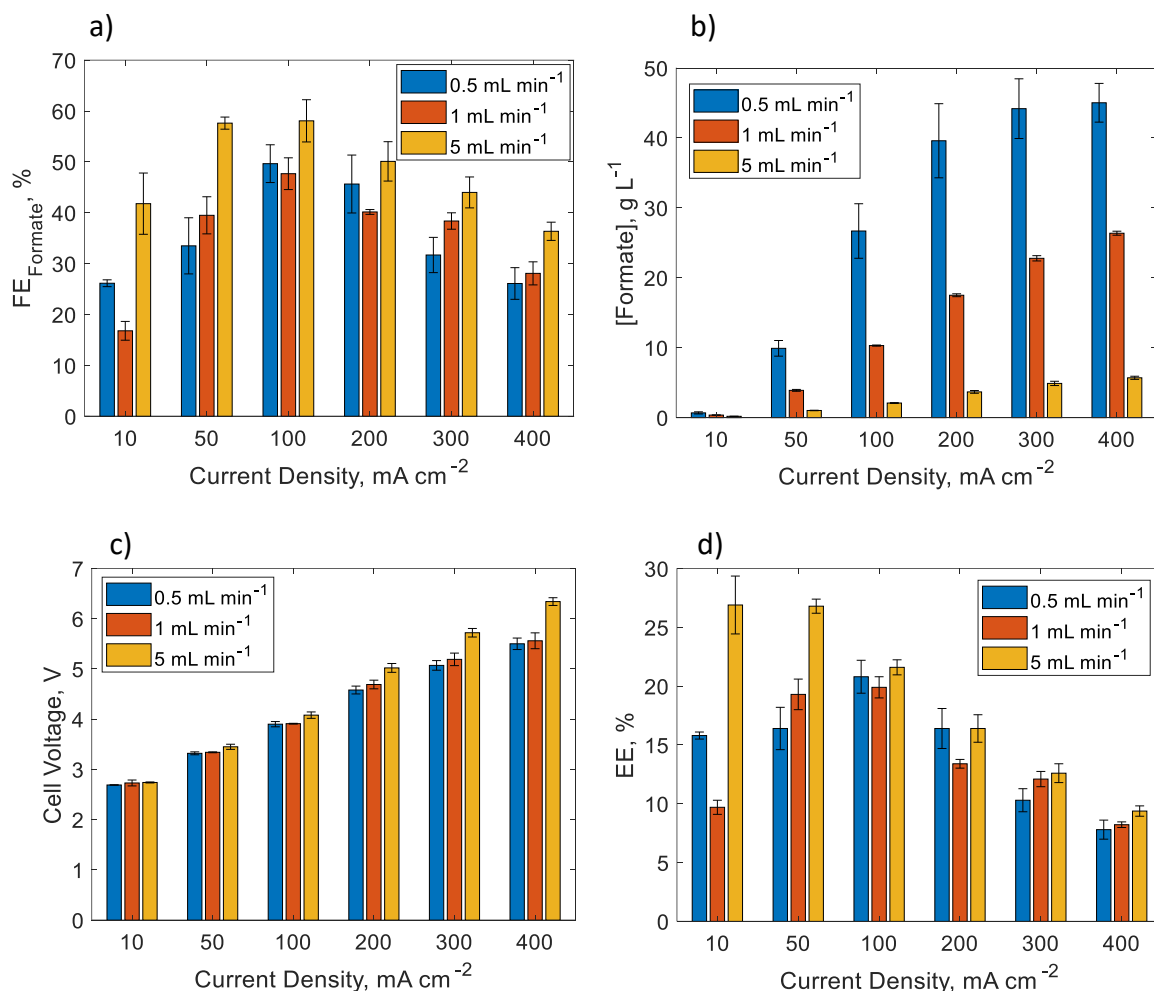


**Figure 8.4.** FE<sub>Formate</sub> (a), concentration of formate (b), V<sub>Cell</sub> (c) and EE (d) of the electrolysis of a KHCO<sub>3</sub> 3 M solution with a flow rate of catholyte of 0.5, 1 or 5 mL min<sup>-1</sup>

The increase in the concentration of formate is directly proportional to the flow rate although there are small variations due to the differences in the FE for each flow rate. This trend was not strictly followed along with the screening of CD when the flow rate is 0.5 mL min<sup>-1</sup> because the decrease in the FE as the CD increases is more significant (very little changes in concentration of formate from 200 to 400 mA cm<sup>-2</sup>). Interestingly when the flow rate was 0.5 mL min<sup>-1</sup>, at 200, 300 and 400 mA cm<sup>-2</sup> the concentration of formate was 40, 44 and 46 g L<sup>-1</sup> respectively, very close to the target concentration for downstream processing needed for upscaling the technology, mentioned before. At the highest flow rate, 5 mL min<sup>-1</sup>, although the overall highest FE was obtained, the

concentration of formate was not that interesting in terms of product processing (the maximum obtained was  $5.7 \text{ g L}^{-1}$  at  $400 \text{ mA cm}^{-2}$ ).

Initially, the flow rate had no noticeable influence on the  $V_{\text{Cell}}$  since it has the same value of  $2.7 \text{ V}$  at  $10 \text{ mA cm}^{-2}$ . Interestingly the  $V_{\text{Cell}}$  at  $5 \text{ mL min}^{-1}$  rose more rapidly with the CD than the experiment at  $0.5$  and  $1 \text{ mL min}^{-1}$ . At  $400 \text{ mA cm}^{-2}$ , a difference in  $V_{\text{Cell}}$  of  $800 \text{ mV}$  was noted (Figure 8.4c). Although with the experiments performed in this study we cannot give a precise explanation on this effect, we strongly believe the increase in the  $V_{\text{Cell}}$  at high CD and high flow rate is caused by the loss of the stability of the electrode/electrolyte interface. More detailed research involving techniques such as EIS would give further information and a proper evaluation of this effect. Therefore, for the flow rates studied, since the changes in the  $V_{\text{Cell}}$  were not significant, the variation in the EE is mostly given by the FE, following the same trend. Then, as the CD increases, the effect of the increase of the  $V_{\text{Cell}}$  becomes noticeable and the EE decreased. The most energy-efficient systems were found at  $5 \text{ mL min}^{-1}$  and  $10$  and  $50 \text{ mA cm}^{-2}$  (27 %).

From the results described above, it is clear that the most efficient performance was obtained at increased bicarbonate flowrate, although the difference is only noticeable at  $5 \text{ mL min}^{-1}$ . Little difference was found between  $0.5$  and  $1 \text{ mL min}^{-1}$ . It is hypothesized that this is caused due to the longer residence time of the in-situ generated gas bubbles at a lower flow rate such as  $0.5$  and  $1 \text{ mL min}^{-1}$  (mainly  $\text{CO}_2$  and  $\text{H}_2$ ). These bubbles will cover part of the catalyst surface and thereby will reduce the overall electrochemical active surface area, which obviously will negatively affect the cell's performance. However, by increasing the flow rate of the bicarbonate, the gas/liquid ratio of the cell will decrease (i.e., more liquid will be present in the cell) and thus less of the catalyst surface will be shielded, resulting in higher  $\text{FE}_{\text{Formate}}$  and EE. In addition to  $\text{CO}_2$ , most of the gas formed is  $\text{H}_2$  produced during the reaction. When the flow rate is low, these  $\text{H}_2$  bubbles stay on the surface of the electrode or in the zero-gap interface, decreasing the performance of the reactor. A higher electrolyte flow rate will mechanically remove the  $\text{H}_2$  bubbles and allow most of the surface of the electrode to be fully operational for the

duration of the experiment. Additionally, an increased flow rate will increase the turbulence in the cell and thereby promote the convective mass transfer of (ionic) species towards and away from the electrochemically active surface and mass transport-related losses are reduced. Finally, the retention time of the produced formate in the cell is lower at an increased flow rate, thus the crossover flux through the membrane is smaller. However, as shown in literature the crossover through BPM is rather limited thus this effect will be minimal.[113,231]

### 8.3.3 Effect of the temperature of the electrolyser

We studied the effect of the temperature by building the electrolyser up in an oven and fixing the value of the temperature in a way that the whole reactor is in isothermal conditions. By doing this, not only the KHCO<sub>3</sub> electrolyte but also the electrodes and the rest of the components of the electrolyser will be affected by the temperature. We expected to affect the system in different ways by changing the temperature. First, the electrochemical thermodynamic parameters, such as the electrochemical reduction and oxidation potentials ( $E_{\text{red}}$  in the cathode and  $E_{\text{ox}}$  in the anode), will be decreased with the increase of temperature, as the Nernst equation indicates, leading to a decrease in the  $V_{\text{Cell}}$ . On the other hand, the solubility of CO<sub>2</sub> (already low at room temperature, 0.033 M) will decrease with the increase of temperature, as Henry's law indicates, and we show in Figure 8.7. For instance, at 40 °C the solubility of CO<sub>2</sub> in water is 0.026 M and at 60 °C the solubility is 0.018 M, decreasing the amount of dissolved CO<sub>2</sub> in the electrolyte. In a bicarbonate solution, there is always a fraction of dissolved CO<sub>2</sub> derived from the equilibrium of bicarbonate with water, which is determined by the pH (see Bjerrum plot in *Annex A.3.1*). At the working pH of 8.3, this fraction is 1.2%. Therefore, in a 3 M KHCO<sub>3</sub> solution, there is 0.036 M of dissolved CO<sub>2</sub> which is higher than the solubility of CO<sub>2</sub> in water at 25 °C, 0.033 M. Thus, in a 3 M KHCO<sub>3</sub> solution at 25 °C only 0.033 M remains as dissolved CO<sub>2</sub>. As the temperature increases, not only does the solubility of CO<sub>2</sub> decrease but the solubility of KHCO<sub>3</sub> increases stabilizing the solution to detriment of the depletion of HCO<sub>3</sub><sup>-</sup> to dissolved CO<sub>2</sub> and H<sub>2</sub>O. [232] Since in bicarbonate electrolysis the dissolved



CO<sub>2</sub> is the active substrate of the reaction instead of CO<sub>2</sub> gas, it means a decrease in the amount of available CO<sub>2</sub> to react and thus a decrease in the FE. In addition, the thermodynamic acidic constant ( $K_{a1}$ ) of the equilibrium reaction between HCO<sub>3</sub><sup>-</sup> and CO<sub>2</sub> will be modified. The increase in temperature increases the value of the  $K_{a1}$ , meaning that the ratio HCO<sub>3</sub><sup>-</sup>/CO<sub>2</sub> will increase in favour of HCO<sub>3</sub><sup>-</sup> (more HCO<sub>3</sub><sup>-</sup> and less CO<sub>2</sub> will be present at equilibrium after the BPM donates H<sup>+</sup>). Furthermore, the ionic conductivity of the electrolyte will increase favouring the mobility of ions, thus decreasing the resistivity of the electrolyte and improving the V<sub>Cell</sub>. Then, we can assume that increasing the temperature is favourable for decreasing the V<sub>Cell</sub> but unfavourable for the electrochemical conversion of CO<sub>2</sub> (FE) since less dissolved CO<sub>2</sub> and more HCO<sub>3</sub><sup>-</sup> (HER promotor) will be available in the reactor. However, we also must consider the effect of the temperature in the kinetics of the reaction and the diffusion of reactants. The increase of temperature promotes the exchange current density and the diffusion constant and thus the reaction rate of CO<sub>2</sub> to formate. Nevertheless, we must investigate if the increase in the kinetics of the reaction and the decrease of the V<sub>Cell</sub> is enough to overcome the drawbacks of decreasing the solubility of CO<sub>2</sub> and increasing the rate of HCO<sub>3</sub><sup>-</sup>/CO<sub>2</sub> in the electrolyte. In this regard, the EE is a parameter that can be used to evaluate the performance of each system since we can then compare both the contributions of the temperature to the V<sub>Cell</sub> and the conversion of CO<sub>2</sub> (FE).

To properly evaluate the effect of temperature we performed electrolysis at 25, 40 and 60 °C fixing the concentration of KHCO<sub>3</sub> at 3 M and the flow rate at 5 mL min<sup>-1</sup>. As shown in Figure 8.5a, the FE<sub>Formate</sub> decreases with the increase of temperature at CD below 100 mA cm<sup>-2</sup> (for instance 58, 51 and 43% at 25, 40 and 60 °C respectively) confirming the mentioned effect of the lack of dissolved CO<sub>2</sub> present and the increase in the solubility of KHCO<sub>3</sub>. After 100 mA cm<sup>-2</sup>, the difference of the FE<sub>Formate</sub> at 25 and 40 °C is not significant (44% at 300 mA cm<sup>-2</sup>), but it still decreases at 60 °C (41% at 300 mA cm<sup>-2</sup>). At 40 °C the decrease in the concentration of dissolved CO<sub>2</sub> is compensated by the improvement in the kinetics of the reaction and the diffusion when the CD is over 100 mA cm<sup>-2</sup>. Below 100

mA cm<sup>-2</sup>, these improvements are not compensating for the lack of dissolved CO<sub>2</sub> present in the electrolyte. At CD higher than 100 mA cm<sup>-2</sup>, the FE<sub>Formate</sub> is similar to 25 °C, in contrast with 60 °C, where even at high CD the low solubility of CO<sub>2</sub> is more significant than the increase in kinetics. Another observation is that the highest FE<sub>Formate</sub> obtained at 25 °C is at 50 mA cm<sup>-2</sup> (58%), while at 40 and 60 °C it is at 100 mA cm<sup>-2</sup> (59 and 52% respectively), confirming the improvement in the kinetics of the reaction when the temperature is increased (the reaction is kinetically controlled at larger voltage). In this case and contrast with the flow rate, the difference of the concentration of formate at the outlet catholyte with the temperature appears to be solely dependent on the FE, as it follows the same trend (higher FE, higher concentration). Since formic acid is not a very volatile compound at mild conditions (boiling point 101 °C at 1 atm) there is not any special effect of applying 40 and 60 °C (Figure 8.5b).

If we take a look at the EE (Figure 8.5d), although the FE<sub>Formate</sub> is lower, the system is more efficient at converting CO<sub>2</sub> to formate at 40 and 60 °C when the CD is higher than 100 mA cm<sup>-2</sup> (13 and 14% EE at 300 mA cm<sup>-2</sup> at 40 and 60 °C respectively), due to the drastic decrease of the V<sub>Cell</sub> induced to the system (from 5.7 at 25 °C to 5.4 and 4.8 V at 300 mA cm<sup>-2</sup> at 40 and 60 °C respectively) and the decrease of the electrolyte resistivity (Figure 8.5c). However, the most energy-efficient system was still at 25 °C, specifically when 50 mA cm<sup>-2</sup> were applied (27%). We can then conclude that the effect of increasing the temperature is beneficial when working at a higher CD than 100 mA cm<sup>-2</sup>, where the decrease in the V<sub>Cell</sub> has a huge impact on the EE of the system. However, CD below 100 mA cm<sup>-2</sup> is still desired for achieving the highest EE. In addition, taking into account that for the EE calculations we did not consider the energy invested to heat up the system to the desired temperature (since it is a very variable parameter that depends on the setup used) we can further conclude that there is no interest in increasing the temperature if we want to achieve higher EE. This adds value to the technology as the best performance is at room temperature, a very attractive parameter for upscaling the technology.

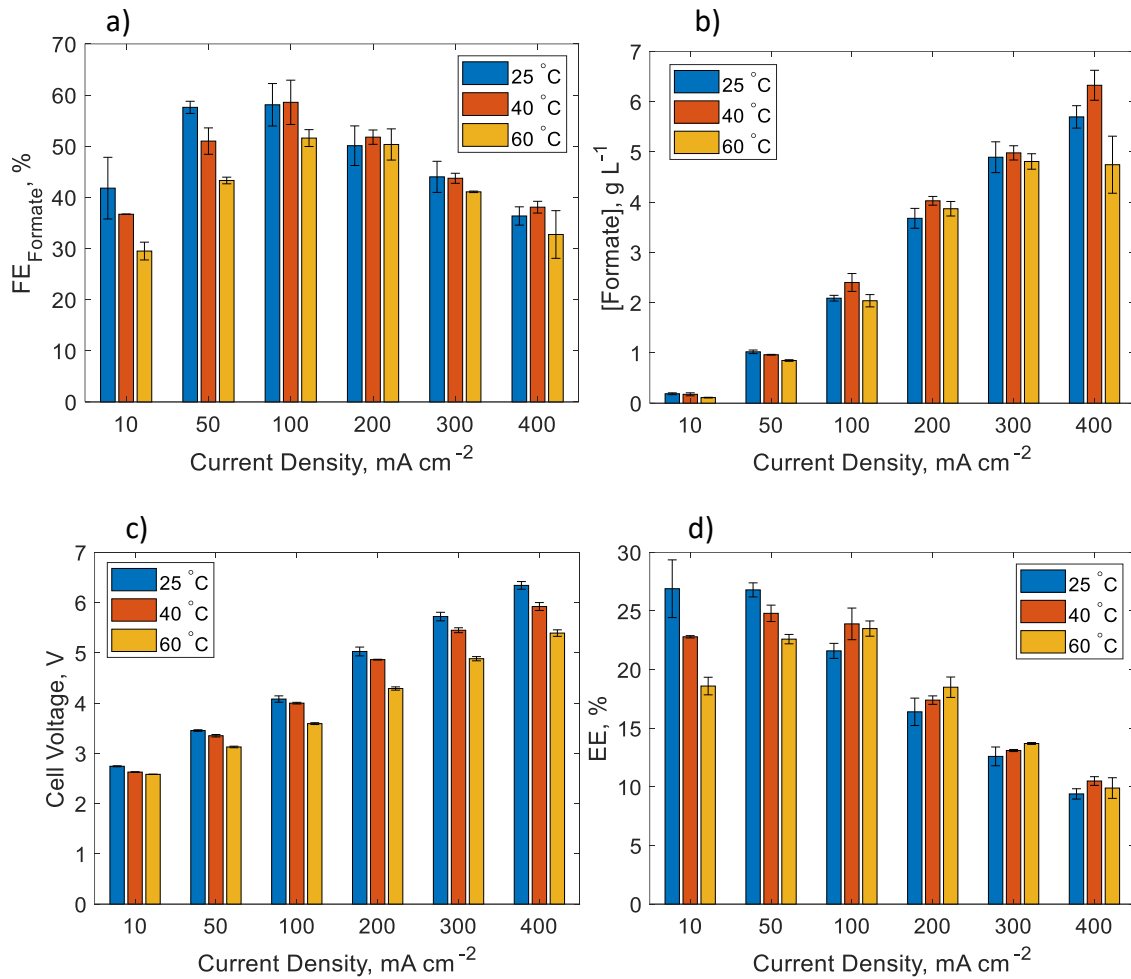


**Figure 8.5.** FE<sub>Formate</sub> (a), concentration of formate (b), V<sub>Cell</sub> (c) and EE (d) of the electrolysis of a KHCO<sub>3</sub> solution at 25, 40 and 60 °C.

### 8.3.4 Effects of the concentration of carbon load (bicarbonate)

To increase the FE towards eCO<sub>2</sub>R products from KHCO<sub>3</sub> electrolytes it is desired to use as high concentration of KHCO<sub>3</sub> as possible since then the highest amount of dissolved CO<sub>2</sub> will be present (for instance 0.036 M CO<sub>2</sub> in KHCO<sub>3</sub> 3 M, comparable to saturated CO<sub>2</sub> solutions, 0.033 M). However, obtaining a 3 M KHCO<sub>3</sub> solution from DAC or flue gas capture using KOH solution as capturing agent is still unrealistic and ambitious from an industrial point of view due to the low amount of CO<sub>2</sub> present in the air (400-420 ppm) and thus the low concentrated KHCO<sub>3</sub> solution obtained during the capturing step. For the experiments performed in this study up to this section, the concentration of the

solution of KHCO<sub>3</sub> used as electrolyte was 3 M since the highest concentration of CO<sub>2</sub> dissolved can be achieved and it was the state-of-the-art solution used in previous reports.[165,220] However, KHCO<sub>3</sub> 3 M is an oversaturated solution, thus unstable over time and unrealistic from a CO<sub>2</sub> capture technology perspective. For this reason, we electrolyzed unsaturated KHCO<sub>3</sub> solutions and compared them to the oversaturated KHCO<sub>3</sub> 3 M solution to evaluate if the zero-gap electrolyser can still convert CO<sub>2</sub> from less concentrated KHCO<sub>3</sub> solutions. To perform these experiments, we fixed the temperature to 25 °C and the flow rate to 5 mL min<sup>-1</sup> and we used KHCO<sub>3</sub> solutions of 1, 2 and 3 M as electrolytes.

The results in Figure 8.6a show how the FE<sub>Formate</sub> decreases when the concentration of KHCO<sub>3</sub> decreases, which was expected since less dissolved CO<sub>2</sub> and carbon donor (KHCO<sub>3</sub>) is present in the electrolyte (0.036, 0.024 and 0.012 M CO<sub>2</sub> in KHCO<sub>3</sub> 3, 2 and 1 M respectively). For instance, at 100 mA cm<sup>-2</sup>, the FE<sub>Formate</sub> goes from 58 to 41 and 33% when the concentration of KHCO<sub>3</sub> is 3, 2 and 1 M, respectively. The trend of FE<sub>Formate</sub> with the CD is the same for every KHCO<sub>3</sub> concentration used: there is an increase in the FE<sub>Formate</sub> up to 50 mA cm<sup>-2</sup> and then it decreases (slowly in KHCO<sub>3</sub> 3 M electrolytes) as the CD increases, forming a plateau from 300 mA cm<sup>-2</sup> onwards when the concentration of KHCO<sub>3</sub> is 2 and 1 M. As shown, the FE<sub>Formate</sub> when using unsaturated KHCO<sub>3</sub> solutions is relatively high taking into consideration the low concentration of dissolved CO<sub>2</sub> present, although the highest FE<sub>Formate</sub> obtained is still when using oversaturated KHCO<sub>3</sub> solutions as electrolyte (as thus higher dissolved CO<sub>2</sub> present). For instance, 41% of FE<sub>Formate</sub> at 50 mA cm<sup>-2</sup> when using KHCO<sub>3</sub> 1 M as an electrolyte is an interesting result for upscaling technologies, taking into account that the amount of dissolved CO<sub>2</sub> in a KHCO<sub>3</sub> 1 M solution is 0.012 M (three times less than a saturated CO<sub>2</sub> and KHCO<sub>3</sub> solution). This is likely caused by the proton donor ability of bicarbonate, less dominating when the concentration is lower like 1 M. The changes in the concentration of formate at the outlet catholyte with the different concentration of bicarbonate follow the same trend as the FE like it happened in the case of the temperature (Figure 8.6b). Therefore, there is not a

special role of the initial concentration of  $\text{KHCO}_3$  on the final concentration of formate, as expected.

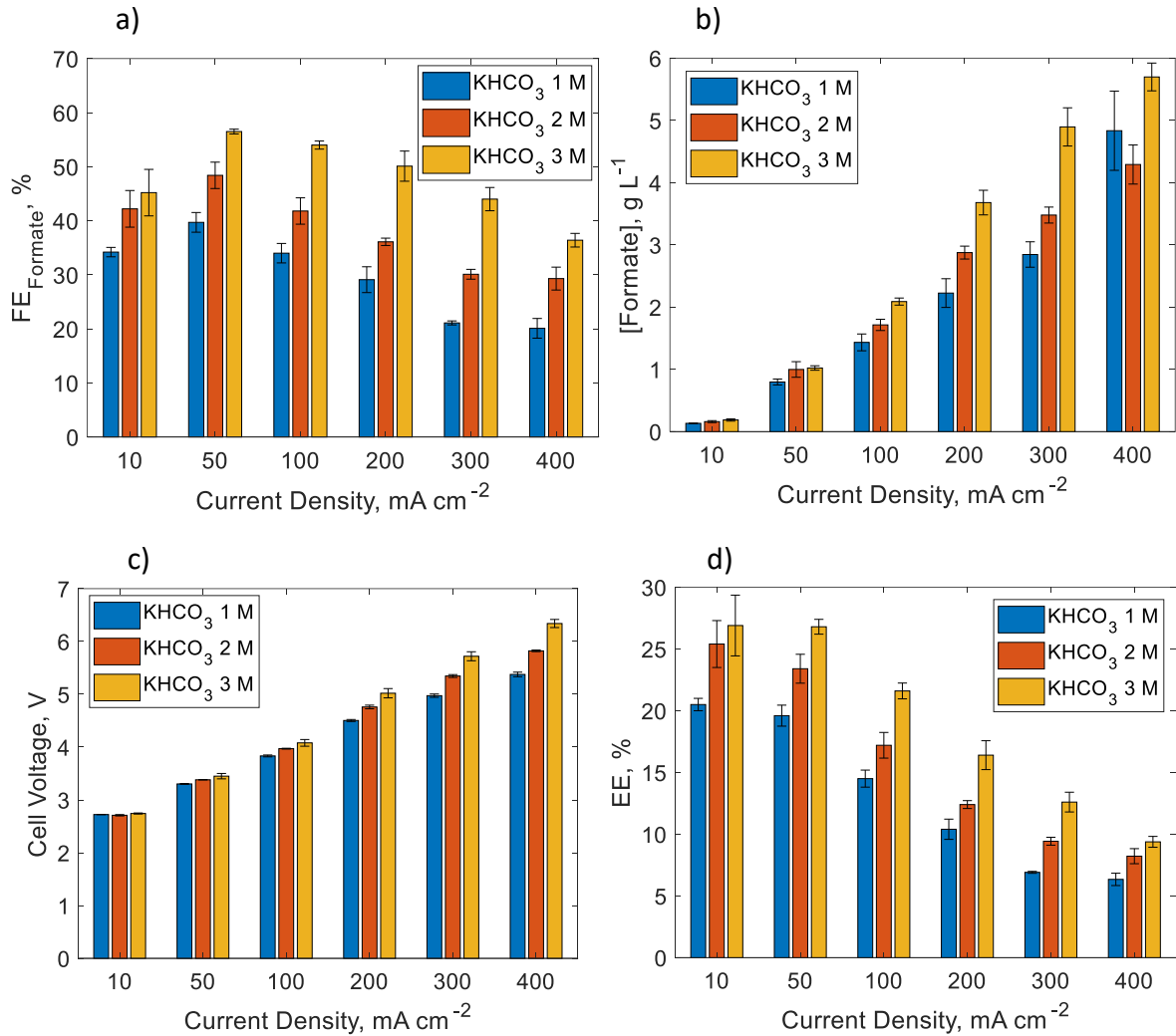


**Figure 8.6.**  $\text{FE}_{\text{Formate}}$  (a), concentration of formate (b),  $V_{\text{Cell}}$  (c) and EE (d) of the electrolysis of  $\text{KHCO}_3$  solutions of 1, 2 and 3 M.

The  $V_{\text{Cell}}$  also decreased when the concentration of  $\text{KHCO}_3$  decreased (Figure 8.6c). This effect is better observed at high CD, as we previously explained when discussing the effects of the flowrate (*vide supra*). However, in this case, there is another parameter to consider. As observed, the  $V_{\text{Cell}}$  is not directly linked to the  $\text{FE}_{\text{Formate}}$  like it did when the flow rate was studied. For instance, from 50  $\text{mA cm}^{-2}$  onwards, the difference in the  $\text{FE}_{\text{Formate}}$  between the three concentrations of  $\text{KHCO}_3$  used remained similar

(approximately 15% between 3 and 2 M and 8% between 2 and 1 M) but the difference in the  $V_{\text{Cell}}$  increases with the CD. This is because  $\text{KHCO}_3$  loses buffering effect as the concentration decreases, meaning that the acidification of the catholyte by the depletion of  $\text{H}_2\text{O}$  in the BPM will decrease the local pH close to the surface of the electrode and thus increase the concentration of  $\text{H}^+$ , decreasing the overall  $V_{\text{Cell}}$ . Even though the  $V_{\text{Cell}}$  decreases when the concentration of  $\text{KHCO}_3$  decreases (for instance 4.9, 5.3 and 5.9 V at  $300 \text{ mA cm}^{-2}$  for  $\text{KHCO}_3$  1, 2 and 3 M respectively) and then we should expect an increase in the EE of the process, the EE of the conversion of  $\text{CO}_2$  is still higher as the concentration of  $\text{KHCO}_3$  is higher (Figure 8.6d). For instance, 15, 17 and 22% at  $100 \text{ mA cm}^{-2}$  for  $\text{KHCO}_3$  1, 2 and 3 M, respectively. Therefore, in this case, the increase in the  $\text{FE}_{\text{Formate}}$  has a higher impact on the overall EE than the decrease in  $V_{\text{Cell}}$ . The most energy-efficient experiment, 27%, was when using  $\text{KHCO}_3$  3 M at  $50 \text{ mA cm}^{-2}$  since the  $\text{FE}_{\text{Formate}}$  obtained is the highest (58%) and the polarization of the electrode is not enough to increase the  $V_{\text{Cell}}$  significantly (3.3, 3.4 and 3.5 V for  $\text{KHCO}_3$  1, 2 and 3 M respectively).

## 8.4 Conclusions

Due to the necessity to reduce the costs of the overall  $\text{CO}_2$  Capture and Conversion systems, the attention is focused not only on the optimization of the  $\text{CO}_2$  electrochemical reactors but also on the capture and release of  $\text{CO}_2$  to the electrochemical cell. Bicarbonate reduction, which was declared inefficient and its applicability was in doubt, is starting to gain attention since it is one of the most promising routes towards developing an efficient integrated  $\text{CO}_2$  capture and conversion system involving the electrochemical reduction of  $\text{CO}_2$ . Thanks to the recent knowledge gained in reactor design and on the mechanism of bicarbonate reduction, the process is now feasible at a lab scale and easier to be upscaled. In this chapter, we have displayed how different engineering aspects such as the inlet flow rate, the temperature of the reactor or the concentration of bicarbonate, not yet evaluated for the current reactor used for bicarbonate conversion (zero-gap electrolyser involving a BPM as a separator) affect the

parameters often used to evaluate the performance of an eCO<sub>2</sub>R electrolyser such as the CD, the FE, the concentration of product formed, the  $V_{\text{Cell}}$  and the EE. Overall, the most efficient systems were found at low CD (10, 50 mA cm<sup>-2</sup>), high flow rate (5 mL min<sup>-1</sup>), room temperature and high KHCO<sub>3</sub> concentration (3 M), with a maximum EE of 27% (well comparable to commonly reported EE in gas-fed CO<sub>2</sub> electrolysers). Nevertheless, from a product processing perspective, the most interesting system is found at a low flow rate (>40 g L<sup>-1</sup> of formate were produced at 0.5 mL min<sup>-1</sup>). As a final observation, the electrocatalyst can be further optimized, especially focusing on its stability. The system's EE drops to 27 to 17% after 3 hours of reaction time (Figure 8.8) which is assumed because of the loss of catalyst activity, probably caused by the lack of binder material during the electrode manufacturing.[233,234] Nonetheless the findings in this work show promising results towards the implementation of fine-designed bicarbonate electrolysers for the integrated capture and conversion of CO<sub>2</sub>.

## 8.5 Supporting information

Assumptions and approximations:

The pH of the catholyte determines the half-reaction and the reduction potential of an eCO<sub>2</sub>R system. The zero-gap configuration of the setup did not allow us to measure the exact pH of the catholyte. Therefore, the pH of the catholyte is measured before entering the electrolyser. For a bicarbonate solution, the pH is 8.33. Then, for the calculation of the CE (and then the EE), bicarbonate is selected as the substrate of the electrochemical half-reaction although the bicarbonate solution is acidified to CO<sub>2</sub> prior the reaction and in-situ the electrolyser (due to the water dissociation in the BPM). We must assume then that the water dissociation overpotential of the BPM is included in this model.

Half-reaction	pH <sub>electrolyte</sub>	E (V <sub>SHE</sub> )	E (V <sub>RHE</sub> )
$\text{HCO}_3^- + 2\text{H}^+ + 2\text{e}^- \rightarrow \text{HCOO}^- + \text{H}_2\text{O}$	8.33	-0.0780 (6.38 < pH < 10.34)	0.424
$\text{H}_2\text{O} \rightarrow \frac{1}{2}\text{O}_2 + 2\text{H}^+ + 2\text{e}^-$	14	1.23	2.060

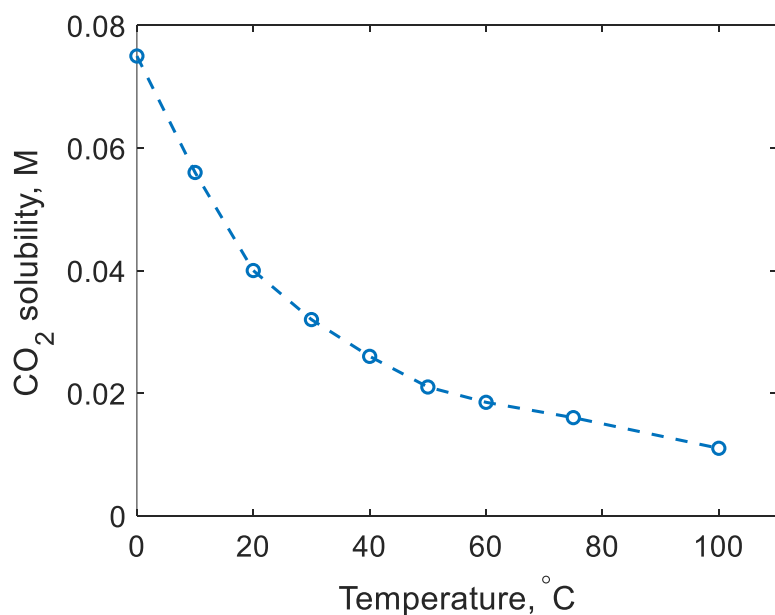


**Figure 8.7.** Solubility of dissolved CO<sub>2</sub> in water at different temperature and at 1 atm based on Henry's law constant at given temperature.

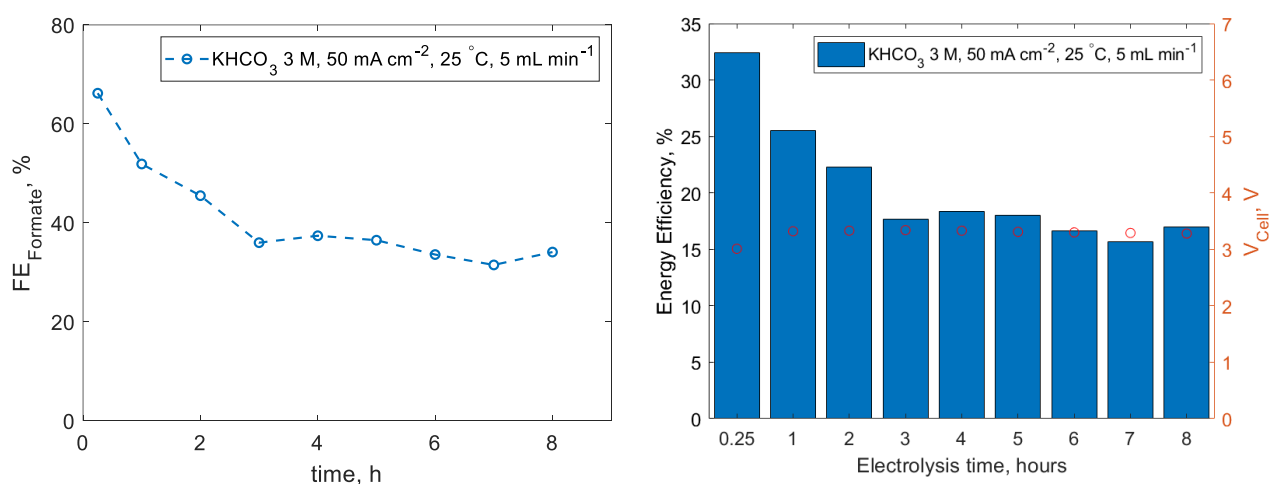


**Figure 8.8.** Stability test of 8 hours. Parameters: KHCO<sub>3</sub> 3 M catholyte, 5 mL min<sup>-1</sup> flow rate, room temperature (25 °C) and 50 mA cm<sup>-2</sup>.



# CHAPTER 9

## Electrochemical CO<sub>2</sub> Conversion from Direct Air Capture solutions

IN THIS FINAL EXPERIMENTAL CHAPTER, ALL THE KNOW-HOW GAINED FROM THE OTHER CHAPTERS ARE PUT INTO PRACTICE IN FORM OF A DIRECT AIR CAPTURE CO<sub>2</sub> ELECTROLYSER. THE CO<sub>2</sub> IS CAPTURED FROM THE AIR IN FORM OF A BICARBONATE/CARBONATE SOLUTION AND, THANKS TO THE OPTIMAL CONDITIONS FOR HIGH EFFICIENCY FOUND IN CHAPTER 8, THE ZERO-GAP ELECTROLYSER IS ABLE TO CONVERT THIS CAPTURED CO<sub>2</sub> TO FORMATE AND CARBON MONOXIDE.

The findings of this chapter are currently under review to be published as: O. Gutierrez-Sanchez, B. De Mot, N. Daems, M. Bulut, J. Vaes, D. Pant and T. Breugelmans, Electrochemical CO<sub>2</sub> Conversion from Direct Air Capture solutions, ACS Energy Letters, 2022

## 9.1 Introduction

Using the results from *Chapter 8*, a procedure to electrolyze bicarbonate solutions was benchmarked and thus electrolyzing CO<sub>2</sub> post-capture solutions is potentially available. In this chapter, we report for the first time, the electrochemical conversion of CO<sub>2</sub> that has been obtained directly from the air, integrating both the capture and the conversion steps in one and only proof-of-concept carbon capture and conversion system. By capturing the CO<sub>2</sub> from the air in form of (bi)carbonate with a DAC system and then electrolyzing the (bi)carbonate solution in a zero-gap flow electrolyser, CO<sub>2</sub> was converted to formate and CO by using a SnO<sub>2</sub>-based and an Ag-based electrocatalyst, respectively. This study sets a new benchmark in the field of CCU since the integrated capture and conversion of CO<sub>2</sub> is proposed as one of the most promising strategies to reach the milestone of closing the CO<sub>2</sub> cycle with a positive techno-economic balance.

## 9.2 Experimental

### 9.2.1 Materials and solutions

All the chemicals were obtained from commercial sources and used without purification unless stated otherwise. The capturing solution and the anolyte were prepared by dissolving the corresponding amount of 1 M of potassium hydroxide pellets (Chem-Lab) in Ultra-Pure water (MilliQ, 18.2 MΩ cm). The capillary module 3M™ Liqui-Cel™ MM-1.7x8.75 was chosen as membrane contactor for CO<sub>2</sub> sequestration based on a previous evaluation performed at VITO. Tin (IV) oxide nanopowder (<100 nm, >99%) and Ag nanopowder (<100 nm, >99.5%) from Sigma-Aldrich were used as the electrocatalyst and porous carbon paper AvCarb MGL 190 (Fuel Cell Store) was used as catalyst support. For the counter electrode, Ni foam (Nanografi) was used. To separate the catholyte and the anolyte, a Bipolar Membrane (FumaSep) was used.

### 9.2.2 Direct Air Capture: Procedure

The set-up used for the DAC experiments is shown in Figure A.13. A sealed bottle was filled with 300 mL of the capture solution: 1 M KOH. This time, the concentration of KOH chosen was 1 M instead of 2 M as precaution since high alkaline solutions might damage the DAC setup. The capture solution is pumped through the valve at 75 mL min<sup>-1</sup>, towards the inside (lumen side) of the capillaries. The fan is set to an operational airflow velocity of 0.22 m s<sup>-1</sup>. The channel displaces a volumetric flow of ~12 m<sup>3</sup> h<sup>-1</sup> air (fan system's exit area: 180 cm<sup>2</sup>) to the module holder, which corresponds to a CO<sub>2</sub> flow of ~0.2 mol h<sup>-1</sup>. The pH of the solution is continuously monitored and registered to evaluate the evolution of the acidity of the solution. The experiment is stopped after 8.5 hours of duration and the solution is stored. The solution remained stable for several weeks (pH invariant at ~10.6).

### 9.2.3 Working electrode manufacturing

Working electrodes were manufactured by spray coating a catalyst ink (SnO<sub>2</sub> or Ag nanoparticles) on top of a 4x4 cm porous carbon paper following the procedure described in *Chapter 8.2.2* and *8.3.1* and inspired by the electrode optimization study of Lees *et al.*[166,168] To maximize the performance of the catalyst in terms of FE and partial CD, no microporous layer and PTFE layer were added to the carbon support and no binder was added to the ink. It is assumed that the stability of the catalyst is affected by the lack of binder, however, in this study, we did not evaluate the stability of the system. Every electrode used in the experiments had a final loading of 2.0 ± 0.2 mg cm<sup>-2</sup> of nanoparticles. The resulting electrode SnO<sub>2</sub>/C was used to convert the DAC solution to formate while Ag/C was used to convert the DAC solution to CO in separated experiments.

#### 9.2.4 (Bi)carbonate electrolysis: setup and procedure

The electrochemical experiments were performed in a custom build zero-gap flow electrolyser (Figure A.16). The same electrolyser was used in the previous chapter and the details are described in *Annex A.5.2*. The (bi)carbonate solution obtained from DAC was used as the catholyte. The catholyte enters the electrolyser from the bottom, where it flows through the interdigitated designed graphite flow channel pressed against the working electrode to the top of the electrolyser thereby optimizing the mass transfer of the electrolyte towards the catalyst surface. On the other face, on top of the electrode, the BPM is placed. The anodic compartment of the electrolyser is like the previously described cathode side. However, here a nickel foam was used as an electrode and 1 M KOH as an anolyte. The electrolyser was connected to an Autolab potentiostat (model PGSTAT302N).

The experimental conditions were set based on the optimization study for bicarbonate electrolysis performed in *Chapter 8*.<sup>[168]</sup> From this study, the most optimal flow rate, temperature and CD to achieve the highest energy efficiency were chosen. The DAC solution was fed in single-pass mode to the cathode side of the electrolyser using a HPLC pump which allowed for accurate control of the flow rate at 5 mL min<sup>-1</sup>. On the anode side, a peristaltic pump was used to recirculate the 1 L of anolyte at a flow rate of 20 mL min<sup>-1</sup>. The complete electrolyser was placed in an oven (Binder Oven) to fix the temperature of the system at 25 °C. Chronopotentiometry (CP) experiments were performed at 50 mA cm<sup>-2</sup>. After 30 minutes, for liquid analysis (formate), samples were taken and stored, while for gas analysis (CO), in-situ gas analysis was performed (see *Chapter 9.3.2*).

## 9.3 Product analysis and characterization

### 9.3.1 Characterization of DAC solutions

After capturing CO<sub>2</sub> for 8.5 hours and after reaching equilibrium, the DAC solution is a mixture of dissolved CO<sub>2</sub>, bicarbonate and carbonate, known as DIC. By measuring the final pH and using the corresponding equilibrium equations and the total concentration of DIC present in the solution, the concentration of each species (carbonate, bicarbonate and dissolved CO<sub>2</sub>) is obtained (Figure A.8, Eq. A.14-16). We can assume a negligible concentration of dissolved CO<sub>2</sub> (<0.01%) at the working pH range (14-10). At the final pH obtained in this study (~10.6), since the carbonate/bicarbonate half-neutralization point is surpassed and thus the initial KOH was already converted to carbonate, the total DIC is equal to the concentration of KOH used as capturing solution (1 M). However, for this study, we could not make this assumption. As we disassembled the capture setup after the experiment, we observed (bi)carbonate salt precipitation around the capillary structure of the membrane contactor (Figure 9.1).

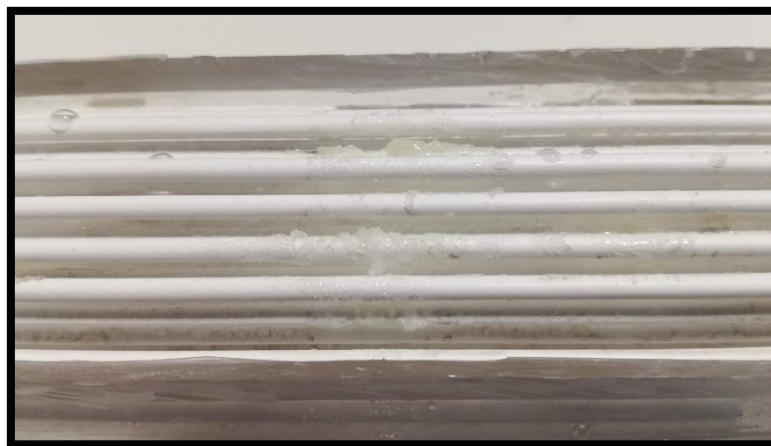


**Figure 9.1.** Salt precipitation (K<sub>2</sub>CO<sub>3</sub>/KHCO<sub>3</sub>) present at the membrane contactor after the CO<sub>2</sub> capture step.

Therefore, alkalinity is lost during the capture experiment and thus the concentration of DIC is lower than the initial concentration of KOH (although the ratio of bicarbonate/carbonate is maintained as it only depends on the pH). Even for upscaled and optimized DAC setups, we believe other methods must be used to properly quantify the (bi)carbonate species in DAC solutions since there will always be a loss of alkalinity to a certain extent due to the pH and concentration gradients in the contactor-solution interface. Thus, in this study, we wanted to benchmark a procedure to properly characterize DAC solutions for the integrated capture and conversion of CO<sub>2</sub>. We chose Fourier Transformed Infrared Spectroscopy (FT-IR) as the technique to characterize (bi)carbonate solutions. FT-IR has been previously used for instance by Joshi *et al.* to quantify bicarbonate and carbonate in solid mixtures and by Baldassarre *et al.* to measure the pH using (bi)carbonate systems.[235,236] We can then use FT-IR to quantify bicarbonate and carbonate in aqueous solutions and then use the pH ratio calculated as a validation of the method.

The trigonal planar carbonate (CO<sub>3</sub><sup>2-</sup>) has symmetry D<sub>3h</sub> and their vibrational modes  $\nu_2$  (A<sub>2</sub>''),  $\nu_1$  (A<sub>1</sub>') and  $\nu_3$  (E') are active in the infrared (IR) spectra. On the other hand, bicarbonate (HCO<sub>3</sub><sup>-</sup>) has symmetry C<sub>2v</sub> and, in addition to the modified CO<sub>3</sub> modes, the vibrational modes corresponding to the presence of OH  $\nu_5$  (A'),  $\nu_4$  (A') and  $\nu_1$  (A') are also active in the IR spectra (Table 9.1).[237] To quantify the concentration of each species present in the DAC solutions, we calibrated the absorption peak  $\nu_3$  (E') found at 1380 cm<sup>-1</sup>, corresponding to carbonate, and the absorption peak  $\nu_2$  (A') found at 1620 cm<sup>-1</sup>, corresponding to bicarbonate, with different bicarbonate/carbonate buffer solutions (Figure 9.2). The carbonate peak  $\nu_3$  (E') was corrected by subtracting the contribution of the bicarbonate's vibrational mode  $\nu_2$  (A') using the absorbance correction method. Therefore, FT-IR was used on the DAC solutions and the absorption peaks found at 1380 and 1620 cm<sup>-1</sup> were interpolated to the calibration slope, obtaining thus the real concentration of bicarbonate and carbonate in the solution.

**Table 9.1.** Vibrational modes of bicarbonate and carbonate in aqueous solutions.

<b>Bicarbonate (HCO<sub>3</sub><sup>-</sup>, C<sub>2v</sub>)</b>		
<i>Frequency (cm<sup>-1</sup>)</i>	<i>Vibrational mode</i>	<i>Description</i>
840	$\nu_8 (A'')$	CO <sub>3</sub> out-of-plane deformation
1000	$\nu_5 (A')$	C-OH stretch
1300	$\nu_4 (A')$	COH bend
1355	$\nu_3 (A')$	symmetric CO stretch
1620	$\nu_2 (A')$	asymmetric CO stretch
2620	$\nu_1 (A')$	OH stretch
<b>Carbonate (CO<sub>3</sub><sup>2-</sup>, D<sub>3h</sub>)</b>		
<i>Frequency (cm<sup>-1</sup>)</i>	<i>Vibrational mode</i>	<i>Description</i>
880	$\nu_2 (A_2'')$	CO <sub>3</sub> out-of-plane deformation
1056	$\nu_1 (A_1')$	symmetric CO stretch
1375 - 1430	$\nu_3 (E')$	asymmetric CO stretch

As a validation of the characterization technique, a similar bicarbonate/carbonate ratio was obtained either by calculating it with the pH (33%/67% ± 4%) or with FT-IR (25%/75% ± 8%). The concentration of DIC, carbonate and bicarbonate are given as an average of three independent DAC experiments. As mentioned, the relative abundance of dissolved CO<sub>2</sub> is negligible (<0.01%) at the pH range of the study and therefore not considered as part of the DIC. The error bars correspond to the standard deviation. Thermo Scientific spectrometer (model Nicolet iS10) was used to characterize the DAC solutions with FT-IR. The DAC solutions were not previously treated.

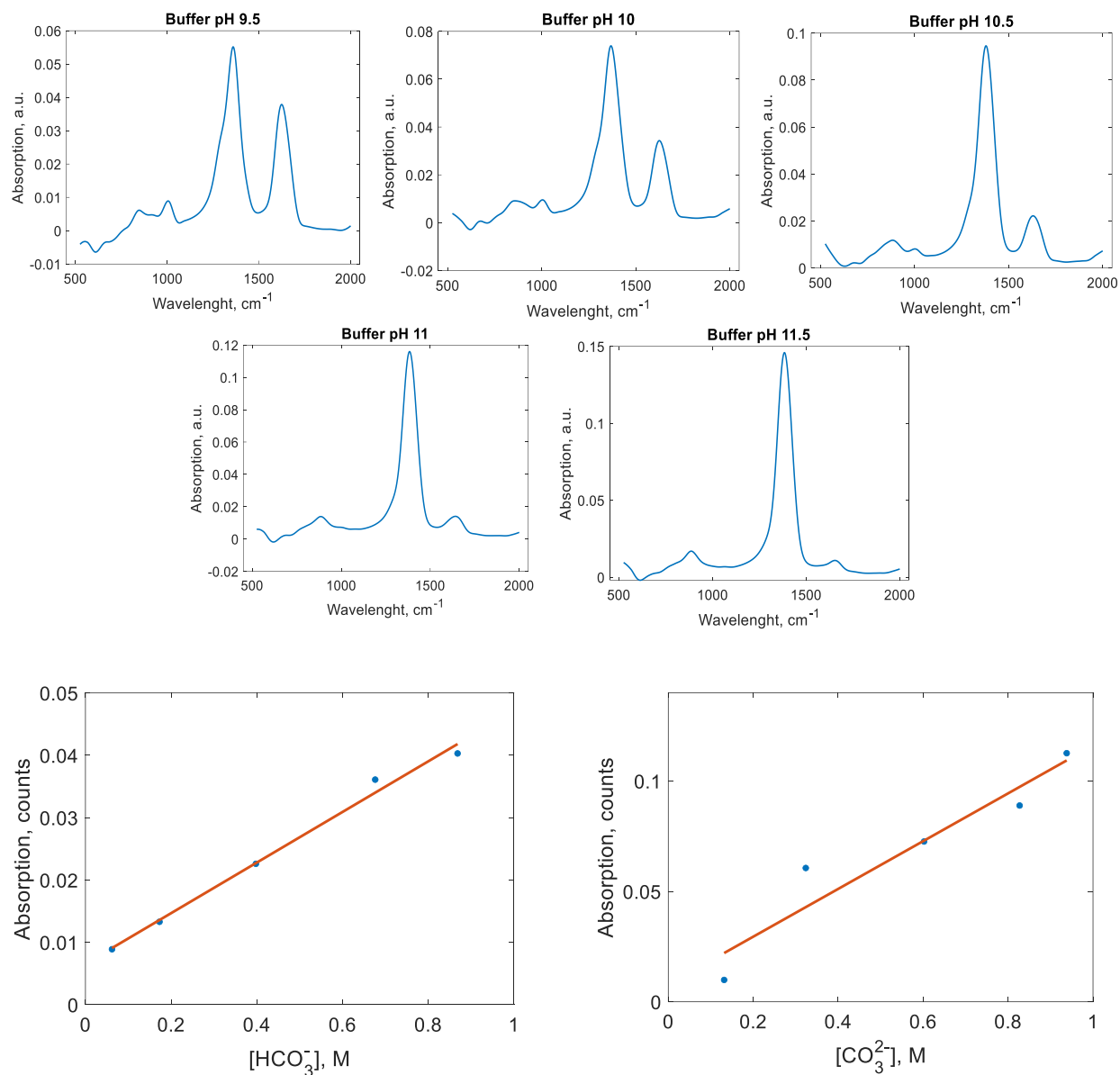


**Figure 9.2.** FT-IR spectra of the buffer solutions and calibration points of the absorption peak 1380 cm<sup>-1</sup> (carbonate, right) and 1620 cm<sup>-1</sup> (bicarbonate, left).

### 9.3.2 (Bi)carbonate electrolysis product analysis

For liquid product analysis, Agilent 1200 HPLC with Agilent Hi-Plex H 7.7×300 mm column was used to separate the product and Agilent 1260 RID detector to detect and quantify formate in the form of formic acid. The samples were previously diluted with water and acidified with H<sub>2</sub>SO<sub>4</sub> to avoid bubble formation and obstruction in the column. H<sub>2</sub>SO<sub>4</sub> 0.01



M was used as the mobile phase. For electrolysis experiments using SnO<sub>2</sub>/C as an electrocatalyst, only formate was analysed as a product.

For gas product analysis, Shimadzu 2014 Gas Chromatography with ShinCarbon St 100/120 2mx1mm column (Restek, USA) installed was used. Helium gas (10 mL min<sup>-1</sup>) was used as the carrier and the temperature of the column was set at 40 °C for 180 s. After the initial stage, the column's temperature was raised from 40 °C min<sup>-1</sup> to 250 °C. Detection of CO was done by a thermal conductivity detector at 280 °C. For electrolysis experiments using Ag/C as an electrocatalyst, only CO was analysed as a product.

The results are presented in the form of FE and  $V_{\text{Cell}}$  and compared to literature results corresponding to electrolysis experiments of bicarbonate solutions at different concentrations. The results are presented as an average of two independent experiments and the error bars corresponds to the standard deviation.

## 9.4 Results and discussion

### 9.4.1 (Bi)carbonate solution obtained from Direct Air Capture

The chemical reactions occurring when capturing CO<sub>2</sub> with an alkaline capture solution, such as KOH, are detailly described in *Annex A.4*. In Figure 9.3 (blue), where the evolution of the pH overtime for the DAC experiments is displayed, these reactions can be observed. During the first four hours of the experiment, the pH decreased gradually from 13.8 to 13.1 due to the consumption of OH<sup>-</sup>. Until this point, the  $[\text{K}_2\text{CO}_3] > [\text{KHCO}_3]$ . Then, from the fourth to the fifth hour, the half-neutralization point was reached ( $[\text{K}_2\text{CO}_3] = [\text{KHCO}_3]$ ) decreasing abruptly the pH from 13.1 to 10.9. From the fifth hour until the end of the experiment, the  $[\text{K}_2\text{CO}_3] < [\text{KHCO}_3]$  and the pH continued decreasing from 10.9 to 10.4 due to the acidification of the solution. The post-capture solution obtained was a mixture of K<sub>2</sub>CO<sub>3</sub> and KHCO<sub>3</sub>, referred to as (bi)carbonate solution. The ratio of the mixture was determined by the final pH (10.6 after reaching equilibrium) and the equilibrium

equations of carbonic acid in aqueous media (Eq. A.14-16). At pH 10.6, the bicarbonate/carbonate calculated ratio was 33%/67% ± 4% (Figure 9.3, orange).

The concentration of bicarbonate, carbonate (and thus DIC) of the DAC solutions were obtained by characterising the solution with FT-IR. In Figure 9.4, the IR spectra of the DAC solution, averaged from three independent DAC experiments, is displayed. As observed, both the characteristic absorption peaks of carbonate and bicarbonate selected to quantify the concentration are present. The concentration of bicarbonate calculated was 0.166 ± 0.063 M, while the concentration of carbonate was 0.492 ± 0.032 M. The concentration distribution corresponded to a bicarbonate/carbonate ratio of 25%/75% ± 8%, which was in the same range of the one calculated from the equilibrium equations, 33%/67% ± 4%. We assumed the slight deviation to shifts in the equilibrium as the solutions were exposed to open air during the manipulation and the characterisation of the samples.

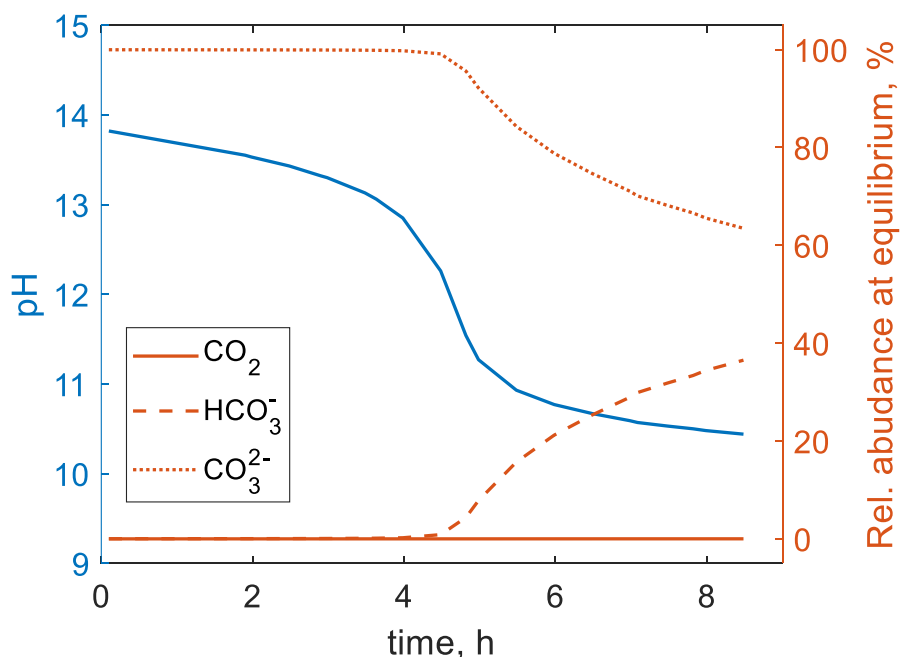


**Figure 9.3.** Evolution of the pH overtime of a DAC experiment using KOH 1 M as capture solution and air as CO<sub>2</sub> source (blue). Relative abundance of the carbonic species presents in the DAC solution after reaching equilibrium (orange).

The total DIC concentration was  $0.658 \pm 0.031$  M in contrast with the initial KOH concentration, 1 M. As we anticipated, there was a loss of alkalinity due to the precipitation of the potassium (bi)carbonate salts, therefore the assumption of  $[\text{DIC}] \neq [\text{KOH}]_0$  was adequate. Approximately, 5.7 g of KOH was lost within the duration of the experiment, corresponding to a loss rate of  $0.7 \text{ g h}^{-1}$ . It is very important to highlight this observation, as it is crucial for the techno-economic validation of a potential upscaled technology to minimize losses in every step. A huge alkalinity loss rate would require human maintenance more often, increasing the costs of the technology. Therefore, to minimize this effect, engineering efforts are required both for lab and upscaled levels. On the other hand, the CO<sub>2</sub> capture efficiency (captured CO<sub>2</sub> vs. CO<sub>2</sub> flow) was  $14.8 \pm 0.7$  %. This capture efficiency allowed up to capture CO<sub>2</sub> with a rate of  $1.4 \pm 0.7 \text{ g h}^{-1}$  and thus obtain a relatively high concentrated (bi)carbonate solution after 8.5 h. However, in long term capture experiments we observed that the pH almost did not drop further from 10 after more than 48 h of experiment. We attributed this effect to the loss of alkalinity mentioned earlier and the fact that the DAC solution acts as a buffer (CO<sub>2</sub>-bicarbonate-carbonate equilibrium). An increase in the mass transport of CO<sub>2</sub> from the air to the solution by a combination of minimizing the alkalinity loss and increasing the capture efficiency (for instance, by adding extra capture modules) would allow going lower in the pH, therefore capturing a more CO<sub>2</sub>.

In this section, we have captured CO<sub>2</sub> from the air using a KOH 1 M solution and we have validated FT-IR as a method to characterize DAC solutions. A total DIC concentration of  $0.658 \pm 0.031$  M ( $0.166 \pm 0.063$  M of bicarbonate and  $0.492 \pm 0.032$  M carbonate) was obtained. The DAC solutions obtained in the CO<sub>2</sub> capture experiment were mixed and evaluated as a single electrolyte in the following (bi)carbonate electrolysis experiment to avoid misevaluation of the results.

[HCO <sub>3</sub> <sup>-</sup> ] (M)	0.166 ± 0.063
[CO <sub>3</sub> <sup>2-</sup> ] (M)	0.492 ± 0.032
[DIC] (M)	0.658 ± 0.031
Capture rate (g h <sup>-1</sup> )	1.40 ± 0.07
Capture eff. (%)	14.8 ± 0.7

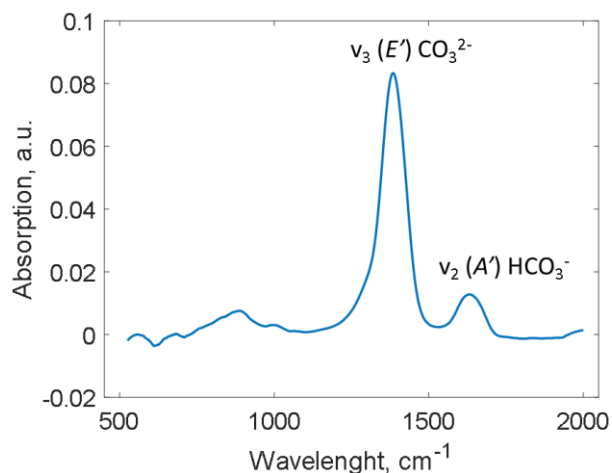


**Figure 9.4.** FT-IR spectra of the DAC solution, and concentration of each species, capture rate and capture efficiency calculated based on the data obtained from the FT-IR characterisation.

#### 9.4.2 Electrolysis of the Direct Air Capture solution

As mentioned, the DAC solution was used as the catholyte in a zero-gap (bi)carbonate flow electrolyser. A SnO<sub>2</sub>/C catalyst was used to convert DAC to formate and an Ag/C catalyst to convert DAC to CO, in separate experiments. In the past, carbonate and bicarbonate were studied separately as carbon donors for eCO<sub>2</sub>R, but a mixture of both has been never studied.[57,165] However, since the BPM was dissociating water and thus the species in the catholyte were acidified, we expected that approximately most of the species present on the surface of the electrode were bicarbonate and dissolved CO<sub>2</sub> (from carbonate and bicarbonate, respectively), depending on the protonating rate of the catholyte. Therefore, the performance of the electrolyser should be around or slightly less efficient than in using pure bicarbonate electrolytes. For this reason, we have compared the results obtained from electrolyzing DAC solutions to the state-of-the-art in bicarbonate electrolysis at different concentrations (1, 2 and 3 M). Our previous work on bicarbonate electrolysis to formate and the work of Li *et al.* on bicarbonate electrolysis to CO were used as references.[166,168]

The results of electrolyzing the DAC solution to formate are shown in Figure 9.5 (left). As observed on the state-of-the-art, there is a clear trend of decrease of the FE as the concentration of KHCO<sub>3</sub> decreases, which is understandable as less carbon donor species is present in the solution. For instance, the state-of-the-art FE is 58, 48 and 38% at 3, 2 and 1 M KHCO<sub>3</sub>, respectively, meaning that there is a decrease of 10% FE for each unit of molarity diminished. In this work, where we used a  $0.658 \pm 0.031$  M of DIC solution, the FE obtained was 16%, instead of 28%. However, the DAC solution is not a pure KHCO<sub>3</sub> solution, but instead, K<sub>2</sub>CO<sub>3</sub> is the most abundant species ( $0.492 \pm 0.032$  M). Therefore, it was expected that the trend was not followed exactly for DAC solutions. Two units of H<sup>+</sup> (dissociated from H<sub>2</sub>O in the BPM) were needed to convert K<sub>2</sub>CO<sub>3</sub> to dissolved CO<sub>2</sub>, while only one was needed to convert KHCO<sub>3</sub> to dissolved CO<sub>2</sub>, explaining why lower FE than hypothetically in pure 0.5 M KHCO<sub>3</sub> solutions was obtained. On the other hand, the  $V_{\text{cell}}$  slightly decreased, following the trend of the state-of-the-art, but few changes were observed.

The results of the analogous experiments, this time using an Ag/C electrocatalyst to convert DAC to CO, are shown in Figure 9.5 (right). The trend of the FE and the concentration of KHCO<sub>3</sub> observed previously for bicarbonate electrolysis to formate in the state-of-the-art (FE decreased when the concentration of KHCO<sub>3</sub> decreased) was observed here, too. However, in the case of bicarbonate electrolysis to CO, the decrease of the FE followed a multiplicative inverse trend ( $1/x$ ) instead of lineal, as was the case when formate was produced. For instance, the state-of-the-art FE is 70, 37 and 22% at 3, 2 and 1 M KHCO<sub>3</sub>, respectively, meaning that the decrease of the FE is approximately halved from 33 (from 3 to 2 M) to 15 % (from 2 to 1 M). When we electrolyzed the DAC solution, a FE towards CO of 13% was obtained, thus the FE decreased by 7% (approximately halved) compared to using KHCO<sub>3</sub> 1 M as electrolyte (from 22 to 13%), following the same trend as in the state-of-the-art KHCO<sub>3</sub> solutions, unlike when formate was the product of the electrolysis. However, we cannot assume that both systems (KHCO<sub>3</sub> and DAC as electrolyte) behave equally, although we agree they do it similarly.

On the one hand, the zero-gap reactor used by Lees *et al.* and ours were not identical, adding an error factor (which was not the case for the previous experiments where formate was the product of the electrolysis). Additionally, the cell voltage was higher in our system due to, precisely, this factor. On the other hand, the concentration of DIC is  $0.658 \pm 0.031$  M instead of 0.5 M (assuming every DIC is converted to KHCO<sub>3</sub>). The concentration of KHCO<sub>3</sub> in the DAC solution is  $0.166 \pm 0.063$  M. To compare both systems, we should assume that the consumption of KHCO<sub>3</sub> is compensated by the acidification of K<sub>2</sub>CO<sub>3</sub> and therefore the concentration of KHCO<sub>3</sub> in the electrolyser is approximately 0.5 M, which we cannot confirm without further analysis. However, we believe that indeed the concentration of both KHCO<sub>3</sub> and dissolved CO<sub>2</sub> might be similar in a 0.658 M DAC solution and a 0.5 M KHCO<sub>3</sub> solution during electrolysis or that, at least, the composition of the electrolyte led to similar electrochemical behaviour, leading to the similarities found in the results.

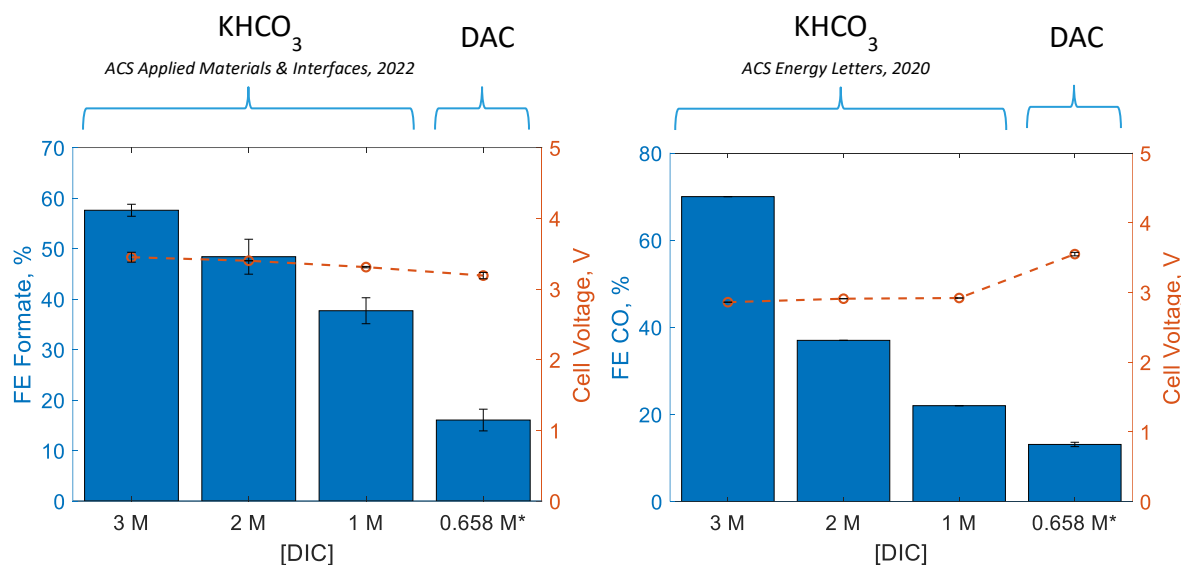


**Figure 9.5.** FE towards formate (left) and CO (right) of the electrolysis of a DAC solution of  $0.658 \pm 0.031$  M DIC at  $50 \text{ mA cm}^{-2}$ . The results are compared to state-of-the-art FE from KHCO<sub>3</sub> electrolysis. [166,168]

The results of the electrolysis presented revealed, for the first time reported, the conversion of CO<sub>2</sub>, which comes directly from a DAC solution, towards formate and CO.

The electrolysis of the DAC solutions, although they were a mixture of bicarbonate and carbonate (33%/67%), followed a similar trend to when using 100% KHCO<sub>3</sub> solutions (FE decreased similarly). Therefore, the know-how on bicarbonate electrolysis can be accurately extrapolated to DAC electrolysis (or to the electrolysis of bicarbonate/carbonate mixtures). Although the conversion of DAC to formate is most interesting from a proof-of-concept point of view (since no OH<sup>-</sup> is generated in the reaction), the conversion of DAC to CO is of high interest due to the formation of OH<sup>-</sup> as co-product of the eCO<sub>2</sub>R. Therefore, the alkalinity is regenerated and can be used as a capture solution in a closed cycle. In addition, low FE towards CO can be of interest for certain applications such as in the syngas industry. From our point of view, since in bicarbonate electrolysis good FE (>40%) has been obtained at high current densities (> 200 mA cm<sup>-2</sup>) when the concentration of bicarbonate is high (>1 M), it is crucial that higher loaded DAC solutions are tested in (bi)carbonate electrolyzers. The overall efficiency of the CCU technology strongly depends on that.

## 9.5 Conclusions

In this study, we have converted electrochemically the CO<sub>2</sub> that comes directly from the air by electrolyzing a DAC solution in a bicarbonate zero-gap flow electrolyser. After 8.5 h of capturing CO<sub>2</sub> with a 1 M KOH solution, a mixture solution of (bi)carbonate was obtained. By developing a procedure to characterize DAC solutions with FT-IR, the concentration of each species and the alkalinity loss were accurately quantified. The DAC solution was directly used as catholyte in the electrolyser and, by applying 50 mA cm<sup>-2</sup>, a FE of 16% towards formate (when using a SnO<sub>2</sub>/C as electrocatalyst) and 13% towards CO (when using Ag/C) were obtained, showing conversion of atmospheric CO<sub>2</sub> towards industrially relevant carbon products. By comparing the results obtained to state-of-the-art data on KHCO<sub>3</sub> electrolysis we observed that the ratio of FE with the concentration of carbon load is maintained (higher FE when the concentration is higher) for DAC solutions, too. Therefore, the concentration of DIC in the DAC solution is crucial to increase the

efficiency of the electrochemical conversion step, which should be considered as a priority in further steps. In conclusion, this proof-of-concept study sets a new benchmark for integrating the capture and the (electrochemical) conversion of CO<sub>2</sub> within the field of CCU.



# **Part V**

**Conclusions and future perspectives**



# CHAPTER 10

## Conclusions and future perspectives

YOU HAVE REACHED THE FINAL CHAPTER OF THIS DOCTORAL THESIS. TO SUMMARIZE OUR WORK, WE WILL CONCLUDE ALL THE FINDINGS FROM THE PREVIOUS CHAPTERS. ALSO, WE PROVIDE THE READERS WITH A CLEAR PERSPECTIVE ON THE NEXT STEPS IN FUTURE RESEARCH ON INTEGRATING THE CAPTURE AND THE ELECTROCHEMICAL CONVERSION OF CO<sub>2</sub>.

## 10.1 Conclusions

The goal of this doctoral thesis was to provide know-how on integrating the capture and the electrochemical conversion of CO<sub>2</sub>, which is proposed as one of the most promising strategies to reach the final milestone of developing an efficient CCU technology. When this thesis was started, the integrated concept was already considered as an option to overcome the high energy cost of treating the CO<sub>2</sub> capture solutions. However, research on the topic was barely existent, especially when the CO<sub>2</sub> was captured in the form of bicarbonate (bicarbonate electrolysis was almost unreported). Therefore, at the beginning of this thesis, we launched two questions: 1) What is the mechanism of bicarbonate electrochemical reduction? And 2) How can we make bicarbonate electrolysis work? Now, after the realization of this thesis, the mechanism of the electrochemical reduction of bicarbonate is described and designs of the firsts flow electrolyzers working at high current densities ( $>100 \text{ mA cm}^{-2}$ ) are reported. We proposed two main routes to convert bicarbonate solutions, one by inhibiting the proton donor ability and the other by promoting the carbon donor ability of the bicarbonate anion. Although the first route was more suitable for mechanistic studies (since it works in a batch, steady state configuration), the second route was the most promising towards upscaling (since higher currents were reached). Nevertheless, although overall the know-how is acquired, there are individual aspects to discuss on each of the studies done on this thesis.

### 10.1.1 Current state of the industrial eCO<sub>2</sub>R

From the TEA analysis done in *Chapter 1* it is shown that most of the costs of capturing and converting electrochemically CO<sub>2</sub> (even in an integrated strategy) come from the electricity usage. These costs are still blocking the technology towards applicability, consequently high valorisation of the products (productivity per unit of energy invested) is needed, which is still a challenging aspect. The electricity usage does not only come

from the operational aspects but also from the energy efficiency of the electrolysis. This energy efficiency depends primarily on the overall cell efficiency, secondarily on the selectivity of the reaction (Faradaic efficiency). It is thus of high importance to find high selective and stable catalysts while the energy losses of the electrolyser are minimized (i.e., ohmic drop, Joule effect...). However, as we discussed in *Chapters 3 and 4*, solely focusing on research and advancements in the individual components on small scale (i.e., catalyst, catholyte, membrane, capture solution, etc.) is not effective enough to upscale the technology, since there are complications when integrating the strategies. Instead, system-level optimization and demonstrations on the combination of all parameters are required.

### 10.1.2 Bicarbonate electrolysis

After identifying in *Chapter 5* the role of the bicarbonate anion as proton donor, and thus as HER promotor, we were able to design strategic pathways to reduce electrochemically bicarbonate solutions. On the one hand, the proton donor ability of bicarbonate was inhibited by covering the surface of the electrocatalyst with cationic surfactants, thus making it hydrophobic. This allowed a significant increase in the FE (i.e., >70% towards formate) and a better understanding of the mechanism of bicarbonate reduction, as it is described in *Chapters 5 and 6*. However, since the electrode was more hydrophobic, the total current dropped severely (i.e., from 30 to 3 mA cm<sup>-2</sup>) thus decreasing the feasibility towards upscaling. Furthermore, the addition of extra components to the electrolyte such as cationic surfactants increase the complexity of a potential downstream processing of separation of products. Nevertheless, the use of cationic surfactants in eCO<sub>2</sub>R is a promising strategy, since the HER competition is one of the main drawbacks of using aqueous solutions for eCO<sub>2</sub>R.

On the other hand, the other strategy we proposed to reduce electrochemically bicarbonate solutions is to promote the carbon donor ability of the bicarbonate anion. As it was already hypothesized in former studies and described by our findings in *chapter 6*,

the actual substrate of bicarbonate electrolysis is dissolved CO<sub>2</sub> instead of the bicarbonate anion. This dissolved CO<sub>2</sub> mainly comes from the equilibrium of bicarbonate with water. Therefore, this additional step is added to the reaction mechanism limiting the overall reaction (bicarbonate to products) to the release rate of CO<sub>2</sub> from bicarbonate, thus increasing the mass transfer limitations of the reaction. Thanks to the advances in using BPM for eCO<sub>2</sub>R, mainly as a pH stabilizer, a pathway to increase the release rate of CO<sub>2</sub> from bicarbonate was proposed. The release of protons from the BPM once the potential is applied acidified the bicarbonate solutions to the benefit of the release of CO<sub>2</sub>, thus increasing to great extent the available substrate of the reaction. Thanks to the use of a BPM and to the zero-gap configuration (where the electrode is in contact with the BPM), we designed an electrolyser in *Chapter 8* that is able to convert bicarbonate solutions to formate at least up to 400 mA cm<sup>-2</sup> (>30% FE to formate is achieved this way). However, the use of the BPM increased to a great extent the ohmic drop of the electrolyser at high current densities. Therefore, the most energy-efficient operational current was found at lower current density, 50 mA cm<sup>-2</sup> (58% FE<sub>Formate</sub> at 27% EE reached this way). The design of this bicarbonate electrolyser allows to do research on a higher TRL (higher current and more realistic configurations) compared to lab-scale batch operations used formerly, which were mainly used for fundamental studies.

### 10.1.3 Integrated capture and conversion of CO<sub>2</sub>

After proposing two pathways to convert electrochemically bicarbonate solutions, we integrated the capture and the conversion step by using these two strategies. Firstly, by getting inspired by nature, in *Chapter 7* we synthesized an artificial enzyme that is both able to catalyse the conversion of CO<sub>2</sub> to bicarbonate during the capture step (increasing the capture rate by up to 84%) and inhibit the HER in a similar way cationic surfactants do (up to 60% FE is achieved this way). However, the stability of the material was compromised at high concentrations, thus limiting its effect at least with the conditions proposed in the study. Nevertheless, this route showed promising results in combining

the research of both the capture and the conversion of CO<sub>2</sub> in one and a single system, as we proposed at the beginning of Chapter 10.1. Materials that are commonly used just to study the capture of CO<sub>2</sub>, such as the artificial enzymes, has been now proven to be functional also for the conversion step.

Finally, we tested the bicarbonate flow electrolyser designed in *Chapter 8* with real CO<sub>2</sub> from the air instead of pure CO<sub>2</sub> coming from commercial suppliers, which is commonly used in the state-of-the-art research. By designing a DAC set-up and by using KOH 1 M as capture solution, a 0.654 M DIC (bicarbonate + carbonate) solution was obtained in 8.5 h of capture time (corresponding to ~11 g CO<sub>2</sub>). This solution was used as an electrolyte and as CO<sub>2</sub>-source in the bicarbonate zero-gap flow electrolyser and it was converted, for the first time ever reported, to formate and CO. Although, compared to state-of-the-art eCO<sub>2</sub>R, low FE was obtained (16 and 13%, respectively), that was mostly due to the low carbon loading of the electrolyte, therefore it can be potentially improved if more CO<sub>2</sub> is captured in the capture step. If we compare this results (i.e., 13% FE<sub>CO</sub>, 50 mA cm<sup>-2</sup> and 3.4 V) to the parameters used in the TEA of *Chapter 1.5* (30% FE<sub>CO</sub>, 200 mA cm<sup>-2</sup> and 3.4 V), where the integrated route had reduced costs compared to the two-step route, we clearly see that an improvement in FE<sub>CO</sub> and V<sub>cell</sub> at higher current densities (i.e., 200 mA cm<sup>-2</sup>) is needed to reach industrially relevant results, discussed in *Chapter 10.2*. Nevertheless, we proved that the proposed procedure to convert bicarbonate used in *Chapter 8* and in the state-of-the-art can be used to convert DAC solutions such as we did in *Chapter 9*.

## 10.2 Future perspectives

After concluding the work presented in this doctoral thesis, the know-how of the electrochemical reduction of bicarbonate solutions is acquired. In addition, a proof-of-concept integrated capture and electrochemical CO<sub>2</sub> conversion system is delivered.

However, since at most aspects our research was very new, there is still room of improvement and further steps to venture towards new opportunities and strategies.

A first general next approach is to target other eCO<sub>2</sub>R products. In this thesis we targeted mainly formate since its electrochemical reaction is well-known and Sn catalysts are well established in the state-of-the-art as high selective materials. In addition, the valorisation of eCO<sub>2</sub>R strategies targeting formate is one of the highest of the field. Therefore, as a starting point to study the bicarbonate electrolysis it was an adequate product to target. However, for integrated capture and electrochemical CO<sub>2</sub> conversion systems, other products, with higher profitability than formate, might be interesting to explore, too. Those electrolytic systems that produce OH<sup>-</sup> as product (such as CO, CH<sub>3</sub>OH and most of C<sub>2</sub> products) are of high interest in the integrated approach since then the alkalinity is regenerated to be used in the captured step again, increasing the valorisation of the technology. For this reason, in *chapter 9* we tested the electrolyser to produce CO, too, although only preliminary results were obtained. Studying specifically the electrolysis of bicarbonate solutions to CO is the priority because even obtaining low FE (20-30%) the technology can be valorised as a syngas production method (CO+H<sub>2</sub>). Parallely, the production of CH<sub>3</sub>OH from bicarbonate solutions must be investigated, too. At this point, only Sn, Bi (for formate production) and Ag (for CO production) have been tested as electrocatalyst for bicarbonate electrolysis. Cu-based electrodes, which lead to CH<sub>3</sub>OH and C<sub>2</sub> products, must be introduced as soon as possible now that the reaction is well-known, and the configuration of the firsts flow electrolysers is delivered.

Regarding the use of cationic surfactants as HER inhibitors for bicarbonate electrolysis, with the results obtained in this thesis, we demonstrated that the functionality of cationic surfactants can be improved with little modifications of its structure, giving the chance to broaden this field of study and overall improve the effectiveness of the surfactants used nowadays, not only in electrocatalysis but in any other field of study. For instance, an interesting approach could be to add, in addition to hydrophobic functional groups like alkyl chains or benzyl groups, CO<sub>2</sub>-philic groups that could promote the stabilization of



the CO<sub>2</sub> molecule at the surface of the electrode and the diffusion of CO<sub>2</sub> from the bulk bicarbonate electrolyte. These functional groups, mainly amino-based, have been studied from the theoretical and fundamental point of view but their application remains still unvalidated and could be an interesting future work.[238–240] Another interesting approach is to combine this technology to current HER inhibitors, mainly based on the modification of the structure/morphology of the catalyst to further improve the inhibition effects.[182] However, when adding cationic surfactants in the electrolyte, low current densities are obtained due to the hydrophobic acquired properties of the electrode (1-5 mA cm<sup>-2</sup>, up to 90% of total current density in the absence of surfactant is cut). This is serious aspect to consider when trying to upscale the technology. It is still unknown how the system behaves in a flow configuration and at high currents (>100 mA cm<sup>-2</sup>) since then, the EDL and thus the hydrophobic layer is more unstable. One strategy to avoid this is to integrate the surfactant on the configuration of the electrocatalyst instead of as a suspension in the electrolyte (this will also decrease the complexity of downstream processing).

Looking at *Chapter 7*, where we synthesized an artificial enzyme to improve the CO<sub>2</sub> capture and conversion rates, there is still room for improvement. Although [Zn(cyclen)]<sup>2+</sup> is a promising artificial CAH for this application, other metal co-factors (such as Cu<sup>2+</sup> or Fe<sup>2+</sup>) and ligands (like other chelating agents) could outperform it. It is thus interesting to perform a further screening of potential artificial CAH. Another interesting approach is to test the artificial enzyme on real systems such as in the DAC set-up used in *chapter 9*. If the capture rate improvement of >80% can be obtained also for DAC, the potential of these materials would very high. On the other hand, in this study we also observed a similar issue as in *Chapter 6*, which was the low total current obtained due to HER inhibition and to the increase of the hydrophobicity of the surface of the electrode. We propose the same approach: to perform electrolysis experiments at higher current to properly evaluate the system. However, in this case the stability of the artificial CAH is of interest of study, too. Since it is based on a metal cation, high reductive currents may lead

to the reduction of the cation and thus the deactivation of the artificial enzyme. If this is the case, an extra step in between the capture and the conversion where the artificial CAH is extracted from the solution must be considered, although the costs of the technology would thus increase. It depends on the improvement of the capture and conversion steps to overcome this drawback, which will be solely know by continuing this research route.

Regarding the bicarbonate zero-gap flow electrolyzer, there are different routes to improve the performance of the system. By looking at the operational parameters, it is observed that the best performance was obtained at 5 mL min<sup>-1</sup>, then it is interesting to evaluate the effect of higher flow rate, for instance at 50 mL min<sup>-1</sup>. On the other hand, one of the biggest reasons for the loss of EE of the system is the increase of cell voltage with the applied current density due to the use of a BPM. Therefore, new and more optimized BPM can be used to minimize this effect, which requires to be alert on the research done on BPM technology, since it is a relatively new field of application for eCO<sub>2</sub>R (few commercial BPM are currently available). Other options for membranes have been considered, however, the ability of BPM to maintain the pH gradients and product crossover (in addition to the additional application of generating protons to produce CO<sub>2</sub> from bicarbonate) makes the BPM the best choice for upscaling bicarbonate electrolyzers.[114] Further understanding of the effects of different parameters, such as the ones considered in this thesis, in addition to the ohmic and the charge transfer resistance of the reactor is still needed. For example, elaborating a deep study including techniques such as EIS will allow us to understand better how the flow rate and the retention of bubbles affect the performance of the bicarbonate zero-gap electrolyser.

Finally, for integrating the DAC and bicarbonate conversion in a single system, in addition to the investigation on the improvement of the efficiency of the electrolyser, further research should focus on how to capture more CO<sub>2</sub> from KOH solutions. For instance, starting from a higher concentration of KOH would allow capturing more CO<sub>2</sub>, although the integrity of the setup, the alkalinity loss and the increased duration of the operational

capture time must be considered, too. Another strategy, if increasing the concentration of KOH is detrimental for the capture system, is to use flue gas as CO<sub>2</sub> carrier instead of air (%CO<sub>2</sub> 1-10% instead of 0.04%). Using flue gas is of high interest for industry, too, as mentioned in the introduction. However, to properly evaluate these systems, the effect of the impurities (ppm of NO<sub>x</sub> and SO<sub>x</sub> among others) must be investigated, too. Finally, further integrating both systems, for instance by coupling the electrolyser to the DAC setup, is an interesting viewpoint, too, although the separate optimization of both systems should be provided, first.



# Annex



# **ANNEX**

## **Fundamental concepts and experimental techniques**

THIS ANNEX EXPLAINS THE THEORETICAL BACKGROUND OF THE FUNDAMENTAL ASPECTS OF THE CAPTURE AND ELECTROCHEMICAL CO<sub>2</sub> CONVERSION.

## **A.1 Physicochemical concepts of the capture of CO<sub>2</sub> using membrane contactors**

In this first section, a general overview of CO<sub>2</sub> capture using membrane contactors will be given. In this context, the capture mechanism and the role of the capture solution are explained. The outline of all basic principles handled in this annex are based on the following references: [16, 54, 55, 241-248].

### **A.1.1 CO<sub>2</sub> capture with membrane contactors**

The CO<sub>2</sub> capture accounts an important fraction of the costs of CCU.[241] Therefore, developing an effective method to capture CO<sub>2</sub> cost-efficiently is crucial for decreasing the overall costs.[242] The most common approach is to use liquid absorbents to capture CO<sub>2</sub> from the air or flue gasses. However, since there are other gases present in the gaseous solution, such as N<sub>2</sub>, O<sub>2</sub>, NO<sub>2</sub> or SO<sub>2</sub>, the CO<sub>2</sub> must compete for a contact site if it is not previously separated from the rest of the gases. In addition, the low concentration of CO<sub>2</sub> in these gaseous solutions limits the contacting of CO<sub>2</sub> with the liquid absorbent, thus increasing the operational time and thus making the process inefficient. In this context, membrane contactors are proposed as a tool to promote the CO<sub>2</sub>-liquid absorbent contacting process.[243] These membranes do not only separate the CO<sub>2</sub> from the rest of the gases, but also provides a large surface area where CO<sub>2</sub> is adsorbed and the contacting time with the capture solution is improved, thus promoting the mass transfer and diffusion of CO<sub>2</sub>. As such, membrane contactors keep the liquid phase separated from the gas flow, preventing that the liquid escapes as an aerosol. Other devices such as conventional gas-liquid contactors were proposed, too, however, membrane contactors outperformed them in terms of foaming, flooding, liquid contact and operational costs.[244]



Membrane contactors were first used in the 80s where polypropylene was used as membrane contactor and sodium hydroxide as liquid absorbent.[245] Since then, abundant research on the topic led towards the optimal configuration of a membrane contactor for CO<sub>2</sub> capture applications. Firstly, the membrane needs to be highly porous to ensure high flux contact. Secondly, the pores of the membrane should remain unflooded to avoid the loss of gas active sites and the decrease of the mass transfer. Finally, a proper selection of a material and liquid absorbent (*Annex A.1.2*) with high affinity towards CO<sub>2</sub> is very important, too.[246]

Air or flue gas that contains CO<sub>2</sub> flow at one site, through the pores or through the capillary structure of the membrane (depending the membrane contactor on use) while the liquid absorbent, from now onwards the capture solution, is supplied to the other site (Figure A.1). The concentration gradient forces the CO<sub>2</sub> to diffuse through the membrane and react with the capture agent.

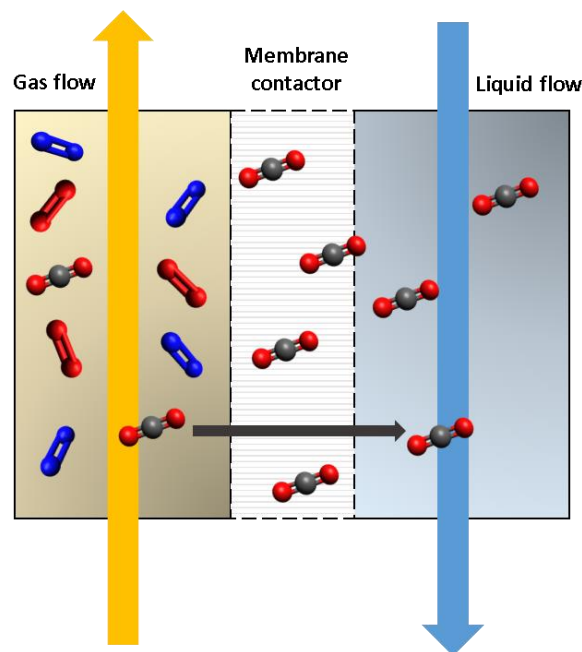


**Figure A.1.** CO<sub>2</sub> diffusion mechanism in a membrane contactor. CO<sub>2</sub> is transported through concentration gradients from the gas phase to the liquid phase.

### A.1.2 CO<sub>2</sub> capture solution

As mentioned in the previous section, the reactivity of the liquid absorbent to CO<sub>2</sub> is crucial to propose an optimal method to capture CO<sub>2</sub> from air or from flue gas. After CO<sub>2</sub> diffuses through the membrane contactor, it reacts with the capturing agent, forming a stable compound. CO<sub>2</sub> is recovered from the post-capture solution. Therefore, the carbonate or carbamate, product of the reaction of the CO<sub>2</sub> with the capture solution, not only allows continuous operation (by avoiding an intermittent CO<sub>2</sub> desorption step, as is the case in solid-state capture) but the recovery of the CO<sub>2</sub> for posterior utilization. Currently, two main capture solutions are proposed as liquid absorbents to capture CO<sub>2</sub> from the air or from flue gas in the frame of CCU: alkaline and amine-based solutions.[169]

For DAC applications, strong alkaline solutions, such as KOH or NaOH, are commonly used for capturing CO<sub>2</sub> in the form of (bi)carbonate.[247] As mentioned in *Chapter 1.2.1*, to recover the CO<sub>2</sub> in the form of a high purity concentrated gas, the (bi)carbonate is typically precipitated with Ca(OH)<sub>2</sub> and then calcinated to generate CaO and CO<sub>2</sub>. [16] On the other hand, for flue gas capture applications, since the concentration of CO<sub>2</sub> is higher, amines such as monoethanolamine (MEA) or triethanolamine, are commonly used for capturing CO<sub>2</sub> in the form of carbamate.[248] To recover back the CO<sub>2</sub>, the carbamate is treated at elevated temperatures and both the CO<sub>2</sub> and the amine are recovered in the amine scrubbing process. Nevertheless, since post-capture steps are costly, there is interest in using directly the CO<sub>2</sub> in the form of (bi)carbonates or carbamates (Figure A.2) without any post-capture treatment other than the conversion step.[160] Capturing CO<sub>2</sub> in the form of (bi)carbonate and carbamate and then using these products directly as substrate in the electrochemical cell for the conversion toward carbon products is challenging due to the low electro-reactivity nature they present. However, being able to directly convert with high efficiency (bi)carbonate or carbamate would increase to a great extent the overall energy efficiency of the CCU technology and thus decrease the operational costs.[54,55]

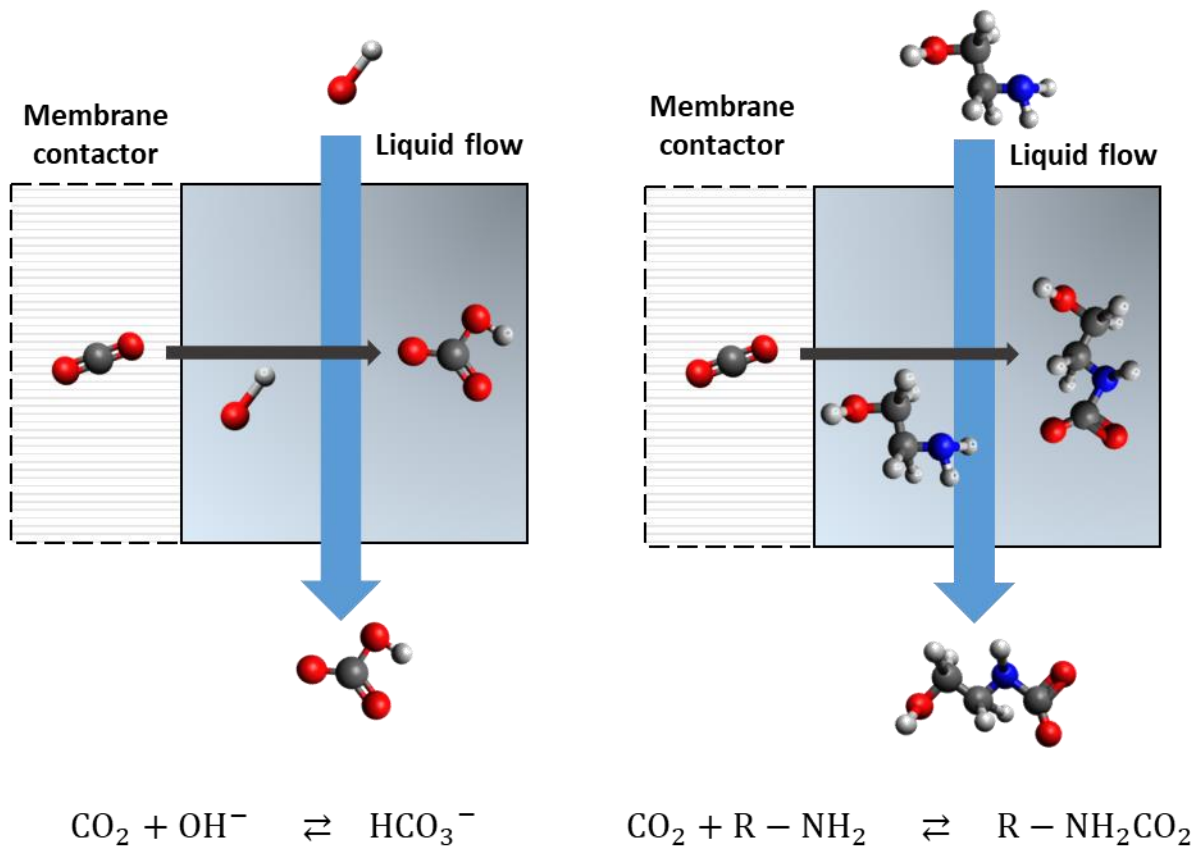


**Figure A.2.** Reactions undergoing when using an alkaline (left) or an amino-based solution (right) as CO<sub>2</sub> capture solution.

## A.2 Basic principles on electrocatalysis

In this section, the basic principles of electrocatalysis will be discussed. The reader will be given a general explanation on what an electrochemical reaction is, focusing on the specific reaction concerning the CO<sub>2</sub> as substrate. Then, a general overview on the thermodynamic aspects and different parameters that involves an electrolytic process will be discussed. The outline of all basic principles is based on the following references: [39, 249-256].

### A.2.1 Electrocatalysis

An electrochemical reaction is a chemical process that is either caused or accompanied by the flux of an electric current and involves, most of the times, the transfer of electrons between two species, mainly between the electrolyte and the electrode, in an electrochemical cell (Eq. A.1). In an electrochemical reaction, one species is reduced (electron acceptor) and the other is oxidized (electron donor), each reaction defined as half-reactions. On the other hand, a catalytic action is a chemical reaction between an agent called catalyst and a reactant, forming chemical intermediates that can react more easily with each other to form the desired product. In this context, electrocatalysis is defined as the catalytic action during an electrochemical reaction where the electrode plays both the role of electron donor/acceptor and of (electro)catalyst.[249]



An electrochemical cell (Figure A.3) typically consists of two electrodes (alternatively three as it will be discussed later): the electrode where the oxidation takes place, namely the anode, and the electrode where the reduction takes place, namely the cathode. The two processes occur at the same time, and one cannot occur without the other. To close the electronic circuit, an electrolyte is needed. The electrolyte is a compound that allows the free movement of ions from one electrode to the other, allowing an electric current to flow between them when the circuit is closed. Additionally, to avoid product crossover while maintaining the transfer of ions, a membrane is placed (detailed in *Annex A.3.2*).

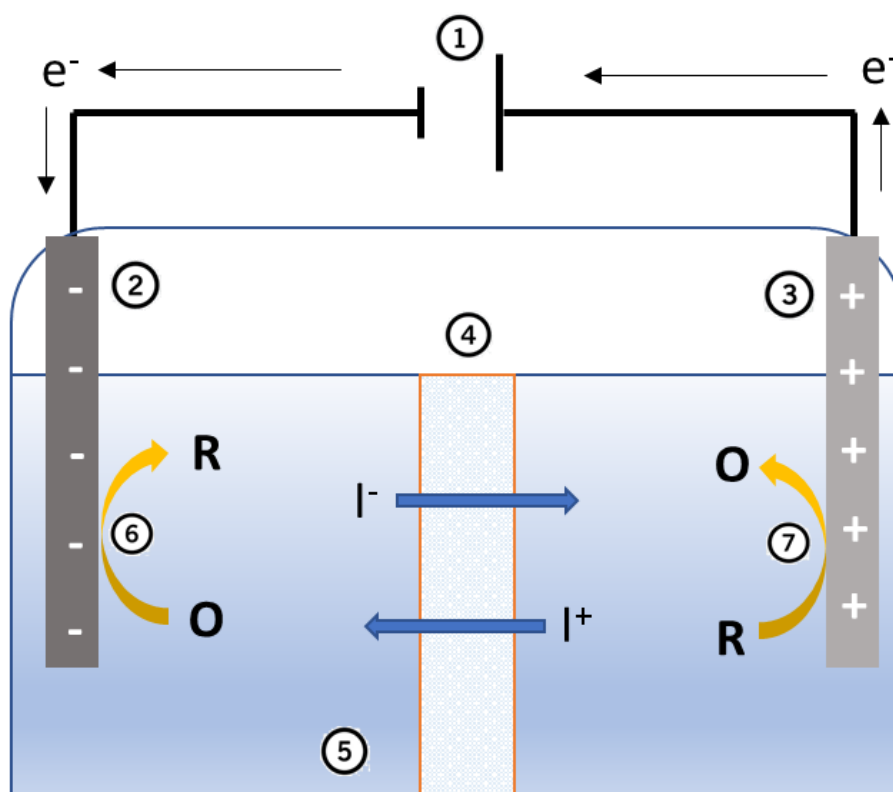


**Figure A.3:** A schematic representation of an electrochemical cell. On the image: 1) power source. 2) Cathode 3) Anode. 4) Membrane 5) Electrolyte 6) Reduction reaction 7) Oxidation reaction.

When the electrical circuit is closed, the flow of electrons can either move spontaneously or non-spontaneously. The spontaneity of a chemical reaction is given by the Gibbs free energy of the reaction ( $\Delta G^\circ$ ), a parameter that tells how easy is to drive a reaction towards a certain direction based on the free energy of the reactants and the products ( $\Delta G^\circ < 0$  for spontaneous reactions and  $\Delta G^\circ > 0$  for non-spontaneous reactions). A spontaneous electrochemical circuit is called galvanic cell. A typical galvanic cell is, for instance, a battery. On the other hand, if the electrochemical reaction does not occur spontaneously, energy must be applied from an energy source. Non-spontaneous electrochemical cells are called electrolytic cell, and the reaction is called electrolysis. In an electrolysis, energy, in form of a difference of potential (in volts), needs to be applied, which is detailed further in the next *Annex A.2.3*.

### A.2.2 Electrochemical thermodynamics: the cell potential

In this section, the main thermodynamic parameter of an electrochemical reaction, the equilibrium potential,  $E_{eq}$ , will be discussed. For standard conditions (25 °C, 1 atm and no ionic interactions) the standard equilibrium potential ( $E^{\circ}_{eq}$ ) is calculated from the standard reduction potential ( $E^{\circ}_{red}$ ) of the half-reactions taking place (Eq. A.2). The  $E^{\circ}_{red}$  is the potential at equilibrium and standard conditions of a theoretical electrochemical cell where one of the reactions is the half-reaction of study and the counter-reaction is the hydrogen oxidation/reduction in the formation of H<sup>+</sup> or H<sub>2</sub>, namely the reversible hydrogen electrode (RHE). The  $E^{\circ}_{red}$  is understood as the tendency of a half-reduction reaction to occur and it is benchmarked as 0 for the reduction of H<sup>+</sup> to H<sub>2</sub>. After obtaining  $E^{\circ}_{eq}$ , the spontaneity of the electrochemical reaction can be guessed by calculating  $\Delta G^{\circ}$  (Eq. A.3), where  $z$  is the number of electrons transferred in the half-cell reactions and  $F$  is the Faraday constant.

$$E^{\circ}_{eq} = E^{\circ}_{red(cathode)} - E^{\circ}_{red(anode)} \quad (\text{Eq. A.2})$$

$$\Delta G^{\circ} = -zFE^{\circ}_{eq} \quad (\text{Eq. A.3})$$

Nevertheless, since the working conditions have variations to standard conditions,  $E^{\circ}_{eq}$  cannot be considered as the equilibrium potential of an electrochemical reaction. In a real system, considering 1 atm as atmospheric pressure, the variations in temperature and in the activity of the chemicals present (ionic interactions) must be considered. To correct these variations, the Nernst equation is used (Eq. A.4), where  $E_{eq}$  is the equilibrium potential,  $E^{\circ}_{eq}$  is the standard equilibrium potential,  $R$  is the ideal gas constant,  $T$  is the temperature,  $z$  is the number of electrons transferred in the half-cell reactions,  $F$  is the Faraday constant, and  $a$  is the activity of the species that are reduced and oxidized.

$$E_{eq} = E^{\circ}_{eq} - \frac{RT}{zF} \ln \frac{a_{red}}{a_{ox}} \quad (\text{Eq. A.4})$$

For conventional electrolysis systems involving the electrochemical reduction of CO<sub>2</sub> to different carbon products and the oxygen evolution reaction (oxidation of H<sub>2</sub>O/OH<sup>-</sup> to O<sub>2</sub>) as counter reaction, the  $E_{eq}^{\circ}$  are shown in Table A.1. As observed, if  $E_{eq}^{\circ}$  is calculated in an electrochemical cell where CO<sub>2</sub> is reduced at the cathode and oxygen is evolved at the anode, the value is negative (for example, -1.335 V<sub>RHE</sub> for a cell producing CO and oxygen), therefore the reaction is non-spontaneous and applying a potential from an external source is needed. Since transferring the electrons from the cathode to the CO<sub>2</sub> is needed to start the reaction, the electrochemical reduction of CO<sub>2</sub> is then an electrocatalytic and an electrolytic process. When a certain potential is applied, the CO<sub>2</sub>, dissolved in the electrolyte or supplied to the electrode in gas form, adsorbs to the surface of the cathode and is reduced to different carbon products, such as carbon monoxide (A.1), with an electrocatalyst, which is the agent determining the product of the reaction (*Chapter 1.3*). At the anode side, a counter reaction is needed to close the electrochemical circuit. Typically, the oxygen evolution reaction is the reaction occurring in the anode (A.2). [250] When combining both half-reactions (reduction and oxidation) the cell reaction is obtained (A.3) and thus  $E_{eq}$  can be calculated.

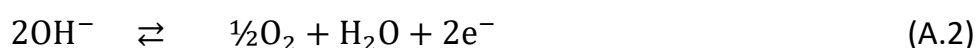
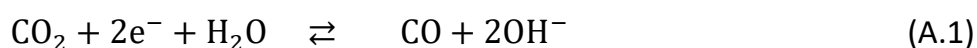


**Table A.1.** Standard reduction potentials found in conventional eCO<sub>2</sub>R systems at 25 °C. OER potential corresponds to pH 14.[251]

Product	Half-reaction	E° <sub>eq</sub> (V <sub>RHE</sub> )
CO <sub>(g)</sub>	CO <sub>2(g)</sub> + H <sub>2</sub> O <sub>(l)</sub> + 2e <sup>-</sup> ⇌ CO <sub>(g)</sub> + 2OH <sub>(aq)</sub> <sup>-</sup>	-0.934
HCOO <sub>(aq)</sub> <sup>-</sup>	CO <sub>2(g)</sub> + H <sub>2</sub> O <sub>(l)</sub> + 2e <sup>-</sup> ⇌ HCOO <sub>(aq)</sub> <sup>-</sup> + OH <sub>(aq)</sub> <sup>-</sup>	-1.078
CH <sub>3</sub> OH <sub>(aq)</sub>	CO <sub>2(g)</sub> + 5H <sub>2</sub> O <sub>(l)</sub> + 6e <sup>-</sup> ⇌ CH <sub>3</sub> OH <sub>(aq)</sub> + 6OH <sub>(aq)</sub> <sup>-</sup>	-0.812
CH <sub>4(g)</sub>	CO <sub>2(g)</sub> + 6H <sub>2</sub> O <sub>(l)</sub> + 8e <sup>-</sup> ⇌ CH <sub>4(g)</sub> + 8OH <sub>(aq)</sub> <sup>-</sup>	-0.659
C <sub>2</sub> O <sub>4</sub> <sup>2-</sup> <sub>(l)</sub>	2CO <sub>2(g)</sub> + 2e <sup>-</sup> ⇌ C <sub>2</sub> O <sub>4</sub> <sup>2-</sup> <sub>(l)</sub>	-0.590
CH <sub>3</sub> CO <sub>2</sub> <sub>(aq)</sub> <sup>-</sup>	2CO <sub>2(g)</sub> + 5H <sub>2</sub> O <sub>(l)</sub> + 8e <sup>-</sup> ⇌ CH <sub>3</sub> CO <sub>2</sub> <sub>(aq)</sub> <sup>-</sup> + 7OH <sub>(aq)</sub> <sup>-</sup>	-0.703
C <sub>2</sub> H <sub>5</sub> OH <sub>(aq)</sub>	2CO <sub>2(g)</sub> + 9H <sub>2</sub> O <sub>(l)</sub> + 12e <sup>-</sup> ⇌ CH <sub>3</sub> CH <sub>2</sub> OH <sub>(aq)</sub> + 12OH <sub>(aq)</sub> <sup>-</sup>	-0.744
C <sub>2</sub> H <sub>4(g)</sub>	2CO <sub>2(g)</sub> + 8H <sub>2</sub> O <sub>(l)</sub> + 12e <sup>-</sup> ⇌ C <sub>2</sub> H <sub>4(g)</sub> + 12OH <sub>(aq)</sub> <sup>-</sup>	-0.764
O <sub>2(g)</sub>	4OH <sub>(aq)</sub> <sup>-</sup> ⇌ O <sub>2(g)</sub> + 2H <sub>2</sub> O <sub>(l)</sub> + 4e <sup>-</sup>	+0.401

### A.2.3 Applied potential, equilibrium potential and overpotential

The electrocatalytic reactions occur in the electrode-electrolyte interface, therefore they are heterogeneous catalytic reactions. As a catalytic reaction, the kinetic study plays an important role to understand the behavior of the system, which is composed of several mechanistic steps, each of them with a specific kinetic mechanism (Figure A.4).



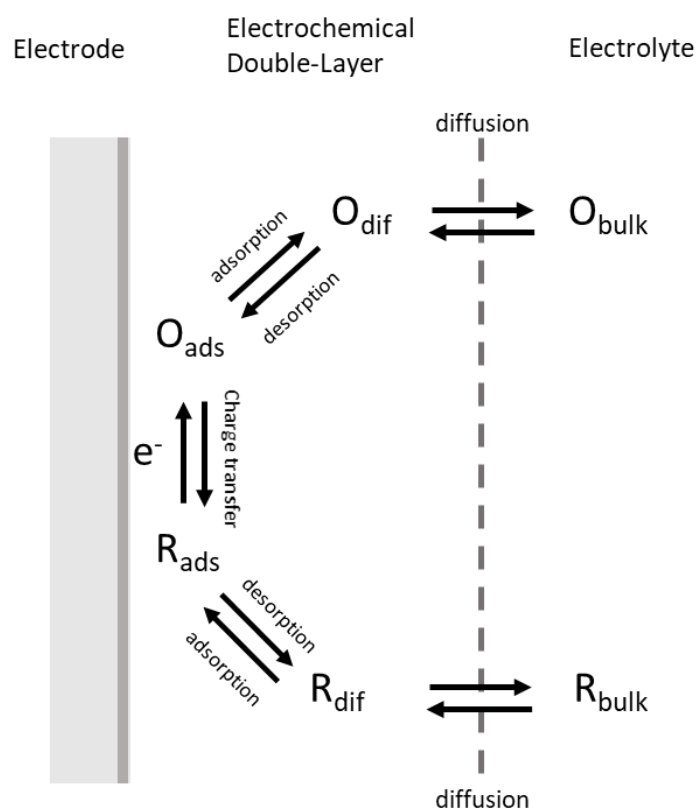


**Figure A.4.** Simplified reaction steps during an electrochemical reaction. Redrawn from [252].

Therefore, in a conventional electrocatalytic reaction, five reversible steps are identified: the diffusion of the reactants from the bulk electrolyte to the electrochemical double layer, the adsorption of the reactant to the surface of the electrode, the charge transfer on the interface (where the electrochemical reaction occurs), the desorption of the products from the surface of the electrode and the diffusion of the products from the electrochemical double layer to the bulk electrolyte. The reaction rate will be determined by the slowest step, namely the limiting step. However, usually, electrocatalytic reactions are more complex and involve several reactants or the charge transfer between two or more species.[39] Nevertheless, to simplify the explanation to the reader, the previous generalization is valid as an overview of the electrocatalytic kinetics.

To determine which step is limiting the electrochemical reaction rate, the current,  $I$ , (in amperes) of the electron flow that travels through the system is studied. The  $I$  is equivalent to the rate of reaction,  $\nu$  (Eq. A.5). Since  $\nu$  and  $I$  are extensive magnitudes (depending on the size of the system), the current density (CD),  $j$ , is used to evaluate the system. In an electrocatalytic system, the  $j$  is amount of current per unit of the electrode surface. By standard, the cathodic current is negative, and the anodic current is positive.

$$I = zF\nu \quad (\text{Eq. A.5})$$

However, to evaluate  $j$ , first the activation overpotential,  $\eta$ , must be determined. The  $\eta$  is the potential difference between the potential at which the electrochemical reaction is experimentally observed,  $E$ , and the  $E_{eq}$  (Eq. A.6). The existence of  $\eta$  implies that the cell requires more energy than thermodynamically expected to drive the reaction, thus being closely related to the efficiency of the system. The additional energy requirement might come, for instance, from the activation energy of the electrochemical reaction (energy required to transfer an electron from the electrode to the electrolyte), tied to the binding energy of the reactant to the electrocatalyst, or from the resistance overpotential (such as capacitive effects), tied to the cell design.

$$\eta = E - E_{eq} \quad (\text{Eq. A.6})$$

As an example of how the nature of the electrocatalyst affects the activation energy of the electrochemical reaction, in this case of the HER and the OER, the  $\eta$  for different catalyst are shown in Table A.2. For the electrochemical reduction of CO<sub>2</sub>, this affects directly to the selectivity of the reaction. The reader is referred to the Table 1.1, where the selectivity of eCO<sub>2</sub>R of different electrocatalyst (each of them with different activation energies) are provided.

**Table A.2.**  $\eta$  for the HER and OER on various electrocatalyst at 25 °C. [253]

Electrocatalyst	$\eta_{HER}$ (V <sub>RHE</sub> )	$\eta_{OER}$ (V <sub>RHE</sub> )
Ag	-0.59	+0.61
Au	-0.12	+0.96
Cu	-0.50	+0.58
Fe	-0.40	+0.41
Pt	-0.09	+1.11
Ni	-0.32	+0.61

When  $\eta$  is determined,  $E$  and  $j$  can be related using the Butler-Volmer equation (Eq. A.7). The  $j$  is the current density,  $j_o$  is the exchange current density,  $\alpha_a$  and  $\alpha_c$  are the charge transfer coefficient for the anodic and cathodic reaction, respectively,  $\eta$  is the activation overpotential,  $R$  is the ideal gas constant and  $T$  is the temperature of the system. Based on the equation, the  $j$ , and thus the rate of the reaction, depends on  $\eta$ ,  $\alpha$  and  $j_o$ . The  $\eta$  is obtained from  $E$  and the Nernst equation, the  $\alpha$  is the fraction of potential of the electrode-electrode interface that helps in lowering the activation energy of the electrochemical reaction, while the  $j_o$  is the current in the absence of net electrolysis and at zero overpotential. In many cases,  $\alpha$  and  $j_o$  are values that are tabulated or can be experimentally obtained.

$$j = j_o \left\{ \exp \left[ \frac{\alpha_a z F \eta}{RT} \right] - \exp \left[ - \frac{\alpha_c z F \eta}{RT} \right] \right\} \quad (\text{Eq. A.7})$$

In Figure A.5, the  $I$  vs  $\eta$  curve and the changes in the limiting steps are shown. When  $\eta$  is zero, the system is in equilibrium and the  $I$  is zero (center of the curve). When  $\eta$  is applied, the system enters the charge transfer controlled range, following the exponential trend of the Butler-Volmer equation (red and yellow area). In this range, the electrochemical reaction is controlled by the transfer of the electrons from the electrode to the electrolyte. When  $\eta$  is close to zero,  $e^x \approx 1+x$ . Therefore, the Butler-Volmer equation can be approximated to a lineal equation (Eq. A.8). This equation is independent to  $\alpha$ , then  $j_o$  can be easily measured with experimental data (red area).

$$j = j_o \frac{F\eta}{RT} \quad ; \quad E \approx E_{eq} \quad (\text{Eq. A.8})$$

As  $\eta$  increases, the system enters the diffusion-controlled zone (green area). From this point, the Butler-Volmer equation is not followed anymore and the  $I$  stops increasing exponentially with  $\eta$ , reaching a plateau. From this  $\eta$ , the charge transfer stops being the limiting step and are now the diffusion of the reactants from the electrolyte to the surface of the electro what is limiting the rate of the electrochemical reaction. The fast consumption of reactants due to the high  $\eta$ , empties the feedstock of reactant close to the surface of the electrode. To calculate  $j$  in a diffusion-controlled range, the first Fick's law is used (Eq. A.9). The  $D$  is the diffusion constant of the reactant,  $C_i$  is the concentration of reactant on the surface of the electrode,  $C^*$  is the bulk concentration and  $\delta$  is the thickness of the diffusion layer. Therefore, the maximum  $j$  is reached when  $C_i=0$  (when there is no reactant on the surface of the electrode).

$$j = -zFD \frac{C_i - C^*}{\delta} \quad (\text{Eq. A.9})$$

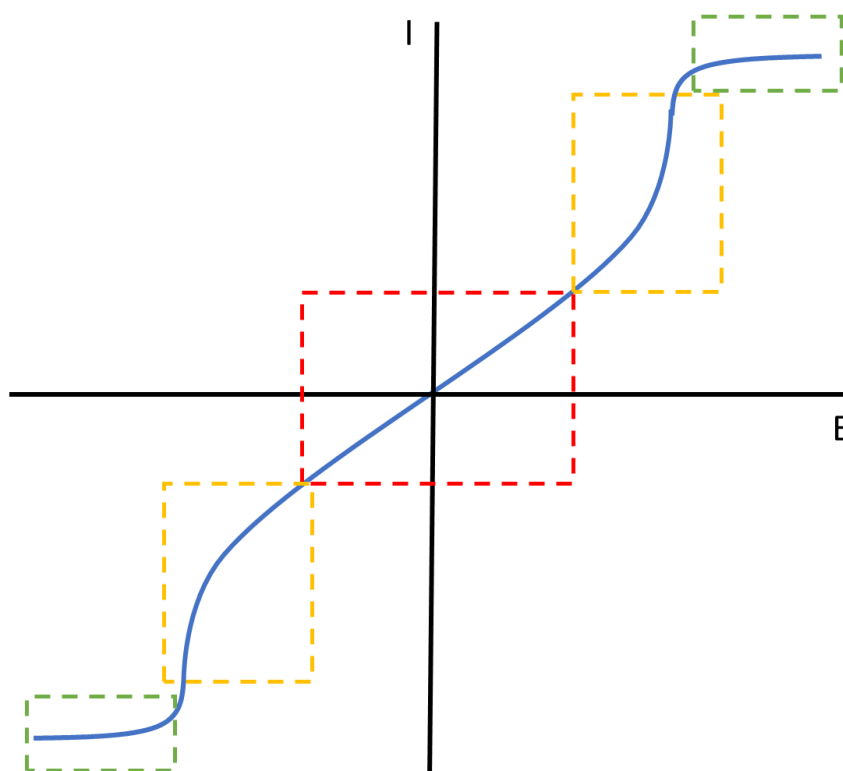


**Figure A.5.** Current-overpotential curve of a system  $O + e \rightleftharpoons R$  with  $\alpha=0.5$  and  $j_c=j_a$ .

The evaluation of the relation between the applied potential and the current is crucial to understand how the electrochemical system of study works. For this reason, different electrochemical techniques will be used in this thesis, described in the *Chapter A.6*.

#### **A.2.4 The electrode-electrolyte interface: the electrochemical double layer**

As mentioned, in an electrocatalytic cell, the oxidation and the reduction reaction occur in the electrode-electrolyte interface, namely the electrochemical double layer (EDL). The EDL refers to two parallel layers of charge surrounding the surface of the electrode (Figure A.6). This structure is formed by polarizing the electrode and can be caused either by applying a potential or by the intrinsic electronic nature of the electrode and the electrolyte. When an electrode is polarized, the charges present in the vicinity of the electrode migrate to the surface of the electrode forming a positive charged layer (at the cathode) or a negative charged layer (at the anode), forming the Inner Helmholtz Plane

(IHP). These ions are, in most cases, adsorbed to the surface of the electrode. Next to this structure, a less compact layer, the Outer Helmholtz Layer (OHL) is formed, consisting of the counter-ionic species present in the electrolyte (anions to the cathode and cations to the anode).

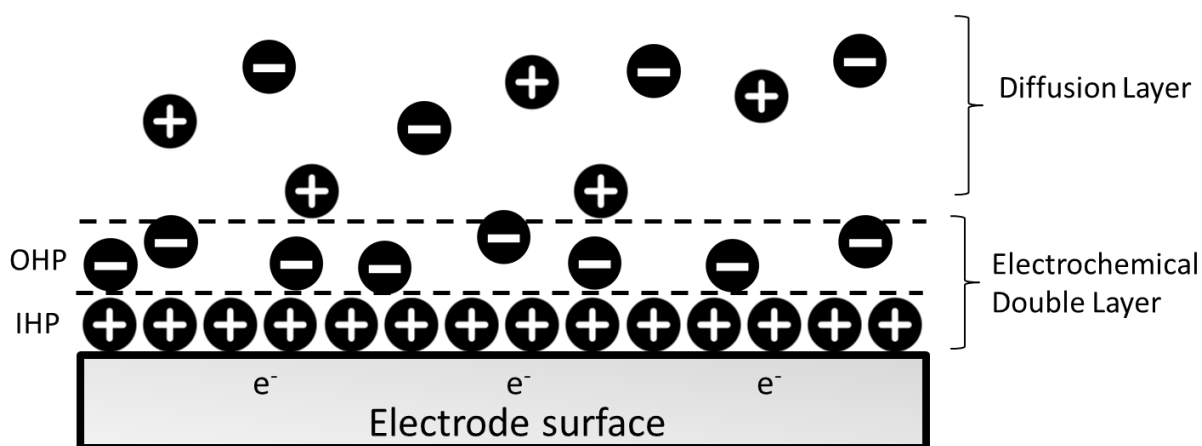


**Figure A.6.** Schematic interpretation of the different layers formed close to the surface of the electrode (in this case, the cathode) after applying a negative potential.

For eCO<sub>2</sub>R where the CO<sub>2</sub> is dissolved in the electrolyte and an aqueous KHCO<sub>3</sub> solution is used as electrolyte, the IHP of the cathode is formed by the cationic species H<sup>+</sup> and K<sup>+</sup> and the OHL is formed by the anionic species HCO<sub>3</sub><sup>-</sup> and OH<sup>-</sup>. The H<sub>2</sub>O molecules, as a non-charged, polar molecule will be present in both layers. The CO<sub>2</sub>, as a non-charged, non-polar molecule will be mostly present outside the EDL, in the diffusion layer.[163] This is one of the reasons why, in most of the systems reported, the eCO<sub>2</sub>R is a diffusion-controlled reaction at relatively low  $\eta$ . [254]

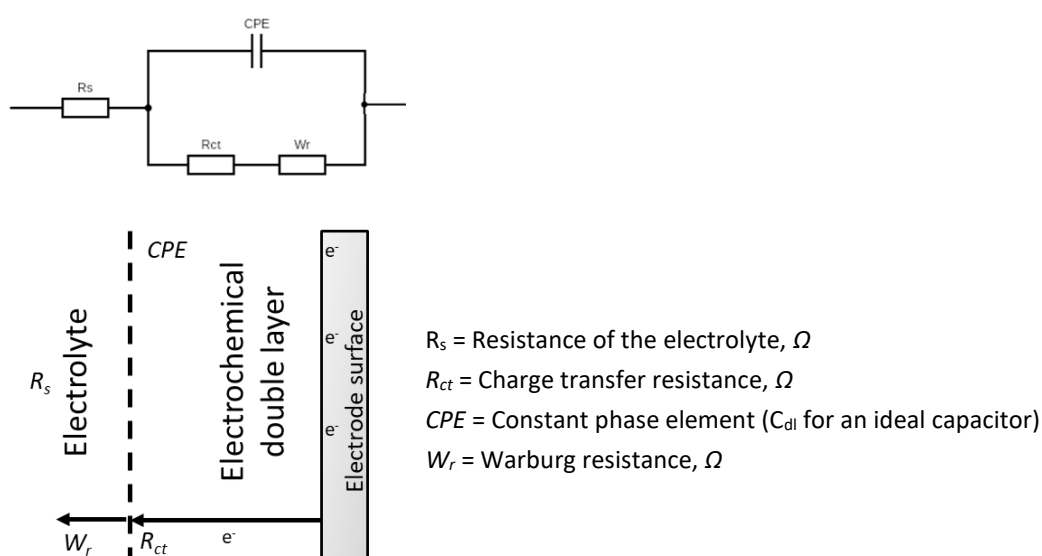


**Figure A.7.** Equivalent electronic circuit of a typical electrode-electrolyte system.

It is common to display the EDL by its schematic representation as an electrical circuit, namely the equivalent circuit, that includes capacitors, resistors and inductors. This equivalent circuit must contain every physicochemical aspect of the EDL to have validation, therefore a model cannot define a system, but the system must define the model proposed. For a system such as the one displayed in Figure A.6, the equivalent circuit, shown in Figure A.7, involves a capacitor ( $C_{dl}$ ), or a constant phase element ( $CPE$ ) if the capacitor is non-ideal, and three resistors: the resistor of the electrolyte ( $R_s$ ), the resistor of the charge transfer ( $R_{ct}$ ) and the resistor of the diffusion ( $W_r$ ). The equivalent circuit is used to study the properties of the electrode-electrolyte interface from the most fundamental perspective, thus allowing the proper evaluation of the system. Aspects such as the permeability of the electrode, the ohmic drop of your system or the kinetics of the reaction can be studied using the equivalent circuit and the adequate electrochemical technique, like the Electrochemical Impedance Spectroscopy (EIS), which will be detailed in *Annex A.6.3*.

The disposition of the charges and the structure of the EDL depends on the Potential of Zero Charge (PZC) of the electrode used. When the potential surpasses the PZC

(negatively for cathodes, positively for anodes), the charges present in the electrolyte will adsorb to the surface of the electrode and form the EDL. In eCO<sub>2</sub>R, the CO<sub>2</sub> does not take part of this EDL as mentioned earlier, therefore it must first cross this EDL to adsorb to the surface and react. It becomes clear that the composition of the EDL has a big impact in determining which species can easily reach the surface and react or, on the other hand, in inhibiting certain undesired co-reactions, like the HER, by preventing a precursor to reach the surface of the electrode.[255,256]

### A.2.5 The Faraday's law, the cell efficiency and the energy efficiency

The charge required to produce a certain amount of product during electrolysis is given by the Faraday's law (Eq. A.10). The  $Q$  is the charge,  $n$  is the amount of product formed in moles,  $z$  is the number of electrons transferred in the half-cell reaction and  $F$  is the Faraday constant.

$$Q = nzF \quad (\text{Eq. A.10})$$

In an electrocatalytic system, such as the eCO<sub>2</sub>R, multiple reactions occur simultaneously. For instance, different carbon products can be produced from CO<sub>2</sub> from the same electrocatalyst at the working potential of study, as well as other co-reactions such as HER. In this case, the  $Q$  is divided among these multiple reactions. The FE is used to illustrate the fraction of charge which is used by a specific half-reaction (Eq. A.11). The  $Q_i$  is the charge that is used for a specific half-reaction,  $\int I dt$  is the total current supplied to the cell within an amount of time. Therefore, the FE is a metric to evaluate the selectivity of an electrocatalytic process. Undesired co-reactions decrease the selectivity towards a specific product and thus, the FE of the process.

$$FE_i = \frac{Q_i}{Q} = \frac{n_i F z}{\int I dt} \quad (\text{Eq. A.11})$$



Apart from the selectivity, other parameters such as the activation energy, the ohmic drop or the Joule effect must be considered when evaluating an electrocatalytic system. All these parameters are englobed in the cell efficiency (CE) which is calculated with the cell voltage of the system. As mentioned in *Annex A.2.3*, there is a thermodynamic reduction potential at which a half-reaction occurs, however, in a real system an overpotential is needed to drive the reaction to a desired current. The CE is referred as the fraction of the potential that is used for the electrochemical reaction (Eq. A.12).

$$CE = \frac{E_{eq}}{E} \quad (\text{Eq. A.12})$$

The parameter that englobes both the contribution of the selectivity (FE) and the contribution on the energy losses (CE) is the EE (Eq. A.13). The EE is the end-metric used to evaluate an electrocatalytic system and one of the most important for validating the applicability of upscaling a technology.

$$EE = FE \times CE \quad (\text{Eq. A.13})$$

### **A.3 Reactor aspects for integrating the capture and conversion of CO<sub>2</sub>**

In this section, the preliminary concepts for understanding bicarbonate electrolysis, as well as the engineering parameters, are given. In this context, considering bicarbonate as a CO<sub>2</sub> source instead of as substrate of the electrochemical reaction and the role of the membrane used as separator during bicarbonate electrolysis are discussed. The outline of all basic principles is based on the following references: [39, 108, 115, 161, 178, 187 257-263].

### A.3.1 Bicarbonate as CO<sub>2</sub> source

As mentioned in the *Chapter 2.1*, there were two schools of thoughts in the scientific community about the electrochemical reduction pathway of the bicarbonate anion: either bicarbonate is the substrate of the electrochemical reaction or bicarbonate is a precursor and it is actually the CO<sub>2</sub> derived from the equilibrium with water the substrate of the reaction (or both). Back in the 80s, it was Hori *et al.*, who first reported the electrochemical reduction of the bicarbonate anion.[257] In their study, the pathway where CO<sub>2</sub> is the substrate and is supplied from the dissociation of bicarbonate, was already proposed. However, the direct electrochemical reduction of bicarbonate has been also reported, although a mechanistic study was still lacking.[258,259] Recently, Dunwell *et al.*, unraveled the role of low concentrated bicarbonate (0-0.1 M) during eCO<sub>2</sub>R (in saturated CO<sub>2</sub> solutions).[178] Surprisingly, they proved how it was the CO<sub>2</sub> coming from the bicarbonate the preferred substrate of the reaction, instead of the dissolved CO<sub>2</sub>. Nevertheless, the effect of high concentrated bicarbonate solutions in the absence of CO<sub>2</sub> pre-saturation, was still a mystery. In fact, the FE towards carbon products was very low (1-5%) when using 0.5, 1 or 2 M bicarbonate solutions.[161]

The approach where CO<sub>2</sub> is the actual substrate and bicarbonate is a precursor by delivering this CO<sub>2</sub> from the equilibrium with water, is proposed for the elaboration of this thesis. The reasoning is two-folded. Firstly, in any bicarbonate solution, there is always a fraction of dissolved CO<sub>2</sub> present, being the pH, the agent determining the ratio. The Bjerrum plot for carbonic species (Figure A.8) shows the relative abundance of each species (dissolved CO<sub>2</sub>, bicarbonate, and carbonate) in function of the pH. By using the equilibrium equations (Eq. A.14-A.16), the fraction of dissolved CO<sub>2</sub> in a pure bicarbonate solution (pH 8.3) can be calculated, being 1.2%. Then, in a 0.5, 1, 2 and 3 M bicarbonate solution, there is 0.006, 0.012, 0.024 and 0.036 M of dissolved CO<sub>2</sub> present. By comparing these concentrations with the solubility of CO<sub>2</sub> in water, 0.033 M, it can be said that they

lay within the same range. Therefore, the concentration of dissolved CO<sub>2</sub> in bicarbonate solutions is comparable to saturated CO<sub>2</sub> solutions (commonly used in eCO<sub>2</sub>R).

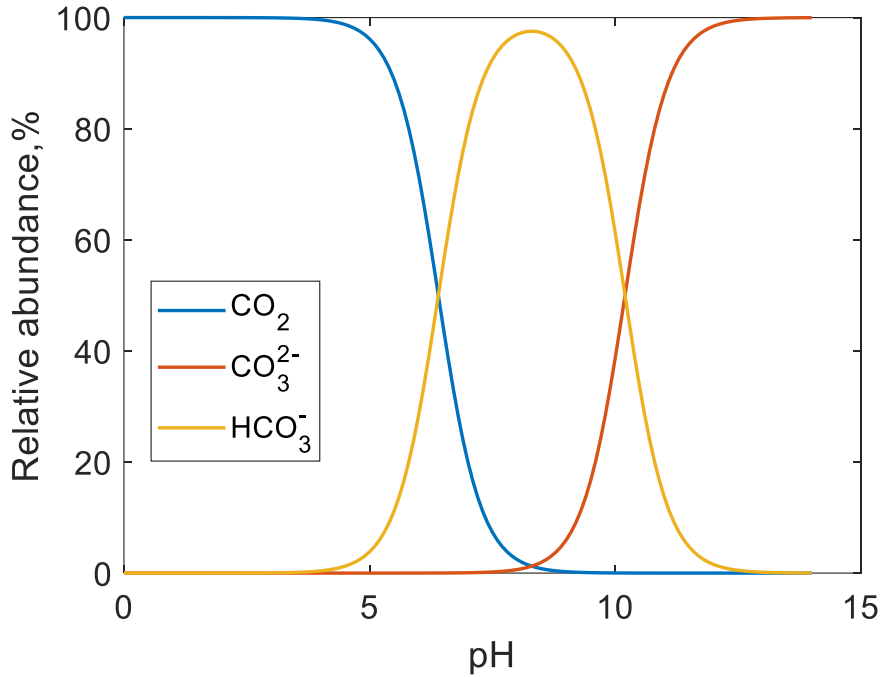


**Figure A.8.** Bjerrum plot for carbonic species in water at 25 °C.

$$\%CO_2 = \frac{1}{\left(\frac{K_{a1}}{10^{-pH}}\right)+1} \times 100 \quad (\text{Eq. A.14})$$

$$\%CO_3^{2-} = \frac{1}{\left(\frac{10^{-pH}}{K_{a2}}\right)+1} \times 100 \quad (\text{Eq. A.15})$$

$$\%HCO_3^- = \frac{1}{\left(\frac{10^{-pH}}{K_{a1}}\right)+\left(\frac{K_{a2}}{10^{-pH}}\right)+1} \times 100 \quad (\text{Eq. A.16})$$

Secondly, it is highly unlikely that the bicarbonate anion, negatively charged, can easily cross the IHP and adsorb to the negatively polarized cathode (Figure A.9). By migration effects, the bicarbonate anion will prefer to stay away from the surface and take part of the OHP. On the other hand, CO<sub>2</sub> is a non-polar molecule, thus it is unaffected by the

charges present in the EDL. Additionally, most of the mechanism proposed for eCO<sub>2</sub>R requires the bending of the molecule to activate the carbon atom.[39] CO<sub>2</sub> can easily bend from 180° to 120° without the interference of π orbitals due to the lineal, non-polar configuration. Contrary, the bending of the bicarbonate anion is highly impeded both sterically and electronically since there is repulsion of the π orbitals.

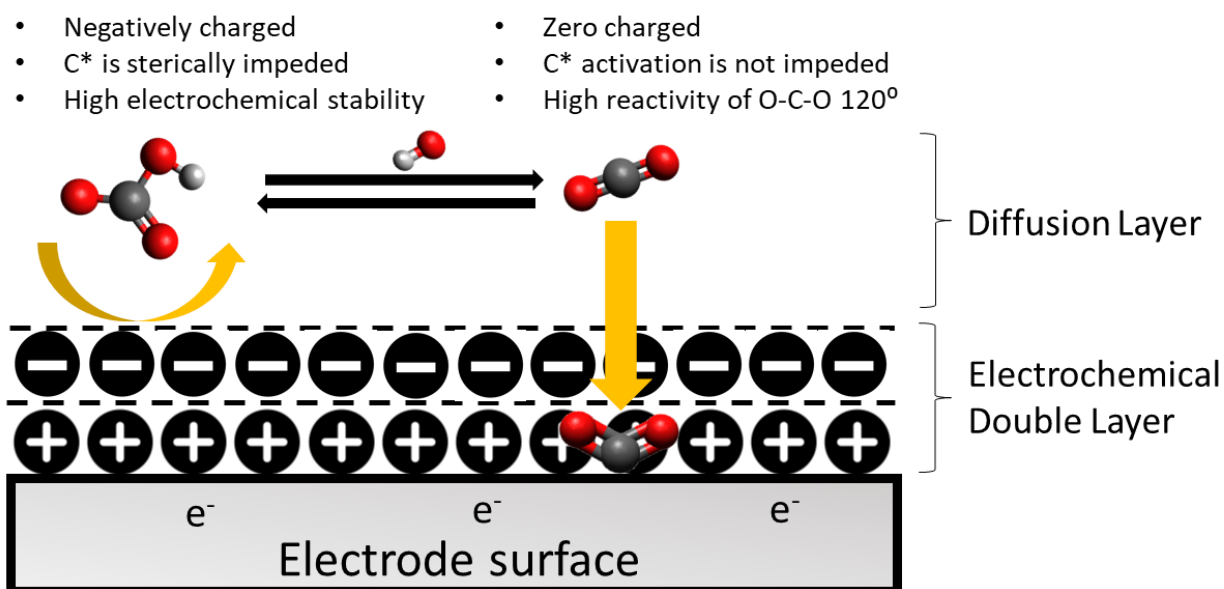


**Figure A.9.** Proposed mechanism for the bicarbonate electrochemical reaction.

Therefore, based on the discussion of the scientific community found in literature and in the independent physicochemical evaluation performed, the mechanism of bicarbonate electrochemical reaction where CO<sub>2</sub> is the substrate of the reaction is proposed and reaffirmed in this doctoral thesis. In fact, the experiments performed, and the conclusions drawn confirm this pathway, benchmarking it, at least, for the strategies followed in this thesis.

### A.3.2 Bicarbonate electrolysis and membrane engineering

Another important aspect to consider when designing experiments involving bicarbonate electrolysis is the choice of the membrane used as separator in the electrochemical cell. In electrochemical engineering, membranes are not only used to separate the anolyte and the catholyte and to avoid re-oxidation of products, but are also functional materials that affect the composition of the electrolytes and the efficiency of the reactor to a great extent.[108,115,187,260] In eCO<sub>2</sub>R usually three types of membranes are used: cation exchange membranes (CEM), anion exchange membranes (AEM) and bipolar membranes (BPM).

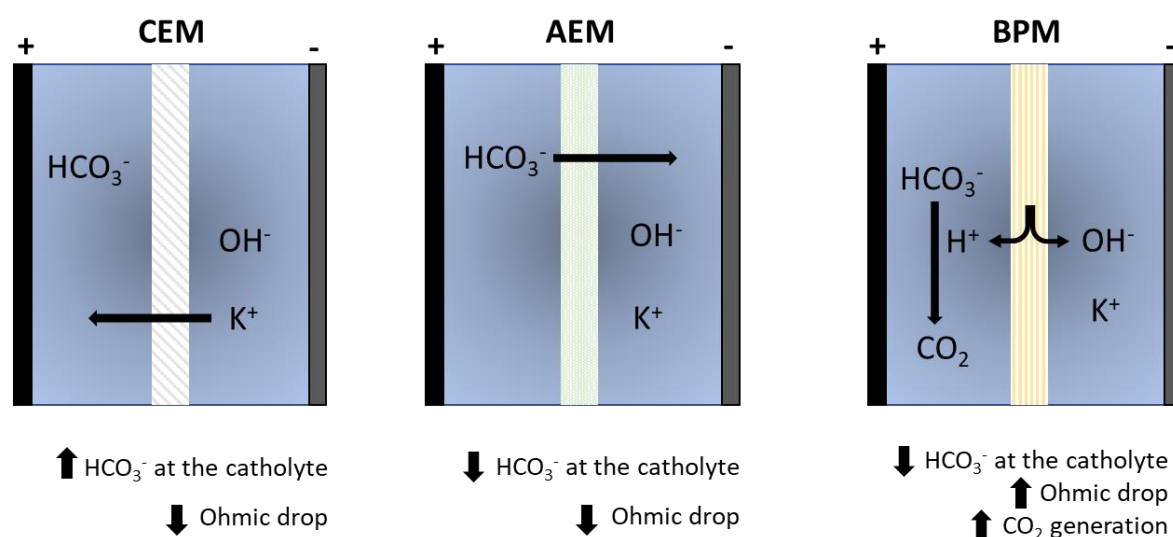


**Figure A.10.** Effects of using CEM, AEM and BPM for bicarbonate electrolysis.

In Figure A.10 the effect of using different membranes for bicarbonate electrolysis is presented. Since bicarbonate anion is the precursor of the reaction (by delivering CO<sub>2</sub>) it is important that it stays in the catholyte and does not migrate to the anolyte. For fundamental studies on bicarbonate electrolysis (*Part II* of this thesis), to evaluate properly parameters such as the effect of the concentration of bicarbonate as catholyte, it is crucial that the initial concentration remains almost unaltered. Therefore, AEM are excluded from these experiments, since bicarbonate, as an anion, will migrate to the

anodic compartment. Then, CEM are selected for fundamental experiments on bicarbonate electrolysis. Alternatively, BPM could be selected, too, but since they present a three-layer configuration, the ohmic drop (resistance of the system) is very high, interfering with the evaluation of the experiments. BPM will be used too, though, but for upscaled experiments. BPM are very efficient for bicarbonate electrolysis, if the ohmic drop can be diminished by, for instance, designing a zero-gap flow reactor. They present a unique function for this application, the water dissociation to H<sup>+</sup> (to the catholyte, converting bicarbonate to CO<sub>2</sub>) and OH<sup>-</sup> (to the anolyte). This will be explained in detail in *Chapter 8*.

#### **A.4 CO<sub>2</sub> capture: experimental set-up**

In this section, the design of the set-up and the procedure used for capturing CO<sub>2</sub> are provided. Two different set-ups were used depending the objective of the experiment: one to study the kinetics of the reaction between the CO<sub>2</sub> and the capture solution KOH, used in *Chapter 7*; and one for capturing CO<sub>2</sub> from the air (DAC) also with KOH as capture solution, used in *Chapter 9*. However, firstly, the chemical reactions occurring when capturing CO<sub>2</sub> with an alkaline capture solution, such as KOH, must be understood.

When CO<sub>2</sub>, coming from a bottle or from the air, starts flushing the capture solution, upon monitoring the pH, a titration-like curve is obtained (Figure A.11). In the beginning, the pH decreases gradually. This is because the capture solution was acts as a buffer (A.4, A.5):

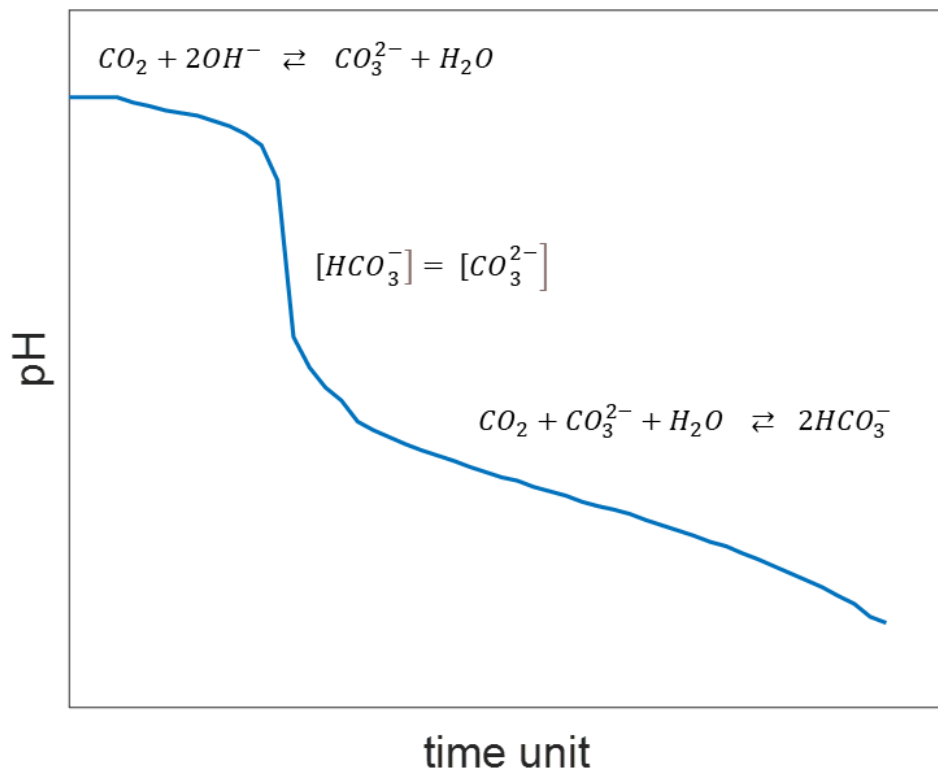
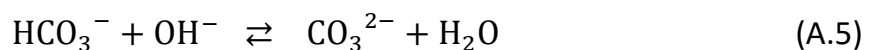
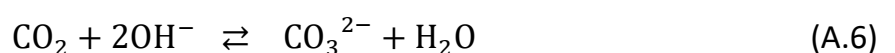


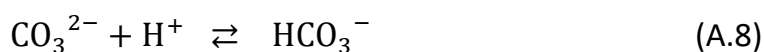
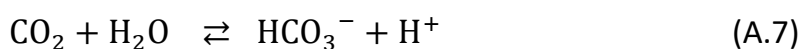
**Figure A.11.** Evolution of pH when saturating an alkaline capture solution with gaseous CO<sub>2</sub>.



This trend is continued until the supplied amount of acid (i.e., CO<sub>2</sub>) becomes larger than the buffer capacity can support, upon which the base is fully converted to carbonate (A.6):



Afterwards, the pH continues decreasing due to the continued introduction of CO<sub>2</sub> and interaction with the solvent (i.e., water) (A.7, A.8) until the point where half of the carbonate is converted to bicarbonate (point of half-neutralization):



After this point the pH decreases gradually again due to the buffering effect of the solution. Finally, when the pH is stable, the solution is saturated. All the carbonate is fully converted to bicarbonate. At 25 °C, if the pH < 8.3, some free CO<sub>2</sub> remains in solution as the maximum fraction of bicarbonate is reached at pH 8.3 (see Bjerrum plot as Figure A.8).

#### A.4.1 CO<sub>2</sub> capture set-up for kinetic studies

The set-up used for the kinetic studies of the CO<sub>2</sub> capture experiments is shown in Figure A.11. A jacketed electrochemical half-cell was filled with the capture solution. Since the kinetics of the reaction are very sensitive to the temperature (Arrhenius' law), the cell was connected to a thermostat to fix the desired temperature of the solution and avoid artifacts in the measurement.[261] The CO<sub>2</sub> was flushed from a gas bottle with a gas sparger connected to a gas flow controller. A second valve was opened on top of the gas sparger to allow the transpiration of the solution and avoid overpressure (which affects the solubility of the species and the kinetics of the reaction).[262] The cell was placed on top of a magnetic stirrer to homogenize the solution and increase the collisions between CO<sub>2</sub> and the capture solution. The pH of the solution was digitally monitored, registered, and used to determine the concentration of the species present in solution (Eq. A.14-A.16). The upper limit of detection of the digital pH-meter was 14, thus if the capture solution was very alkaline, the first moments of reaction (pH > 14) were not monitored. However, this was considered upon the design of the kinetic study and did not affect the outcome of the experiment. This set-up was used in *Chapter 7*.



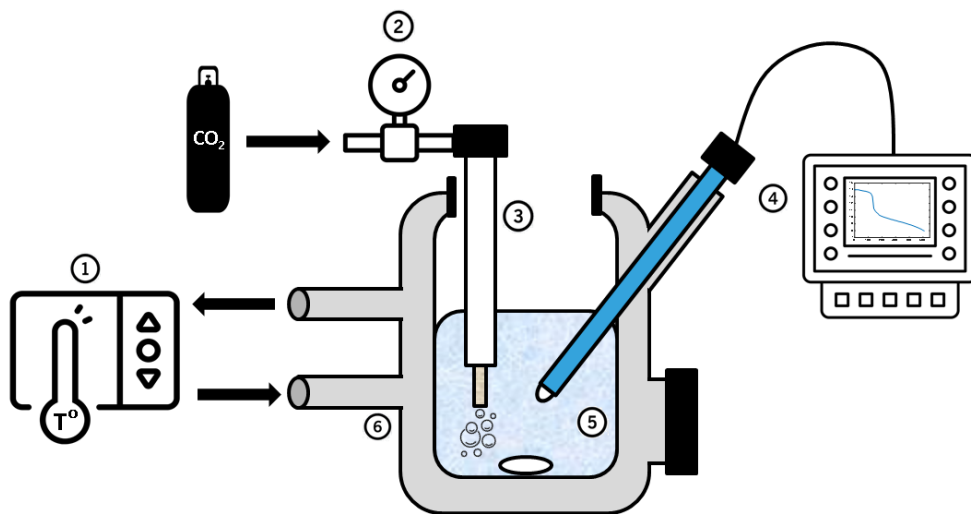
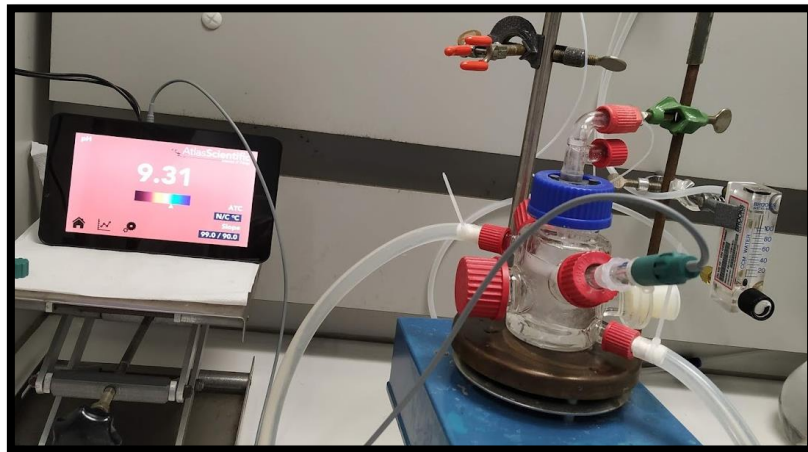


**Figure A.12.** Experimental set-up for kinetic studies of CO<sub>2</sub> capture experiments. 1) thermostat; 2) Gas flow controller; 3) Gas sparger; 4) Digital pH meter; 5) Capture solution; and 6) jacketed electrochemical half-cell.

#### A.4.2 Air tunnel for Direct Air Capture applications

For DAC experiments, instead of a pure CO<sub>2</sub> gas bottle, the air was used as CO<sub>2</sub> source. Since the concentration of CO<sub>2</sub> in the air is very low compared to a gas bottle (0.04% vs >99%), a new set-up had to be built. As mentioned in *Annex A.1*, membrane contactors are commonly used to separate the CO<sub>2</sub> from the air and dissolve it in a capture solution.[263] Then, the it is important to design a system that contains a membrane

contactor, a flow system for the capture solution and a fan system that direct the air flow towards the membrane contactor.

The set-up used to capture CO<sub>2</sub> from the air is show in Figure A.13. A capillary module was charged into the bench-scale setup and contained in a tailor-made module holder. The module housing was cut on two sides to allow free air movement through the capture module (in vertical position) in and out, perpendicular to the capillaries' direction. The capture solution was pumped through the valve at a controlled flow rate, towards the inside (lumen side) of the capillaries. In the capillary module, the membrane contactor allowed an enhanced CO<sub>2</sub> transport from the atmospheric air to the capture solution. The fan system could set to an operational airflow to control the velocity the air, and therefore control the flow of CO<sub>2</sub>. The airflow that exits the fan system went through a stack of tubes, to obtain a laminar flow. After the module holder, an exit channel was foreseen to avoid shape turbulence. The purpose of such design is to avoid pressure drops, in addition to the resistance from the tested module and capillaries. To avoid water losses due to evaporation, adequate humidification was integrated into the capture system to avoid/minimize this effect, making water compensation in the capture solution vessel unnecessary. The pH of the solution was monitored, registered, and used to determine the concentration of the species present in solution like it was described in *Annex A.4.1*.

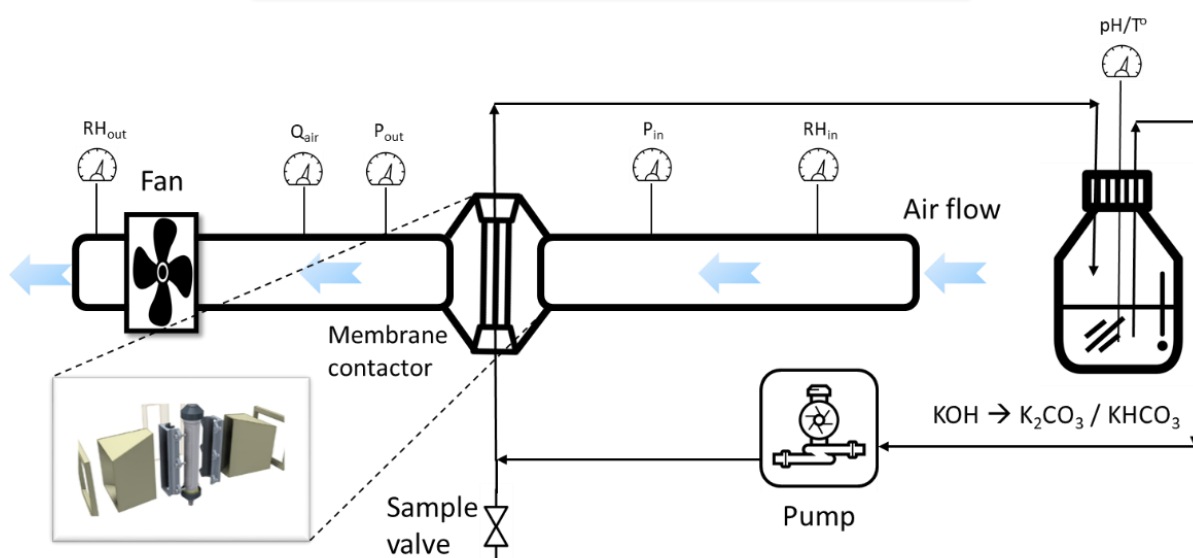


**Figure A.13:** Bench scale and schematic CO<sub>2</sub> capture test setup. It consists of a fan system and channel that guides the airflow to a central module holder, followed by an exit channel. The test module holder is located at the center of the bench-scale setup, through which the capture solution flows. The module is adapted such that it can be placed vertically and receive the airflow.

### A.5 Electrochemical cell: experimental set-up

For electrolysis experiments, it is often desired to convert large amounts of the reactant to obtain analytically relevant amounts of product and as such evaluate properly a system. Hence, a large electrode surface area and cell volume are commonly used. Electrolysis cells can be designed considering different specifications: single or multiple

cells, batch or flow configuration, two or three electrode system, temperature control, gas inlet, etc.

The separation of the electrodes using multiple cells is a common classification for electrolytic cells. If the electrodes are not separated in different cells, the products formed can interact with the other electrode (i.e., re-oxidation or re-reduction). In addition, in many applications it is desired to use different composition in the anolyte and the catholyte (i.e., in eCO<sub>2</sub>R), thus separating the compartments is necessary by, for instance, using membranes (as described in *Annex A.3.2*).

Other important specification is to use two electrodes (working and counter) or three electrodes (working, counter and reference). Two electrodes are commonly used in chronopotentiometry operations where the conversion of product is the main metric of interest (i.e., a fixed current is applied) and the cell voltage is measured between the working and the counter electrode, suitable for conversion experiments. On the other hand, the three-electrode system adds a reference electrode which allows the control of the working electrode potential, thus providing additional information of the system, more suitable for electroanalysis and the deep evaluation of the different components of the electrolyser such as the electrocatalysts or the electrolyte.

Besides the separation of the electrodes and the optional addition of a third electrode, another important classification is the operation in batch or continuous flow. Batch operation is the simplest way and therefore mostly applied in laboratory scale electrochemistry. This method is suitable for electroanalysis and fundamental studies, such as the electrochemical response of an electrode. Since the process conditions changes during the experiment (i.e., pH, consumption of reactants and formation of products), reactions are often carried out until a certain amount of charge has passed through the electrodes (chronoamperometry, detailed in *Annex A.6.2*). Constant process conditions can be performed in a flow configuration, where the reactants are

continuously replenished, and the products flushed out. Flow electrolyzers are more complex to operate and commonly used for upscaled experiments, since it is a more realistic system.

In this thesis, two main electrolytic cells are used for the experiments, a H-cell for batch operation (fundamental studies) and a flow-cell for continuous operation (upscaling studies).

### **A.5.1 H-Cell for batch operation**

The set-up used for batch operation is shown in Figure A.14. In a H-Cell the working and the counter electrode are separated in two compartments, connected by a channel where a membrane separator is placed, avoiding product crossover. Next to the working compartment, in the catholyte, a reference electrode is placed to control the potential of the working electrode. The H-Cell is connected to a thermostat, where the temperature is set. This set-up allows the study of the most fundamental parameters of the bicarbonate electrochemical reduction such as the selectivity of an electrocatalyst, the effect of certain additives of the electrolyte. In addition, electrochemical techniques that require (in our study) steady state, such as voltammetry (detailed in *Annex A.6.1*) or electrochemical impedance spectroscopy (EIS, detailed in *Annex A.6.3*) are performed in this set-up.

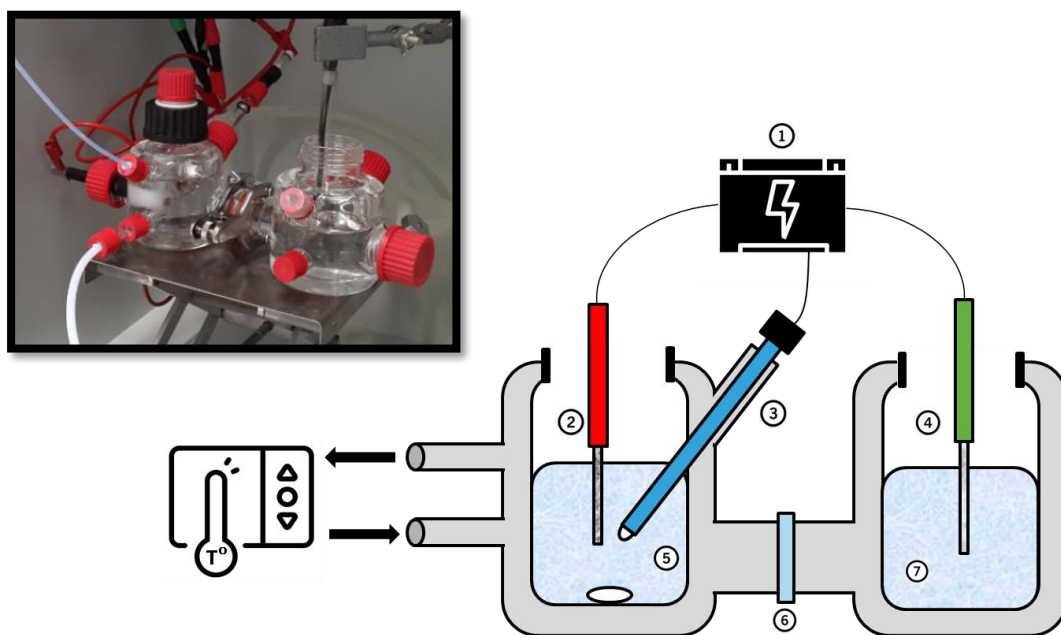


**Figure A.14.** Experimental set-up for bicarbonate electrolysis experiments (components labelled in Figure A.11 are not displayed in this figure): 1) Potentiostat; 2) Sn electrocatalyst, working electrode; 3) Ag/AgCl 3 M KCl, reference electrode; 4) Pt mesh, counter electrode; 5) Bicarbonate solutions; 6) Nafion CEM; and 7) KOH 1 M solution, anolyte.

### A.5.2 Zero-gap electrolyser for continuous flow operation

As an alternative to conventional flow electrolyzers, researchers have developed zero-gap flow electrolyzers for eCO<sub>2</sub>R (Figure A.15). This configuration has shown great results mainly in the field of fuel cells.[264] In a zero-gap configuration, the catholyte and the anolyte compartments are removed and the electrodes are pressed directly against the membrane, forming a membrane electrode assembly.[265] The main advantage of using zero gap electrolyzers instead of conventional flow electrolyzers is the significant decrease of the ohmic drop of the cell, since the catholyte and anolyte compartment are removed.[266] Another interesting reason to use a zero-gap electrolyser is to couple it with functional membranes, such as catalyst coated membranes or BPM.[164,266–268] Since the membrane is directly pressed to the electrode surface, it can affect to a great

extent the performance of the reaction. For instance, BPM avoid the crossover of the molecules and ions from the cathode and the anode and vice versa by dissociating water at the centre of the membrane. The  $H^+$  migrate towards the cathode while the  $OH^-$  migrate towards the anode.[269] Further functionality of BPM is found specifically for bicarbonate electrolysis, as the  $H^+$  generated protonate the bicarbonate thus increasing the amount of  $CO_2$  available two react.[165,220] A more detailed discussion of this practical application is provided in *chapter 8*.

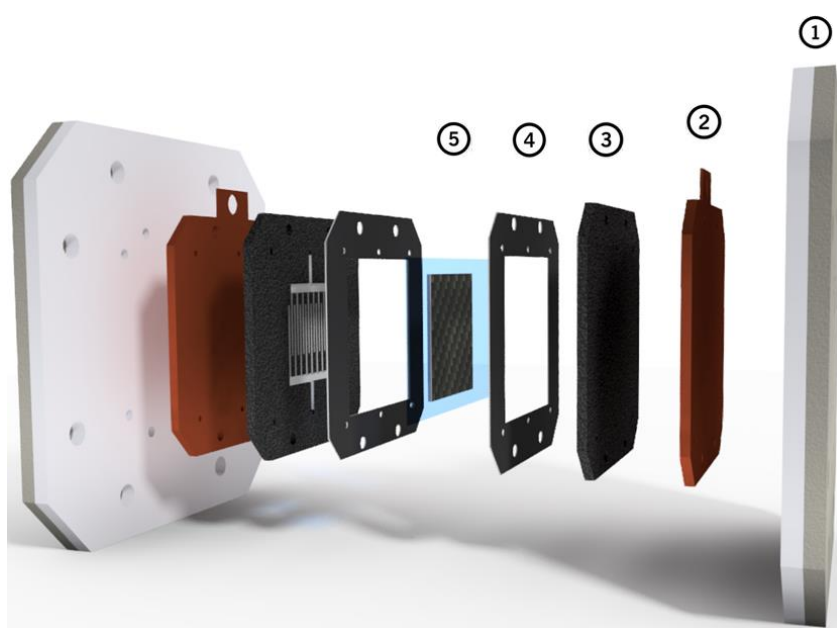


**Figure A.15.** Schematic representation of a zero-gap flow electrolyser: 1) End-plates; 2) Cu current collectors; 3) Flow channel; 4) Catalysts gaskets; 5) Membrane separator.

## A.6 Experimental techniques

### A.6.1 Lineal sweep voltammetry

Voltammetry is the study of the current response of an electrochemical system under a potential difference. Voltammetry experiments can provide huge information about the reduction and oxidation thermodynamics, as well as the kinetics of the electrochemical

reactions, thus being an essential technique to unravel the mechanism of an electrochemical reaction or to study the behavior of an electrocatalyst under certain systems' influence. There exist different voltammetry methods, being the sweep types the most widely used in electrochemistry. Sweep voltammetry are techniques where the current response of a system is measured under a continuous potential range at a certain scan rate (time within two consecutive potential). Within sweep voltammetry, the cyclic and the lineal sweep are the most interesting types to study an electrochemical system. Linear sweep voltammetry (LSV) is probably one of the most widely used techniques to study the electrochemistry of an electrode.

LSV consists of applying a linearly varying potential and measuring the current response (Figure A.16). The potential-current curve is called a polarization curve. The scan rate at which the potential is changed must be low enough to ensure equilibrium conditions at every step of the LSV. The technique is most often used to investigate the reaction mechanism of an electrode by distinguishing the different reactions taking place at the electrode as a function of the applied potential. In stationary conditions, the overall current is determined by the slowest process (rate limiting step), meaning that LSV can only give mechanistic information about the rate limiting reactions.

In Figure A.16, an example of a LSV is shown. The scan begins from the left side of the of the plot ( $V_1$ ) where there is no current flow. As the voltage is swept to the right, a current appears and increases until eventually reach a peak before dropping. To explain this effect the effect of the voltage on the system must be understood. The current appears at the oxidation/reduction potential of the species of study, calculated with the Nernst equation (Eq. A.4). At this potential, the electrochemically active species starts to react (oxidizes or reduces). As the current increases the overpotential ( $\eta$ ) rises, thus converting more reactant. The peak is reached since at some point the  $\eta$  is high enough to reach the diffusion control zone (the diffusion layer has grown sufficiently so that the flux of



reactant to the surface of the electrode is not fast enough), as described in *Annex A.2.3*. After this situation, the current begins to drop, following the Cottrell equation (Eq. A.17).

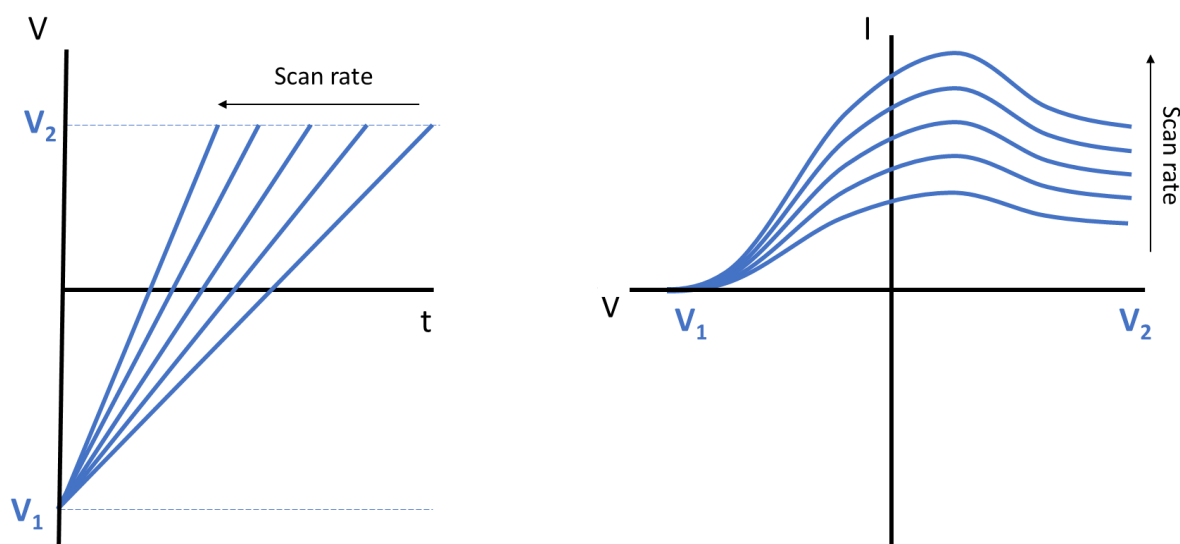


**Figure A.16.** Variation of the applied potential over time in a LSV experiment at different scan rate (left). LSV of a system showing an electrochemical reaction as the potential is swept at different scan rate (right).

$$i = \frac{zFSc^*\sqrt{D_i}}{\sqrt{\pi t}} \quad (\text{Eq. A.17})$$

The characteristics of the LSV recorded strongly depend on the scan rate. If the scan rate is altered the current response also changes. In Figure A.16, the LSV of a system at different scan rates is shown. Each voltammogram has the same shape (i.e., the peak is located at the same voltage) but the current increases with the scan rate. Again, the diffusion layer plays a role here. In a slow scan rate, the diffusion layer is larger than in fast scan rate. Consequently, the flux of reactants at slow scan rate is considerably smaller than at fast scan rate.

In this thesis, LSV will be used to check the performance of an electrode (i.e., current response to a certain applied potential) and to identify the electrochemical reactions

taking place on the electrode. This will help to choosing of an optimal potential to get a desired current for conversion experiments as well as evaluate the effect of different additives in the electrolyte on the potential/current response.

### **A.6.2 Chronoamperometry and chronopotentiometry**

Chronoamperometry (CA) is a potentiostatic method (i.e., a fixed potential is applied and the variation of the current in time is measured) while chronopotentiometry (CP) is an amperostatic method (i.e., a fixed current is applied and the variation of the potential is measured). These experiments allow the calculation of the total charge that goes through the electrochemical system, which is used to calculate the rate and the FE of a conversion reaction (Eq. A.11). In CA experiments, when a potential is applied, initially there is an abrupt increase in the current due to the abundance of electroactive species on the surface of the electrode. Then, this current decreases over time until it reaches a steady state (if the conditions of the reactions do not change, i.e., the formation of a product does not affect the performance of the reaction). The current measured corresponds of a Faradaic current (caused by the transfer of electrons) and of a capacitive current (caused by the charge of the electrochemical double layer, see *Annex A.2.4*). CA are commonly used in laboratory-scale conversion experiments following a voltammetry experiment. With the voltammetry, the potential where the desired current (or reaction) is reached is chosen and used for the CA. On the other hand, CP experiments are commonly used for upscaled experiments, where the fixed variable is the current instead of the potential, as it is the metric that approximately predicts the amount of product formed and thus the productivity of the process

In this thesis, CA is used for bicarbonate electrolysis in the most fundamental experiments (*Chapters 5-7*) while CP is used for upscaled experiments (*Chapters 8 and 9*).

### A.6.3 Electrochemical Impedance Spectroscopy

EIS is a technique used for the analysis of interfacial properties related to the events occurring at the electrode surface. EIS measures the impedance of a system in dependence of an alternate circuit potential frequency. In electrochemistry, EIS can be used to obtain various information about the system of study such as the distinction between two or more reactions, the identification of diffusion-limited reaction, the capacitive behaviour and the electron transfer rate.

In Ohm's Law, resistance is defined as the ability of a circuit element to resist a flow of electrical current, described by Eq. A.18. However, Ohm's Law can only be applied to a single circuit element, the ideal resistor. This ideal resistor follows Ohm's law at all current and voltage levels, its value is independent of frequency and the alternate circuit current and voltage signals are in phase. However, in real, non-ideal, systems, circuit elements present more complex behaviors. In this complex system, the  $R_i$  is substituted by the impedance,  $Z$ , a generic parameter that describes the whole system instead of being limited to a single circuit component.

$$R_i = \frac{E}{I} \quad (\text{Eq. A.18})$$

Impedance is normally measured using a small excitation signal. The current response will be sinusoid at the same frequency but shifted in phase (Figure A.17) caused by a capacitor.

Each excitation signal (peak) is expressed in function of time, being the current shifted in phase (Eq. A.19 and A.20). Where  $E_o$  is the amplitude,  $I_o$  the current response to the amplitude,  $\omega$  is the radial frequency and  $\Phi$  is the phase shift.

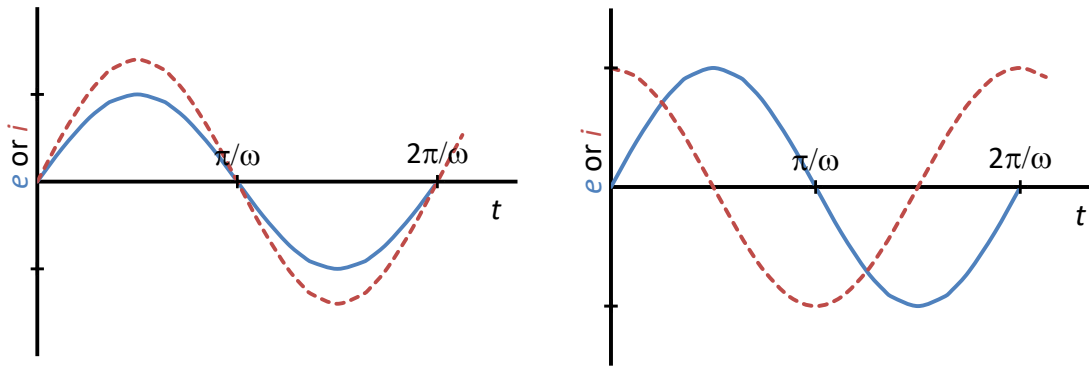


**Figure A.17.** Voltage and current response on time in phase in an ideal resistor that follows Ohm's Law (left). Voltage and current response on time out of phase in a non-ideal resistor (right)

$$E_t = E_o \sin(\omega t) \quad \text{Eq. A.19}$$

$$I_t = I_o \sin(\omega t + \Phi) \quad \text{Eq. A.20}$$

Therefore, analogous expression to the Ohm's law can be formulated to find the  $Z$  of the system (Eq. A.21). By using the Euler's relationship ( $e^{i\Phi} = \cos\Phi + i\sin\Phi$ ), the  $Z$  can be represented as a complex number expressed as a function of the radial frequency (Eq. A.22).

$$Z = \frac{E_o \sin(\omega t)}{I_o \sin(\omega t + \Phi)} = Z_o \frac{\sin(\omega t)}{\sin(\omega t + \Phi)} \quad \text{Eq. A.21}$$

$$Z(\omega) = Z_o(\cos\Phi + i\sin\Phi) \quad \text{Eq. A.22}$$

By looking at Eq. A.22, the impedance is composed of a real and an imaginary part. If the real part ( $Z'$ ) is plotted against the imaginary part ( $Z''$ ) at a series of frequencies  $\omega$  ( $f$ ), the Nyquist plot is obtained (Figure A.18, left). However, in a Nyquist plot it is hard to tell what frequency was used to record each point. For that reason, another popular representation of impedance is the Bode plot (Figure A.18, right). In a Bode plot, both the

absolute value of impedance  $Z$  and the  $\Phi$  are plotted with the log of frequency, therefore obtaining a broad range of information about the system.

**Table A.3.** Some important parameters obtainable when plotting the EIS data with the equivalent circuit model.

Circuit element	Description	Related physicochemical element
$R_s$	Electrolyte resistance. It depends on the ionic concentration, type of ions, temperature, and the geometry of the area in which current is carried	Resistivity ( $\rho$ ) and conductivity ( $\kappa$ ). $R_s = \rho \frac{l}{A} = \frac{l}{\kappa A}$
$R_{ct}$	Charge transfer resistance. Formed by a single, kinetically controlled electrochemical reaction	Exchange current density ( $j_o$ ) Obtainable at low $\eta$ as described in section 3.2.3. $R_{ct} = \frac{RT}{zFj_o}$
$W_r$	Warburg resistance. Models the impedance caused due to the lack of species present at the electrode (diffusion process)	Diffusion constant ( $D_i$ ) Obtainable from Cottrell equation. $W_r = \frac{\sigma}{\sqrt{2\pi f}} - j \frac{\sigma}{\sqrt{2\pi f}}$ ; $\sigma = \frac{RT}{Az^2F^2\sqrt{2}} \left( \frac{1}{D_o c_o^b} + \frac{1}{D_r c_r^b} \right)$
CPE	Constant Phase Element. Describes the EDL as a capacitor. Parameters like the roughness of the electrode or the polycrystallinity disturb the EDL	Double layer capacitance ( $C_{dl}$ ). $C_{dl} = (R_{ct}^{(1-N)} CPE)^{\frac{1}{N}}$ Where $N$ describes how ideal is of the capacitor

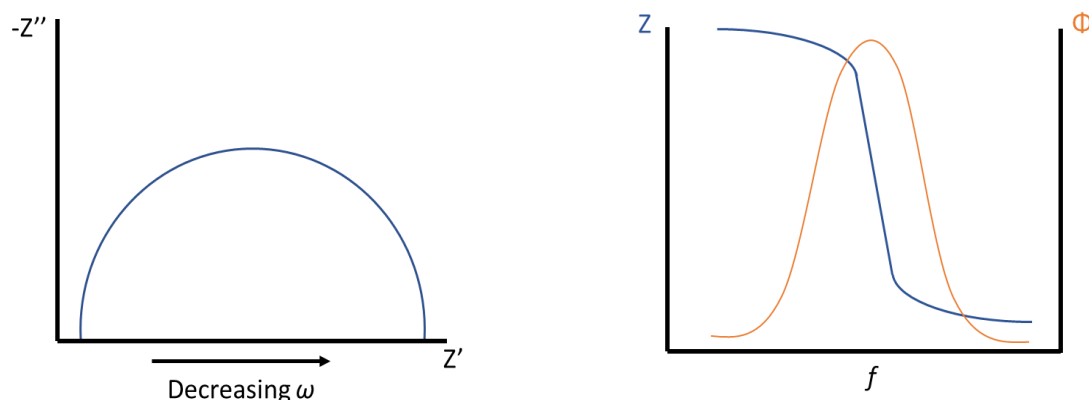


**Figure A.18.** Nyquist plot (left) and Bode plot with one time constant (right) of a hypothetical electrochemical circuit.

To obtain the Nyquist and Bode plots of a system, first it must be defined electronically with an equivalent circuit model. EIS data are commonly analysed by fitting to this equivalent circuit model. Most of the elements in the model are common electrical such as resistors, capacitors and inductors. As explained in *Annex A.2.4*, an electrochemical system can also be defined by these circuit elements. To properly define an equivalent circuit, each element must describe a specific activity of the system (i.e., the resistance of the electrolyte, the capacitance of the electrochemical double layer or the charge transfer resistance of the electrochemical reaction) and the model must have a physicochemical sense (i.e., elements cannot be added just to fit the data without a meaning). For instance, the Nyquist and Bode plots of Figure A.18 correspond to the equivalent circuit model of Figure A.7. Once the model is found, by using specific software the experimental data can be fitted and the value of each element is calculated. In Table A.3, some parameters that can be calculated with the information obtained in EIS are described. From these parameters, the most relevant for this doctoral thesis will be the double layer capacitance (DL-Capacitance) calculated from the CPE.

A capacitor is formed once there is a separation of charges like, for instance, the EDL (described in *Annex A.2.4*). The electrode potential, the temperature, the concentration

and types of ions or the presence of adsorbed species are some of the factors that influence the properties of this capacitor. The parameter that describes the capacitor of the electrochemical double layer is the DL-Capacitance. The capacitance can be easily calculated by obtaining the Nyquist plot of the system (Eq. A.23). However, this is only true if the capacitor is considered ideal (perfect EDL is formed). Parameters like the roughness of the electrode or the turbulence can alter how ideal is the capacitor formed in the EDL. In realistic systems, or in systems where the DL-Capacitance is the main factor of study, the CPE must be used instead. CPE is a parameter that describes the non-ideality of a capacitor by introducing an  $N$  factor, a value between 0 and 1, where 1 is a perfect capacitor (see formula of  $C_{dl}$  in Table A.3). The  $N$  value is a useful factor while proposing an equivalent circuit for a system since an equivalent circuit is considered valid when the  $N > 0.85$ . A lower  $N$  would indicate that there are missing elements in the circuit and thus it must be revised.

In this thesis, EIS and the DL-Capacitance are used to study the hydrophobicity of the electrodes in *Chapters 6* and *7*, being crucial to understand the behaviour of the system and thus draw the proper conclusions of the observations made.





# List of figures

<b>Figure 1.1.</b>	Global atmospheric carbon dioxide concentrations (CO <sub>2</sub> ) in parts per million for the past 800,000 years. Graph by NOAA Climate.gov based on data from Lüthi, <i>et al.</i> , 2008, via NOAA NCEI Paleoclimatology Program.[1].....	2
<b>Figure 1.2.</b>	Amount of CO <sub>2</sub> emitted per year (grey). The International Panel for Climate Change set a scenario for the global CO <sub>2</sub> emissions to achieve a temperature anomaly of no more than 2 °C, ideally 1.5 °C (red). A net CO <sub>2</sub> emission approaches 10 Gt in 2050 and is zero in 2070.[6].....	3
<b>Figure 1.3.</b>	CO <sub>2</sub> net cycle proposed in the CCU technology.....	5
<b>Figure 1.4.</b>	DAC Process using sodium hydroxide as the absorbent and including a solvent regeneration step. Re-drawn from [23].....	8
<b>Figure 1.5.</b>	CO <sub>2</sub> capture from flue gas by using an amine solution as an absorber and regenerating the solvent in the stripper. Re-drawn from [24].....	8
<b>Figure 1.6.</b>	Overview of reaction pathways for eCO <sub>2</sub> R towards different products. Reproduced with the permission of [29].....	11
<b>Figure 1.7.</b>	Schematic representation of an integrated CO <sub>2</sub> capture and electrochemical conversion system involving KOH as capture solution.....	13
<b>Figure 1.8.</b>	Comparison of the capture cost of the integrated and two-step route.....	18
<b>Figure 1.9.</b>	Comparison of syngas production cost of the two-step and integrated routes (IR).....	19

<b>Figure 1.10.</b>	Impact of electrolyte losses in the integrated route on syngas production cost.....	21
<b>Figure 1.11.</b>	Impact of the cell potential in the integrated route on syngas production cost.....	21
<b>Figure 1.12.</b>	Impact of the amount of exist CO <sub>2</sub> and DSP cost on syngas production cost (integrated route only).....	22
<b>Figure 2.1.</b>	TRL scale of eCO <sub>2</sub> R technologies.....	27
<b>Figure 2.2.</b>	Schematic outline of this doctoral thesis.....	30
<b>Figure 3.1.</b>	Various configurations for electrochemical flow reactors. (A) general design; (B-D) membrane reactors depending on the state of catholyte and anolyte; (E) classical microfluidic reactor; (F) Solid-oxide electrolyser. This figure is reproduced with permission from reference.[81].....	41
<b>Figure 3.2.</b>	Schematic of a gas diffusion electrode including interrelated effects of the GDL and CL design parameters. Parameters shown in the black, brown and green boxes refer to the microporous layer, catalyst layer and macroporous layer respectively. Positive effects are shown in blue and negative effects in red colored boxes.....	46
<b>Figure 4.1.</b>	Mechanism of the hydration of CO <sub>2</sub> in the metal cofactor of the enzyme CAH.....	58
<b>Figure 4.2.</b>	Schematic representation of the mechanism of bicarbonate electrochemical reduction in reactors involving a BPM.....	62
<b>Figure 5.1.</b>	Volmer-Heyrovsky mechanism of HER involving water and bicarbonate.....	70

- Figure 5.2.** LSV voltammograms of a Sn electrode in different  $\text{KHCO}_3$  solutions (left).  $\text{FE}_{\text{Formate}}$  at different potentials in various  $\text{KHCO}_3$  solutions (right). ..... 76
- Figure 5.3.** LSV of a Sn electrode in  $\text{KHCO}_3$  2 M electrolytes in presence and in the absence of 1000  $\mu\text{M}$  of surfactants of different nature. .... 77
- Figure 5.4.** LSV of a Cu electrode in  $\text{KHCO}_3$  2 M electrolytes in presence and in the absence of 1000  $\mu\text{M}$  of CKC. .... 78
- Figure 5.5.** LSV of a Sn electrode in  $\text{KHCO}_3$  2 M in presence and in the absence of 1000  $\mu\text{M}$  of CTAB and CTAC. .... 79
- Figure 5.6.** a)  $\text{FE}_{\text{Formate}}$  at different applied potential in  $\text{KHCO}_3$  2 M in presence and in the absence of CKC. b) Corresponding  $\text{FE}_{\text{HER}}$  c) Partial current density towards formate; d) partial current density towards HER. .... 80
- Figure 5.7.**  $\text{FE}_{\text{Formate}}$  at  $-0.9 \text{ V}_{\text{RHE}}$  in 2 M  $\text{KHCO}_3$  in presence and in the absence of different concentrations of CKC (left) LSV voltammograms of a Sn electrode in  $\text{KHCO}_3$  2 M in presence and in the absence of different concentrations of CKC. .... 81
- Figure 5.8.**  $\text{FE}_{\text{Formate}}$  at  $-0.9 \text{ V}_{\text{RHE}}$  in different concentrations of  $\text{KHCO}_3$  electrolytes in presence and in the absence of 1000  $\mu\text{M}$  of CKC. .... 82
- Figure 5.9.**  $\text{FE}_{\text{Formate}}$  at different potentials in  $\text{KHCO}_3$  2 M with and without 1000  $\mu\text{M}$  of CTAB (left).  $\text{FE}_{\text{Formate}}$  at  $-0.9 \text{ V}_{\text{RHE}}$  in different concentrations of  $\text{KHCO}_3$  with and without 1000  $\mu\text{M}$  of CTAB (right). .... 84
- Figure 6.1.** Schematic interpretation of the  $\text{eCO}_2\text{R}$  to formate when using bicarbonate as a carbon source. A cationic surfactant is used and a non-polar layer is formed close to the surface of the cathode, promoting the reaction. 1)  $\text{CO}_2$  is formed from the equilibrium with bicarbonate with water. 2)  $\text{CO}_2$  (non-

polar) diffuses through the non-polar layer and reaches the surface of the electrode. 3) CO<sub>2</sub> is reduced to formate. .... 87

**Figure 6.2.** LSV at 10 mV s<sup>-1</sup> of a Sn electrode in KHCO<sub>3</sub> 2 M in presence or in the absence of different surfactants (left) F<sub>EFormate</sub> and c) Partial CD for formate and H<sub>2</sub> production after one hour CA of a Sn electrode in KHCO<sub>3</sub> 2 M in presence and in the absence of 1 mM of different surfactants (right). .... 94

**Figure 6.3.** LSV at 10 mV s<sup>-1</sup> of a Cu electrode in KHCO<sub>3</sub> 2 M in presence and in the absence of different concentrations of a) CTAB and b) CKC. c) Comparison plot of LSV at 10 mV s<sup>-1</sup> of a Cu electrode in KHCO<sub>3</sub> 2 M in presence and in the absence of 1 mM of CTAB and CKC. d) Current drop observed at -1.0 V<sub>RHE</sub> when adding CTAB or CKC in a LSV experiment using Sn or Cu as cathode. .... 96

**Figure 6.4.** LSV at 1 mV s<sup>-1</sup> of a Sn RDE electrode in KHCO<sub>3</sub> 2 M while rotating the electrode at different speeds (0 – 3200 rpm). .... 98

**Figure 6.5.** LSV at 1 mV s<sup>-1</sup> of a Sn RDE electrode in KHCO<sub>3</sub> 2 M while rotating the electrode at different speeds in presence of 1 mM CKC (left) and 0.5 mM CKC (right). .... 99

**Figure 6.6.** Comparison of the highest current density reached for the CKC characteristic reduction peak between 1 mM and 0.5 mM CKC when rotating at different speeds. .... 100

**Figure 6.7.** Phase shift extracted from the EIS of a Sn electrode in KHCO<sub>3</sub> 2 M in presence of 1 mM of CTAB (left) or SDS (right). .... 102

- Figure 6.8.** Equivalent electrical circuit model used for the EIS simulations to fit the experimental data of systems in presence of CKC. A Warburg resistor was added after  $R_{ct}$  at potentials -0.9 and -1.0  $V_{RHE}$ . .....102
- Figure 6.9.** Phase shift at different frequencies extracted from the EIS of a Sn electrode in  $KHCO_3$  2 M in the absence of surfactant (left) and in presence of 1 mM of CKC (right). .....103
- Figure 6.10.** Double-layer Capacitance extracted by modelling EIS of a Sn electrode (left) and Cu electrode (right) in  $KHCO_3$  2 M solutions in presence and in the absence of 1 mM of different surfactants. ....105
- Figure 6.11.** Phase shift at different frequencies extracted from EIS of a Cu electrode in  $KHCO_3$  2 M in the absence (left) and presence of 1 mM of CKC (right). ....105
- Figure 6.12.** LSV at  $10\text{ mV s}^{-1}$  of a Sn electrode in  $KHCO_3$  2 M in presence and in the absence of 1 mM of benzyl-functionalized substances (left) and structure of the benzyl-functionalized species used (right). .....106
- Figure 6.13.** Structure and identity of the impurities found in (a) CKC and (b) CTAB. ...108
- Figure 6.14.** LSV at  $10\text{ mV s}^{-1}$  of a Sn RDE electrode in  $KHCO_3$  2 M previously saturated with  $N_2$  (blue) or  $CO_2$  (orange). .....111
- Figure 6.15.** Nyquist plot (experimental and simulation) for EIS experiments carried out in  $KHCO_3$  2 M electrolyte and using a Sn electrode in the absence of surfactants. ....112
- Figure 6.16.** Nyquist plot (experimental and simulation) for EIS experiments carried out in  $KHCO_3$  2 M electrolyte and using a Sn electrode in presence of 1 mM CTAB. ....113

<b>Figure 6.17.</b>	Nyquist plot for EIS experiments carried out in KHCO <sub>3</sub> 2 M electrolyte and using a Sn electrode in presence of 1 mM SDS.	114
<b>Figure 6.18.</b>	Nyquist plot for EIS experiments carried out in KHCO <sub>3</sub> 2 M electrolyte and using a Sn electrode in presence of 1 mM CKC.	115
<b>Figure 6.19.</b>	Nyquist plot for EIS experiments carried out in KHCO <sub>3</sub> 2 M electrolyte and using a Cu electrode in the absence of surfactants.	116
<b>Figure 6.20.</b>	Nyquist plot for EIS experiments carried out in KHCO <sub>3</sub> 2 M electrolyte and using a Cu electrode in presence of 1 mM CKC.	117
<b>Figure 6.21.</b>	Nyquist plot for EIS experiments carried out in KHCO <sub>3</sub> 2 M electrolyte and using a Cu electrode in presence of 1 mM CTAB.	118
<b>Figure 6.22.</b>	LC of a CKC solution and MS spectra of the species detected.	120
<b>Figure 6.23.</b>	LC of a CTAB solution and MS spectra of the species detected.	122
<b>Figure 7.1.</b>	Schematic representation of the catalytic mechanism of the conversion of CO <sub>2</sub> to bicarbonate in the metal co-factor of CAH (hydrogen atoms are not displayed). 1) H <sub>2</sub> O coordination to the unoccupied position of the tetrahedral structure; 2) Reaction between CO <sub>2</sub> and coordinated OH <sup>-</sup> and; 3) formation of bicarbonate and substitution with a new H <sub>2</sub> O molecule. [202]	125
<b>Figure 7.2.</b>	Potential ligands chosen to form the artificial CAH. Log <i>k<sub>b</sub></i> refer to the binding constant Zn <sup>2+</sup> -L. The <i>pK<sub>a</sub></i> corresponds to the H <sub>2</sub> O after being fixated to the complex. [210–214]	128

- Figure 7.3.** Evolution of pH and equilibrium reactions of the species present when saturating a 2 M KOH solution with gaseous CO<sub>2</sub>. ..... 130
- Figure 7.4.** Linear regression fitting of the evolution of pH when saturating 2 M KOH solutions with gaseous CO<sub>2</sub>. The time range chosen belongs to the conversion of carbonate to bicarbonate. .... 132
- Figure 7.5.** Scheme of the experimental procedure to evaluate the effectiveness of the bio-mimetic catalyst and the conditions of the CO<sub>2</sub> capture in a 2 M KOH media. .... 133
- Figure 7.6.** Evolution of  $\ln[\text{H}^+]$  over time (left) and  $K_c^*$  calculated (right) from the corresponding linear regression equation (Figure 7.14) of a CO<sub>2</sub> capture solution in the presence and in the absence of  $[\text{Zn}(\text{L})_x]^{2+}$ , where L are different ligands tested (histidine, imidazole and cyclen). .... 136
- Figure 7.7.** Evolution of  $\ln[\text{H}^+]$  over time (left) and  $K_c^*$  calculated (right) from the corresponding linear regression equation (Figure 7.15) of a CO<sub>2</sub> capture solution in the presence and the absence of  $[\text{Zn}(\text{cyclen})]^{2+}$  at different concentrations. .... 139
- Figure 7.8.** Evolution of  $\ln[\text{H}^+]$  over time (left) and calculated  $K_c^*$  (right) from the corresponding linear regression equation (Figure 7.16) of a CO<sub>2</sub> capture solution at different temperatures in the presence and the absence of 20 mM of  $[\text{Zn}(\text{cyclen})]^{2+}$ . .... 141
- Figure 7.9.**  $\text{FE}_{\text{Formate}}$  (measured) and H<sub>2</sub> (approximated) of the electrolysis of a 2 M KHCO<sub>3</sub> solution (prepared from a 2 M KOH capture solution) in the presence and the absence of 20 mM of cyclen, 20 mM of  $[\text{Zn}(\text{cyclen})]^{2+}$  or 1 mM of CKC. .... 143

<b>Figure 7.10.</b> Partial CD towards formate and H <sub>2</sub> (approximated) of the electrolysis of a 2 M KHCO <sub>3</sub> solution (prepared from a 2 M KOH capture solution) in the presence and the absence of 20 mM of cyclen, 20 mM of [Zn(cyclen)] <sup>2+</sup> or 1 mM of CKC.....	143
<b>Figure 7.11.</b> LSV (left) and DL-Capacitance (right) of 2 M KHCO <sub>3</sub> solutions in the presence and the absence of cyclen and [Zn(cyclen)] <sup>2+</sup> .....	144
<b>Figure 7.12.</b> EDL representation for each case scenario (absence of artificial CA, presence of cyclen and presence of [Zn(cyclen)] <sup>2+</sup> ) and HER inhibition model proposed.....	146
<b>Figure 7.13.</b> Nyquist plots (experimental and simulation) for EIS experiments carried out in this chapter.....	147
<b>Figure 7.14.</b> Linear regression fitting of the evolution of pH when saturating 2 M KOH solutions with gaseous CO <sub>2</sub> in presence and in the absence of [Zn(L) <sub>x</sub> ] <sup>2+</sup> , where L are different ligands tested (histidine, imidazole and cyclen).....	148
<b>Figure 7.15.</b> Linear regression fitting of the evolution of pH when saturating 2 M KOH solutions with gaseous CO <sub>2</sub> in presence and in the absence of [Zn(cyclen)] <sup>2+</sup> at different concentrations.....	149
<b>Figure 7.16.</b> Linear regression fitting of the evolution of pH when saturating 2 M KOH solutions at different temperature with gaseous CO <sub>2</sub> in presence and in the absence of 20 mM [Zn(cyclen)] <sup>2+</sup> .....	150
<b>Figure 7.17.</b> Evolution of pH when saturating a 2 M KOH solution with gaseous CO <sub>2</sub> at different temperature in the presence of 20 mM of [Zn(cyclen)] <sup>2+</sup> .....	151



- Figure 7.18.** Sn working electrode after 1 h electrolysis in  $\text{KHCO}_3$  2 M in presence of 20 mM of  $[\text{Zn}(\text{cyclen})]^{2+}$  (left) and 2 mM of  $[\text{Zn}(\text{imidazole})_3]^{2+}$  (right). ..... 151
- Figure 8.1.** Schematic representation of the mechanism of bicarbonate electrochemical reduction to formate in reactors involving a BPM (CEL: Cation Exchange Layer. AEL: Anion Exchange Layer). ..... 157
- Figure 8.2.** Schematic representation of the experimental set-up of the zero-gap electrolyser for bicarbonate electrochemical reduction. .... 161
- Figure 8.3.**  $\text{FE}_{\text{Formate}}$  when using Sn or  $\text{SnO}_2$  nanoparticles as electrocatalysts on top of a porous carbon substrate (left).  $\text{FE}_{\text{Formate}}$  when using a  $\text{SnO}_2/\text{C}$  catalyst with a Nafion binder, a Sustainion binder or without a binder (right). ..... 163
- Figure 8.4.**  $\text{FE}_{\text{Formate}}$  (a), concentration of formate (b),  $V_{\text{Cell}}$  (c) and EE (d) of the electrolysis of a  $\text{KHCO}_3$  3 M solution with a flow rate of catholyte of 0.5, 1 or 5  $\text{mL min}^{-1}$ . ..... 166
- Figure 8.5.**  $\text{FE}_{\text{Formate}}$  (a), concentration of formate (b),  $V_{\text{Cell}}$  (c) and EE (d) of the electrolysis of a  $\text{KHCO}_3$  solution at 25, 40 and 60 °C. .... 171
- Figure 8.6.**  $\text{FE}_{\text{Formate}}$  (a), concentration of formate (b),  $V_{\text{Cell}}$  (c) and EE (d) of the electrolysis of  $\text{KHCO}_3$  solutions of 1, 2 and 3 M. .... 173
- Figure 8.7.** Solubility of dissolved  $\text{CO}_2$  in water at different temperature based on Henry's law constant at given temperature. .... 176
- Figure 8.8.** Stability test of 8 hours. Parameters:  $\text{KHCO}_3$  3 M catholyte, 5  $\text{mL min}^{-1}$  flow rate and room temperature (25 °C). ..... 176

<b>Figure 9.1.</b>	Salt precipitation (K <sub>2</sub> CO <sub>3</sub> /KHCO <sub>3</sub> ) present at the membrane contactor after the CO <sub>2</sub> capture step. ....	181
<b>Figure 9.2.</b>	FT-IR spectra of the buffer solutions and calibration points of the absorption peak 1380 cm <sup>-1</sup> (carbonate, right) and 1620 cm <sup>-1</sup> (bicarbonate, left). ....	184
<b>Figure 9.3.</b>	Evolution of the pH of a DAC experiment using KOH 1 M as capture solution and air as CO <sub>2</sub> source (blue). Relative abundance of the carbonic species present in the DAC solution after reaching equilibrium (orange). ....	186
<b>Figure 9.4.</b>	FT-IR spectra of the DAC solution, and concentration of each species, capture rate and capture efficiency calculated based on the data obtained from the FT-IR characterisation. ....	188
<b>Figure 9.5.</b>	FE towards formate (left) and CO (right) of the electrolysis of a DAC solution of 0.658 ± 0.031 M DIC at 50 mA cm <sup>-2</sup> . The results are compared to state-of-the-art FE from KHCO <sub>3</sub> electrolysis. [166,168]. ....	190
<b>Figure A.1.</b>	CO <sub>2</sub> diffusion mechanism in a membrane contactor. CO <sub>2</sub> is transported through concentration gradients from gas phase to liquid phase. ....	209
<b>Figure A.2.</b>	Reactions undergoing when using an alkaline (left) or an amino-based solution (right) as CO <sub>2</sub> capture solution. ....	211
<b>Figure A.3.</b>	A schematic representation of an electrochemical cell. On the image: 1) power source. 2) Cathode 3) Anode. 4) Membrane 5) Electrolyte 6) Reduction reaction 7) Oxidation reaction. ....	213
<b>Figure A.4.</b>	Simplified reaction steps during an electrochemical reaction. Redraw from [252]. ....	217

- 
- Figure A.5.** Current-overpotential of a system  $O + e \rightleftharpoons R$  with  $\alpha=0.5$  and  $j_c=j_a$ ......221
- Figure A.6.** Schematic interpretation of the different layers formed close to the surface of the electrode (in this case, the cathode) after applying a negative potential. ....222
- Figure A.7.** Equivalent electronic circuit of a typical electrode-electrolyte system. ....223
- Figure A.8.** Bjerrum plot for carbonic species in water. ....227
- Figure A.9.** Proposed mechanism for the bicarbonate electrochemical reaction. ....228
- Figure A.10.** Effects of using CEM, AEM and BPM for bicarbonate electrolysis. ....229
- Figure A.11.** Evolution of pH when saturating an alkaline capture solution with gaseous  $CO_2$ . ....231
- Figure A.12.** Experimental set-up for kinetic studies of  $CO_2$  capture experiments. 1) thermostat; 2) Gas flow controller; 3) Gas sparger; 4) Digital pH meter; 5) Capture solution; and 6) jacketed electrochemical half-cell. ....233
- Figure A.13.** Bench scale and schematic  $CO_2$  capture test setup. It consists of a fan system and channel that guides the airflow to a central module holder, followed by an exit channel. The test module holder is located at the center of the bench-scale setup, through which the capture solution flows. The module is adapted such that it can be placed vertically and receive the airflow. ....235
- Figure A.14.** Experimental set-up for bicarbonate electrolysis experiments (components labelled in Figure A.12 are not displayed in this figure): 1) potentiostat; 2) Sn electrocatalyst, working electrode; 3) Ag/AgCl 3 M KCl, reference

electrode; 4) Pt mesh, counter electrode; 5) Bicarbonate solutions; 6) Nafion CEM; and 7) KOH 1 M solution, anolyte.....238

**Figure A.15.** Schematic representation of a zero-gap flow electrolyser: 1) End-plates; 2) Cu current collectors; 3) Flow channel; 4) Catalysts gaskets; 5) Membrane separator.....239

**Figure A.16.** Variation of the applied potential over time in a LSV experiment at different scan rate (left). LSV of a system showing an electrochemical reaction as the potential is swept at different scan rate (right).....241

**Figure A.17.** Voltage and current response on time in phase in an ideal resistor that follows Ohm's Law (left). Voltage and current response on time out of phase in a non-ideal resistor (right).....244

**Figure A.18.** Nyquist plot (left) and Bode plot with one time constant (right) of a hypothetical electrochemical circuit.....246

# List of tables

<b>Table 1.1.</b>	Some technologies proposed to convert CO <sub>2</sub> [21].....	6
<b>Table 1.2.</b>	Market price and yearly global production of some eCO <sub>2</sub> R products (2018). Some high selective electrocatalysts for the conversion of CO <sub>2</sub> to specific products. [39,40].....	10
<b>Table 1.3.</b>	Comparison of the process performance of the two-step and integrated route. Cell potentials at which industrially relevant current densities (> 200 mA cm <sup>-2</sup> ) have been achieved are chosen.....	15
<b>Table 1.4.</b>	Economic assumptions. Data refer to an N-th kind of a plant, as described by Keith <i>et al.</i> (2018).[32] .....	17
<b>Table 3.1.</b>	Some representative electrochemical CO <sub>2</sub> reduction projects.....	37
<b>Table 3.2.</b>	Main advantages and drawbacks of eCO <sub>2</sub> R reactor configurations.....	44
<b>Table 4.1.</b>	Some of the current operational DAC (pilot) plants in Europe, the United States and Canada.....	54
<b>Table 5.1.</b>	Structure and properties of the surfactants tested.....	73
<b>Table 6.1.</b>	LUMO energy of CKC, CTAB and the impurities found.....	108
<b>Table 9.1.</b>	Vibrational modes of bicarbonate and carbonate aqueous solutions.....	183
<b>Table A.1.</b>	Standard reduction potentials of conventional eCO <sub>2</sub> R systems.[251].....	216
<b>Table A.2.</b>	η for the HER and OER on various electrocatalyst at 25 °C. [253].....	219
<b>Table A.3.</b>	Some important parameters obtainable when plotting the EIS data with the equivalent circuit model.....	245



# Bibliography

- [1] D. Lüthi, M. le Floch, B. Bereiter, T. Blunier, J.-M. Barnola, U. Siegenthaler, D. Raynaud, J. Jouzel, H. Fischer, K. Kawamura, T.F. Stocker, High-resolution carbon dioxide concentration record 650,000–800,000 years before present, *Nature*. 453 (2008) 379–382. <https://doi.org/10.1038/nature06949>.
- [2] Rebecca Lindsey, *Climate Change: Atmospheric Carbon Dioxide*, Climate.Gov. (2021). <https://www.climate.gov/news-features/understanding-climate/climate-change-atmospheric-carbon-dioxide> (accessed June 24, 2022).
- [3] T. Dietz, E.A. Rosa, Effects of population and affluence on CO<sub>2</sub> emissions, *Proceedings of the National Academy of Sciences*. 94 (1997) 175–179. <https://doi.org/10.1073/pnas.94.1.175>.
- [4] I. Nagelkerken, S.D. Connell, Global alteration of ocean ecosystem functioning due to increasing human CO<sub>2</sub> emissions, *Proceedings of the National Academy of Sciences*. 112 (2015) 13272–13277. <https://doi.org/10.1073/pnas.1510856112>.
- [5] J. Blunden, T. Boyer, State of the Climate in 2020, *Bull Am Meteorol Soc*. 102 (2021) S1–S475. <https://doi.org/10.1175/2021BAMSStateoftheClimate.1>.
- [6] V. Masson-Delmotte, P. Zhai, H.-O. Pörtner, D. Roberts, J. Skea, P.R. Shukla, A. Pirani, W. Moufouma-Okia, C. Péan, R. Pidcock, S. Connors, J.B.R. Matthews, Y. Chen, X. Zhou, M.I. Gomis, E. Lonnoy, T. Maycock, M. Tignor, T. Waterfield (eds.), Annex I: Glossary. *Global Warming of 1.5°C.*, 2018. <https://www.ipcc.ch/sr15/> (accessed June 24, 2022).
- [7] N. Cavallaro, G. Shrestha, R. Birdsey, M.A. Mayes, R.G. Najjar, S.C. Reed, P. Romero-Lankao, Z. Zhu, eds., *Second State of the Carbon Cycle Report*, Washington, DC, 2018. <https://doi.org/10.7930/Soccr2.2018>.
- [8] J. Tollefson, The hard truths of climate change — by the numbers, *Nature*. 573 (2019) 324–327. <https://doi.org/10.1038/d41586-019-02711-4>.
- [9] J. Rogelj, A. Popp, K. v. Calvin, G. Luderer, J. Emmerling, D. Gernaat, S. Fujimori, J. Strefler, T. Hasegawa, G. Marangoni, V. Krey, E. Kriegler, K. Riahi, D.P. van Vuuren, J. Doelman, L. Drouet, J. Edmonds, O. Fricko, M. Harmsen, P. Havlík, F. Humpenöder, E. Stehfest, M. Tavoni, Scenarios towards limiting global mean

temperature increase below 1.5 °C, *Nature Climate Change*. 8 (2018) 325–332. <https://doi.org/10.1038/s41558-018-0091-3>.

- [10] P. Gabrielli, M. Gazzani, M. Mazzotti, The Role of Carbon Capture and Utilization, Carbon Capture and Storage, and Biomass to Enable a Net-Zero-CO<sub>2</sub> Emissions Chemical Industry, *Industrial & Engineering Chemistry Research*. 59 (2020) 7033–7045. <https://doi.org/10.1021/acs.iecr.9b06579>.
- [11] O.S. Bushuyev, P. de Luna, C.T. Dinh, L. Tao, G. Saur, J. van de Lagemaat, S.O. Kelley, E.H. Sargent, What Should We Make with CO<sub>2</sub> and How Can We Make It?, *Joule*. 2 (2018) 825–832. <https://doi.org/10.1016/j.joule.2017.09.003>.
- [12] N. mac Dowell, P.S. Fennell, N. Shah, G.C. Maitland, The role of CO<sub>2</sub> capture and utilization in mitigating climate change, *Nature Climate Change*. 7 (2017) 243–249. <https://doi.org/10.1038/nclimate3231>.
- [13] O.G. Sánchez, Y.Y. Birdja, M. Bulut, J. Vaes, T. Breugelmans, D. Pant, Recent advances in industrial CO<sub>2</sub> electroreduction, *Current Opinion in Green and Sustainable Chemistry*. 16 (2019) 47–56. <https://doi.org/10.1016/j.cogsc.2019.01.005>.
- [14] A.I. Osman, M. Hefny, M.I.A. Abdel Maksoud, A.M. Elgarahy, D.W. Rooney, Recent advances in carbon capture storage and utilisation technologies: a review, *Environmental Chemistry Letters*. 19 (2021) 797–849. <https://doi.org/10.1007/s10311-020-01133-3>.
- [15] P. Mores, N. Scenna, S. Mussati, CO<sub>2</sub> capture using monoethanolamine (MEA) aqueous solution: Modeling and optimization of the solvent regeneration and CO<sub>2</sub> desorption process, *Energy*. 45 (2012) 1042–1058. <https://doi.org/10.1016/j.energy.2012.06.038>.
- [16] M. Mahmoudkhani, D.W. Keith, Low-energy sodium hydroxide recovery for CO<sub>2</sub> capture from atmospheric air—Thermodynamic analysis, *International Journal of Greenhouse Gas Control*. 3 (2009) 376–384. <https://doi.org/10.1016/J.IJGGC.2009.02.003>.
- [17] P.C. Sahoo, R. Kumar, M. Kumar, S. Kumar Puri, S.S.V. Ramakumar, Rational design of a porous gel encapsulated bio-hybrid solvent for accelerated CO<sub>2</sub> capture and low energy stripping, *International Journal of Greenhouse Gas Control*. 90 (2019) 102785. <https://doi.org/10.1016/j.ijggc.2019.102785>.



- [18] D.T. Whipple, P.J.A. Kenis, Prospects of CO<sub>2</sub> utilization via direct heterogeneous electrochemical reduction, *Journal of Physical Chemistry Letters*. 1 (2010) 3451–3458. <https://doi.org/10.1021/jz1012627>.
- [19] Q. Zhu, Developments on CO<sub>2</sub>-utilization technologies, *Clean Energy*. 3 (2019) 85–100. <https://doi.org/10.1093/ce/zkz008>.
- [20] S. Valluri, V. Claremboux, S. Kawatra, Opportunities and challenges in CO<sub>2</sub> utilization, *Journal of Environmental Sciences*. 113 (2022) 322–344. <https://doi.org/10.1016/j.jes.2021.05.043>.
- [21] Emily Nishikawa, CO<sub>2</sub> conversion & utilization pathways: Techno-economic insights, *Prescouter*. (2022). <https://www.prescouter.com/2022/04/co2-conversion-utilization-pathways/> (accessed June 24, 2022).
- [22] C. Bergins, K.-C. Tran, E.-I. Koytsoumpa, E. Kakaras, T. Buddenberg, Ó. Sigurbjörnsson, *Power to Methanol Solutions for Flexible and Sustainable Operations in Power and Process Industries*, (2015). [http://www.mefco2.eu/pdf/1.\\_Power\\_to\\_Methanol\\_Solutions\\_for\\_Flexible\\_and\\_Sustainable\\_Operations\\_in\\_Power\\_and\\_Process\\_Industries.pdf](http://www.mefco2.eu/pdf/1._Power_to_Methanol_Solutions_for_Flexible_and_Sustainable_Operations_in_Power_and_Process_Industries.pdf) (accessed June 24, 2022).
- [23] J. Walters, *SkyMine Beneficial CO<sub>2</sub> Use Project*, Pittsburgh, PA, and Morgantown, WV (United States), 2016. <https://doi.org/10.2172/1241314>.
- [24] R. Kungas, Review—Electrochemical CO<sub>2</sub> Reduction for CO Production: Comparison of Low- and High-Temperature Electrolysis Technologies, *Journal of The Electrochemical Society*. 167 (2020) 044508. <https://doi.org/10.1149/1945-7111/ab7099>.
- [25] J.M. Spurgeon, B. Kumar, A comparative technoeconomic analysis of pathways for commercial electrochemical CO<sub>2</sub> reduction to liquid products, *Energy & Environmental Science*. 11 (2018) 1536–1551. <https://doi.org/10.1039/C8EE00097B>.
- [26] I. Pikaar, J. Guest, R. Ganigué, P. Jensen, K. Rabaey, T. Seviour, J. Trimmer, O. van der Kolk, C. Vaneckhaute, W. Verstraete, eds., *Resource Recovery from Water*, IWA Publishing, 2022. <https://doi.org/10.2166/9781780409566>.
- [27] C.A. Trudewind, A. Schreiber, D. Haumann, Photocatalytic methanol and methane production using captured CO<sub>2</sub> from coal power plants. Part II – Well-to-Wheel

analysis on fuels for passenger transportation services, *Journal of Cleaner Production*. 70 (2014) 38–49. <https://doi.org/10.1016/j.jclepro.2014.02.024>.

- [28] S. Xie, Q. Zhang, G. Liu, Y. Wang, Photocatalytic and photoelectrocatalytic reduction of CO<sub>2</sub> using heterogeneous catalysts with controlled nanostructures, *Chemical Communications*. 52 (2016) 35–59. <https://doi.org/10.1039/C5CC07613G>.
- [29] A. Bogaerts, G. Centi, Plasma Technology for CO<sub>2</sub> Conversion: A Personal Perspective on Prospects and Gaps, *Frontiers in Energy Research*. 8 (2020). <https://doi.org/10.3389/fenrg.2020.00111>.
- [30] Sara Budinis, Direct Air Capture, IEA, Paris. (2020). <https://www.iea.org/reports/direct-air-capture-2> (accessed November 2, 2021).
- [31] A. Raksajati, M.T. Ho, D.E. Wiley, Reducing the Cost of CO<sub>2</sub> Capture from Flue Gases Using Aqueous Chemical Absorption, *Industrial & Engineering Chemistry Research*. 52 (2013) 16887–16901. <https://doi.org/10.1021/ie402185h>.
- [32] D.W. Keith, G. Holmes, D. st. Angelo, K. Heidel, A Process for Capturing CO<sub>2</sub> from the Atmosphere, *Joule*. 2 (2018) 1573–1594. <https://doi.org/10.1016/j.joule.2018.05.006>.
- [33] H.M. Stowe, G.S. Hwang, Fundamental Understanding of CO<sub>2</sub> Capture and Regeneration in Aqueous Amines from First-Principles Studies: Recent Progress and Remaining Challenges, *Industrial & Engineering Chemistry Research*. 56 (2017) 6887–6899. <https://doi.org/10.1021/acs.iecr.7b00213>.
- [34] K. Beydoun, K. Thenert, J. Wiesenthal, C. Hoppe, J. Klankermayer, Utilization of Formic Acid as C1 Building Block for the Ruthenium-Catalyzed Synthesis of Formaldehyde Surrogates, *ChemCatChem*. 12 (2020) 1944–1947. <https://doi.org/10.1002/cctc.201902332>.
- [35] Z. Ma, U. Legrand, E. Pahija, J.R. Tavares, D.C. Boffito, From CO<sub>2</sub> to Formic Acid Fuel Cells, *Industrial & Engineering Chemistry Research*. 60 (2021) 803–815. <https://doi.org/10.1021/acs.iecr.0c04711>.
- [36] P. Chen, Y. Jiao, Y.-H. Zhu, S.-M. Chen, L. Song, M. Jaroniec, Y. Zheng, S.-Z. Qiao, Syngas production from electrocatalytic CO<sub>2</sub> reduction with high energetic efficiency and current density, *Journal of Materials Chemistry A*. 7 (2019) 7675–7682. <https://doi.org/10.1039/C9TA01932D>.

- [37] T. Pardal, S. Messias, M. Sousa, A.S.R. Machado, C.M. Rangel, D. Nunes, J. v. Pinto, R. Martins, M.N. da Ponte, Syngas production by electrochemical CO<sub>2</sub> reduction in an ionic liquid based-electrolyte, *Journal of CO<sub>2</sub> Utilization*. 18 (2017) 62–72. <https://doi.org/10.1016/j.jcou.2017.01.007>.
- [38] K. van Daele, B. de Mot, M. Pupo, N. Daems, D. Pant, R. Kortlever, T. Breugelmans, Sn-Based Electrocatalyst Stability: A Crucial Piece to the Puzzle for the Electrochemical CO<sub>2</sub> Reduction toward Formic Acid, *ACS Energy Letters*. 6 (2021) 4317–4327. <https://doi.org/10.1021/acsenerylett.1c02049>.
- [39] Y.Y. Birdja, E. Pérez-Gallent, M.C. Figueiredo, A.J. Göttle, F. Calle-Vallejo, M.T.M. Koper, Advances and challenges in understanding the electrocatalytic conversion of carbon dioxide to fuels, *Nature Energy*. 4 (2019) 732–745. <https://doi.org/10.1038/s41560-019-0450-y>.
- [40] M. Jouny, W. Luc, F. Jiao, General Techno-Economic Analysis of CO<sub>2</sub> Electrolysis Systems, *Industrial & Engineering Chemistry Research*. 57 (2018) 2165–2177. <https://doi.org/10.1021/acs.iecr.7b03514>.
- [41] S. Hernández, M. Amin Farkhondehfal, F. Sastre, M. Makkee, G. Saracco, N. Russo, Syngas production from electrochemical reduction of CO<sub>2</sub> : current status and prospective implementation, *Green Chemistry*. 19 (2017) 2326–2346. <https://doi.org/10.1039/C7GC00398F>.
- [42] E.R. Cave, J.H. Montoya, K.P. Kuhl, D.N. Abram, T. Hatsukade, C. Shi, C. Hahn, J.K. Nørskov, T.F. Jaramillo, Electrochemical CO<sub>2</sub> reduction on Au surfaces: mechanistic aspects regarding the formation of major and minor products, *Physical Chemistry Chemical Physics*. 19 (2017) 15856–15863. <https://doi.org/10.1039/C7CP02855E>.
- [43] Y. Hori, H. Wakebe, T. Tsukamoto, O. Koga, Electrocatalytic process of CO selectivity in electrochemical reduction of CO<sub>2</sub> at metal electrodes in aqueous media, *Electrochimica Acta*. 39 (1994) 1833–1839. [https://doi.org/10.1016/0013-4686\(94\)85172-7](https://doi.org/10.1016/0013-4686(94)85172-7).
- [44] M. Duarte, B. de Mot, J. Hereijgers, T. Breugelmans, Electrochemical Reduction of CO<sub>2</sub> : Effect of Convective CO<sub>2</sub> Supply in Gas Diffusion Electrodes, *ChemElectroChem*. 6 (2019) 5596–5602. <https://doi.org/10.1002/celec.201901454>.
- [45] T. Hatsukade, K.P. Kuhl, E.R. Cave, D.N. Abram, T.F. Jaramillo, Insights into the electrocatalytic reduction of CO<sub>2</sub> on metallic silver surfaces, *Phys. Chem. Chem. Phys.* 16 (2014) 13814–13819. <https://doi.org/10.1039/C4CP00692E>.

- [46] H. Wu, J. Song, C. Xie, Y. Hu, B. Han, Highly efficient electrochemical reduction of CO<sub>2</sub> into formic acid over lead dioxide in an ionic liquid–catholyte mixture, *Green Chemistry*. 20 (2018) 1765–1769. <https://doi.org/10.1039/C8GC00471D>.
- [47] X. Min, M.W. Kanan, Pd-Catalyzed Electrohydrogenation of Carbon Dioxide to Formate: High Mass Activity at Low Overpotential and Identification of the Deactivation Pathway, *J Am Chem Soc*. 137 (2015) 4701–4708. <https://doi.org/10.1021/ja511890h>.
- [48] D. Yang, Q. Zhu, C. Chen, H. Liu, Z. Liu, Z. Zhao, X. Zhang, S. Liu, B. Han, Selective electroreduction of carbon dioxide to methanol on copper selenide nanocatalysts, *Nature Communications*. 10 (2019) 677. <https://doi.org/10.1038/s41467-019-08653-9>.
- [49] Y. Liu, F. Li, X. Zhang, X. Ji, Recent progress on electrochemical reduction of CO<sub>2</sub> to methanol, *Current Opinion in Green and Sustainable Chemistry*. 23 (2020) 10–17. <https://doi.org/10.1016/j.cogsc.2020.03.009>.
- [50] A. Sedighian Rasouli, X. Wang, J. Wicks, G. Lee, T. Peng, F. Li, C. McCallum, C.-T. Dinh, A.H. Ip, D. Sinton, E.H. Sargent, CO<sub>2</sub> Electroreduction to Methane at Production Rates Exceeding 100 mA/cm<sup>2</sup>, *ACS Sustainable Chemistry & Engineering*. 8 (2020) 14668–14673. <https://doi.org/10.1021/acssuschemeng.0c03453>.
- [51] K.P. Kuhl, E.R. Cave, D.N. Abram, T.F. Jaramillo, New insights into the electrochemical reduction of carbon dioxide on metallic copper surfaces, *Energy & Environmental Science*. 5 (2012) 7050. <https://doi.org/10.1039/c2ee21234j>.
- [52] D. Chi, H. Yang, Y. Du, T. Lv, G. Sui, H. Wang, J. Lu, Morphology-controlled CuO nanoparticles for electroreduction of CO<sub>2</sub> to ethanol, *RSC Adv*. 4 (2014) 37329–37332. <https://doi.org/10.1039/C4RA05415F>.
- [53] D. Ren, Y. Deng, A.D. Handoko, C.S. Chen, S. Malkhandi, B.S. Yeo, Selective Electrochemical Reduction of Carbon Dioxide to Ethylene and Ethanol on Copper(I) Oxide Catalysts, *ACS Catalysis*. 5 (2015) 2814–2821. <https://doi.org/10.1021/cs502128q>.
- [54] I. Sullivan, A. Goryachev, I.A. Digdaya, X. Li, H.A. Atwater, D.A. Vermaas, C. Xiang, Coupling electrochemical CO<sub>2</sub> conversion with CO<sub>2</sub> capture, *Nature Catalysis*. 4 (2021) 952–958. <https://doi.org/10.1038/s41929-021-00699-7>.

- [55] O. Gutiérrez-Sánchez, B. Bohlen, N. Daems, M. Bulut, D. Pant, T. Breugelmans, A State-of-the-Art Update on Integrated CO<sub>2</sub> Capture and Electrochemical Conversion Systems, *ChemElectroChem*. (2022).  
<https://doi.org/10.1002/celec.202101540>.
- [56] S. Verma, Y. Hamasaki, C. Kim, W. Huang, S. Lu, H.-R.M. Jhong, A.A. Gewirth, T. Fujigaya, N. Nakashima, P.J.A. Kenis, Insights into the Low Overpotential Electroreduction of CO<sub>2</sub> to CO on a Supported Gold Catalyst in an Alkaline Flow Electrolyzer, *ACS Energy Letters*. 3 (2018) 193–198.  
<https://doi.org/10.1021/acseenergylett.7b01096>.
- [57] Y.C. Li, G. Lee, T. Yuan, Y. Wang, D.-H. Nam, Z. Wang, F.P. García de Arquer, Y. Lum, C.-T. Dinh, O. Voznyy, E.H. Sargent, CO<sub>2</sub> Electroreduction from Carbonate Electrolyte, *ACS Energy Letters*. 4 (2019) 1427–1431.  
<https://doi.org/10.1021/acsenergylett.9b00975>.
- [58] A. Mayyas, Ruth. Mark, B. Pivovar, G. Bender, K. Wipke, Manufacturing Cost Analysis for Proton Exchange Membrane Water Electrolyzers, 2019.  
<https://www.nrel.gov/docs/fy19osti/72740.pdf>.
- [59] M. Ramdin, A.R.T. Morrison, M. de Groen, R. van Haperen, R. de Kler, E. Irtem, A.T. Laitinen, L.J.P. van den Broeke, T. Breugelmans, J.P.M. Trusler, W. de Jong, T.J.H. Vlugt, High-Pressure Electrochemical Reduction of CO<sub>2</sub> to Formic Acid/Formate: Effect of pH on the Downstream Separation Process and Economics, *Industrial & Engineering Chemistry Research*. 58 (2019) 22718–22740.  
<https://doi.org/10.1021/acs.iecr.9b03970>.
- [60] M.G. Kibria, J.P. Edwards, C.M. Gabardo, C. Dinh, A. Seifitokaldani, D. Sinton, E.H. Sargent, Electrochemical CO<sub>2</sub> Reduction into Chemical Feedstocks: From Mechanistic Electrocatalysis Models to System Design, *Advanced Materials*. 31 (2019) 1807166. <https://doi.org/10.1002/adma.201807166>.
- [61] H.R.M. Jhong, S. Ma, P.J. Kenis, Electrochemical conversion of CO<sub>2</sub> to useful chemicals: Current status, remaining challenges, and future opportunities, *Current Opinion in Chemical Engineering*. 2 (2013) 191–199.  
<https://doi.org/10.1016/j.coche.2013.03.005>.
- [62] J. Qiao, Y. Liu, F. Hong, J. Zhang, A review of catalysts for the electroreduction of carbon dioxide to produce low-carbon fuels, *Chem. Soc. Rev.* 43 (2014) 631–675.  
<https://doi.org/10.1039/c3cs60323g>.

- [63] J. Durst, A. Rudnev, A. Dutta, Y. Fu, J. Herranz, V. Kaliginedi, A. Kuzume, A.A. Permyakova, Y. Paratcha, P. Broekmann, T.J. Schmidt, Electrochemical CO<sub>2</sub> Reduction – A Critical View on Fundamentals, Materials and Applications, CHIMIA International Journal for Chemistry. 69 (2015) 769–776. <https://doi.org/10.2533/chimia.2015.769>.
- [64] S. Verma, B. Kim, H.R.M. Jhong, S. Ma, P.J.A. Kenis, A gross-margin model for defining technoeconomic benchmarks in the electroreduction of CO<sub>2</sub>, ChemSusChem. 9 (2016) 1972–1979. <https://doi.org/10.1002/cssc.201600394>.
- [65] O.S. Bushuyev, P. De Luna, C.T. Dinh, L. Tao, G. Saur, J. van de Lagemaat, S.O. Kelley, E.H. Sargent, What Should We Make with CO<sub>2</sub> and How Can We Make It?, Joule. 2 (2018) 825–832. <https://doi.org/10.1016/j.joule.2017.09.003>.
- [66] J. Spurgeon, B. Kumar, A comparative technoeconomic analysis of pathways for commercial electrochemical CO<sub>2</sub> reduction to liquid products, Energy Environ. Sci. 11 (2018) 1536–1551. <https://doi.org/10.1039/C8EE00097B>.
- [67] X. Li, P. Anderson, H.-R.M. Jhong, M. Paster, J.F. Stubbins, P.J.A. Kenis, Greenhouse Gas Emissions, Energy Efficiency, and Cost of Synthetic Fuel Production Using Electrochemical CO<sub>2</sub> Conversion and the Fischer–Tropsch Process, Energy Fuels. 30 (2016) 5980–5989. <https://doi.org/10.1021/acs.energyfuels.6b00665>.
- [68] A. ElMekawy, H.M. Hegab, G. Mohanakrishna, A.F. Elbaz, M. Bulut, D. Pant, Technological advances in CO<sub>2</sub> conversion electro-biorefinery: A step toward commercialization, Bioresource Technology. 215 (2016) 357–370. <https://doi.org/10.1016/j.biortech.2016.03.023>.
- [69] N. Sridhar, D. Hill, Carbon Dioxide Utilization. Electrochemical Conversion of CO<sub>2</sub>- Opportunities and Challenges, 2011. [http://www.dnv.com/resources/position\\_papers/new\\_frontiers.asp](http://www.dnv.com/resources/position_papers/new_frontiers.asp) (accessed June 24, 2022).
- [70] C. OLOMAN, H. LI, Continuous Co-Current Electrochemical Reduction of Carbon Dioxide, WO/2007/041872, 2007.
- [71] Carbon Recycling International, Recycling CO<sub>2</sub> to produce methanol, (2006). <https://www.carbonrecycling.is/co2-methanol> (accessed June 24, 2022).
- [72] Mitsui Chemicals, Mitsui Chemicals to Establish a Pilot Facility to Study a Methanol Synthesis Process from CO<sub>2</sub>, (2008).

- <https://jp.mitsuichemicals.com/en/release/2008/080825e.htm> (accessed June 24, 2022).
- [73] Air Company, Technology, (2022). <https://aircompany.com/pages/technology> (accessed June 24, 2022).
- [74] Z. Liu, R.I. Masel, Q. Chen, R. Kutz, H. Yang, K. Lewinski, M. Kaplun, S. Luopa, D.R. Lutz, Electrochemical generation of syngas from water and carbon dioxide at industrially important rates, *Journal of CO<sub>2</sub> Utilization*. 15 (2016) 50–56. <https://doi.org/10.1016/j.jcou.2016.04.011>.
- [75] T. Haas, R. Krause, R. Weber, M. Demler, G. Schmid, Technical photosynthesis involving CO<sub>2</sub> electrolysis and fermentation, *Nature Catalysis*. 1 (2018) 32–39. <https://doi.org/10.1038/s41929-017-0005-1>.
- [76] T. Burdyny, P.J. Graham, Y. Pang, C.-T. Dinh, M. Liu, E.H. Sargent, D. Sinton, Nanomorphology-Enhanced Gas-Evolution Intensifies CO<sub>2</sub> Reduction Electrochemistry, *ACS Sustainable Chemistry & Engineering*. 5 (2017) 4031–4040. <https://doi.org/10.1021/acssuschemeng.7b00023>.
- [77] P. de Luna, R. Quintero-Bermudez, C.-T. Dinh, M.B. Ross, O.S. Bushuyev, P. Todorović, T. Regier, S.O. Kelley, P. Yang, E.H. Sargent, Catalyst electro-redeposition controls morphology and oxidation state for selective carbon dioxide reduction, *Nature Catalysis*. 1 (2018) 103–110. <https://doi.org/10.1038/s41929-017-0018-9>.
- [78] Kendra Kuhl, Electrochemical conversion of coal-derived CO<sub>2</sub> into fuels and chemicals using a modified PEM electrolyzer, U.S. Department of Energy. National Energy Technology Laboratory, 2020. [https://netl.doe.gov/sites/default/files/netl-file/20VPRCU\\_Kuhl.pdf](https://netl.doe.gov/sites/default/files/netl-file/20VPRCU_Kuhl.pdf) (accessed June 24, 2022).
- [79] D.M. Weekes, D.A. Salvatore, A. Reyes, A. Huang, C.P. Berlinguette, Electrolytic CO<sub>2</sub> Reduction in a Flow Cell, *Accounts of Chemical Research*. 51 (2018) 910–918. <https://doi.org/10.1021/acs.accounts.8b00010>.
- [80] M. Bevilacqua, J. Filippi, H.A. Miller, F. Vizza, Recent Technological Progress in CO<sub>2</sub> Electroreduction to Fuels and Energy Carriers in Aqueous Environments, *Energy Technology*. 3 (2015) 197–210. <https://doi.org/10.1002/ente.201402166>.
- [81] B. Endródi, G. Bencsik, F. Darvas, R. Jones, K. Rajeshwar, C. Janáky, Continuous-flow electroreduction of carbon dioxide, *Progress in Energy and Combustion Science*. 62 (2017) 133–154. <https://doi.org/10.1016/j.pecs.2017.05.005>.

- [82] I. Merino-Garcia, E. Alvarez-Guerra, J. Albo, A. Irabien, Electrochemical membrane reactors for the utilisation of carbon dioxide, *Chemical Engineering Journal*. 305 (2016) 104–120. <https://doi.org/10.1016/j.cej.2016.05.032>.
- [83] D.T. Whipple, E.C. Finke, P.J.A. Kenis, Microfluidic Reactor for the Electrochemical Reduction of Carbon Dioxide: The Effect of pH, *Electrochemical and Solid-State Letters*. 13 (2010) B109. <https://doi.org/10.1149/1.3456590>.
- [84] X. Lu, D.Y.C. Leung, H. Wang, M.M. Maroto-Valer, J. Xuan, A pH-differential dual-electrolyte microfluidic electrochemical cells for CO<sub>2</sub> utilization, *Renewable Energy*. 95 (2016) 277–285. <https://doi.org/10.1016/j.renene.2016.04.021>.
- [85] F. Bidrawn, G. Kim, G. Corre, J.T.S. Irvine, J.M. Vohs, R.J. Gorte, Efficient Reduction of CO<sub>2</sub> in a Solid Oxide Electrolyzer, *Electrochemical and Solid-State Letters*. 11 (2008) B167–B170. <https://doi.org/10.1149/1.2943664>.
- [86] S.D. Ebbesen, M. Mogensen, Electrolysis of carbon dioxide in Solid Oxide Electrolysis Cells, *Journal of Power Sources*. 193 (2009) 349–358. <https://doi.org/10.1016/j.jpowsour.2009.02.093>.
- [87] G. Cinti, G. Discepoli, A. Lanzini, M. Santarelli, Co-electrolysis of water and CO<sub>2</sub> in a solid oxide electrolyzer (SOE) stack, *Int. J. Energy Res.* 40 (2016) 207–215. <https://doi.org/10.1002/er>.
- [88] K. So, K. Sakai, K. Kano, Gas diffusion bioelectrodes, *Current Opinion in Electrochemistry*. 5 (2017) 173–182. <https://doi.org/10.1016/j.coelec.2017.09.001>.
- [89] R. Omrani, B. Shabani, Gas diffusion layer modifications and treatments for improving the performance of proton exchange membrane fuel cells and electrolyzers: A review, *International Journal of Hydrogen Energy*. 42 (2017) 28515–28536. <https://doi.org/10.1016/j.ijhydene.2017.09.132>.
- [90] S. Bajracharya, K. Vanbroekhoven, C.J.N. Buisman, D. Pant, D.P.B.T.B. Strik, Application of gas diffusion biocathode in microbial electrosynthesis from carbon dioxide, *Environmental Science and Pollution Research*. 23 (2016) 22292–22308. <https://doi.org/10.1007/s11356-016-7196-x>.
- [91] L.-C. Weng, A.T. Bell, A.Z. Weber, Modeling gas-diffusion electrodes for CO<sub>2</sub> reduction, *Physical Chemistry Chemical Physics*. 20 (2018) 16973–16984. <https://doi.org/10.1039/C8CP01319E>.



- [92] L. Han, W. Zhou, C. Xiang, High-Rate Electrochemical Reduction of Carbon Monoxide to Ethylene Using Cu-Nanoparticle-Based Gas Diffusion Electrodes, *ACS Energy Letters*. 3 (2018) 855–860. <https://doi.org/10.1021/acsenergylett.8b00164>.
- [93] D. Kopljar, A. Inan, P. Vindayer, N. Wagner, E. Klemm, Electrochemical reduction of CO<sub>2</sub> to formate at high current density using gas diffusion electrodes, *Journal of Applied Electrochemistry*. 44 (2014) 1107–1116. <https://doi.org/10.1007/s10800-014-0731-x>.
- [94] H.R.Q. Jhong, F.R. Brushett, P.J.A. Kenis, The effects of catalyst layer deposition methodology on electrode performance, *Advanced Energy Materials*. 3 (2013) 589–599. <https://doi.org/10.1002/aenm.201200759>.
- [95] S. Ma, R. Luo, J.I. Gold, A.Z. Yu, B. Kim, P.J.A. Kenis, Carbon nanotube containing Ag catalyst layers for efficient and selective reduction of carbon dioxide, *Journal of Materials Chemistry A*. 4 (2016) 8573–8578. <https://doi.org/10.1039/c6ta00427j>.
- [96] C. Dinh, T. Burdyny, G. Kibria, A. Seifitokaldani, M. Christine, CO<sub>2</sub> electroreduction to ethylene via hydroxide-mediated copper catalysis at an abrupt interface, *Science* (1979). 360 (2018) 783–787. <https://doi.org/10.1126/science.aas9100>.
- [97] B. Kim, F. Hillman, M. Ariyoshi, S. Fujikawa, P.J.A. Kenis, Effects of composition of the micro porous layer and the substrate on performance in the electrochemical reduction of CO<sub>2</sub> to CO, *Journal of Power Sources*. 312 (2016) 192–198. <https://doi.org/10.1016/j.jpowsour.2016.02.043>.
- [98] Q. Wang, H. Dong, H. Yu, H. Yu, Enhanced performance of gas diffusion electrode for electrochemical reduction of carbon dioxide to formate by adding polytetrafluoroethylene into catalyst layer, *Journal of Power Sources*. 279 (2015) 1–5. <https://doi.org/10.1016/j.jpowsour.2014.12.118>.
- [99] H. Wang, J. Jia, P. Song, Q. Wang, D. Li, S. Min, C. Qian, L. Wang, Y.F. Li, C. Ma, T. Wu, J. Yuan, M. Antonietti, G.A. Ozin, Efficient Electrocatalytic Reduction of CO<sub>2</sub> by Nitrogen-Doped Nanoporous Carbon / Carbon Nanotube Membranes : A Step Towards the Electrochemical CO<sub>2</sub> Refinery, *Angew. Chem. Int. Ed*. 56 (2017) 7847–7852. <https://doi.org/10.1002/anie.201703720>.
- [100] J.J. Walsh, G. Neri, C.L. Smith, A.J. Cowan, Electrocatalytic CO<sub>2</sub> reduction with a membrane supported manganese catalyst in aqueous solution, *Chemical Communications*. 50 (2014) 12698–12701. <https://doi.org/10.1039/c4cc06404f>.

- [101] W. Luc, J. Rosen, F. Jiao, An Ir-based anode for a practical CO<sub>2</sub> electrolyzer, *Catalysis Today*. 288 (2017) 79–84. <https://doi.org/10.1016/j.cattod.2016.06.011>.
- [102] M. Bevilacqua, J. Filippi, A. Lavacchi, A. Marchionni, H.A. Miller, W. Oberhauser, E. Vesselli, F. Vizza, Energy Savings in the Conversion of CO<sub>2</sub> to Fuels using an Electrolytic Device, *Energy Technology*. 2 (2014) 522–525. <https://doi.org/10.1002/ente.201402014>.
- [103] R. Zhang, W. Lv, G. Li, M.A. Mezaal, L. Lei, Electrochemical reduction of carbon dioxide to formate with a Sn cathode and an Ir<sub>x</sub>Sn<sub>y</sub>Ru<sub>z</sub>O<sub>2</sub>/Ti anode, *RSC Adv*. 5 (2015) 68662–68667. <https://doi.org/10.1039/C5RA13618K>.
- [104] S. Ma, R. Luo, S. Moniri, Y. Lan, P.J.A. Kenis, Efficient Electrochemical Flow System with Improved Anode for the Conversion of CO<sub>2</sub> to CO, *J Electrochem Soc*. 161 (2014) F1124–F1131. <https://doi.org/10.1149/2.1201410jes>.
- [105] S. Verma, B. Kim, H.R.M. Jhong, S. Ma, P.J.A. Kenis, A gross-margin model for defining technoeconomic benchmarks in the electroreduction of CO<sub>2</sub>, *ChemSusChem*. 9 (2016) 1972–1979. <https://doi.org/10.1002/cssc.201600394>.
- [106] T.E. Lister, E.J. Dufek, Chlor-syngas: Coupling of electrochemical technologies for production of commodity chemicals, *Energy and Fuels*. 27 (2013) 4244–4249. <https://doi.org/10.1021/ef302033j>.
- [107] T. Li, Y. Cao, J. He, C.P. Berlinguette, Electrolytic CO<sub>2</sub> Reduction in Tandem with Oxidative Organic Chemistry, *ACS Central Science*. 3 (2017) 778–783. <https://doi.org/10.1021/acscentsci.7b00207>.
- [108] H. Yang, J.J. Kaczur, S.D. Sajjad, R.I. Masel, Electrochemical conversion of CO<sub>2</sub> to formic acid utilizing Sustainion™ membranes, *Journal of CO<sub>2</sub> Utilization*. 20 (2017) 208–217. <https://doi.org/10.1016/j.jcou.2017.04.011>.
- [109] D.M. Weekes, D.A. Salvatore, A. Reyes, A. Huang, C.P. Berlinguette, Electrolytic CO<sub>2</sub> Reduction in a Flow Cell, *Acc. Chem. Res*. 51 (2018) 910–918. <https://doi.org/10.1021/acs.accounts.8b00010>.
- [110] D.A. Salvatore, D.M. Weekes, J. He, K.E. Dettelbach, Y.C. Li, T.E. Mallouk, C.P. Berlinguette, Electrolysis of Gaseous CO<sub>2</sub> to CO in a Flow Cell with a Bipolar Membrane, *ACS Energy Letters*. 3 (2018) 149–154. <https://doi.org/10.1021/acseenergylett.7b01017>.

- [111] Y.C. Li, D. Zhou, Z. Yan, R.H. Gonçalves, D.A. Salvatore, C.P. Berlinguette, T.E. Mallouk, Electrolysis of CO<sub>2</sub> to Syngas in Bipolar Membrane-Based Electrochemical Cells, *ACS Energy Letters*. 1 (2016) 1149–1153. <https://doi.org/10.1021/acseenergylett.6b00475>.
- [112] D.A. Vermaas, W.A. Smith, Synergistic Electrochemical CO<sub>2</sub> Reduction and Water Oxidation with a Bipolar Membrane, *ACS Energy Letters*. 1 (2016) 1143–1148. <https://doi.org/10.1021/acseenergylett.6b00557>.
- [113] Y.C. Li, Z. Yan, J. Hitt, R. Wycisk, P.N. Pintauro, T.E. Mallouk, Bipolar Membranes Inhibit Product Crossover in CO<sub>2</sub> Electrolysis Cells, *Advanced Sustainable Systems*. 1700187 (2018) 1700187. <https://doi.org/10.1002/adsu.201700187>.
- [114] M.A. Blommaert, D. Aili, R.A. Tufa, Q. Li, W.A. Smith, D.A. Vermaas, Insights and Challenges for Applying Bipolar Membranes in Advanced Electrochemical Energy Systems, *ACS Energy Letters*. 6 (2021) 2539–2548. <https://doi.org/10.1021/acsenergylett.1c00618>.
- [115] M. Ramdin, A.R.T. Morrison, M. de Groen, R. van Haperen, R. de Kler, L.J.P. van den Broeke, J.P.M. Trusler, W. de Jong, T.J.H. Vlugt, High Pressure Electrochemical Reduction of CO<sub>2</sub> to Formic Acid/Formate: A Comparison between Bipolar Membranes and Cation Exchange Membranes, *Industrial & Engineering Chemistry Research*. 58 (2019) 1834–1847. <https://doi.org/10.1021/acs.iecr.8b04944>.
- [116] R.B. Kutz, Q. Chen, H. Yang, S.D. Sajjad, Z. Liu, I.R. Masel, Sustainion Imidazolium-Functionalized Polymers for Carbon Dioxide Electrolysis, *Energy Technology*. 5 (2017) 929–936. <https://doi.org/10.1002/ente.201600636>.
- [117] J.J. Kaczur, H. Yang, Z. Liu, S.D. Sajjad, R.I. Masel, Carbon Dioxide and Water Electrolysis Using New Alkaline Stable Anion Membranes, *Frontiers in Chemistry*. 6 (2018). <https://doi.org/10.3389/fchem.2018.00263>.
- [118] L.M. Aeshala, R. Uppaluri, A. Verma, Electrochemical conversion of CO<sub>2</sub> to fuels: tuning of the reaction zone using suitable functional groups in a solid polymer electrolyte, *Phys. Chem. Chem. Phys.* 16 (2014) 17588–17594. <https://doi.org/10.1039/C4CP02389G>.
- [119] Y.Y. Birdja, R.E. Vos, T.A. Wezendonk, L. Jiang, F. Kapteijn, M.T.M. Koper, Effects of Substrate and Polymer Encapsulation on CO<sub>2</sub> Electroreduction by Immobilized Indium(III) Protoporphyrin, *ACS Catalysis*. 8 (2018) 4420–4428. <https://doi.org/10.1021/acscatal.7b03386>.

- [120] A.S. Reis Machado, M. Nunes da Ponte, CO<sub>2</sub> capture and electrochemical conversion, *Current Opinion in Green and Sustainable Chemistry*. 11 (2018) 86–90. <https://doi.org/10.1016/j.cogsc.2018.05.009>.
- [121] Y. Deng, J. Li, Y. Miao, D. Izikowitz, A comparative review of performance of nanomaterials for Direct Air Capture, *Energy Reports*. 7 (2021) 3506–3516. <https://doi.org/10.1016/j.egyr.2021.06.002>.
- [122] S. Sjostrom, H. Krutka, Evaluation of solid sorbents as a retrofit technology for CO<sub>2</sub> capture, *Fuel*. 89 (2010) 1298–1306. <https://doi.org/10.1016/j.fuel.2009.11.019>.
- [123] I. Ghiat, T. Al-Ansari, A review of carbon capture and utilisation as a CO<sub>2</sub> abatement opportunity within the EWF nexus, *Journal of CO<sub>2</sub> Utilization*. 45 (2021) 101432. <https://doi.org/10.1016/j.jcou.2020.101432>.
- [124] E.S. Sanz-Pérez, C.R. Murdock, S.A. Didas, C.W. Jones, Direct Capture of CO<sub>2</sub> from Ambient Air, *Chemical Reviews*. 116 (2016) 11840–11876. <https://doi.org/10.1021/acs.chemrev.6b00173>.
- [125] G. Realmonte, L. Drouet, A. Gambhir, J. Glynn, A. Hawkes, A.C. Köberle, M. Tavoni, An inter-model assessment of the role of direct air capture in deep mitigation pathways, *Nature Communications*. 10 (2019) 3277. <https://doi.org/10.1038/s41467-019-10842-5>.
- [126] Climeworks, Capricorn, (n.d.). <https://climeworks.com/roadmap/capricorn> (accessed November 4, 2021).
- [127] Climeworks, Orca, (n.d.). <https://climeworks.com/roadmap/orca> (accessed November 4, 2021).
- [128] Carbon Engineering, Carbon Engineering, (n.d.). <https://carbonengineering.com/> (accessed November 4, 2021).
- [129] Global Thermostat, Global Thermostat, (n.d.). <https://globalthermostat.com/> (accessed November 4, 2021).
- [130] IEA, The world's first million-tonne Direct Air Capture plant, (n.d.). <https://www.iea.org/reports/ccus-around-the-world/dac-1> (accessed November 4, 2021).

- [131] Prometheus Fuels, Technology, (n.d.). <https://prometheusfuels.com/technology> (accessed November 4, 2021).
- [132] S.R. Shewchuk, A. Mukherjee, A.K. Dalai, Selective carbon-based adsorbents for carbon dioxide capture from mixed gas streams and catalytic hydrogenation of CO<sub>2</sub> into renewable energy source: A review, *Chemical Engineering Science*. 243 (2021). <https://doi.org/10.1016/j.ces.2021.116735>.
- [133] M. Wang, A.S. Joel, C. Ramshaw, D. Eimer, N.M. Musa, Process intensification for post-combustion CO<sub>2</sub> capture with chemical absorption: A critical review, *Applied Energy*. 158 (2015) 275–291. <https://doi.org/10.1016/j.apenergy.2015.08.083>.
- [134] G.T. Rochelle, Amine Scrubbing for CO<sub>2</sub> Capture, *Science* (1979). 325 (2009) 1652–1654. <https://doi.org/10.1126/science.1176731>.
- [135] G.T. Rochelle, Conventional amine scrubbing for CO<sub>2</sub> capture, in: *Absorption-Based Post-Combustion Capture of Carbon Dioxide*, Elsevier Inc., 2016: pp. 35–67. <https://doi.org/10.1016/B978-0-08-100514-9.00003-2>.
- [136] L. Chen, F. Li, Y. Zhang, C.L. Bentley, M. Horne, A.M. Bond, J. Zhang, Electrochemical Reduction of Carbon Dioxide in a Monoethanolamine Capture Medium, *ChemSusChem*. 10 (2017) 4109–4118. <https://doi.org/10.1002/cssc.201701075>.
- [137] D. Filotás, T. Nagy, L. Nagy, P. Mizsey, G. Nagy, Extended Investigation of Electrochemical CO<sub>2</sub> Reduction in Ethanolamine Solutions by SECM, *Electroanalysis*. 30 (2018) 690–697. <https://doi.org/10.1002/elan.201700693>.
- [138] A. Ratanpara, A. Shaw, M. Thomas, R.N. Patel, M. Kim, Microfluidic analysis of seawater-based CO<sub>2</sub> capture in an amine solution with nickel nanoparticle catalysts, *Journal of CO<sub>2</sub> Utilization*. 53 (2021). <https://doi.org/10.1016/j.jcou.2021.101712>.
- [139] M. Ishaq, M.A. Gilani, M.R. Bilad, A. Faizan, A.A. Raja, Z.M. Afzal, A.L. Khan, Exploring the potential of highly selective alkanolamine containing deep eutectic solvents based supported liquid membranes for CO<sub>2</sub> capture, *Journal of Molecular Liquids*. 340 (2021). <https://doi.org/10.1016/j.molliq.2021.117274>.
- [140] A. Khurram, L. Yan, Y. Yin, L. Zhao, B.M. Gallant, Promoting Amine-Activated Electrochemical CO<sub>2</sub> Conversion with Alkali Salts, *The Journal of Physical Chemistry C*. 123 (2019) 18222–18231. <https://doi.org/10.1021/acs.jpcc.9b04258>.

- [141] M. Wang, H.J. Herzog, T.A. Hatton, CO<sub>2</sub> Capture Using Electrochemically Mediated Amine Regeneration, *Industrial & Engineering Chemistry Research*. 59 (2020) 7087–7096. <https://doi.org/10.1021/acs.iecr.9b05307>.
- [142] X. Li, J. Liu, W. Jiang, G. Gao, F. Wu, C. Luo, L. Zhang, Low energy-consuming CO<sub>2</sub> capture by phase change absorbents of amine/alcohol/H<sub>2</sub>O, *Separation and Purification Technology*. 275 (2021). <https://doi.org/10.1016/j.seppur.2021.119181>.
- [143] F. Liu, Y. Shen, L. Shen, Y. Zhang, W. Chen, Q. Wang, S. Li, S. Zhang, W. Li, Sustainable ionic liquid organic solution with efficient recyclability and low regeneration energy consumption for CO<sub>2</sub> capture, *Separation and Purification Technology*. 275 (2021). <https://doi.org/10.1016/j.seppur.2021.119123>.
- [144] X. Wu, H. Fan, M. Sharif, Y. Yu, K. Wei, Z. Zhang, G. Liu, Electrochemically-mediated amine regeneration of CO<sub>2</sub> capture: From electrochemical mechanism to bench-scale visualization study, *Applied Energy*. 302 (2021). <https://doi.org/10.1016/j.apenergy.2021.117554>.
- [145] M. Rahimi, K.M. Diederichsen, N. Ozbek, M. Wang, W. Choi, T.A. Hatton, An Electrochemically Mediated Amine Regeneration Process with a Mixed Absorbent for Postcombustion CO<sub>2</sub> Capture, *Environmental Science and Technology*. 54 (2020) 8999–9007. <https://doi.org/10.1021/acs.est.0c02595>.
- [146] K.R. Putta, H.F. Svendsen, H.K. Knuutila, Kinetics of CO<sub>2</sub> Absorption in to Aqueous MEA Solutions Near Equilibrium, *Energy Procedia*. 114 (2017) 1576–1583. <https://doi.org/10.1016/j.egypro.2017.03.1288>.
- [147] S.S.W. Effendi, I.S. Ng, The prospective and potential of carbonic anhydrase for carbon dioxide sequestration: A critical review, *Process Biochemistry*. 87 (2019) 55–65. <https://doi.org/10.1016/j.procbio.2019.08.018>.
- [148] J. Berg, J. Tymoczko, L. Stryer, Making a Fast Reaction Faster: Carbonic Anhydrases, in: *Biochemistry*, 5th ed., Freeman, W.H., 2002.
- [149] S. Aoki, E. Kimura, Zinc Hydrolases, in: *Comprehensive Coordination Chemistry II*, Elsevier, 2003: pp. 601–640. <https://doi.org/10.1016/B0-08-043748-6/08139-1>.
- [150] S. Peirce, R. Perfetto, M.E. Russo, C. Capasso, M. Rossi, P. Salatino, A. Marzocchella, Characterization of technical grade carbonic anhydrase as biocatalyst for CO<sub>2</sub> capture in potassium carbonate solutions, *Greenhouse Gases: Science and Technology*. 8 (2018) 279–291. <https://doi.org/10.1002/ghg.1738>.

- [151] D. Park, M.S. Lee, Kinetic study of catalytic CO<sub>2</sub> hydration by metal-substituted biomimetic carbonic anhydrase model complexes, *Royal Society Open Science*. 6 (2019) 190407. <https://doi.org/10.1098/rsos.190407>.
- [152] H. Wen, L. Zhang, Y. Du, Z. Wang, Y. Jiang, H. Bian, J. Cui, S. Jia, Bimetal based inorganic-carbonic anhydrase hybrid hydrogel membrane for CO<sub>2</sub> capture, *Journal of CO<sub>2</sub> Utilization*. 39 (2020) 101171. <https://doi.org/10.1016/j.jcou.2020.101171>.
- [153] C. Jin, S. Zhang, Z. Zhang, Y. Chen, Mimic Carbonic Anhydrase Using Metal–Organic Frameworks for CO<sub>2</sub> Capture and Conversion, *Inorganic Chemistry*. 57 (2018) 2169–2174. <https://doi.org/10.1021/acs.inorgchem.7b03021>.
- [154] S. Kim, K. il Joo, B.H. Jo, H.J. Cha, Stability-Controllable Self-Immobilization of Carbonic Anhydrase Fused with a Silica-Binding Tag onto Diatom Biosilica for Enzymatic CO<sub>2</sub> Capture and Utilization, *ACS Applied Materials & Interfaces*. 12 (2020) 27055–27063. <https://doi.org/10.1021/acsami.0c03804>.
- [155] C. Molina-Fernández, P. Luis, Immobilization of carbonic anhydrase for CO<sub>2</sub> capture and its industrial implementation: A review, *Journal of CO<sub>2</sub> Utilization*. 47 (2021) 101475. <https://doi.org/10.1016/j.jcou.2021.101475>.
- [156] D. Sivanesan, M.H. Youn, A. Murnandari, J.M. Kang, K.T. Park, H.J. Kim, S.K. Jeong, Enhanced CO<sub>2</sub> absorption and desorption in a tertiary amine medium with a carbonic anhydrase mimic, *Journal of Industrial and Engineering Chemistry*. 52 (2017) 287–294. <https://doi.org/10.1016/j.jiec.2017.03.058>.
- [157] J.M. Hanusch, I.P. Kerschgens, F. Huber, M. Neuburger, K. Gademann, Pyrrolizidines for direct air capture and CO<sub>2</sub> conversion, *Chemical Communications*. 55 (2019) 949–952. <https://doi.org/10.1039/C8CC08574A>.
- [158] A. Zubrienè, D. Matulis, Characterization of Carbonic Anhydrase Thermal Stability, in: *Carbonic Anhydrase as Drug Target*, Springer International Publishing, Cham, 2019: pp. 51–59. [https://doi.org/10.1007/978-3-030-12780-0\\_4](https://doi.org/10.1007/978-3-030-12780-0_4).
- [159] G. Lee, Y.C. Li, J.Y. Kim, T. Peng, D.H. Nam, A. Sedighian Rasouli, F. Li, M. Luo, A.H. Ip, Y.C. Joo, E.H. Sargent, Electrochemical upgrade of CO<sub>2</sub> from amine capture solution, *Nature Energy*. 6 (2021) 46–53. <https://doi.org/10.1038/s41560-020-00735-z>.
- [160] E. Pérez-Gallent, C. Vankani, C. Sánchez-Martínez, A. Anastasopol, E. Goetheer, Integrating CO<sub>2</sub> Capture with Electrochemical Conversion Using Amine-Based

Capture Solvents as Electrolytes, *Industrial & Engineering Chemistry Research*. 60 (2021) 4269–4278. <https://doi.org/10.1021/acs.iecr.0c05848>.

- [161] O. Gutiérrez-Sánchez, N. Daems, W. Offermans, Y.Y. Birdja, M. Bulut, D. Pant, T. Breugelmans, The inhibition of the proton donor ability of bicarbonate promotes the electrochemical conversion of CO<sub>2</sub> in bicarbonate solutions, *Journal of CO<sub>2</sub> Utilization*. 48 (2021) 101521. <https://doi.org/10.1016/j.jcou.2021.101521>.
- [162] H. Ooka, M.C. Figueiredo, M.T.M. Koper, Competition between Hydrogen Evolution and Carbon Dioxide Reduction on Copper Electrodes in Mildly Acidic Media, *Langmuir*. 33 (2017) 9307–9313. <https://doi.org/10.1021/acs.langmuir.7b00696>.
- [163] O. Gutiérrez-Sánchez, N. Daems, M. Bulut, D. Pant, T. Breugelmans, Effects of Benzyl-Functionalized Cationic Surfactants on the Inhibition of the Hydrogen Evolution Reaction in CO<sub>2</sub> Reduction Systems, *ACS Applied Materials & Interfaces*. 13 (2021) 56205–56216. <https://doi.org/10.1021/acsami.1c17303>.
- [164] B. de Mot, J. Hereijgers, N. Daems, T. Breugelmans, Insight in the behavior of bipolar membrane equipped carbon dioxide electrolyzers at low electrolyte flowrates, *Chemical Engineering Journal*. 428 (2022) 131170. <https://doi.org/10.1016/j.cej.2021.131170>.
- [165] T. Li, E.W. Lees, M. Goldman, D.A. Salvatore, D.M. Weekes, C.P. Berlinguette, Electrolytic Conversion of Bicarbonate into CO in a Flow Cell, *Joule*. 3 (2019) 1487–1497. <https://doi.org/10.1016/j.joule.2019.05.021>.
- [166] E.W. Lees, M. Goldman, A.G. Fink, D.J. Dvorak, D.A. Salvatore, Z. Zhang, N.W.X. Loo, C.P. Berlinguette, Electrodes Designed for Converting Bicarbonate into CO, *ACS Energy Letters*. (2020) 2165–2173. <https://doi.org/10.1021/acsenergylett.0c00898>.
- [167] T. Li, E.W. Lees, Z. Zhang, C.P. Berlinguette, Conversion of Bicarbonate to Formate in an Electrochemical Flow Reactor, *ACS Energy Letters*. 5 (2020) 2624–2630. <https://doi.org/10.1021/acsenergylett.0c01291>.
- [168] O. Gutierrez-Sanchez, B. de Mot, M. Bulut, D. Pant, T. Breugelmans, Engineering Aspects for the Design of a Bicarbonate Zero-Gap Flow Electrolyzer for the Conversion of CO<sub>2</sub> to Formate, *ACS Applied Materials & Interfaces*. (In press) (2022). <https://doi.org/10.1021/acsami.2c05457>.



- [169] C. Halliday, T.A. Hatton, Sorbents for the Capture of CO<sub>2</sub> and Other Acid Gases: A Review, *Industrial & Engineering Chemistry Research*. 60 (2021) 9313–9346. <https://doi.org/10.1021/ACS.IECR.1C00597>.
- [170] M. Ding, R.W. Flaig, H.-L. Jiang, O.M. Yaghi, Carbon capture and conversion using metal–organic frameworks and MOF-based materials, *Chemical Society Reviews*. 48 (2019) 2783–2828. <https://doi.org/10.1039/C8CS00829A>.
- [171] J. Ozdemir, I. Mosleh, M. Abolhassani, L.F. Greenlee, R.R. Beitle, M.H. Beyzavi, Covalent Organic Frameworks for the Capture, Fixation, or Reduction of CO<sub>2</sub>, *Frontiers in Energy Research*. 7 (2019) 77. <https://doi.org/10.3389/FENRG.2019.00077/BIBTEX>.
- [172] M. Aghaie, N. Rezaei, S. Zندهboudi, A systematic review on CO<sub>2</sub> capture with ionic liquids: Current status and future prospects, *Renewable and Sustainable Energy Reviews*. 96 (2018) 502–525. <https://doi.org/10.1016/J.RSER.2018.07.004>.
- [173] W. Lu, B. Jia, B. Cui, Y. Zhang, K. Yao, Y. Zhao, J. Wang, Efficient Photoelectrochemical Reduction of Carbon Dioxide to Formic Acid: A Functionalized Ionic Liquid as an Absorbent and Electrolyte, *Angewandte Chemie*. 129 (2017) 12013–12016. <https://doi.org/10.1002/ange.201703977>.
- [174] H. Liu, J. Chu, Z. Yin, X. Cai, L. Zhuang, H. Deng, Covalent Organic Frameworks Linked by Amine Bonding for Concerted Electrochemical Reduction of CO<sub>2</sub>, *Chem*. 4 (2018) 1696–1709. <https://doi.org/10.1016/J.CHEMPR.2018.05.003/ATTACHMENT/80ED0FF4-F136-442C-9FFD-51F3C40842B9/MMC1.PDF>.
- [175] B.A. Rosen, A. Salehi-Khojin, M.R. Thorson, W. Zhu, D.T. Whipple, P.J.A. Kenis, R.I. Masel, Ionic liquid-mediated selective conversion of CO<sub>2</sub> to CO at low overpotentials, *Science* (1979). 334 (2011) 643–644. [https://doi.org/10.1126/SCIENCE.1209786/SUPPL\\_FILE/ROSEN.SOM.PDF](https://doi.org/10.1126/SCIENCE.1209786/SUPPL_FILE/ROSEN.SOM.PDF).
- [176] A. Kahyarian, A. Schumacher, S. Nestic, Mechanistic Investigation of Hydrogen Evolution Reaction from Multiple Proton Donors: The Case of Mildly Acidic Solutions Containing Weak Acids, *Journal of The Electrochemical Society*. 166 (2019) H320–H330. <https://doi.org/10.1149/2.0411908jes>.
- [177] A. Goyal, G. Marcandalli, V.A. Mints, M.T.M. Koper, Competition between CO<sub>2</sub> Reduction and Hydrogen Evolution on a Gold Electrode under Well-Defined Mass Transport Conditions, *J Am Chem Soc*. 142 (2020) 4154–4161. <https://doi.org/10.1021/jacs.9b10061>.

- [178] M. Dunwell, Q. Lu, J.M. Heyes, J. Rosen, J.G. Chen, Y. Yan, F. Jiao, B. Xu, The Central Role of Bicarbonate in the Electrochemical Reduction of Carbon Dioxide on Gold, *J Am Chem Soc.* 139 (2017) 3774–3783. <https://doi.org/10.1021/jacs.6b13287>.
- [179] S. Banerjee, Z.-Q. Zhang, A.S. Hall, V.S. Thoi, Surfactant Perturbation of Cation Interactions at the Electrode–Electrolyte Interface in Carbon Dioxide Reduction, *ACS Catalysis.* 10 (2020) 9907–9914. <https://doi.org/10.1021/acscatal.0c02387>.
- [180] S. Banerjee, X. Han, V.S. Thoi, Modulating the Electrode-Electrolyte Interface with Cationic Surfactants in Carbon Dioxide Reduction, *ACS Catalysis.* 9 (2019) 5631–5637. <https://doi.org/10.1021/acscatal.9b00449>.
- [181] Z.-Q. Zhang, S. Banerjee, V.S. Thoi, A. Shoji Hall, Reorganization of Interfacial Water by an Amphiphilic Cationic Surfactant Promotes CO<sub>2</sub> Reduction, *The Journal of Physical Chemistry Letters.* 11 (2020) 5457–5463. <https://doi.org/10.1021/acs.jpcllett.0c01334>.
- [182] D. Wakerley, S. Lamaison, F. Ozanam, N. Menguy, D. Mercier, P. Marcus, M. Fontecave, V. Mougél, Bio-inspired hydrophobicity promotes CO<sub>2</sub> reduction on a Cu surface, *Nature Materials.* 18 (2019) 1222–1227. <https://doi.org/10.1038/s41563-019-0445-x>.
- [183] Y. Zhong, Y. Xu, J. Ma, C. Wang, S. Sheng, C. Cheng, M. Li, L. Han, L. Zhou, Z. Cai, Y. Kuang, Z. Liang, X. Sun, An Artificial Electrode/Electrolyte Interface for CO<sub>2</sub> Electroreduction by Cation Surfactant Self-Assembly, *Angewandte Chemie International Edition.* 59 (2020) 19095–19101. <https://doi.org/10.1002/anie.202005522>.
- [184] C.J. Bondue, M. Graf, A. Goyal, M.T.M. Koper, Suppression of Hydrogen Evolution in Acidic Electrolytes by Electrochemical CO<sub>2</sub> Reduction, *J Am Chem Soc.* 143 (2021) 279–285. <https://doi.org/10.1021/jacs.0c10397>.
- [185] G. Marcandalli, A. Goyal, M.T.M. Koper, Electrolyte Effects on the Faradaic Efficiency of CO<sub>2</sub> Reduction to CO on a Gold Electrode, *ACS Catalysis.* 11 (2021) 4936–4945. <https://doi.org/10.1021/acscatal.1c00272>.
- [186] M. König, J. Vaes, E. Klemm, D. Pant, Solvents and Supporting Electrolytes in the Electrocatalytic Reduction of CO<sub>2</sub>, *IScience.* 19 (2019) 135–160. <https://doi.org/10.1016/j.isci.2019.07.014>.

- [187] R.A. Tufa, D. Chanda, M. Ma, D. Aili, T.B. Demissie, J. Vaes, Q. Li, S. Liu, D. Pant, Towards highly efficient electrochemical CO<sub>2</sub> reduction: Cell designs, membranes and electrocatalysts, *Applied Energy*. 277 (2020) 115557. <https://doi.org/10.1016/j.apenergy.2020.115557>.
- [188] E. Lust, Zero Charge Potentials and Electrical Double Layer at Solid Electrodes, in: *Encyclopedia of Interfacial Chemistry*, Elsevier, 2018: pp. 316–344. <https://doi.org/10.1016/B978-0-12-409547-2.13613-3>.
- [189] M. Pugh, L.M. Warner, D.R. Gabe, Some passivation studies on tin electrodes in alkaline solutions, *Corrosion Science*. 7 (1967) 807–820. [https://doi.org/10.1016/S0010-938X\(67\)80114-8](https://doi.org/10.1016/S0010-938X(67)80114-8).
- [190] S. Zhao, S. Li, T. Guo, S. Zhang, J. Wang, Y. Wu, Y. Chen, Advances in Sn-Based Catalysts for Electrochemical CO<sub>2</sub> Reduction, *Nano-Micro Letters*. 11 (2019) 62. <https://doi.org/10.1007/s40820-019-0293-x>.
- [191] W. Lv, R. Zhang, P. Gao, L. Lei, Studies on the faradaic efficiency for electrochemical reduction of carbon dioxide to formate on tin electrode, *Journal of Power Sources*. 253 (2014) 276–281. <https://doi.org/10.1016/j.jpowsour.2013.12.063>.
- [192] S. Zhang, P. Kang, T.J. Meyer, Nanostructured Tin Catalysts for Selective Electrochemical Reduction of Carbon Dioxide to Formate, *J Am Chem Soc*. 136 (2014) 1734–1737. <https://doi.org/10.1021/ja4113885>.
- [193] G.B. Damas, C.R. Miranda, R. Sgarbi, J.M. Portela, M.R. Camilo, F.H.B. Lima, C.M. Araujo, On the Mechanism of Carbon Dioxide Reduction on Sn-Based Electrodes: Insights into the Role of Oxide Surfaces, *Catalysts*. 9 (2019) 636. <https://doi.org/10.3390/catal9080636>.
- [194] M.F. Baruch, J.E. Pander, J.L. White, A.B. Bocarsly, Mechanistic Insights into the Reduction of CO<sub>2</sub> on Tin Electrodes using in Situ ATR-IR Spectroscopy, *ACS Catalysis*. 5 (2015) 3148–3156. <https://doi.org/10.1021/acscatal.5b00402>.
- [195] S. Dobberschütz, M. Rimmen, T. Hassenkam, M.P. Andersson, S.L.S. Stipp, Specific ion effects on the hydrophobic interaction of benzene self-assembled monolayers, *Physical Chemistry Chemical Physics*. 17 (2015) 21432–21441. <https://doi.org/10.1039/C5CP01803J>.

- [196] P. Peljo, H.H. Girault, Electrochemical potential window of battery electrolytes: the HOMO–LUMO misconception, *Energy & Environmental Science*. 11 (2018) 2306–2309. <https://doi.org/10.1039/C8EE01286E>.
- [197] F. Sabatino, A. Grimm, F. Gallucci, M. van Sint Annaland, G.J. Kramer, M. Gazzani, A comparative energy and costs assessment and optimization for direct air capture technologies, *Joule*. 5 (2021) 2047–2076. <https://doi.org/10.1016/j.joule.2021.05.023>.
- [198] L. Fradette, S. Lefebvre, J. Carley, Demonstration Results of Enzyme-Accelerated CO<sub>2</sub> Capture, *Energy Procedia*. 114 (2017) 1100–1109. <https://doi.org/10.1016/j.egypro.2017.03.1263>.
- [199] Z. Fisher, C.D. Boone, S.M. Biswas, B. Venkatakrisnan, M. Aggarwal, C. Tu, M. Agbandje-McKenna, D. Silverman, R. McKenna, Kinetic and structural characterization of thermostabilized mutants of human carbonic anhydrase II, *Protein Engineering Design and Selection*. 25 (2012) 347–355. <https://doi.org/10.1093/protein/gzs027>.
- [200] S. Lindskog, Structure and mechanism of carbonic anhydrase, *Pharmacology & Therapeutics*. 74 (1997) 1–20. [https://doi.org/10.1016/S0163-7258\(96\)00198-2](https://doi.org/10.1016/S0163-7258(96)00198-2).
- [201] A. Bottoni, C.Z. Lanza, G. Pietro Miscione, D. Spinelli, New Model for a Theoretical Density Functional Theory Investigation of the Mechanism of the Carbonic Anhydrase: How Does the Internal Bicarbonate Rearrangement Occur?, *J Am Chem Soc*. 126 (2004) 1542–1550. <https://doi.org/10.1021/ja030336j>.
- [202] D.S. Goodsell, Carbonic Anhydrase, *RCSB Protein Data Bank*. (2004). [https://doi.org/10.2210/rcsb\\_pdb/mom\\_2004\\_1](https://doi.org/10.2210/rcsb_pdb/mom_2004_1).
- [203] M.E. Russo, G. Olivieri, A. Marzocchella, P. Salatino, P. Caramuscio, C. Cavaleiro, Post-combustion carbon capture mediated by carbonic anhydrase, *Separation and Purification Technology*. 107 (2013) 331–339. <https://doi.org/10.1016/j.seppur.2012.06.022>.
- [204] J.K.J. Yong, G.W. Stevens, F. Caruso, S.E. Kentish, The use of carbonic anhydrase to accelerate carbon dioxide capture processes, *Journal of Chemical Technology and Biotechnology*. 90 (2015) 3–10. <https://doi.org/10.1002/jctb.4502>.
- [205] O. Alvizo, L.J. Nguyen, C.K. Savile, J.A. Bresson, S.L. Lakhapatri, E.O.P. Solis, R.J. Fox, J.M. Broering, M.R. Benoit, S.A. Zimmerman, S.J. Novick, J. Liang, J.J. Lalonde, Directed evolution of an ultrastable carbonic anhydrase for highly efficient carbon

- capture from flue gas, *Proceedings of the National Academy of Sciences*. 111 (2014) 16436–16441. <https://doi.org/10.1073/pnas.1411461111>.
- [206] W.C. Floyd, S.E. Baker, C.A. Valdez, J.K. Stolaroff, J.P. Bearinger, J.H. Satcher, R.D. Aines, Evaluation of a Carbonic Anhydrase Mimic for Industrial Carbon Capture, *Environmental Science & Technology*. 47 (2013) 10049–10055. <https://doi.org/10.1021/es401336f>.
- [207] T. Knaus, C.E. Paul, C.W. Levy, S. de Vries, F.G. Mutti, F. Hollmann, N.S. Scrutton, Better than Nature: Nicotinamide Biomimetics That Outperform Natural Coenzymes, *J Am Chem Soc*. 138 (2016) 1033–1039. <https://doi.org/10.1021/jacs.5b12252>.
- [208] P.C. Sahoo, Y.-N. Jang, S.-W. Lee, Immobilization of carbonic anhydrase and an artificial Zn(II) complex on a magnetic support for biomimetic carbon dioxide sequestration, *Journal of Molecular Catalysis B: Enzymatic*. 82 (2012) 37–45. <https://doi.org/10.1016/j.molcatb.2012.05.020>.
- [209] I. Nath, J. Chakraborty, F. Verpoort, Metal organic frameworks mimicking natural enzymes: a structural and functional analogy, *Chemical Society Reviews*. 45 (2016) 4127–4170. <https://doi.org/10.1039/C6CS00047A>.
- [210] X. Zhang, R. van Eldik, A functional model for carbonic anhydrase: thermodynamic and kinetic study of a tetraazacyclododecane complex of zinc(II), *Inorganic Chemistry*. 34 (1995) 5606–5614. <https://doi.org/10.1021/ic00126a034>.
- [211] A. Morita, S. Ariyasu, S. Ohya, I. Takahashi, B. Wang, K. Tanaka, T. Uchida, H. Okazaki, K. Hanaya, A. Enomoto, M. Neno, M. Ikekita, S. Aoki, Y. Hosoi, Evaluation of Zinc (II) chelators for inhibiting p53-mediated apoptosis, *Oncotarget*. 4 (2013) 2439–2450. <https://doi.org/10.18632/oncotarget.1535>.
- [212] Y.-F. Lin, E.N. Yousef, E. Torres, L. Truong, J.M. Zahnow, C.B. Donald, Y. Qin, L.A. Angel, Weak Acid-Base Interactions of Histidine and Cysteine Affect the Charge States, Tertiary Structure, and Zn(II)-Binding of Heptapeptides, *J Am Soc Mass Spectrom*. 30 (2019) 2068–2081. <https://doi.org/10.1007/s13361-019-02275-7>.
- [213] H. Sigel, A. Saha, N. Saha, P. Carloni, L.E. Kapinos, R. Griesser, Evaluation of intramolecular equilibria in complexes formed between substituted imidazole ligands and nickel(II), copper(II) or zinc(II), *Journal of Inorganic Biochemistry*. 78 (2000) 129–137. [https://doi.org/10.1016/S0162-0134\(99\)00219-6](https://doi.org/10.1016/S0162-0134(99)00219-6).

- [214] H. Song, D.L. Wilson, E.R. Farquhar, E.A. Lewis, J.P. Emerson, Revisiting Zinc Coordination in Human Carbonic Anhydrase II, *Inorganic Chemistry*. 51 (2012) 11098–11105. <https://doi.org/10.1021/ic301645j>.
- [215] K.G. Schulz, U. Riebesell, B. Rost, S. Thoms, R.E. Zeebe, Determination of the rate constants for the carbon dioxide to bicarbonate inter-conversion in pH-buffered seawater systems, *Marine Chemistry*. 100 (2006) 53–65. <https://doi.org/10.1016/j.marchem.2005.11.001>.
- [216] J.E. House, Ligand fields and molecular orbitals, *Inorganic Chemistry*. (2020) 687–715. <https://doi.org/10.1016/B978-0-12-814369-8.00017-0>.
- [217] K. Datta, A.J. Wowor, A.J. Richard, V.J. LiCata, Temperature Dependence and Thermodynamics of Klenow Polymerase Binding to Primed-Template DNA, *Biophysical Journal*. 90 (2006) 1739–1751. <https://doi.org/10.1529/biophysj.105.071837>.
- [218] Y. Zhu, M.L. Free, R. Woollam, W. Durnie, A review of surfactants as corrosion inhibitors and associated modeling, *Progress in Materials Science*. 90 (2017) 159–223. <https://doi.org/10.1016/j.pmatsci.2017.07.006>.
- [219] D. Wakerley, S. Lamaison, J. Wicks, A. Clemens, J. Feaster, D. Corral, S.A. Jaffer, A. Sarkar, M. Fontecave, E.B. Duoss, S. Baker, E.H. Sargent, T.F. Jaramillo, C. Hahn, Gas diffusion electrodes, reactor designs and key metrics of low-temperature CO<sub>2</sub> electrolyzers, *Nature Energy*. 7 (2022) 130–143. <https://doi.org/10.1038/s41560-021-00973-9>.
- [220] T. Li, E.W. Lees, Z. Zhang, C.P. Berlinguette, Conversion of Bicarbonate to Formate in an Electrochemical Flow Reactor, *ACS Energy Letters*. 5 (2020) 2624–2630. <https://doi.org/10.1021/acscenergylett.0c01291>.
- [221] A.R. Akbashev, Electrocatalysis Goes Nuts, *ACS Catalysis*. (2022) 4296–4301. <https://doi.org/10.1021/acscatal.2c00123>.
- [222] A. del Castillo, M. Alvarez-Guerra, J. Solla-Gullón, A. Sáez, V. Montiel, A. Irabien, Electrocatalytic reduction of CO<sub>2</sub> to formate using particulate Sn electrodes: Effect of metal loading and particle size, *Applied Energy*. 157 (2015) 165–173. <https://doi.org/10.1016/j.apenergy.2015.08.012>.
- [223] B. de Mot, M. Ramdin, J. Hereijgers, T.J.H. Vlugt, T. Breugelmans, Direct Water Injection in Catholyte-Free Zero-Gap Carbon Dioxide Electrolyzers, *ChemElectroChem*. 7 (2020) 3839–3843. <https://doi.org/10.1002/celec.202000961>.

- [224] H. Liu, B. Miao, H. Chuai, X. Chen, S. Zhang, X. Ma, Nanoporous tin oxides for efficient electrochemical CO<sub>2</sub> reduction to formate, *Green Chemical Engineering*. (2021). <https://doi.org/10.1016/j.gce.2021.11.001>.
- [225] S.A. Al-Tamreh, M.H. Ibrahim, M.H. El-Naas, J. Vaes, D. Pant, A. Benamor, A. Amhamed, Electroreduction of Carbon Dioxide into Formate: A Comprehensive Review, *ChemElectroChem*. 8 (2021) 3207–3220. <https://doi.org/10.1002/celec.202100438>.
- [226] B. de Mot, J. Hereijgers, M. Duarte, T. Breugelmans, Influence of flow and pressure distribution inside a gas diffusion electrode on the performance of a flow-by CO<sub>2</sub> electrolyzer, *Chemical Engineering Journal*. 378 (2019) 122224. <https://doi.org/10.1016/j.cej.2019.122224>.
- [227] I. Merino-Garcia, L. Tinat, J. Albo, M. Alvarez-Guerra, A. Irabien, O. Durupthy, V. Vivier, C.M. Sánchez-Sánchez, Continuous electroconversion of CO<sub>2</sub> into formate using 2 nm tin oxide nanoparticles, *Applied Catalysis B: Environmental*. 297 (2021) 120447. <https://doi.org/10.1016/j.apcatb.2021.120447>.
- [228] C.W. Li, M.W. Kanan, CO<sub>2</sub> Reduction at Low Overpotential on Cu Electrodes Resulting from the Reduction of Thick Cu<sub>2</sub>O Films, *J Am Chem Soc*. 134 (2012) 7231–7234. <https://doi.org/10.1021/ja3010978>.
- [229] J.T. Feaster, C. Shi, E.R. Cave, T. Hatsukade, D.N. Abram, K.P. Kuhl, C. Hahn, J.K. Nørskov, T.F. Jaramillo, Understanding Selectivity for the Electrochemical Reduction of Carbon Dioxide to Formic Acid and Carbon Monoxide on Metal Electrodes, *ACS Catalysis*. 7 (2017) 4822–4827. <https://doi.org/10.1021/acscatal.7b00687>.
- [230] C. Oloman, H. Li, Electrochemical Processing of Carbon Dioxide, *ChemSusChem*. 1 (2008) 385–391. <https://doi.org/10.1002/cssc.200800015>.
- [231] N. Wang, R.K. Miao, G. Lee, A. Vomiero, D. Sinton, A.H. Ip, H. Liang, E.H. Sargent, Suppressing the liquid product crossover in electrochemical CO<sub>2</sub> reduction, *SmartMat*. 2 (2021) 12–16. <https://doi.org/10.1002/smm2.1018>.
- [232] W.L. Bourcier, J.K. Stolaroff, M.M. Smith, R.D. Aines, Achieving Supercritical Fluid CO<sub>2</sub> Pressures Directly from Thermal Decomposition of Solid Sodium Bicarbonate, *Energy Procedia*. 114 (2017) 2545–2551. <https://doi.org/10.1016/j.egypro.2017.03.1412>.

- [233] D. Franzen, B. Ellendorff, M.C. Paulisch, A. Hilger, M. Osenberg, I. Manke, T. Turek, Influence of binder content in silver-based gas diffusion electrodes on pore system and electrochemical performance, *Journal of Applied Electrochemistry*. 49 (2019) 705–713. <https://doi.org/10.1007/s10800-019-01311-4>.
- [234] G. Arinton, A. Rianto, F. Faizal, D. Hidayat, S. Hidayat, C. Panatarani, I.M. Joni, Effect of binders on natural graphite powder-based gas diffusion electrode for Mg-air cell, in: 2016: p. 030055. <https://doi.org/10.1063/1.4943750>.
- [235] S. Joshi, S. Kalyanasundaram, V. Balasubramanian, Quantitative Analysis of Sodium Carbonate and Sodium Bicarbonate in Solid Mixtures Using Fourier Transform Infrared Spectroscopy (FT-IR), *Applied Spectroscopy*. 67 (2013) 841–845. <https://doi.org/10.1366/12-06915>.
- [236] M. Baldassarre, A. Barth, The carbonate/bicarbonate system as a pH indicator for infrared spectroscopy, *Analyst*. 139 (2014) 2167. <https://doi.org/10.1039/c3an02331a>.
- [237] A.R. Davis, B.G. Oliver, A vibrational-spectroscopic study of the species present in the CO<sub>2</sub>?H<sub>2</sub>O system, *Journal of Solution Chemistry*. 1 (1972) 329–339. <https://doi.org/10.1007/BF00715991>.
- [238] C. James, J. Eastoe, Ion specific effects with CO<sub>2</sub>-philic surfactants, *Current Opinion in Colloid & Interface Science*. 18 (2013) 40–46. <https://doi.org/10.1016/j.cocis.2012.12.004>.
- [239] E. Girard, T. Tassaing, J.-D. Marty, M. Destarac, Structure–Property Relationships in CO<sub>2</sub>-philic (Co)polymers: Phase Behavior, Self-Assembly, and Stabilization of Water/CO<sub>2</sub> Emulsions, *Chemical Reviews*. 116 (2016) 4125–4169. <https://doi.org/10.1021/acs.chemrev.5b00420>.
- [240] B. Farbos, T. Tassaing, Substituent effect on the interaction of aromatic primary amines and diamines with supercritical CO<sub>2</sub> from infrared spectroscopy and quantum calculations, *Physical Chemistry Chemical Physics*. 11 (2009) 5052. <https://doi.org/10.1039/b818956k>.
- [241] K. Sumida, D.L. Rogow, J.A. Mason, T.M. McDonald, E.D. Bloch, Z.R. Herm, T.-H. Bae, J.R. Long, Carbon Dioxide Capture in Metal–Organic Frameworks, *Chemical Reviews*. 112 (2012) 724–781. <https://doi.org/10.1021/cr2003272>.



- [242] P. Brandl, M. Bui, J.P. Hallett, N. mac Dowell, Beyond 90% capture: Possible, but at what cost?, *International Journal of Greenhouse Gas Control*. 105 (2021) 103239. <https://doi.org/10.1016/j.ijggc.2020.103239>.
- [243] C.Y. Chuah, K. Kim, J. Lee, D.-Y. Koh, T.-H. Bae, CO<sub>2</sub> Absorption Using Membrane Contactors: Recent Progress and Future Perspective, *Industrial & Engineering Chemistry Research*. 59 (2020) 6773–6794. <https://doi.org/10.1021/acs.iecr.9b05439>.
- [244] R. Klaassen, P.H.M. Feron, A.E. Jansen, Membrane Contactors in Industrial Applications, *Chemical Engineering Research and Design*. 83 (2005) 234–246. <https://doi.org/10.1205/cherd.04196>.
- [245] Z. Qi, E.L. Cussler, Microporous hollow fibers for gas absorption, *Journal of Membrane Science*. 23 (1985) 321–332. [https://doi.org/10.1016/S0376-7388\(00\)83149-X](https://doi.org/10.1016/S0376-7388(00)83149-X).
- [246] M.T. Ho, D.E. Wiley, Liquid absorbent-based post-combustion CO<sub>2</sub> capture in industrial processes, *Absorption-Based Post-Combustion Capture of Carbon Dioxide*. (2016) 711–756. <https://doi.org/10.1016/B978-0-08-100514-9.00028-7>.
- [247] A.J. Welch, E. Dunn, J.S. DuChene, H.A. Atwater, Bicarbonate or Carbonate Processes for Coupling Carbon Dioxide Capture and Electrochemical Conversion, *ACS Energy Letters*. 5 (2020) 940–945. <https://doi.org/10.1021/acsenergylett.0c00234>.
- [248] S.-Y. Oh, M. Binns, H. Cho, J.-K. Kim, Energy minimization of MEA-based CO<sub>2</sub> capture process, *Applied Energy*. 169 (2016) 353–362. <https://doi.org/10.1016/j.apenergy.2016.02.046>.
- [249] J.-M. Léger, F. Hahn, Contribution of In-situ Infrared Reflectance Spectroscopy in the Study of Nanostructured Fuel Cell Electrodes, in: *In-Situ Spectroscopic Studies of Adsorption at the Electrode and Electrocatalysis*, Elsevier, 2007: pp. 63–98. <https://doi.org/10.1016/B978-044451870-5/50004-X>.
- [250] Y. Meng, X. Zhang, W.-H. Hung, J. He, Y.-S. Tsai, Y. Kuang, M.J. Kenney, J.-J. Shyue, Y. Liu, K.H. Stone, X. Zheng, S.L. Suib, M.-C. Lin, Y. Liang, H. Dai, Highly active oxygen evolution integrated with efficient CO<sub>2</sub> to CO electroreduction, *Proceedings of the National Academy of Sciences*. 116 (2019) 23915–23922. <https://doi.org/10.1073/pnas.1915319116>.

- [251] R. Lin, J. Guo, X. Li, P. Patel, A. Seifitokaldani, Electrochemical Reactors for CO<sub>2</sub> Conversion, *Catalysts*. 10 (2020) 473. <https://doi.org/10.3390/catal10050473>.
- [252] L.R.F.H.S.W. Allen J. Bard, *Electrochemical Methods: Fundamentals and Applications*, 3rd Edition, Wiley, 2022.
- [253] D.M. Heard, A.J.J. Lennox, Electrode Materials in Modern Organic Electrochemistry, *Angewandte Chemie International Edition*. 59 (2020) 18866–18884. <https://doi.org/10.1002/anie.202005745>.
- [254] S.-F. Qin, Y.-J. Xie, Y. Wang, L.-X. You, J.-H. Fang, J.-J. Sun, Fundamentals on kinetics of electrochemical reduction of CO<sub>2</sub> at a bismuth electrode, *Journal of Electroanalytical Chemistry*. 904 (2022) 115924. <https://doi.org/10.1016/j.jelechem.2021.115924>.
- [255] S. Ringe, E.L. Clark, J. Resasco, A. Walton, B. Seger, A.T. Bell, K. Chan, Understanding cation effects in electrochemical CO<sub>2</sub> reduction, *Energy & Environmental Science*. 12 (2019) 3001–3014. <https://doi.org/10.1039/C9EE01341E>.
- [256] M. Dunwell, Y. Yan, B. Xu, Understanding the influence of the electrochemical double-layer on heterogeneous electrochemical reactions, *Current Opinion in Chemical Engineering*. 20 (2018) 151–158. <https://doi.org/10.1016/j.coche.2018.05.003>.
- [257] Y. Hori, S. Suzuki, Electrolytic Reduction of Bicarbonate Ion at a Mercury Electrode, *Journal of The Electrochemical Society*. 130 (1983) 2387–2390. <https://doi.org/10.1149/1.2119593>.
- [258] R. Kortlever, K.H. Tan, Y. Kwon, M.T.M. Koper, Electrochemical carbon dioxide and bicarbonate reduction on copper in weakly alkaline media, *Journal of Solid State Electrochemistry*. 17 (2013) 1843–1849. <https://doi.org/10.1007/s10008-013-2100-9>.
- [259] A. Bonet Navarro, A. Nogalska, R. Garcia-Valls, Direct Electrochemical Reduction of Bicarbonate to Formate Using Tin Catalyst, *Electrochem*. 2 (2021) 64–70. <https://doi.org/10.3390/electrochem2010006>.
- [260] I. Merino-Garcia, E. Alvarez-Guerra, J. Albo, A. Irabien, Electrochemical membrane reactors for the utilisation of carbon dioxide, *Chemical Engineering Journal*. 305 (2016) 104–120. <https://doi.org/10.1016/j.cej.2016.05.032>.

- [261] P. Servio, P. Englezos, Effect of temperature and pressure on the solubility of carbon dioxide in water in the presence of gas hydrate, *Fluid Phase Equilibria*. 190 (2001) 127–134. [https://doi.org/10.1016/S0378-3812\(01\)00598-2](https://doi.org/10.1016/S0378-3812(01)00598-2).
- [262] R. Wiebe, V.L. Gaddy, The Solubility of Carbon Dioxide in Water at Various Temperatures from 12 to 40° and at Pressures to 500 Atmospheres. *Critical Phenomena* \*, *J Am Chem Soc.* 62 (1940) 815–817. <https://doi.org/10.1021/ja01861a033>.
- [263] C.Y. Chuah, K. Kim, J. Lee, D.-Y. Koh, T.-H. Bae, CO<sub>2</sub> Absorption Using Membrane Contactors: Recent Progress and Future Perspective, *Industrial & Engineering Chemistry Research*. 59 (2020) 6773–6794. <https://doi.org/10.1021/acs.iecr.9b05439>.
- [264] B. Endródi, E. Kecsenovity, A. Samu, F. Darvas, R. v. Jones, V. Török, A. Danyi, C. Janáky, Multilayer Electrolyzer Stack Converts Carbon Dioxide to Gas Products at High Pressure with High Efficiency, *ACS Energy Letters*. 4 (2019) 1770–1777. <https://doi.org/10.1021/acsenergylett.9b01142>.
- [265] C.M. Gabardo, C.P. O'Brien, J.P. Edwards, C. McCallum, Y. Xu, C.-T. Dinh, J. Li, E.H. Sargent, D. Sinton, Continuous Carbon Dioxide Electroreduction to Concentrated Multi-carbon Products Using a Membrane Electrode Assembly, *Joule*. 3 (2019) 2777–2791. <https://doi.org/10.1016/j.joule.2019.07.021>.
- [266] G. Díaz-Sainz, M. Alvarez-Guerra, J. Solla-Gullón, L. García-Cruz, V. Montiel, A. Irabien, Catalyst coated membrane electrodes for the gas phase CO<sub>2</sub> electroreduction to formate, *Catalysis Today*. 346 (2020) 58–64. <https://doi.org/10.1016/j.cattod.2018.11.073>.
- [267] D.M. Weekes, D.A. Salvatore, A. Reyes, A. Huang, C.P. Berlinguette, Electrolytic CO<sub>2</sub> Reduction in a Flow Cell, *Accounts of Chemical Research*. 51 (2018) 910–918. <https://doi.org/10.1021/acs.accounts.8b00010>.
- [268] Y.C. Li, D. Zhou, Z. Yan, R.H. Gonçalves, D.A. Salvatore, C.P. Berlinguette, T.E. Mallouk, Electrolysis of CO<sub>2</sub> to Syngas in Bipolar Membrane-Based Electrochemical Cells, *ACS Energy Letters*. 1 (2016) 1149–1153. <https://doi.org/10.1021/acsenergylett.6b00475>.
- [269] M.A. Blommaert, D. Aili, R.A. Tufa, Q. Li, W.A. Smith, D.A. Vermaas, Insights and Challenges for Applying Bipolar Membranes in Advanced Electrochemical Energy Systems, *ACS Energy Letters*. 6 (2021) 2539–2548. <https://doi.org/10.1021/acsenergylett.1c00618>.



# Personal information

## Publications in international peer-reviewed journals

1. **O. Gutierrez-Sanchez**, Y. Y. Birdja, M. Bulut, J. Vaes, T. Breugelmans and D. Pant. Recent advances in industrial CO<sub>2</sub> electroreduction. *Current Opinion in Green and Sustainable Chemistry*, 2019, 16, 47-56.
2. **O. Gutierrez-Sanchez**, N. Daems, W. Offermans, Y. Y. Birdja, M. Bulut, D. Pant and T. Breugelmans. The inhibition of the proton donor ability of bicarbonate promotes the electrochemical conversion of CO<sub>2</sub> from bicarbonate solutions. *Journal of CO<sub>2</sub> Utilization*, 2021, 48, 101521
3. **O. Gutierrez-Sanchez**, N. Daems, M. Bulut, D. Pant and T. Breugelmans. Effect of benzyl-functionalized cationic surfactants on the inhibition of the hydrogen evolution reaction in CO<sub>2</sub> reduction systems. *ACS Applied Materials & Interfaces*, 2021, 13(47), 56205-56216
4. **O. Gutierrez-Sanchez**, B. Bohlen, N. Daems, M. Bulut, D. Pant and T. Breugelmans. A state-of-the-art update on integrated CO<sub>2</sub> capture and electrochemical conversion systems. *ChemElectroChem*, 2022, 9(5), e202101540
5. **O. Gutierrez-Sanchez\***, B. De Mot\*, M. Bulut, D. Pant and T. Breugelmans. Engineering aspects for the design of a bicarbonate zero-gap flow electrolyser for the conversion of CO<sub>2</sub> to formate. *ACS Applied Materials & Interfaces*, 2022. In press. (\*Equal contribution)

## Publications in review in international peer-reviewed journals

1. **O. Gutierrez-Sanchez**, H. Y. Vincent Ching, N. Daems, M. Bulut, D. Pant and T. Breugelmans. Bifunctional Carbonic Anhydrase for the Integrated Capture and Electrochemical Conversion of CO<sub>2</sub>. *Materials Today Chemistry*, 2022. Under review
2. **O. Gutierrez-Sanchez**, B. De Mot, N. Daems, M. Bulut, D. Pant and T. Breugelmans. Electrochemical CO<sub>2</sub> Conversion from Direct Air Capture solutions. *ACS Energy Letters*, 2022. Under review.

## Oral presentations at international conferences

1. **O. Gutierrez-Sanchez**, N. Daems, W. Offermans, Y. Y. Birdja, M. Bulut, D. Pant and T. Breugelmans. The inhibition of the proton donor ability of bicarbonate promotes the electrochemical conversion of CO<sub>2</sub> from bicarbonate solutions. *29<sup>th</sup> Topical Meeting of the International Society of Electrochemistry*, 19 April, 2021. Mikulov, Czech Republic.
2. **O. Gutierrez-Sanchez**, N. Daems, M. Bulut, D. Pant and T. Breugelmans. Electrochemical conversion of CO<sub>2</sub> from bicarbonate solutions. *41<sup>st</sup> Meeting of the Electrochemistry Group of the Spanish Royal Society of Electrochemistry*, 6 July, 2021. Paris, France.
3. **O. Gutierrez-Sanchez**, N. Daems, M. Bulut, D. Pant and T. Breugelmans. Electrochemical conversion of CO<sub>2</sub> from bicarbonate solutions. *72<sup>nd</sup> Annual Meeting of the International Society of Electrochemistry*, 29 August, 2021. Jeju Island, Korea.

## Oral presentations at a national conference

1. **O. Gutierrez-Sanchez**, N. Daems, M. Bulut, D. Pant and T. Breugelmans. Integrated capture and electrochemical conversion of CO<sub>2</sub>. *CAPTURE Science Talks*, 30 April, 2021. Online event.

## Poster presentations at international conferences

1. **O. Gutierrez-Sanchez**, N. Daems, W. Offermans, Y. Y. Birdja, M. Bulut, D. Pant and T. Breugelmans. Electrocatalytic conversion of bicarbonate promoted by surface hydrophobicity, *71<sup>st</sup> Annual Meeting of the International Society of Electrochemistry*, 31 August, 2020. Belgrade, Serbia.
2. **O. Gutierrez-Sanchez**, N. Daems, W. Offermans, Y. Y. Birdja, M. Bulut, D. Pant and T. Breugelmans. Electrochemical conversion of bicarbonate to formate promoted by the inhibition of the hydrogen evolution reaction, *International Conference on Electrocatalysis for Energy Applications and Sustainable Chemicals*, 23 November, 2020. Online event.





